UNIVERSITAT
ROVIRA I VIRGILI

DEQ

Universitat Rovira i Virgili
Escola Tecnica Superior d'Enginyeria Quimica
Departament d'Enginyeria Quimica

Study of a torus bioreactor for the enzymatic elimination of phenol

Dissertation submitted to obtain the degree:
Doctor in Chemical Engineering from Universitat Rovira i Virgili

Presented by: Laura Mariela Pramparo
Supervised by: Dr. Christophe Bengoa (URV)

Tarragona, June 2008

Universitat Rovira i Virgili

Departament d'Enginyeria Química

Escola Tècnica Superior d'Enginyeria Química

Study of a torus bioreactor for the enzymatic elimination of phenol

Memoria presentada por:

Laura Mariela Pramparo

Para optar al Grado de

Doctora en Ingeniería Química

Tesis dirigida por el Dr. Christophe Bengoa

Miembros del Tribunal de Tesis

Dr. Henry Delmas   Dr. Jérémy Pruvost

Dr. Frank Stüber   Dra. Magdalena Constantí

Dr. Agustí Fortuny   Dr. Julián Carrera

Dr. Anton Vernet

Evaluadores Externos (Doctorado Europeo)

Dr. Jack Legrand   Dr. Yves Popineau

Junio de 2008

El Dr. Christophe Bengoa, Profesor Agregado del Departament d'Enginyeria Química de la Universitat Rovira i Virgili de Tarragona, fair constar que el present treball, amb el títol:

Study of a torus bioreactor for the enzymatic elimination of phenol

que presenta la doctoranda LAURA MARIELA PRAMPARO

per a optar al grau de Doctora en Enginyeria Química, ha estat dut a terme sota la nostra immediata direcció i que tots els resultats obtinguts són fruit del treball i l'anàlisi realitzats per l'esmentada doctoranda.

I per a què es faci saber i tingui els efectes que corresponguin, signen aquesta certificació.

Tarragona, Junio de 2008

Dr. Christophe Bengoa

*"No son las malas hierbas las que ahogan la buena
semilla, sino la negligencia del campesino"*

CONFUCIO

Filósofo chino

Esta tesis esta dedicada a mi
familia por su incondicional amor.

General index

Index of figures

Index of figures

Index of figures

Index of tables

Nomenclature Abbreviations, Acronyms and Symbols

AC	Activated Carbon	$E(t)$	Residence time distribution function
ATSDR	Agency for toxic substances and disease registry	F_g	Geometrical parameter of the impeller
CFD	Computational Fluids Dynamics	H_2O	Water
CPO	Chloroperoxidase	H_2O_2	Hydrogen peroxide
CSTR	Continuous stirred tank reactor	L_t	Reactor average length
CWAO	Catalytic Wet Air Oxidation	N	Rotation velocity of the impeller, rpm
EPA	Environmental Protection Agency		
EPER	European Pollutant Emission Register	Pe	Peclet number
		Q	Flow rate
HPLC	High performance liquid chromatography	R_c	Bend curvature radius
		Re	Reynolds number
HRP	Horseradish peroxidase	Re_m	Mixing Reynolds number
LiP	Lignin peroxidase	Sc	Schmidt number
MRF	Multiple reference frame	T_m	Mixing time
PMMA	Poly(methyl methacrylate)	U_o	Mean bulk velocity
RANS	Reynolds equation obtained for the Navier-Stokes equation	V	Reactor volume
		V_i	Initial reaction rate
RSM	Reynolds stress model	X_{Ph}	Phenol conversion
RTD	Residence time distribution	K'_m	Apparent Michaelis constant
TOC	Total Organic Carbon	t_c	Circulation time
UV	Ultraviolet	$\bar{t}_c$	Mean circulation time
WAO	Wet Air Oxidation	t_{cb}	Batch circulation time
A_2H_2	Polymers	t_{cc}	Continuous circulation time
$AH\cdot$	Phenoxy radical	T_m^{*}	Dimensionless mixing time
AH_2	Phenol	T_m	Mixing time
C_{Ph0}	Initial phenol concentration	U	Axial component of the velocity
C	Concentration	V	Rate consumption
C_{final}	Average final concentration in the reactor	V'_{max}	Apparent maximum reaction rate
$C_T(t)$	Tracer concentration	x	Axial coordinate
D_{ax}	Axial dispersion coefficient	y	Wall distance
D_t	Reactor diameter	z	Longitudinal coordinate
E_i	Compound I in the chemical reaction	μ	Dynamic viscosity
		ρ	Fluid density
E_{ii}	Compound II	τ	Average residence time

Acknowledgments

A lo largo de estos años son muchas las personas que de una u otra manera han contribuido con la realización de esta tesis doctoral. Quisiera agradecer a todas ellas el apoyo, comprensión y ayuda que me han brindado.

En primer lugar quisiera agradecer la beca pre-doctoral que he recibido, los primeros meses de la Universitat Rovira i Virgili y después de la Agència de Gestió d'Ajuts, Universitats i Recerca de la Generalitat de Catalunya.

También quisiera agradecer el soporte económico para desarrollar esta tesis doctoral que ha sido provisto por la Comunidad Europea mediante el proyecto REMOVALS FP6-018525 y por el Ministerio de Educación y Ciencia mediante la concesión de Acciones Integradas Franco-Española ref. HF2003-003 y el proyecto CTM2005-01873/TECNO.

A los doctores H. Delmas, J. Pruvost, F. Stüber, M. Constantí, A. Fortuny, J. Carrera y A. Vernet por aceptar ser miembros del tribunal de tesis.

Quisiera expresar mi gratitud a todos los miembros del Departamento de Ingeniería Química de la Universitat Rovira i Virgili y al grupo de investigación Chemical Reaction Engineering and Process Intensification (CREPI) por recibirme en su grupo y proveerme de todo lo necesario para la realización de este trabajo.

Especialmente quisiera agradecer a mi supervisor Dr. Christophe Bengoa por la confianza depositada en mí y por su constante ayuda en la producción de esta tesis.

Je dois attribuer une grande partie de mes mérites aux stages de recherche que j'ai réalisé au sein du groupe de recherche GEPEA de l'Université de Nantes, dirigé par le Professeur Jack Legrand. Je voudrais remercier tout particulièrement au Dr. Jérémy Pruvost pour son inappréciable aide lors de mes séjours et pour son énorme collaboration lors de la réalisation de cette Thèse. Je tiens à remercier très particulièrement au Professeur Jack Legrand pour ses commentaires qui m'ont toujours été d'un grand secours ainsi qu'au Professeur Patrick Legentilhomme pour sa gentillesse. Finalement, je voudrais remercier Mariana et Daniel Titica qui ont permis que mon séjour à Saint-Nazaire soit si agréable.

De tout mon coeur, j'espère pouvoir collaborer à nouveau avec vous dans un futur proche.

I would like to acknowledge the kindness of Dr. Keith Taylor who helped me during my stay in Windsor, Canada.

Gracias al Departamento de Ingeniería Mecánica de la Universitat Rovira I Virgili, especialmente al Dr. J. Pallares del Grup de Recerca en Experimentació, Computació i Modelització en Mecànica de Fluids i Turbulència por permitirme utilizar sus ordenadores para realizar las simulaciones numéricas.

Mis mejores deseos a Laura García y Verónica Saravia, ha sido una experiencia inolvidable haber vivido con ustedes 4 años. Hemos compartido muchas cosas y espero que podamos seguir compartiendo nuestra amistad en el futuro. Todo lo mejor para ustedes!

A Irama Sánchez y Maretva Baricot, ha sido una experiencia única haber compartido todo este tiempo con ustedes tanto laboratorio, oficina como amistad. A Fernando Salazar y Mariela Labbe, por todos los viajes que hicimos juntos, las fiestas de fin de año haciéndonos compañía y espero que ahora, a pesar de la distancia, no olvidemos nada de esto, que pensemos en todo lo que hemos compartido y que eso mantenga la llama de nuestra amistad.

Quisiera agradecer a Cosmín Burian (ahora si haré empanadas!), a Fredy Avellaneda y Debora Nabarlatz (por todas las comidas, salidas, viajes y momentos compartidos...y espero que haya muchos más!), a Subba Rao Mandava, Luizildo Pitol, Alexey Kolodkin, Jorgelina Pasqualino, Henry Lambis, Camilo Mancera, Alexandre Trentin, Dan y Simona Libotean y Vikas Kumar. Todos hemos pertenecido a esta pequeña ONU que formamos aquí y en la que hemos compartido un montón de vivencias y cosas inolvidables y que, hoy por hoy, considero mis amigos. Gracias a todos!

Quisiera dar un especial agradecimiento a Johann por su amor, su apoyo y su comprensión. Gracias por todo este maravilloso tiempo vivido y compartido. Llenas de alegría y amor mi vida. Gracias por escucharme, ayudarme y hacerme desconectar cada vez que lo necesitaba.

A mi familia, mis padres Silvia y Eduardo, mis hermanos Pablo y Romina y mis dos hermosas sobrinas por su apoyo incondicional, aunque eso significase estar separados por más de 10000 km todo este tiempo. Y también a todas las personas que me quieren y a quienes quiero.

Seguramente se me olvida gente por nombrar, solo les pido perdón y que sepan que les agradezco infinitamente el haber estado allí conmigo.

Laura Mariela Pramparo

Tarragona, Junio de 2008

Resumen

Los compuestos fenólicos son contaminantes prioritarios que se encuentran comúnmente en una gran cantidad de efluentes industriales. Diferentes procesos están disponibles actualmente para la eliminación de fenol desde dicho efluentes pero los mismos presentan algunas desventajas como pueden ser una baja eficiencia, un mayor consumo de energía, la producción de lodos conteniendo hierro o limitaciones en la capacidad de tratamiento. La necesidad de encontrar alternativas a estos problemas ha hecho del proceso enzimático una buena opción. En las últimas dos décadas, varios procesos han sido implementados utilizando diferentes enzimas extraídas de plantas y microorganismos como pueden ser las peroxidasas de diversas fuentes, horseradish peroxidasa, las ligninas peroxidasas obtenidas de hongos de putrefacción blanca y las polifenol oxidasas, como por ejemplo la tyrosinasa, obtenidas de setas.

Diferentes configuraciones de enzimas, libre e inmovilizada y diferentes soportes para la inmovilización han sido también estudiados. En los últimos años, sustancial atención ha sido dedicada a la inmovilización de enzimas por enlace covalente sobre soportes porosos insolubles tales como vidrio, aluminio, sílice y chitosan. Este trabajo muestra una nueva configuración que no ha sido aún probada: la horseradish peroxidase soportada en Eupergit.

La segunda novedad de este trabajo es la utilización de un reactor tórico para la eliminación de contaminantes orgánicos en efluentes. Este reactor, que puede ser considerado como un reactor de bucle, presenta algunas ventajas con respecto a los tradicionales reactores tipo tanque agitado como pueden ser una más eficiente mezcla de los reactivos, un fácil escalado y un diseño que asegura la ausencia de volúmenes muerto dentro del reactor, un bajo consumo de potencia, una alta capacidad de transferencia de calor, la prevención del depósito de los polímeros o biomateriales sobre la pared del reactor y una alta eficiencia.

El objetivo de este trabajo es el estudio de la hidrodinámica dentro de un reactor tórico para su posterior aplicación en la eliminación enzimática de fenol y el acople entre las cinéticas y la modelización.

En una primera etapa, la eliminación enzimática de fenol es estudiada experimentalmente en el reactor tórico. Con el objetivo de comparar el rendimiento de dicho reactor, varios ensayos se realizaron en un reactor agitado tradicional.

Un alto grado de conversión de fenol ha sido obtenido para la eliminación enzimática de fenol en ambos reactores para las cantidades estudiadas de fenol. Ha sido observado que es necesario mantener una relación de 1:1 entre la concentración inicial de fenol y la de peróxido de hidrógeno para lograr la mayor conversión de fenol. Usando el reactor tórico ha sido obtenido un 97% de conversión de fenol cuando las concentraciones óptimas de substratos y enzimas fueron utilizados. También, una inhibición por la concentración de substrato ha sido observada ya que se obtuvo una menor conversión de fenol cuando se agregaba una concentración de peróxido de hidrógeno superior a la relación 1:1 establecida anteriormente. El

Resumen

exceso de peróxido de hidrógeno en la mezcla inhibió la actividad catalítica de la enzima a través de la conversión de la peroxidase a formas inactivas de la misma. Un modelo cinético basado en el modelo de Michaelis-Menten con inhibición ha sido propuesto con el objetivo de obtener un modelo único que pueda ser aplicado a cualquier concentración de fenol estudiada. Un buen ajuste ha sido obtenido utilizando el modelo propuesto para todas las concentraciones estudiadas en este trabajo. De esta manera, ha sido obtenido un modelo cinético que incluye tanto el efecto de la concentración de peróxido de hidrógeno, la influencia de la concentración de fenol como así también la inhibición debido a ambos substratos. Las velocidades iniciales de la reacción obtenidas en ambos reactores han sido muy similares, sin embargo, una mejor conversión de fenol ha sido obtenida utilizando el reactor tórico para todos los casos.

Con el objetivo de mejorar económicamente el proceso y hacerlo factible para su uso a escala industrial, la enzima debería ser utilizada en un proceso en continuo sobre un largo período de tiempo para explotarla completamente. Por esta razón, ha sido necesario inmovilizar la enzima. Tres diferentes técnicas para la inmovilización covalente de la enzima han sido explorados, concluyendo que el método de inmovilización sobre Eupergit que utiliza tratamiento con periodate de la enzima ha dado mejores resultados y por lo tanto, ha sido encontrado un efectivo método para la preparación de biocatalizadores estables. Utilizando esta técnica de inmovilización ha sido encontrado que un valor máximo de actividad de 126 U·g^{-1} es obtenido para una cantidad de enzima cargando sobre el soporte de 17.6 mg·g^{-1}. Este método de inmovilización permitió también reducir la cantidad de enzima necesaria para obtener la máxima actividad de la enzima inmovilizada. Utilizando enzima inmovilizada se ha obtenido una más baja actividad enzimática comparada con la de enzima libre. Sin embargo, un mayo grado de conversión de fenol ha sido obtenido utilizando una menor concentración de enzima.

Asimismo, la caracterización usando CFD del campo de flujo de un reactor tórico similar al experimental de 100 ml ha sido realizada para un reactor trabajando de forma batch y continua. En condiciones batch ha sido obtenida una evolución lineal de las velocidades medias de circulación con respecto a la velocidad de rotación del agitador. Los valores obtenidos para el tiempo de mezclado en todas las condiciones hidrodinámicas han sido muy cortos, menos de 21 segundos en todos los casos estudiados, obteniendo una rápida homogeneización dentro del reactor. El tiempo de mezclado adimensional ha sido también determinado y ha sido encontrado ser independiente del número de Reynolds cuando la velocidad de rotación del agitador era mayor que 1200 rpm (Re > 5800). Así pues, régimen turbulento debería ser obtenido dentro del reactor para valores de número de Reynolds obtenidos para velocidades mayores que 1200 rpm.

En modo continuo, el reactor tórico puede exhibir un comportamiento más complejo debido a la perturbación del flujo dentro del reactor dado por la corriente de entrada (aceleración o desaceleración de la circulación del flujo dentro del reactor). Este hecho ha sido mostrado para condiciones particulares de velocidades de rotación del agitador y caudales de entrada. Para

condiciones de operación normales, la hidrodinámica sin embargo ha sido solo función de la velocidad de rotación del agitador.

Cuando diferentes caudales de entrada fueron comparados, con el objetivo de determinar la mejor configuración a ser usado para el sistema en continuo, solo una pequeña diferencia ha sido encontrada en los tiempos de mezclado. Esta diferencia ha sido observada especialmente para bajas velocidades de rotación del agitador. Para altas velocidades de rotación, despreciables diferencias han sido encontradas para las diferentes configuraciones estudiadas. De esta manera, ha sido posible deducir que cuando el flujo de entrada es localizado de manera perpendicular a la circulación del flujo dentro del reactor, el flujo de entrada no tiene influencia sobre la hidrodinámica del reactor.

Asimismo, un escalado en el volumen del reactor tórico ha sido realizado utilizando CFD para un reactor de 300 ml. En este caso ha sido encontrado que las velocidades medias de circulación dentro del reactor son mayores que en el reactor de 100 ml comportándose de una manera más similar a un reactor tórico de sección circular.

Finalmente, la reacción enzimática de fenol con HRP has sido modelada acoplando el modelo cinético obtenido experimentalmente con las simulaciones del campo de flujo dentro del reactor. En este caso un buen ajuste ha sido obtenido entre los datos experimentales y las simulaciones numéricas realizadas con CFD. Estos resultados permitirán la optimización y el escalado del proceso usando CFD.

Las conclusiones más relevantes obtenidas en este trabajo se pueden resumir en:

- Los resultados experimentales muestran que el proceso enzimático es una buena opción para el tratamiento de compuestos fenólicos.

- El rendimiento del reactor tórico es comparable con el del reactor tanque agitado. La actividad de la enzima es igual en ambos reactores. Sin embargo es obtenida una más baja eliminación de fenol en el tanque agitado. Se obtienen velocidades iniciales de reacción mayores en el reactor tórico debido a un más eficiente mezclado de los reactivos.

- Se ha obtenido un buen método para la inmovilización de la enzima. Este método es una nueva alternativa para la inmovilización de HRP.

- La hidrodinámica del reactor depende principalmente de la velocidad de rotación del agitador.

- Se obtienen tiempos de mezclados muy breves dentro del reactor tórico, lo que implica una rápida homogeneización de la concentración en el reactor.

- Las simulaciones numéricas realizadas con CFD tienen una muy buena aproximación con los datos experimentales. Esto permite predecir los resultados experimentales.

- Finalmente, estos resultados permiten la optimización y el escalado del proceso usando CFD.

Abstract

Phenols are priority pollutants that are commonly found in a large number of industrial wastewaters. Different processes are currently available for the elimination of phenol from wastewater but present some disadvantages like low efficiency, high energy-consumption, the necessity of acclimatisation of the sludges or the limitation of the treatment capacity. The need to find alternatives has made the enzymatic processes a good option. In the last two decades, several processes were implemented with different enzymes from plants and microorganisms, including peroxidases from several sources, horseradish peroxidase, lignin peroxidases from white-rot fungus and the polyphenol oxidases (e.g. tyrosinase) from mushrooms.

Also, different enzyme configurations, free or immobilised enzyme and different supports for immobilisation have been studied. In the last years, substantial attention has been devoted to the covalent immobilisation of enzymes on porous insoluble supports such as glass, alumina, silica, and chitosan. This work presents a new configuration that has never been tested: the horseradish peroxidase supported on Eupergit.

The second novelty of this work is the utilisation of a torus reactor for the removal of organic contaminants from wastewaters. This reactor, that can be considered as a loop reactor, presents some advantages over other stirred tank reactors including an efficient mixing of the reactants, easy scale-up and design ensured by the absence of dead volume, low power consumption, high heat transfer capacity, the prevention of deposition of polymers or biomaterials on the reactor wall and finally, a high efficiency.

The goal of this work is the study of the hydrodynamics of a torus reactor for its further application in the enzymatic elimination of phenol and the coupling of the kinetics and the modelisation.

In a first step, the enzymatic elimination of phenol was experimentally studied in the torus reactor. In order to compare the performances, several assays were also carried out with a stirred reactor.

A high degree of conversion was obtained for the enzymatic elimination of phenol in both reactors with the tested quantities of phenol. It was concluded that, keeping a ratio of 1:1 between the phenol and the H_2O_2 initial molar quantities, the highest final reaction conversion was obtained. Using the torus reactor was obtained 97% of phenol conversion when the optimal concentrations of substrates were used. Also, a substrate inhibition was presented in the reaction, this occurred when the H_2O_2 initial concentration was increased, and thus, the final reaction conversion was lower. The excess of hydrogen peroxide in the mixture inhibited the catalytic activity of the enzyme through the conversion of the peroxidase to inactive forms. A kinetic model based on Michaelis-Menten with inhibition was proposed in order to have a unique kinetic model to be applied for any initial phenol concentration. A good fitting was obtained with the proposed model for all the studied phenol concentrations. In this way, a model that included the effect of the H_2O_2 and the phenol initial concentrations and inhibitions was reached. The

Abstract

initial reaction rates were very similar in both reactors; however, better phenol conversions were obtained in the torus reactor for all cases.

In order to improve economically the process, the enzyme should be used in a continuous regime over a long time period to exploit it completely. For this reason it was necessary to immobilise the enzyme. Three different approaches for the covalent immobilisation of the HRP were explored, concluding that, the periodate-mediated covalent immobilisation of the HRP on Eupergit was found to be an effective method for the preparation of stable biocatalysts. In this case, a maximum value of the immobilised enzyme activity of 126 $U \cdot g^{-1}$ was found using an enzyme loading on the support of 17.6 $mg \cdot g^{-1}$. The activity of the immobilised enzyme was lower than the activity of the free enzyme. However, a high degree of phenol conversion was obtained using less concentration of enzyme.

In a second step, the characterisation using the CFD of the flow-field in a torus reactor of 100 ml, similar to the experimental reactor, was carried out for two different configurations, batch and continuous operating modes.

In batch conditions, a linear evolution of the mean circulation velocities with respect to the impeller rotation speed was obtained. The mixing time values obtained in all hydrodynamic conditions were short, less than 21s, in all the studied cases, achieving rapid concentration homogeneity in the reactor. The dimensionless mixing time was determined and was found to be independent of the Reynolds number when the impeller rotation speed was greater than 1200 rpm (Re > 5800). Thus, fully turbulent regime should be obtained into the torus reactor with values of Reynolds number obtained for N values greater than 1200 rpm.

In continuous mode, the torus reactor can exhibit a more complex behaviour, due to the perturbation of the inside flow by the feeding injection (acceleration or deceleration of the flow circulation in the reactor). This was shown for particular conditions of impeller rotation speeds and feeding flow rates. For common operating conditions, the hydrodynamics was, however, mainly a function of the impeller rotation speed. Further studies will quantify the influence of such perturbation in the case of the enzymatic conversion using the torus reactor in continuous regime.

When different inlet flow rates were compared, in order to determine the best configuration to be used, only a small difference in the mixing times was observed for small values of impeller rotation speeds (200 rpm). For higher velocities of rotation, negligible differences have been found for the different configurations. Thus, it was deductible that when the flow inlet was located in a perpendicular form to the flow circulation inside the reactor, it did not have any influence on the hydrodynamic of the reactor.

Finally, the enzymatic reaction of phenol with the HRP was modelled using the CFD coupled to the kinetic model of the enzymatic reaction to the flow simulation. A very good agreement was obtained between experimental data and the CFD numerical simulations in terms of phenol

Abstract

conversion, initial reaction rates and kinetic comparison. These results allowed the possibility of optimising and scaling-up the process using the CFD modelisation.

Abstract

PART I. Introduction and hypotheses

Chapter 1. Introduction

1.1. Water pollution

Comprising over 70% of the Earth's surface, water is undoubtedly the most precious natural resource that exists on our planet. This invaluable resource is an essential element for everything on our planet to grow and prosper. Although human kind recognizes this fact, it is disregarding it by polluting rivers, lakes, and oceans. In order to combat water pollution, society has to understand the problems and become part of the solution.

This natural resource is becoming scarcer in certain places, and its availability is a major social and economic concern. Currently, about 1 billion people around the world routinely drink unhealthy water. During the G8 Evian summit in 2003, most countries have accepted the challenge of halving the number of people who do not have access to safe water and sanitation by 2015. Even if this difficult goal is achieved, there will be more than half billion people without access to safe drinking water, and also, 1 billion people will not have access to an adequate sanitation. Poor water quality and bad sanitation are deadly; about 2 million deaths a year are caused by drinking polluted or nonpotable water.

UNESCO's World Water Development Report (WWDR, 2003) from its World Water Assessment Program indicates that, in the next 20 years, the quantity of water available to everyone is predicted to decrease by 30%. Currently, 40% of the world's inhabitants have insufficient fresh water for minimal hygiene. More than 2.2 million people died in 2000 from waterborne diseases (related to the consumption of contaminated water) or drought. In 2004, the UK charity Water Aid reported that a child dies every 15 seconds from easily preventable water-related diseases; this often refers to a lack of sewage disposal.

Water, unlike petroleum, is not yet a limited resource, but rather re-circulated as potable water in precipitation in quantities many degrees of magnitude higher than human consumption. Therefore, water replenished in aquifers around every 1 to 10 years is the relatively small quantity of water in reserve in the earth, which corresponds to about 1% of our drinking water supply. That is a non-renewable resource, and it is, rather, the distribution of potable and irrigation water which is scarce, rather than the actual amount of it that exists on the earth.

The pollution of rivers and streams with chemical contaminants has become one of the most crucial environmental problems within the 20th century. Waterborne chemical pollution entering rivers and streams cause a tremendous contamination. Moreover, in the 21st century, 90% of all wastewater still goes untreated into local rivers and streams (UNEP, 2002). Fifty countries, responsible of a third of the world's population, also suffer from medium or high water stress, and 17 of these extract more water annually than is recharged through their natural water cycles

(Ravindranath, 2002). The strain not only affects surface fresh water bodies like rivers and lakes, but degrades also groundwater resources.

In Europe, the past decades have seen significant progress in the treating of sewage and industrial wastes. Treated effluents are still being pumped into the river systems, resulting in the diminishment of levels of most pollutants and a measurable improvement of the water quality. Nowadays, the wastewater treatment and recovery is mandatory.

There are different causes of pollution including sewage and fertilizers that contain nutrients such as nitrates and phosphates. In excess levels, nutrients over stimulate the growth of aquatic plants and algae. An excessive growth of these types of organisms consequently clogs our waterways, consume dissolved oxygen as they decompose, and block light to deeper waters. This, in turn, proves very harmful to aquatic organisms as it affects the respiration ability of fish and other invertebrates that reside in water.

The pollution is also caused when silt and other suspended solids, such as soil, wash off plowed fields, construction and logging sites, urban areas, and eroded river banks when it rains. Under natural conditions, lakes, rivers, and other water bodies undergo Eutrophication, an aging process that slowly fills in the water body with sediment and organic matter. When these sediments enter various bodies of water, fish respiration becomes impaired, plant productivity and water depth become reduced, and aquatic organisms and their environments become suffocated.

The pollution in the form of organic material enters waterways in many different forms as sewage, as leaves and grass clippings, or as runoff from livestock feedlots and pastures. When natural bacteria and protozoan in the water break down this organic material, they begin to consume the oxygen dissolved in the water. Many types of fish and bottom-dwelling animals cannot survive when levels of dissolved oxygen drop below two to five parts per million. When this occurs, it kills aquatic organisms in large numbers which leads to disruptions in the food chain.

Other sources of water pollution are petroleum and radioactive substances. Petroleum often pollutes water bodies in the form of oil, resulting from oil spills. The large-scale accidental discharges of petroleum are an important cause of pollution along shore lines. Radioactive substances are produced in the form of waste from nuclear power plants, and from the industrial, medical, and scientific use of radioactive materials. Specific forms of waste are uranium and thorium mining and refining.

Because of overpopulation, mass consumption, misuse, and water pollution, the availability of drinking water per capita is inadequate and shrinking as of the year 2006. For this reason, water is a strategic resource in the globe and an important element in many political conflicts. It causes health impacts and damage to biodiversity. The serious worldwide water situation is called water crisis.

One of the Millennium Development Goals is to halve, by 2015, the proportion of people without sustainable access to safe drinking water. Fresh water — now more precious than ever in our history for its extensive use in agriculture, high-tech manufacturing, and energy production — is increasingly receiving attention as a resource requiring better water management and sustainable use.

1.2. The Industrial effluents problem

The wastewaters can be divided in two typical categories: urban and industrial. In the urban residues, the main pollutant load is organic, mostly non toxic and biodegradable. Usually, this kind of wastewater is treated in conventional wastewater treatment plants based on biological oxidation.

On the contrary, industrial effluents usually have a very complex and toxic composition, depending on the industry that generated them, which often requires more severe remediation treatments. Examples of toxic and therefore non biodegradable organic pollutants are phenols, surfactants, chlorinated compounds, pesticides, aryl and chlorinated alkysulfonates, polyethylene and aromatic hydrocarbons, among many others (Dojilido 1993, Ozmen 2008).

Despite the banned or severely restricted use of all those chemicals since the late 1970s, their continued presence in groundwater, soil, sediment, surface water, and living tissues emphasises the concern regarding their persistence in the environment.

The organic pollutants tend to accumulate in the tissues of animals and plants, often becoming more concentrated as they move up through the food chain. Moreover, many times, the symptoms of contamination may not manifest themselves until several generations after initial contact with the chemical of concern (Stirling 2000).

The importance of phenolic effluents, besides from their potential toxicity, is outlined by the high quantities that are eventually rejected in the environment. Thus, it is often used as a model compound for the studies of wastewater treatment. This compound was selected as model because it is listed in the Priority Pollutants List (PPL) of the Environmental Protection Agency (EPA). Phenol is also listed in the European Union (EU) Directive 2000/60/EC, the Comprehensive Environmental Response and in the Compensation and Liability Act (CERCLA) Priority List of Hazardous Substances. Moreover, it is recognised, or at least suspected, to be a toxic compound by the International Chemical Safety Cards, the Registry of Toxic Effects of Chemical Substances (RTECS) and the toxicological profiles made by the Agency for Toxic Substances and Disease Registry (ATSDR, 1998) in USA.

The direct emissions to water per Member State of the European Community are shown in figure 1.1 and the indirect emissions in figure 1.2. As it can be seen in the figures, the direct emissions of phenols to water are a significant problem in Spain.
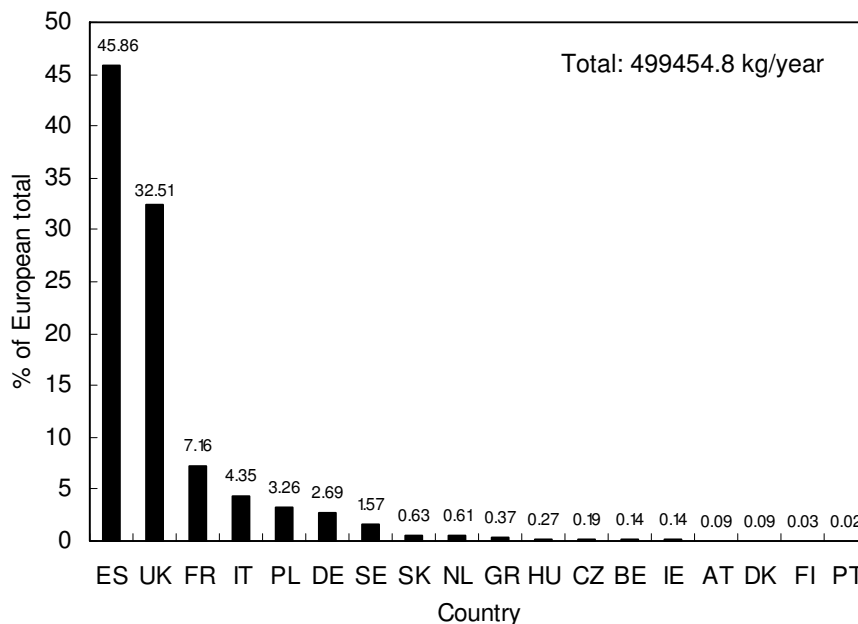
Figure 1.1. Phenols direct emissions to water per European Member State (EPER, 2004).
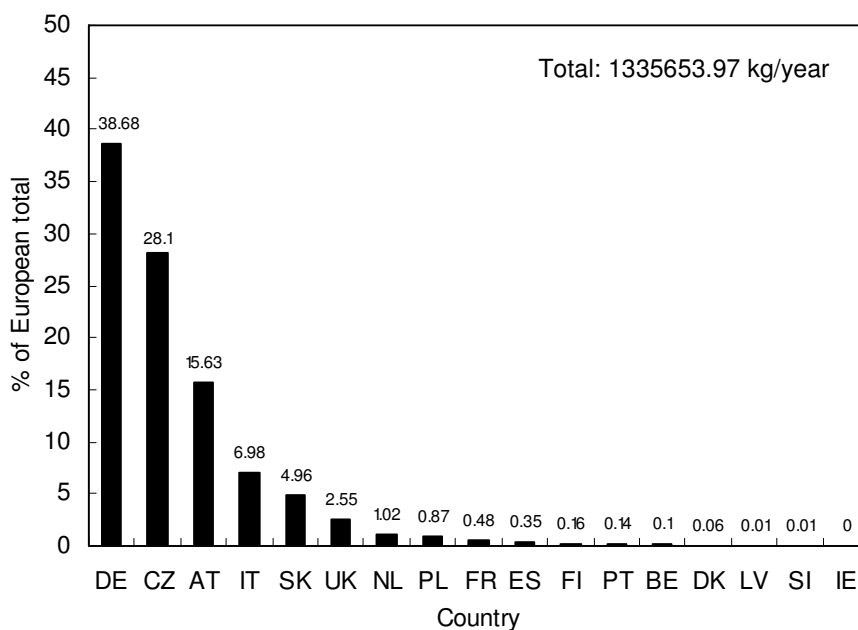
Figure 1.2. Phenols indirect emissions to water per European Member State (EPER, 2004).

In Spain, the total emissions of phenol can be divided depending of the autonomous community. The table 1.1 shows the total emissions of phenol in Spain for each community.

Table 1.1. Spanish direct emissions of phenols to water by communities (EPER-Spain, 2004).

Autonomic Community	Total direct emissions (ton/year)	% of total emissions
Asturias	221.00	94.4
Cataluña	2.77	1.2
Aragón	2.43	1.0
País Vasco	2.24	1.0
Andalucía	2.12	0.9
Valencia	1.50	0.6
Cantabria	1.20	0.5
Galicia	0.63	0.3
Castilla La Mancha	0.40	0.2
Madrid	0.32	0.1
Navarra	0.11	~0.0
Spain	234.00	100.0

As it can be seen in the table, Asturias is the Autonomous Community with the highest level of direct emissions of phenol to water. This can be due to the type of industries presents in that region, mainly for the production and transformation of metals, smelting products and gross steel. Likewise, Cataluña is positioned in the second place, representing a serious problem for the region.

1.3. A case of study: the phenol

Phenol and its derivatives are aromatic compounds and the major class of pollutants commonly found in industrial wastewaters. In general, aromatic hydrocarbons are molecules based on the benzene ring structure. They are important components in petrol (gasoline) and usually contain carcinogenic molecules like benzene, toluene, ethylbenzene and xylene (ortho-, meta- and para). Some of them have non-organic substituents like N, Cl, S, P, so they form important subgroups, termed substituted aromatic hydrocarbons (Bingham, 1979). In table 1.2, the typical use and potential toxicity of these compounds are summarized.

Table 1.2. Aromatic compounds found in wastewaters (EPA-USA, 2001: Data for total annual release).

Group	Material	Toxicity Ranking	Use
Aromatic Hydrocarbons	Xylenes	May contain benzene, a carcinogen [3]	Aviation gasoline, protective coatings, solvent for alkyd resins, rubber cements, synthesis of organic chemicals
Phenols	Phenol	Questionable carcinogen [3]	Making pharmaceuticals, chemicals, plastics, resins, rubber, refining oils, fertilizer, coke, paint removers, asbestos, perfumes, disinfectants, bactericide, fungicide
	Cresols	Toxic	Making disinfectants, perfumes, preserving agents or herbicide
Chlorinated Hydrocarbons	Chlorophenols	Questionable carcinogen, corrosive	Making dyes, making other chemicals
Nitroaromatic Hydrocarbons	Nitrophenols	Toxic [3]	Making fungicide, pesticide, dyes and other chemicals
	Nitrobenzene	Also called oil of mirbane, poison, reproductive effects [3]	Making shoe polish, dyes, explosives, floor and metal polish, other chemicals and paints
	Aniline	Suspected carcinogen, mutagen, allergen [3]	Dyes, coloured pencils, lithographic and other printing inks, perfumes, pharmaceuticals, nylon fibres, resins, industrial solvents, rubber processing
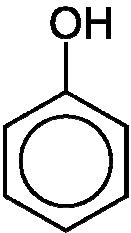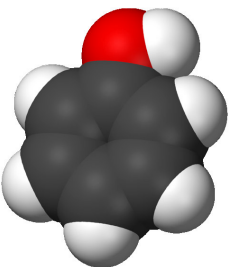
[3] Severe toxicity, materials that can cause injury of sufficient severity to threaten life.

As it can be seen in this table, the important pollutant families are aromatic hydrocarbons (phenols, cresols, xylenes) and substituted hydrocarbons (chlorophenols, nitrophenols, etc.). The effect of these pollutants is high, as they accomplish factors of high toxicity and high annual release (EPA).

Phenolic compounds are found in the waste streams of e.g. fibre bonding production, wood composites, textiles, foundry resins, coatings and abrasives, from chemical, petrochemical, pharmaceutical, agricultural and chemical-manufacturing sources in concentrations ranging from trace quantities to thousands of milligrams per litre (Wu 1993, Stanisavljevic 2004).

Phenol is a monosubstituted aromatic hydrocarbon. In its pure state, it exists as a colourless or white solid. The chemical and physical characteristics of phenol are given in table 1.3.

Table 1.3. Characteristics of phenol.

	IUPAC name	Phenol
	CAS Number	[108-95-2]
	Other names	Carbolic Acid, Benzenol, Phenylic Acid, Hydroxybenzene, Phenic acid
	Molecular formula	C_6H_5OH
	Molar mass	94.11 g/mol
	Appearance	White Crystalline Solid
	Density	1.07 g/cm³
	Melting point	40.5 ℃
	Boiling point	181.7 ℃
	Solubility in water	90 g/l (20 ℃)
	Acidity (pKa)	9.95
	Dipole moment	1.7 D
	EU classification	Toxic (T)-Muta. Cat. 3-Corrosive (C)
	Flash point	79ºC

Phenol gives off a sweet, acrid smell detectable to most people at 40 ppb in air, and at about 1 to 8 mg·l^{-1} in water (ATSDR 1998).

Phenol is toxic to bacteria and fungi, and is also used as disinfectant. Because of its anaesthetic effects, phenol is used in medicines such as ointments, ear and nose drops, cold sore lotions, throat lozenges, and antiseptic lotions. Moreover, due to the bactericidal effect of phenol on microorganisms, it is not possible to treat phenolic wastewaters applying biological sewage processing methods without acclimatizing the biomass (Scully 2006).

The industries that use phenol are listed in Table 1.4 (Pacific Northwest Pollution Prevention Resource Centre, January 2006).

The largest use of phenol is as an intermediate in the production of phenolic resins, which are used in the plywood, adhesive, construction, automotive, and appliance industries. Phenol is also used in the production of synthetic fibbers, such as nylon, and for epoxy resin precursors such as bisphenol-A.

Table 1.4. Uses of phenol in the industry.

Industrial sector	Uses
Primary metals	Blast furnaces and steel mills, non-ferrous wire drawing and insulating, grey and ductile iron foundries, malleable iron foundries, motor vehicle parts and accessories, and aluminium foundries.
Stone, clay and glass product manufacture	Mineral wool, abrasive products, asbestos products, products of purchased glass, non-clay refractories, minerals (ground or treated), cement - hydraulic, lime manufacture.
Rubber and plastic parts manufacture	Laminated plastics plate & sheet, custom compound purchased resins, tires and inner tubes, unsupported plastics film & sheet.
Petroleum products	Petroleum refining, petroleum and coal products, lubricating oils and greases. Transportation Equipment Manufacture - motor vehicle parts and accessories, railroad and aircraft equipment.
Wood products manufacture	Reconstituted wood products, softwood veneer and plywood, hardwood veneer and plywood, structural wood members, sawmills & planing mills.
Textile mills	Tire cord and fabrics, coated fabrics (not rubberised), broad woven fabric mills (wool and cotton).
Electronic equipment manufacture	Engine electrical equipment, commercial lighting fixtures, transformers, electric house wares and fans, non-current carrying wiring devices, semiconductors and related devices, printed circuit boards, switchgear and switchboard, relays and industrial controls.
Industrial machinery manufacture	Paper industries machinery, machine tools (metal cutting types).

The consumer products that may contain phenol are agricultural chemicals, disinfectants, general antibacterials and antiseptics, household hard surface cleaners, lubricating oils, automotive chemicals, paint and varnish removers, pharmaceutical preparations, synthetic resins and rubber adhesives and wood office work surfaces.

The direct emissions of phenol to water per industrial activity are presented in figure 1.3 and the indirect emissions to water by transfer to an off-site waste water treatment are shown in figure 1.4.
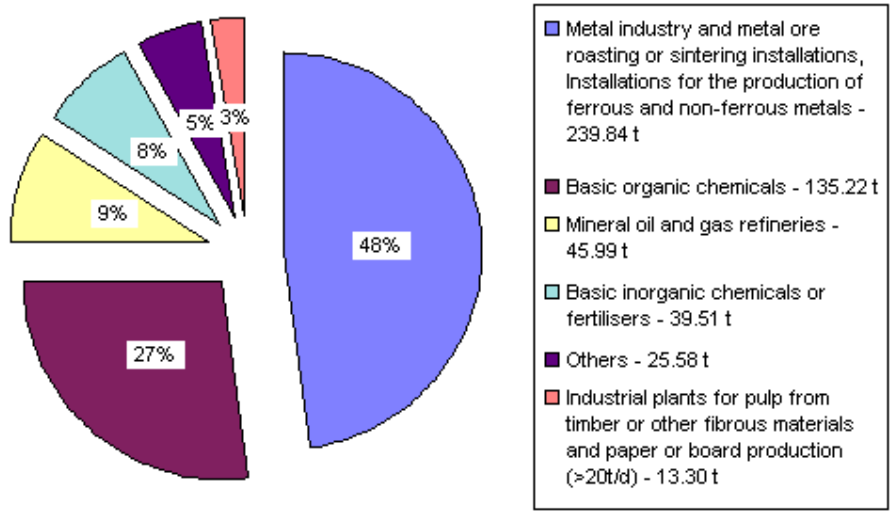
Figure 1.3. Direct emissions of phenol per industrial activity.
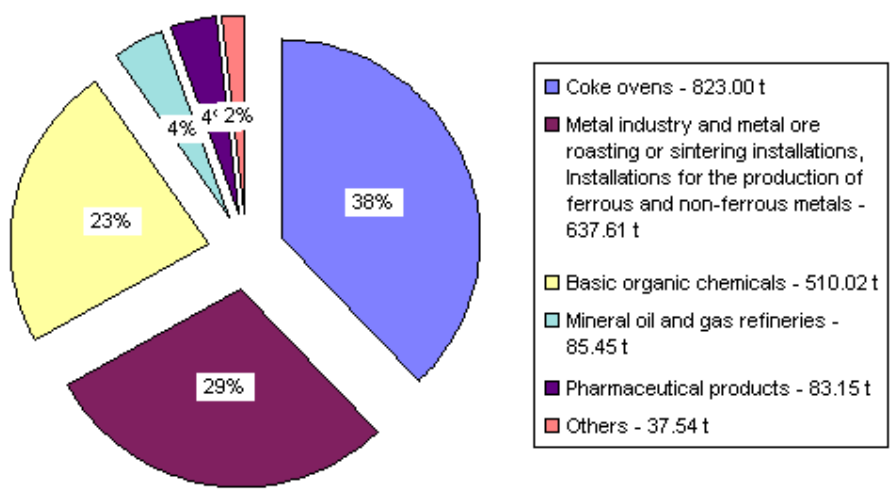
Figure 1.4. Indirect emissions of phenol per industrial activity.

The total direct emissions of phenol to water in the European Union are around 500 ton per year and the indirect emissions are around 2200 ton per year (EPER, 2004). In Spain, the total direct emissions of phenol to water are 229 ton per year and the indirect emissions are 7.69 ton per year. These values represent the 45.86% and the 0.35% of the total emissions of phenol in the European Community.

The majority of phenols and its derivatives are toxic substances; a lot of them have been classified as hazardous wastes, and some of them are known or suspected to be carcinogens (Verschueren 1977). Moreover, if discharged, even at a lower concentration, they are highly hazardous to aquatic life, and confer a particular disagreeable taste and odour to water.

1.4. Water pollution regulations in Europe and in Spain

Environmental action by the European Community (EC) as a whole began in 1972 with the adoption of more than 200 pieces of legislation, chiefly concerned with limiting pollution by introducing minimum standards, notably for waste management, water pollution and air pollution.

The EC policy on waste management involves three complementary principles:

a)   Eliminating waste at source and breaking the link between waste creation and growth, amongst other things by improving product design.

b)   Encouraging waste recycling and re-use, for specific waste flows in particular.

c)   Improving the method of final disposal, for example by reducing pollution caused by waste incineration and using landfill only as a last resort.

Since the adoption of the 1975 framework Directive on waste (Directive 75/442/EEC), legislative developments have been based on these three principles. In the same way, prevention and recycling are gaining more and more weight as the main thematic strategies on that subject.

The Council Directive 76/464/EEC on pollution caused by certain dangerous substances discharged into the aquatic environment was adopted because chemical contamination of Community waters and the oceans had become an increasing and potentially damaging phenomenon. The European governments agreed that this problem required some kind of coordinated action. At the time, Directive 76/464/EEC set relatively ambitious goals for the prevention and minimisation of water pollution from dangerous chemicals. The urge expressed by most Member States to harmonise the implementation of protective measures was however not only inspired by the need to improve the environment, but also to avoid distortion of competition in polluting industries affected by respective policies.

The Directive 76/464/EEC, being at the interface of industrial and environmental policies, has remained a contentious legislative act for 25 years. While its provisions are clear its wording leaves considerable discretion to Member States how to actually implement them. Also, strong industrial pressure has delayed and in many cases altogether prevented the adoption of the required EU daughter directives laying down measures and objectives for individual black substances. As a result, out of 129 Black List candidate substances, only 18 have been regulated, and not a single one has been tackled since 1990 (Lanz 2001).

The purpose of Directive 80/68/EEC on the protection of groundwater against pollution caused by certain dangerous substances is to prevent the discharge of certain toxic, persistent and bioaccumulating substances into groundwater.

The legislation has since moved towards assigning more responsibility to the producer. For instance, the Directive of September 2000 on end-of-life vehicles (Directive 2000/53/EC) establishes a system for collecting such vehicles at the manufacturer's expense. Likewise, two Directives on waste from electrical and electronic equipment and restricting the use of certain

dangerous substances in such equipment were adopted in 2002 (Directive 2002/96/EC, Directive 2002/95/EC).

Reflecting the new environmental conscience, the European Union, in the Directive 2000/60/EC, points out that "water is not a commercial product like any other but, rather, a heritage which must be protected, defended and treated as such".

Finally, the Directive 2000/60/EC and also the Spanish Water Act 1/2001 (article 93) (Spanish Water Act 1/2001) define the pollution as the "direct or indirect introduction, as a result of human activity, of substances or heat into the air, water or land which may be harmful to human health or the quality of aquatic ecosystems or terrestrial ecosystems directly depending on aquatic ecosystems, which result in damage to material property, or which impair or interfere with amenities and other legitimate uses of the environment".

The European Union made a list of dangerous compounds (Directive 2000/60/EC, Annex VIII: Indicative list of the main pollutants), considered as contaminants. The aim of this Directive is to achieve the progressive reduction of emissions of hazardous substances to water. The list of the updated priority pollutants has been presented in the Decision 2001/2455/EC. Further Water Framework Directive obligations are aimed at:

- the progressive reduction of discharges, emissions and losses of priority substances to surface water bodies and,

- the cessation or phasing-out of discharges, emissions and losses of priority hazardous substances to surface water bodies.

The environmental level permitted by the Agency for toxic substances and disease registry (ATSDR) for phenol in water is 1 ppb in unpolluted groundwater and 0.01-1 ppb in unpolluted rivers (data from 1985) (ATSDR 2006).

EPA has a lifetime health advisory for adults for phenol in drinking water of 4 milligrams per litre (4 ppm). EPA also recommends that the level of phenol in surface water (lakes, streams) should be limited to 3.5 mg/l to protect people from drinking contaminated water or eating contaminated fish (ATSDR 1998).

1.5. Conclusions

Phenol is a toxic compound that is commonly found in industrial wastewaters. Several tons of phenol are discharged to water by direct or indirect emissions in the European Community per year. In the same way, the different Autonomous Communities in Spain suffer the same problem, especially in Asturias due to the type of industries present in this region.

The consequences of the water pollution have the capabilities to disrupt life on our planet to a great extent. Governments have approved laws to try to combat water pollution thus acknowledging the fact that water pollution is, indeed, a serious issue.

For countries within the European Union, water-related directives are important for water resource management and environmental and water quality standards. Different regulations have been established in the EC in order to prevent the pollution of water.

But the government alone cannot solve the entire problem. It is ultimately up to the society, to be informed, responsible and involved when it comes to face the problems with water. The society must become familiar with local water resources and learn about ways for disposing harmful household wastes so they do not end up in sewage treatment plants that cannot handle them or landfills not designed to receive hazardous materials.

These are just a few of the many ways in which the civilization has the ability to combat water pollution. As we head into the 21st century, awareness and education will most assuredly continue to be the two most important ways to prevent water pollution. If these measures are not taken and water pollution continues, life on earth will suffer severely.

Global environmental collapse is not inevitable. But the developed countries must work with the developing countries to ensure that new industrialised economies do not add environmental problems to the world. Politicians must think about sustainable development rather than economic expansion. Conservation strategies have to become more widely accepted, and people must learn that energy use can be dramatically diminished without sacrificing comfort. In short, with the technology that currently exists, the years of global environmental mistreatment can begin to be reversed.

Chapter 2. Hypotheses and objectives

2.1. Hypotheses

The torus reactor can be a better option than other conventional reactors for the elimination of contaminants in wastewaters.

The enzymatic elimination of phenolic compounds can compete with other techniques of wastewater treatments.

The use of CFD allows the acquisition of simulated values and, in this way, permits a reduction of the experimentation.

2.2. Objectives

The main objective of the research is to study the performance of a torus reactor in order to be used in a treatment of elimination of contaminants in wastewater. Phenol is used as model compound because it is found commonly in industrial wastewaters.

This whole doctoral research is divided into three specific goals:

The first goal is to use the torus reactor for the elimination of organic contaminants present in wastewaters with enzymes as the biocatalyst of the reaction. For this, the phenol will be used as model compound. The performance of the torus reactor in the process will be compared with a stirred tank reactor. The optimization of the operating conditions will be done with the torus reactor. Finally, the immobilisation of the enzyme will be done to allow the economical improvement of the process.

In a second step, the study of the hydrodynamic behaviour of the torus reactor will be carried out by CFD numerical simulation. The objective is to determine the hydrodynamic characteristics of the torus reactor in batch and continuous mode. The influence of the inlet flow and of the stirring speed will be investigated. Finally, the validation of the experimental data will be achieved.

The last purpose of the work is to simulate by CFD the enzymatic reaction using the torus reactor. The objective of this part will be the coupling between the flow-field and the kinetic reaction obtained experimentally, to allow predicted results of the reaction without any experimental work. Finally, the scale-up of the process will be analysed.

PART II. Enzymatic elimination of phenol

Chapter 3. Literature review

This chapter summarises some of the most important processes currently available for the elimination of organic contaminants present in wastewater, focusing on the enzymatic process. For the enzymatic elimination of phenol there are different alternatives depending on the enzyme and the configuration used. This work is based on the use of the horseradish peroxidase as the biocatalyst.

3.1. Available treatment processes

Due to the characteristics of phenolic compounds presented in chapter 1, it is essential to treat phenol-contaminated water before discharging it. In some cases, the removal of these pollutants to levels specified by discharge standards may not be economically attainable using conventional treatments such as chemical, physical and biological, because the increasing severity of the legislation.

Nowadays, the processes and technologies available can be classified as preliminary, primary, secondary and tertiary treatments (Horan 1990). The conventional treatments for industrial wastewaters are presented in figure 3.1. The preliminary treatment is designed to remove the debris and sandy materials; the primary treatment separates suspended solids and greases; meanwhile, the secondary treatment is usually a biological treatment to remove the dissolved organic matter; and finally, the tertiary treatment focuses on the removal of disease-causing organisms from wastewaters.

In the last decade, several researches have been addressed to a special class of oxidation techniques defined as Advanced Oxidation Processes (AOP). It was shown that AOP could solve the problem of biorecalcitrant water pollutants working at, or near, ambient temperature and pressure.
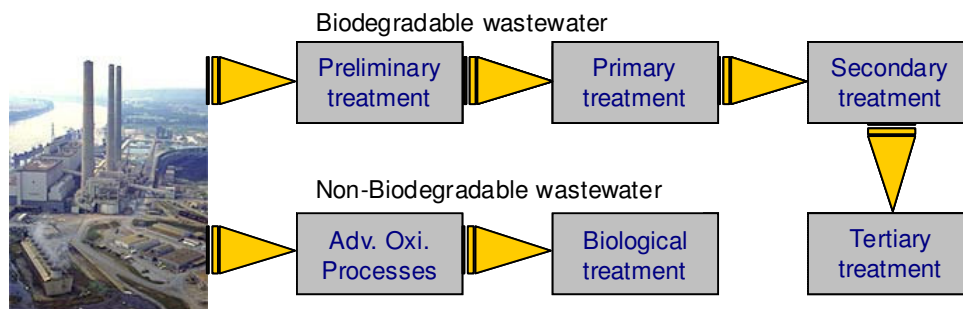
Figure 3.1. The conventional treatments for industrial wastewaters.

There are a lot of treatment methods that are currently utilised or under investigation. These common methods are membrane separation, adsorption by activated carbon or other

adsorbents, Fenton and electro-fenton, photo-oxidation using H_2O_2/UV, electro-oxidation, chlorine or ozone, wet oxidation, catalytic wet air oxidation, peroxide promoted catalytic wet air oxidation and incineration, among a lot of other technologies. Some of these technologies are mapped in the figure 3.2 (Hancock 1999) where, their applicability is evaluated with the effluent COD concentration (measured as TOC) and the effluent flow-rate ($m^3 \cdot h^{-1}$). In definitive, the map shows where the technologies can be applied and they are effective. Generally, in the case of high organic pollutant concentrations (TOC > 1000 mg·l^{-1}) and low flow rates (< 25 $m^3 \cdot h^{-1}$), the classical incineration is the most widely used technology for the destruction of liquid and solid waste (Santoleri 1988). For wastes with only low to moderate concentration of organic material (100 < TOC < 1000 mg·l^{-1}), the process is not self sustainable and auxiliary fuel has to be added. There are several options for the treatment of liquid waste streams. One option is the adsorption on activated carbon (Matatov & Sheintuch 1998), but the saturated carbon is a hazardous waste, requiring either regeneration or transportation to a hazardous waste landfill (Voice 1998). An apparent low cost option offers the biological oxidation, but the organic pollutant has to be biodegradable, dilute and of low toxicity and the process generates a huge amount of sludges (Irvine & Wilderer 1988). This high sludge generation requires physical treatments for sludge volume reduction, and the subsequent landfilled leading to a potential secondary pollution source (Bertanza et al. 2001).
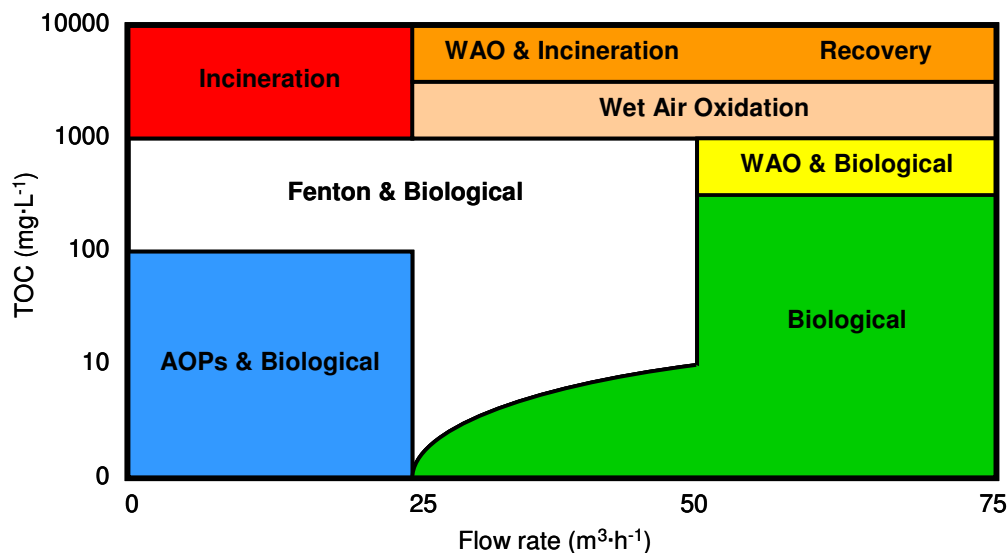
Figure 3.2. The technology map (adapted from Hancock 1999).

The effectiveness of these methods is also impaired due to the drawbacks of either less efficient, more energy-consuming, production of iron containing sludge or limitation of treatment capacity. Wet Air Oxidation (WAO) and Catalytic Wet Air Oxidation (CWAO), use temperature and pressures over 120ºC and 10 bar and air or oxygen as oxidant. Fenton-like process benefits from using H_2O_2 as a liquid oxidant and a homogeneous or heterogeneous catalyst to enhance the oxidation conditions.

In the last decade, the performance of the activated carbon used as a catalyst has been investigated for the WAO of phenol (Fortuny 1998, Fortuny 1999, Eftaxias 2001, Suarez-Ojeda 2005).

These authors used activated carbon and copper catalysts (Cu0803) to compare phenol conversion. The experimental data were obtained from a continuous trickle bed reactor using air as oxidant at different conditions of temperatures (120–160ºC) and oxygen partial pressures (6–12 bar) (Fortuny et al. 1999). In their experiments, Cu0803 was found to lose its activity due to the leaching of the copper phase. On the other hand, AC also exhibited a continuous drop in phenol conversion, finally reaching about 48% (30% with Cu0803). However, the loss of AC efficiency could be ascribed to its consumption during the experiment, thus the absolute activity of AC remained stable during the long term run, while the reactions of the oxidation of phenol and of the activated carbon are competitive.

The integration of catalytic wet air oxidation with aerobic biological treatment allowed the discharge of product reactions in WWTP (Suarez-Ojeda 2005 and 2007). In these works it was demonstrated that the continuous catalytic wet air oxidation (CWAO) was a suitable precursor for the biological treatment of industrial wastewater containing phenols (phenol, o-cresol, 2-chlorophenol, p-nitrophenol), or other organic compounds (aniline, sulfolane, nitrobenzene and sodium dodecylbenzene sulfonate (DBS)). The results showed that the AC without any supported active metal behaved the bifunctionallity of adsorbent and catalyst, and moreover, is active enough to oxidate phenol, o-cresol, 2-chlorophenol and DBS, giving conversions between 30 and 55% at the conditions tested.

The feasibility study of the coupling of an AC/CWAO process, catalysed by activated carbon with an aerobic biological treatment to treat a high-strength o-cresol wastewater was carried out in Suarez-Ojeda (2007). The biodegradation parameters, i.e. the maximum oxygen uptake rate and the oxygen consumption, of the main reaction intermediates allowed their classification into readily biodegradable, inert, toxic or inhibitory compounds. This detailed study, permitted to understand the biodegradability enhancement exhibited by an AC/CWAO effluent and to achieve a successful strategy for coupling the AC/CWAO step with an aerobic biological treatment for a high-strength o-cresol wastewater. For the demonstration, the inlet flow of the pilot scale WWTP was constituted by a 30% of COD of the AC/CWAO elluent. The integrated AC/CWAO-biological treatment achieved a 98% of total COD removal and in particular, a 91% of the AC/CWAO effluent of COD removal and, without any undesirable effect on the biomass.

The viability of the H_2O_2 promoted catalytic wet air oxidation (PP-CWAO) process was studied with activated carbon (AC) as catalyst to increase the biodegradability of phenolic aqueous solutions (Rubalcaba 2007). A trickle bed reactor has been used in this study, the addition of H_2O_2 in the alimentation of the CWAO process not only increased pollutant removal, but also led to obtain a higher mineralization of the remaining oxidation products. For instance, the removal of phenol, o-cresol and p-nitrophenol increased from 45, 33 and 15% in the CWAO process, to 64, 64 and 49% in the PP-CWAO process.

On the other hand, the advanced oxidation processes (AOP) such as ozonation, photocatalysis and electrochemical oxidation (among many others), utilise electron beams, UV light or ultrasound pulses to obtain high oxidation rate through the generation of free OH• radicals (mainly hydroxyl radicals).

The recovery of organics is one of the available techniques for the elimination of phenol, but it requires additional energy costs for the construction and operation of the facilities. There are also combined treatments like AOPs with biological treatment, ozonation with photocatalysis or adsorption on activated carbon with CWAO, etc. A technology commonly used as a last option is the incineration, appropriate for effluents having TOC >1000 $g \cdot L^{-1}$. However, it has an extremely high energetic cost and it is not environmental friendly due to the dust dissemination to the atmosphere and to the related problems associated with dioxins production (Mishra 1995).

Phenol degradation using sonochemical techniques has been widely investigated (Entezari et al. 2004; Papadaki et al. 2004; Kidak et al. 2006). Wu et al. (2001) have studied the effect of UV irradiation on sonochemical degradation of phenol, reporting that while total phenol degradation was possible, the degree of mineralization was no more than 20%; however the latter could be improved by the addition of Fenton's reagent to the solution.

In other studies, Chen et al. (2002) encompassed the combination of Advanced Oxidation with ultrasound and Drijvers et al. (1999) investigated the decomposition of phenol under the combined effect of sonolysis, chemical oxidation (with H_2O_2) and the addition of solid catalyst (e.g. Al_2O_3, ZnO, Ni_2O_3, CuO). The authors have reported that the degradation was significantly enhanced by the presence of H_2O_2 and CuO.

Biological treatments seem to be the most useful method for wastewater treatment but the incapability of conventional biological treatment to remove effectively many industrial biorecalcitrant and/or toxic pollutants evidences that new efficient treatment systems are needed.

Finally, the enzymatic elimination of phenol is one of these alternative and attractive methods. This system has been developed in the last decades and appears to be a destruction method for the treatment of solid, liquid and hazardous wastes (Klibanov 1980, Klibanov 1983, Robb 1984, Tien 1987, Kirk 1987, Griffin 1991, Dunford 1991, Nicell 1992, Aitken 1993, Vasudevan 1996, Karam 1997, Tong 1997, Masuda 2001, Ikehata 2002, Duarte 2002, Ikehata 2005, Bayramoglu 2008). Such method has many advantages over conventional biological treatments, physical and/or chemical processes e.g. specificity, application to a broad range of compounds including biorefractories; ability to operate in wide ranges of temperature, pH and salinity; capacity to manage low and high concentration of contaminants; no necessity to acclimate the biomass with a simpler process control, the possibility to operate under milder and less corrosive conditions and finally, the enzymes are easy to handle and store (Nicell 1993, Bódalo 2006).

3.2. Enzymatic treatment

3.2.1. The beginning

The enzymatic method was firstly introduced by Klibanov and co-workers in 1980. They developed a method for the removal of organic contaminants from industrial wastewater. This technique involved the treatment of aqueous solutions containing the pollutants with an enzyme as the biocatalyst and, the hydrogen peroxide as the precursor of the polymerization.

In the work of Klibanov et al. (1980), different phenols and anilines were used to study the enzymatic method. The study began by examining the effect of the enzyme, horseradish peroxidase (HRP), on phenol, o-chlorophenol, cresol and resorcinol. The study was continuated with o-chlorophenol, where they have shown that the reaction of 0.1 g/L of o-chlorophenol with 1 mM of H_2O_2 in presence of 1 Unit/ml of enzyme removed around 99.8% of the initial o-chlorophenol in about 3 h of treatment. The same efficiency was obtained with low concentrations, 0.1 mg/L.

Since this date, several works have confirmed that the oxidation of phenolic pollutants can be catalysed by a large number of enzymes from plants and microorganisms (Aitken 1993), including horseradish peroxidase (Dunford 1991), soybean peroxidase (Bódalo 2006), turnip peroxidase (Duarte 2002), coprinus cinereus peroxidase (Masuda 2001, Ikehata 2005), chloroperoxidase (Griffin 1991), laccases from several microbial sources (Ikehata 2002), lignin peroxidase from white-rot fungus (Tien 1987, Kirk 1987) and polyphenol oxidase (e.g. tyrosinase) from mushrooms (Ikehata 2002, Robb 1984).

3.2.2. The mechanism

Between the high number of different operative conditions the phenol polymerisation catalysed by HRP is widely the most utilised. The cycle for the HRP was deduced by Roman et al. (1972). In this work, iodide ion is perhaps the best used substrate. The proof is that the two-electron oxidation was obtained by six different methods (Dunford 1991).

$$HRP + H_2O_2 \Rightarrow E_i + H_2O \tag{3.1}$$

$$E_i + I^- \Rightarrow HRP + HOI \tag{3.2}$$

The mechanism of action of the peroxidases was studied in detail by Dunford (1976) and the catalytic cycle was described as following.

In a first step, the H_2O_2 oxidizes the HRP to an active intermediate form of the enzyme, E_i.

$$HRP + H_2O_2 \Rightarrow E_i + H_2O \tag{3.3}$$

Then, E_i reacts with a reducing substrate molecule, AH_2, to produce a free radical, $AH\bullet$, and the enzyme complex E_{ii}, which is a second active intermediate form of the HRP.

$$E_i + AH_2 \text{ (aq)} \Rightarrow E_{ii} + AH\bullet \tag{3.4}$$

Moreover, E_{ii} oxidizes a second substrate molecule producing another free radical and the native HRP.

$$E_{ii} + AH_2 \text{ (aq)} \Rightarrow HRP + AH\bullet \tag{3.5}$$

Finally, the produced free radicals can combine themselves to give bigger chain polymers, as a classical polymerisation.

$$2AH\bullet \Rightarrow A_2H_2\downarrow \tag{3.6}$$

Thus a single two-electron oxidation of the enzyme is followed by two single-electron reductions.

The free radicals produced in the catalytic cycle of the HRP and released into the solution produce polyphenolic products by their combination. These polymers are less soluble in water than phenol and precipitate (Vasudevan 1996, Huixian 1994).

The overall reaction for the enzyme-catalysed oxidation of phenol may therefore be represented as:

$$H_2O_2 + 2AH_2 \Rightarrow 2\ AH\bullet + 2H_2O \tag{3.7}$$

Two free radicals are generated for every molecule of peroxide consumed, since the free radicals polymerize spontaneously, the stoichiometic ratio of peroxide to phenol should be 0.5:1.0. As suggested by Nicell et al (1992), this fact assumes that the dimers are completely insoluble in water. However, the dimers which remain soluble can react again with the HRP to form more free radicals. These radicals can combine itselves to form larger polymers which then precipitate. In short, as long as the polymers remain soluble, the enzyme is able to catalyse the oxidation of phenol and its polymers.

If the precipitation does not occur, the larger polyphenolic compound can react another time with HRP (E_i) resulting in a chain polymerisation reaction while the polymers are still soluble in the media. Polymers which remain soluble can be oxidized again, resulting in the formation of longer chain polymers (A_3H_3, A_4H_4, etc) with further reduced solubilities (Dec 1990). The final polymers obtained are totally insoluble in water. This fact is interesting because the insolubility of the polymers should facilitate a posterior separation of the solids from the solution by sedimentation or filtration procedures. This mechanism has been used in several works (Nicell 1992, Yu 1994, Vasudevan 1996, Wu 1999).

As described above, one electron oxidation of phenols results in the formation of phenoxy radicals, which may diffuse from the enzyme active site and allow a variety of post-enzymatic reactions in aqueous solution (Griffin 1991, Dunford 1991). Products from such reactions include quinones resulting from the loss of another electron from the phenoxy radical (Minard et al. 1981, Hammel et al. 1988) and coupling products resulting from the reaction of two phenoxy radicals, leading to the formation of dimers and higher molecular weight oligomers (Danner et

al. 1973, Bollag et al. 1977, Minard et al. 1981, Schwartz et al. 1981, Sawahata et al. 1982, Maloney et at. 1986).

3.2.3. The kinetics

The kinetics of the HRP catalysed oxidation were investigated by Ryu et al. (1993), Nicell (1994), Vasudevan (1996) and Buchanan (1997) in batch stirred reactors. Traditionally, steady-state models have been used to describe the functions of the enzyme in its reaction environment. While such models may be used to evaluate kinetic parameters of enzyme systems, they do not adequately describe the reaction under non ideal and unsteady-state conditions where competing reactions interfere with the catalytic cycle of the enzyme.

To gain a better understanding of the HRP-hydrogen peroxide-aromatic compound system, a kinetic model was developed by Nicell (1994). This model was successful in predicting the HRP-catalyzed removal of 4-chlorophenol with respect to time in batch reactors. However, the mechanism incorporated multiple mechanisms of enzyme inactivation by lumping them in to a single parameter. The validity of this simplification hinged on the assumption that the extent of enzyme inactivation was directly proportional to the amount of substrate removed from solution and was therefore independent of the instantaneous concentrations of enzyme and substrate. While this assumption was valid for the treatment of 4-chlorophenol, it was noted that this behaviour was not necessarily exhibited for other substances, including Phenol (Buchanan 1997).

In the work of Buchanan et al. (1997), the model presented took into account these deficiencies by explicitly identifying the major mechanisms of enzyme inactivation, formulating reaction rate expressions for reversible and irreversible inactivation processes, incorporating these expressions in an overall kinetic model and calibrating and verifying the model using phenol as a substrate. Since, the pseudo steady-state model for the HRP-H_2O_2-aromatic compound system was significantly improved. The enzyme inactivation by free radicals was modelled as being proportional to the product of the free radical and active enzyme concentrations. The rate of enzyme inactivation due to end-product polymer was modelled as being proportional to the rate of polymer formation.

Nicell et al. (1997) have studied the effect of the hydrogen peroxide concentration using two different enzymes, soybean peroxidase (SBP) and horseradish peroxidase (HRP). They have found a steady-state kinetic model describing the dependence of peroxidase activity on hydrogen peroxide concentration. They have reported the inhibitory effect of the hydrogen peroxide concentration on the catalytic activity of the enzyme. The main drawback of this system is that HRP is inactivated during the enzymatic reaction, most likely by the interaction of the free radicals generated in the catalytic process with the enzyme's active centre.

As reported by Vasudevan et al. (1996), the enzymatic reaction involves two substrates, H_2O_2 and phenol, so, the relevant rate equation will include the concentration terms of the two substrates in a variety of functional forms depending on the reaction mechanism. The rate equation can be modified to include only one substrate as a variable while keeping the initial concentration of the other substrate constant. In this work, they have studied the kinetic behaviour of HRP at pH 8 and at room temperature. They have indicated that the reaction exhibited a normal Michaelis-Menten saturation kinetic. An irreversible reaction mechanism was proposed for the steady-state kinetics which was consistent with the experimental data. No inhibition was identified.

3.2.4. Influence of operating conditions: pH, temperature

The optimisation of the process variables is necessary to avoid the enzyme inactivation (Nicell 1992). This optimisation has the objective on extending the catalytic lifetime to improve the economical feasibility of the process, because the lifetime is one of the most important characteristics.

Some authors have presented works about the optimisation of the process variables. Nicell et al. (1992) studied the HRP catalysed polymerisation and precipitation of aromatic compounds from wastewater. In this study, the removal of phenol, 3-chlorophenol and 4-methylphenol, was clearly function of the value of the pH. The HRP established some activity between pH's 4 and 10 but, only a high efficiency between 6 to 9. In the same way, the optimum temperature was found to be below 35ºC.

Other authors demonstrated that 100% of phenol removal is achievable in a large range of pH (5-9) and temperature (0-60ºC) with an excess of Coprinus cinereus peroxidase (Masuda 2001). This statement is very interesting because the conditions of industrial effluents may vary over a wide range. Similar results were obtained by the same authors (Masuda 2001) with another enzyme, the Coprinus cinereus peroxidase, where the maximum removal efficiency was obtained at 0ºC and at pH=7.5, while the maximum relative activity was at a temperature between 40 and 50ºC and at pH of 9.0.

Finally, in a comparative study between HRP and soybean peroxidase, the maximal phenol elimination was reached at neutral pH and moreover, both enzymes are also able to work at basic medium, better, and at slightly acid medium (Bódalo 2006). No significant differences were found in the behaviour of the reaction with both enzymes in the range of temperature studied (25-40ºC).

An interesting way to increase the thermostability and the performances of the enzyme is by its modification. This can be done with acetic acid N-hydroxysuccinimide ester (Miland 1996), phtalic anhydride or glucosamine hydrochloride (Liu 2002). Liu et al. (2002) determined that the optimal pH for higher phenol removal was 9.0 for both native HRP and modified HRP. The

same results were presented by Miland et al (1996). Moreover, modified HRP were able to work at temperatures above of 60ºC, where native HRP was fastly inactivated. Finally, the efficiency of the phenol removal and the rates of the polymerisation reaction were higher with the modified enzymes.

On the other hand, there are not any studies addressing the effects of solution ionic conditions. Huang 2005 observed that the analyses of the product distributions between dissolved and precipitated forms revealed that ionic conditions significantly impact those distributions and therefore, the product precipitation increased significantly when salt concentration was augmented.

Finally, several methods for the suppression of the HRP inactivation have been reported. These techniques are lowering the substrate concentration to protect the enzymes from free radical attack, using additives such as polyethylene glycol (Wu 1993) or coagulants (Tatsumi 1994). Another possibility is the utilisation of crude enzyme that is less affected by the adsorption.

3.3. The enzyme: Horseradish peroxidase

The Horseradish peroxidase (HRP) (Donor:hydrogen-peroxide oxidoreductase) belongs to the ferroprotoporphyrin group of peroxidases and it is isolated from horseradish roots (*Amoracia rusticana*). The HRP is a single chain polypeptide containing four disulfide bridges. It is a glycoprotein in which the carbohydrate moiety of this enzyme constitutes about 18% of the molecular weight. The carbohydrate composition consists of galactose, arabinose, xylose, fucose, mannose, mannosamine, and galactosamine, depending upon the specific isoenzyme (Shannon, 1966). The structure of the horseradish peroxidase is shown in figure 3.3.
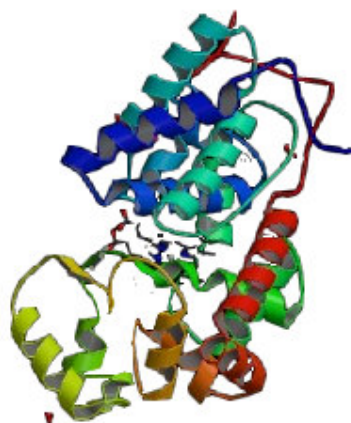
Figure 3.3. Structure of horseradish peroxidase (obtained from www.freeradicalscience.com).

HRP is a globular glycoprotein with a diameter of 50A. The enzyme consists of 308 amino acid residues, a hemin group and 8 neutral carbohydrate side chains attached through N-glycosyl linkages with asparagine. The molecular weight is around 44 kDa, this includes the polypeptide chain, 33890 Da, the hemin plus Ca^{2+}, approx. 700 Da, and the carbohydrate, 9400 Da

(Welinder 1978). The HRP has an extinction coefficient (EmM) of 100 when measured at 403 nm (Delincee 1975). Also, the powdered enzymes are soluble in water and should be refrigerated at 2-8ºC.

HRP readily combines with hydrogen peroxide (H_2O_2) and the resultant [HRP-H_2O_2] complex can oxidise a wide variety of chromogenic hydrogen donors. It can also utilise chemiluminescent substrates such as luminol and isoluminol and fluorogenic substrates such as tyramine, homovanilic acid, 4-hydroxyphenil acetic acid.

HRP is widely used as a label for immunoglobulins in many different immunochemistry applications including ELISA, immunoblotting and immunohistochemistry. HRP can be conjugated to antibodies by several different methods including glutaraldehyde, periodate oxidation, through disulfide bonds, and also via amino and thiol directed cross–linkers. HRP is the most desired label for antibodies since it is the smallest and most stable of the three most popular enzyme labels (HRP, alkaline phosphatase, and B–galactosidase) and its glycosylation leads to lower non–specific binding (Deshpande 1996).

Some compounds are inhibitors of the HRP such as sodium azide, cyanide, L-cystine, dichromate, ehtylenethiourea, hydroxylamine, sulfide, vanadate, p-aminobenzoic acid, Cd^{2+}, Co^{2+}, Cu^+, Fe^{3+}, Mn^{2+}, Ni^{2+}, Pb^{2+} (Zollner 1993).

3.4. Hydrogen peroxide

The hydrogen peroxide (H_2O_2) is a very pale blue liquid which appears colorless in a dilute solution, slightly more viscous than water. It is a weak acid, which has strong oxidising properties and is therefore a powerful bleaching agent that is mostly used for bleaching paper. The hydrogen peroxide is also used as a disinfectant, as an oxidiser, and in rocketry (particularly in high concentrations as high-test peroxide, HTP) as a monopropellant, and in bipropellant systems (Greenwood 1997).

About 50% of the world's production of hydrogen peroxide in 1994 was used for pulp- and paper-bleaching (Hage 2005). Although, other bleaching applications are becoming more important as the hydrogen peroxide is seen as an environmentally benign alternative to chlorine-based bleaches.

Other major industrial applications for the hydrogen peroxide include the manufacture of sodium percarbonate and sodium perborate, used as mild bleaches in laundry detergents. It is used in the production of certain organic peroxides such as dibenzoyl peroxide, used in polymerisations and other chemical processes. The hydrogen peroxide is also used in the production of epoxides such as propylene oxide (Jones 1999).

The hydrogen peroxide is one of the most powerful oxidizers known, stronger than chlorine, chlorine dioxide, and potassium permanganate, as it is shown in Table 3.1, where the oxidation potential of several oxidants are compared with the hydrogen peroxide. Also, when it is used

with a catalyst, the hydrogen peroxide is decomposed into hydroxyl radicals (OH·) with a reactivity that is second only to fluorine.

Table 3.1. Oxidation potential of oxidants.

Oxidant	Oxidation potential (V)
Fluorine	3.0
Hydroxyl radical	2.8
Ozone	2.1
Hydrogen peroxide	1.8
Potassium permanganate	1.7
Chlorine dioxide	1.5
Chlorine	1.4

The hydrogen peroxide can decompose itself spontaneously into water and oxygen. It usually acts as an oxidizing agent, but there are many reactions where it acts as a reducing agent, releasing oxygen as a by-product. For this reason, the hydrogen peroxide is incompatible with many substances that catalyse its decomposition, including most of the transition metals and their compounds, as manganese dioxide, and silver.

On the other hand, the same reaction can be catalysed by the enzyme catalase, commonly found in the liver of various animals, whose main function in the body is the removal of toxic byproducts of metabolism and the reduction of oxidative stress. The decomposition occurs more rapidly in alkali, so acid is often added as a stabilizer.

In the presence of certain catalysts, such as Fe^{2+} or Ti^{3+}, the decomposition may take a different path, with free radicals such as HO· (hydroxyl) and HOO· being formed. A combination of the hydrogen peroxide and Fe^{2+} is known as Fenton's reagent. Some physical properties of the main commercially available grades are recorded in table 3.2 (Strukul 1992).

Table 3.2. Physical properties of commercial hydrogen peroxide solutions.

Property	H_2O_2 strength (wt %)		
	35	50	70
Density at 20ºC (g cm^{-3})	1.1312	1.1953	1.2886
Viscosity at 20 ºC (mPa s)	1.11	1.17	1.23
Freezing point (ºC)	-33.0	-52.2	-40.3
Boiling point (ºC)	107.9	113.8	125.5

3.5. Enzyme Immobilisation

3.5.1. Introduction

The immobilisation of the enzyme can be defined as the fixation of the biocatalyst (e.g. enzymes, microorganisms, organelles) to insoluble carrier supports. The enzyme immobilisation into solid supports provides several advantages like the repeated use of the bio-catalyst due to the possibility to work with a confined bioreactor system. (Magnin 2003). In addition, the enzyme immobilisation allows an easy separation of enzyme from products, the possibility of continuous processes, the rapid stop of reactions, and the improvement of enzymes stability (Dumitriu 1994, Magnin 2003).

These advantages may be very interesting for many applications in biotechnology (Krajewska 1990, Spagna 2001), in biomedicine (Krajewska 1990), for analytical systems (Okuma 1992), for enzyme therapy (Karube 1987). Likewise, for the bio-treatment of industrial and agricultural wastes (Arica 2004, Bayramoglu 2004, Simsek 2007, Yildiz 2007) in order to improve enzymatic processes economically by the development of continuous bioprocesses (Knezevic 2006).

3.5.2. Immobilisation procedures

There are different methods for enzyme immobilisation, such as, covalent attachment, adsorption, entrapment, and crosslinking on various supports (Malcata 1990). To immobilise an enzyme to a surface, the most important is to choose a method of attachment that will prevent the loss of the enzyme activity avoiding the chemical nature or the reactive groups in the binding site of the enzyme. In other words, it is important to attach the enzyme but being careful of making it as few damage as possible. One of the solutions is to protect the active site during the attachment as long as the protective groups can be removed later. In some cases, this protective function can be fulfilled by a substrate or a competitive inhibitor of the enzyme.

The most important methods to immobilise enzymes are (Chibata 1978):
- Carrier-Binding: the binding of enzymes to water-insoluble carriers.
- Cross-Linking: intermolecular cross-linking of enzymes by bi-functional or multi-functional reagents.
- Entrapping: incorporating enzymes into the lattices of a semi-permeable gel or enclosing the enzymes in a semi-permeable polymer membrane.

The carrier-binding method is the oldest immobilisation technique for enzymes. In this method, the amount of enzyme bound to the carrier and the activity after immobilisation depend on the nature of the carrier. The figure 3.4 shows how the enzyme is bound to the carrier.
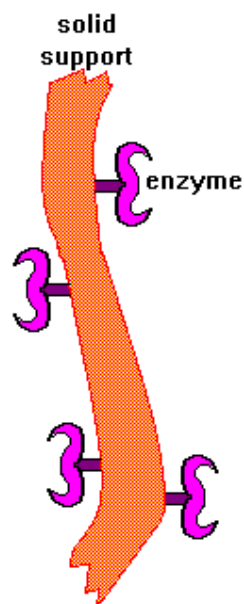
Figure 3.4. Enzyme bounding by carrier binding.

The selection of the carrier depends on the nature of the enzyme itself, as well as the:

- Particle size
- Surface area
- Molar ratio of hydrophilic to hydrophobic groups
- Chemical composition

In general, an increase in the ratio of hydrophilic groups and in the concentration of bound enzymes, results in a higher activity of the immobilised enzymes. Some of the most commonly used carriers for enzyme immobilisation are polysaccharide derivatives such as cellulose, dextran, agarose, and polyacrylamide gel.

According to the binding mode of the enzyme, the carrier-binding method can be further sub-classified into (Bungay 1989):

- Physical Adsorption
- Ionic Binding
- Covalent Binding

The most intensely studied of the immobilisation techniques is the formation of covalent bonds between the enzyme and the support matrix. The selection of the type of immobilisation procedure, the choice is limited by two characteristics: the binding reaction must be performed under conditions that do not cause a loss of the enzymatic activity, and the active site of the enzyme must be unaffected by the reagents used.

The covalent binding method is based on the binding of enzymes and water-insoluble carriers by covalent bonds (Bungay 1989). The functional groups that may take part in this binding are:

- Amino group
- Hydroxyl group
- Thiol group

- Carboxyl group
- Imidazole group
- Threonine group

- Sulfhydryl group
- Phenolic group
- Indole group

Moreover, the covalent binding can be further classified into diazo, peptide and alkylation methods, according to the mode of linkage of the enzyme. The conditions for immobilisation by covalent binding are much more complicated and less mild than in the cases of physical adsorption and ionic binding. Therefore, covalent binding may alter the conformational structure and the active centre of the enzyme, resulting in a major loss of the activity and/or, in changes of the substrate. However, the binding force between the enzyme and the carrier is so strong, that no leakage of the enzymes occurs, even in the presence of substrate or solution of high ionic strength.

Covalent binding to a support matrix must involve only functional groups of the enzyme that are not essential for catalytic action (Voet 1995). Higher activities result from prevention of inactivation reactions with amino acid residues of the active sites. A number of protective methods have been proposed:

- The covalent binding of the enzyme in the presence of a competitive inhibitor or substrate.

- The utilisation of a reversible, covalently linked enzyme-inhibitor complex.

- The use of a chemically modified soluble enzyme whose covalent linkage to the matrix is achieved by newly incorporated residues.

- The utilisation of a zymogen precursor.

The optimum immobilisation technique for a particular process is determined by a large number of considerations: technical, commercial and practical. However, the covalent immobilisation is the method that best follows the purpose of stabilising for a long term the immobilised enzyme. The formation of a covalent bond between the biocatalyst and a support matrix creates a stable conjugate which is unlikely to be dissociated during normal use, and moreover, hence the problem of enzyme leaching out, often encountered in other immobilisation methods (adsorption). There has been a proliferation of covalent binding techniques each seeking to provide a simple, efficient and environmentally safe method of immobilisation.

Covalent immobilisation has been worked out with different kinds of supporting matrices (mostly polysaccharides and other organic polymers) following different activation and coupling procedure.

3.5.3. Most common substrates used for immobilising by covalent binding

In the last decades, substantial attention has been devoted to the covalent immobilisation of enzymes to porous, insoluble supports such as glass (Wehtje 1992), alumina (Hyndmann 1992), silica (Hyndmann 1992), and chitosan (Chellapandian 1998, Itoyama 1994, Miao 2001).

This is due to the fact that they possess a high catalytic activity per unit volume of the catalyst and minimum diffusion limitations and facilitate the diffusion of large substrate molecules into the porous structure of the matrix within which enzymes are bound.

Between them, chitosan has gained importance as an immobilisation matrix in recent years because of its low cost and robust nature. There have been reports on the immobilisation of several enzymes such as urease (Chellapandian 1998), lipase (Itoyama 1994), β-galactosidase (Shin 1998), cellobiase (Abdel-Fattah 1997), tyrosinase (Carvalho 2000), invertase (Gonzalez Siso 1997), β-amylase (Noda 2001), alcohol dehydrogenase (Cochranea 1996), α-L-rhamnopyranosidase (Spagna 2001), protease (Benkhelifa 2005) and horseradish peroxidase (HRP) (Miao 2001) on chitosan.

3.5.4. Our case of study: HRP on Eupergit C

Eupergit C is a very desirable support for industrial scale enzyme immobilisation because it is commercially available worldwide, resistant to mechanical and chemical stresses and adaptable to a variety of configurations and specific processes carried out in reactors (Katchalski-Katzir 2000).

This support has been successfully used for the immobilisation of lipase by several authors and the protocol of preparation was found to allow a better stability than the ones used with other supports (Ivanov 1997, Wirz 1993, Knezevic 2006). In the work of Knezevic et al. (2006), they have studied and compared the results of three different covalent immobilisation methods employed for the immobilisation of lipase from *Candida rugosa* on Eupergit® C supports. The method yielding the highest activity retention of 43.3% was based on coupling lipase via its carbohydrate moiety, previously modified by periodate oxidation. The study of the thermal deactivation kinetics at three temperatures (37, 50 and 75 ºC) revealed that the immobilisation method also produces an appreciable stabilization of the biocatalyst, changing its thermal deactivation profile. They have concluded that the lipase immobilised via carbohydrate moiety was almost 18-fold more stable than the free enzyme and 2-fold than conventionally immobilised lipase. The immobilisation procedure developed was quite simple, easily reproducible, and provided a promising solution for its application with lipase in aqueous and microaqueous reaction system.

Moreover, good results were also obtained in a number of previous studies for immobilisation of other hydrolases such α– and β– galactosidase (Hernaiz 2000, Krizanic 1993), pepsin, trypsin (Katchalski-Katzir 2000), penicillin Gacylase (Rocchietti 2002).

Since 1972, some techniques for protein-protein conjugation have been developed. The most widely used method for this purpose involves the coupling of two compounds by reaction with glutaraldehyde to give a mixture of conjugates of similar and dissimilar components. To avoid

formation of conjugates of similar components, two components with different reactive groups are used for the coupling reaction.

Some researchers have shown that the carbohydrate content of some glycoproteins is not essential to the catalytic properties of the enzyme. Conjugation through these residues is a viable alternative to the modification of amino acid side chains. Several reports from literature utilised hydrazone formation to prepare the conjugates of the proteins with various ligands. The glycoproteins can be chemically or enzymatically oxidized to generate aldehyde groups and then, they can be coupled to low molecular weight ligands containing various types of amino groups, making possible to keep almost the same catalytic activity.

In general, functional aldehyde groups can be introduced in a glycoprotein by oxidizing the carbohydrate moiety by periodate treatment without significantly affecting the enzyme activity. This observation permits conjugation of this enzyme through the carbohydrate moieties.

Enzymes are usually immobilised on Eupergit through their different groups (amino, sulfhydryl, hydroxyl, phenolic) that could be essential for their catalytic action. Hence, it has been often difficult to achieve stable binding of high levels of activity because the active site may be blocked from substrate accessibility, multiple point-binding may occur, or the enzyme may be denatured.

The HRP has acquired considerable interest in the field of organic synthesis in recent years (Adam 1998) because the enzyme catalyzes commercially important reactions such as phenol (Oguchi 1999, Kim 1998), aniline polymerizations (Lim 2000, Bruno 2000), and the synthesis of specialty chemicals, including 3,4 dihydroxyphenylalanine (DOPA) (Klibanov 1981) and bisphenol (Schwartz 1981). The majority of the work on the HRP immobilisation has focused on the use of immobilised enzyme preparations as biosensors (Ortiz 1997, Xu 1998, Vianello 2000).

Epoxy-activated beads are bead polymers formed from a hydrophilic acrylamide with allyl glycidyl (epoxide) groups as the active components responsible for binding. These groups are convenient for the covalent binding of enzymes. The O-C and N-C bonds formed by the epoxide groups are extremely stable, so that the epoxide-containing polymers can be used for the immobilisation of enzymes and proteins (Kramer 1975).

Eupergit C is a copolymer of methacrylamide, N,N'-methylen-bis(acrylamide) and a monomer carrying oxirane groups (epoxy-activated acrylic beads). The matrixes are hydrophilic acrylic beads with approx. 800 µmol per g. The matrix spacers are 3 atoms (when ligands are coupled through the free oxirane groups). The beads have a particle size of approx. 150 µm (macroporous particles).

This support is very stable and has good chemical and mechanical properties (simple immobilisation procedure, high binding capacity, low water uptake, high flow rate in column procedures, excellent performance in stirred bath reactors, etc.) (Kramer 1975; Kramer 1978).

Although Eupergit® is known to be a good support for enzyme immobilisation, its potential for horseradish peroxidase immobilisation has not been explored. Regarding the literature, there does not seem to be prior strategy for the preparation of the HRP linked to Eupergit-NH$_2$ by covalent bonds. Therefore, the specific objectives of this part of the study were to immobilise the HRP on Eupergit C and to study the kinetics of the immobilised enzyme. A different method for the immobilisation of the HRP on Eupergit C is presented. This method of immobilisation eliminates the disadvantages associated with the use of the glutaraldehyde method (Sakuragawa 1998), which requires extensive washing procedures to remove the excess reagent.

3.6. The torus reactor

The torus reactor is a reactor that is characterised to have a toroidal or doughnut-shaped chamber, and for this reason, it can be considered as a loop reactor. A photo of the torus reactor used in this work as experimental reactor can be seen in the figure 3.5.
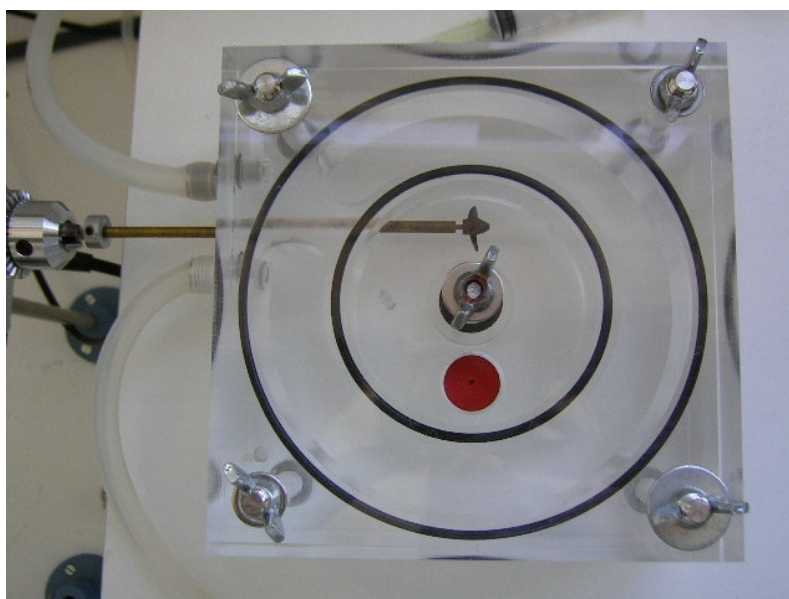
Figure 3.5. Photo of the 100 mL torus reactor.

This reactor presents some advantages over other stirred tank reactors including an efficient mixing of the reactants, an easy scale-up and design ensured by the absence of dead volume, low power consumption (Nouri 1997), a high heat transfer capacity (Sato 1979), a prevention of deposition of the polymer or biomaterial on the reactor wall and finally, a high efficiency (Nouri 1997, Legrand 1997, Benkhelifa 2005). The relative confinement of the reagents and the products as a result of the doughnut-shaped chamber reduces the attenuation of the shockwaves, which reduces the dissipation of the energy imparted by the shockwaves.

Tests have shown that the pressure waves, imparted by the pulsar to the solution in the chamber, propagate in a more confined fashion in a reactor with a torus-shape chamber than in reactors with other chamber configurations. In addition, Belleville et al. (1992) have shown that the torus reactor in batch conditions presents an efficient radial mixing inducing little dead volumes and allowing an easier scale-up of the results.

Other studies have shown the interest of the torus reactor for applications in processes using viscous fluids and in two-phase systems. Hosogai and Tanaka (1992) used a circular loop reactor for the polymerisation in suspension of styrene where, they have shown that the reactor is more efficient for the production of uniform size particles than the conventional stirred reactor.

Though, the torus reactor has been tested by Laederach and Widmer (1984) in batch conditions for the growth of a fermentating culture. With this reactor, the biomass production was around 40% higher than that obtained using a stirred reactor.

On the other hand, Adler and Fiechter (1986), have assessed different types of bioreactors with the help of a microbiologic growth test system. They have shown the interest of the torus reactor with regard to the stirred one for systems subjected to a foam formation. They also showed that, for this application, the extrapolation of the results obtained with a stirred reactor is not possible, but it is for the torus reactor.

Moreover, in 1997 Nouri et al. have studied the enzymatic application of the torus reactor in the hydrolysis of wheat proteins, in this work, the authors made the performance comparison with a stirred reactor in terms of the volumetric power criterion and the hydrolysis degree. For a limited hydrolysis of the wheat proteins, the difference in the reactors performance was not significant, but the process, was perturbated in the stirred reactor by the formation of high amounts of foam that was not detected in the torus reactor.

In addition, the pea acetylation has been investigated in a torus minireactor by Legrand et al. (1997). The minireactor was particularly suited to this biochemical reaction because the acetylation degree obtained was higher in the torus minireactor than in a stirred reactor.

Also, Benkhelifa et al. (2005) studied the hydrolysis of the casein by immobilised enzymes in a batch torus reactor. In this work, chitosan beads of 1–3mm diameter were a suitable support for the enzyme immobilisation by covalent binding. Satisfactory mechanical, chemical and thermal resistances was shown, however, crosslinked beads were more prone to erosion and fragmentation by contact with the propeller blades. Covalent immobilisation by glutaraldehyde allowed binding of protease XIX from *A. sojae*.

On the other hand, the kinetic parameters for free and immobilised enzyme were in the same order of magnitude denoting the same specificity for the substrate but, the activity of the immobilised protease was only 1/20 that of the free enzyme and the maximum apparent reaction rate was lower. Nevertheless, a high degree of hydrolysis was obtained for the casein and the reuse of the immobilised enzyme showed the potential interest of the immobilised enzyme torus reactors for bioprocesses. This work showed promising results in the use of the

torus reactor in bioprocesses involving immobilised enzymes as it was certified by other authors.

For this reason, this study is the starting point of the use of the torus bioreactor in biodegradation processes of wastewater and particularly in the case of the phenol. This reactor may be applied in different industrial sectors as for example, in wastewater from olive oil (Aggelis 2003), wine (Borja 1993), meat and fishing (Artiga 2005) too.

Chapter 4. Methodology

This chapter describes in detail the materials, experimental set-ups and analytical techniques used for the study of the enzymatic elimination of phenol, as well for the determination of the kinetic model and the analysis of the influence of the initial conditions.

4.1. Torus reactor set-up

The enzymatic elimination of phenol was carried out in a thermostatised torus reactor of 100 ml built in Poly(methyl-methacrylate) (PMMA). The scheme of the torus reactor is presented in figure 4.1.
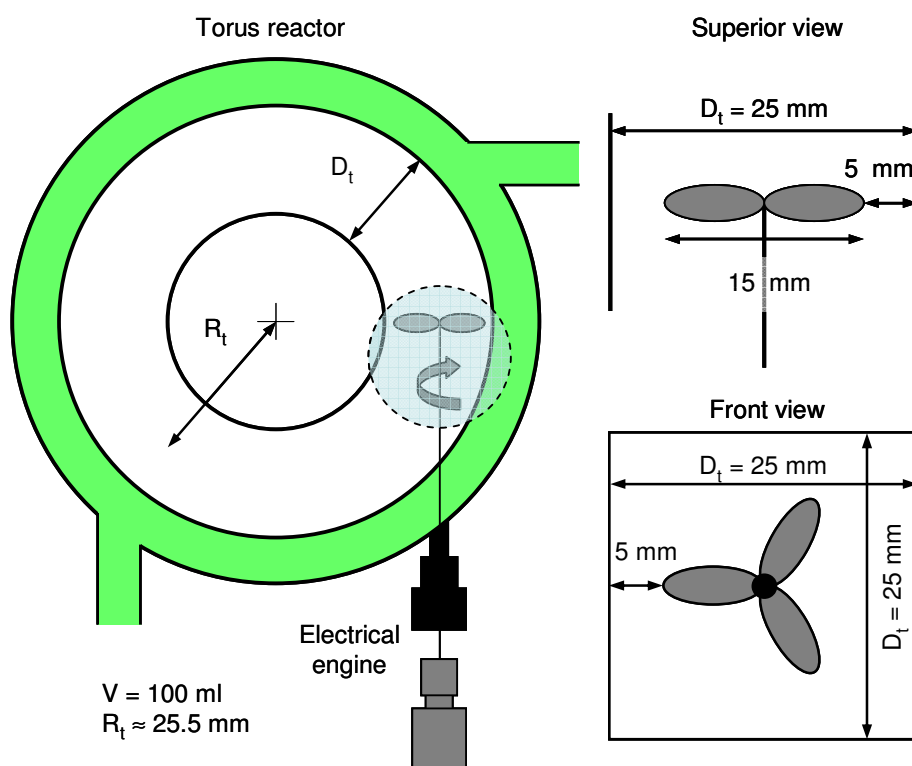
Figure 4.1. Schematic representation of the torus reactor.

The reactor has an annular square section with a gap width of D = 25 mm. The geometric characteristics of the torus reactor are given in table 4.1 where R_t is the mean bend curvature and L_t is the loop length taken in the middle of the channel. The agitation into the reactor is done by a three blades marine impeller with a blade pitch angle of 45º and an external diameter of 15 mm. An electrical engine of variable speed controlled by a tachometer (Heidolph model RZR 2021) was used to manage the rotation of the impeller. An impeller rotation speed of 1500 rpm was used in all experiments.

Table 4.1. Geometric characteristics of the torus reactor.

V_R (ml)	R_t (mm)	L_t (mm)
100.0	25.5	160.0

In a second step, the enzymatic reaction was studied in a stirred glass reactor of 100 ml. In this case, the agitation into the reactor is done by a bar of magnetic agitation.

4.2. Materials

The enzyme horseradish peroxidase (HRP) from Sigma-Aldrich (ref. P8250) with a specific activity of 181 U/mg (according to pyrogallol method performed by the supplier) was used in all the experiments. Aqueous stock solutions of peroxidase were prepared weighing a quantity of 85 mg of enzyme and adding 100 ml of distillated water. The stock solution was separated in several aliquotes of 10 ml and stored at -4ºC.

Aqueous solution of hydrogen peroxide (30% w/v, specific gravity 1.1) was purchased from Panreac (ref. 121076.1211). Phenol crystallized was purchased from Panreac (ref. 144852.1211). A stock solution was prepared weighting 500 mg of phenol and adding distillated water to reach the final volume of 1000 ml. The acetonitrile solution was supplied by Fluka (ref. 00687). The products of the polymerisation as 4,4'-Biphenol (ref. 168734), 4-Phenoxyphenol (ref. 23066-9) and 2,2'-diphenol (ref. 11581-9) were obtained from Sigma-Aldrich.

Hydrogenophosphate of disodium dihydrated (ref. 71644) was purchased from Fluka, sodium chloride (ref. S7653), sodium hydroxide (ref. 5881), chlorhydric acid (ref. 31.894-9) and acetic acid (ref. 10900-8) were purchased from Sigma-Aldrich.

Sodium phosphate dibasic (ref. S0876), sodium phosphate monobasic (ref. S9638), Adipic dihydrazide (ref. A0638), 4-aminoantipyrine (ref. 06800), sodium periodate (ref. 311448), ethylene glycol (ref. 102466) and Eupergit C (ref. 46115) were purchased from Sigma-Aldrich.

More specific details are given in each chapter.

4.3. General procedure

Different initial concentrations of phenol (0.5 to 1.6 mM) and H_2O_2 (0 to 2.65 mM) were used, while HRP was kept to $2 \cdot 10^{-4}$ mM. The phenol solutions were prepared adding deionised water to the appropriated quantity of crystallized phenol to achieve a concentration in phenol of 500 ppm (5.3 mM). This stock solution was then used to achieve the wanted concentration of phenol into the reactor by dilution in deionised water.

The stock solution of hydrogen peroxide was prepared diluting 285 µl of the concentrated solution by the addition of deionised water to reach the final volume of 25 ml. This solution has a concentration of 100 mM. The different H_2O_2 concentrations were obtained by dilution with deionised water in order to achieve the respective concentration inside the reactor.

Both, the phenol and HRP dissolution were kept into the reactor to reach the operating temperature (T=20ºC) before adding the corresponding amount of hydrogen peroxide. The reaction time started when hydrogen peroxide was introduced into the reactor. In a typical experiment, the reaction was initiated by the addition of hydrogen peroxide and terminated by the addition of concentrated acetonitrile solution (a ratio of 1 with the sample) to the sample. The acetonitrile solution decreases the pH, and thus, inhibits the action of the enzyme. All experiments were carried out in batch conditions.

In all experiments, several liquid samples (1 ml) were withdrawn at different times of reaction for the analytical procedure. Then the samples were centrifuged and analysed by HPLC.

The buffer solutions were prepared using the Henderson-Hasselbalch equation which allows the relationship between pH and composition of the mixture. The equation is defined as:

$$pH = pK_a + log_{10}\left(\frac{[basic\ specie]}{[acid\ specie]}\right) \qquad (4.1)$$

The measurements of the pH were performed with a pHmeter Crison series, model GL-21.

These conditions were the general ones used for all the experiments carried out. In the following sections, the operating conditions will be specified for each specific case when it will be necessary.

4.4. Analytical procedures

The phenol concentration of the liquid samples was analysed and quantified by HPLC (High Performance Liquid Chromatography, Agilent Technologies 1100 Series) using a C18 reverse phase column (Hypersil ODS, 5 µm, 25 x 0.4 cm).

To properly separate phenol from the partial oxidation or polymerisation products, the mobile phase was a 40/60 vol. mixture of methanol and deionised water, acidified pH 1.41, at a flow rate of 1 ml/min. The detection of the phenol was performed with an UV with diode array detector (DAD) at a wavelength of 270 nm. The phenol concentration is determined using a calibration curve that was obtained using patterns with different phenol concentration. A typical chromatogram for phenol is presented in figure 4.2.
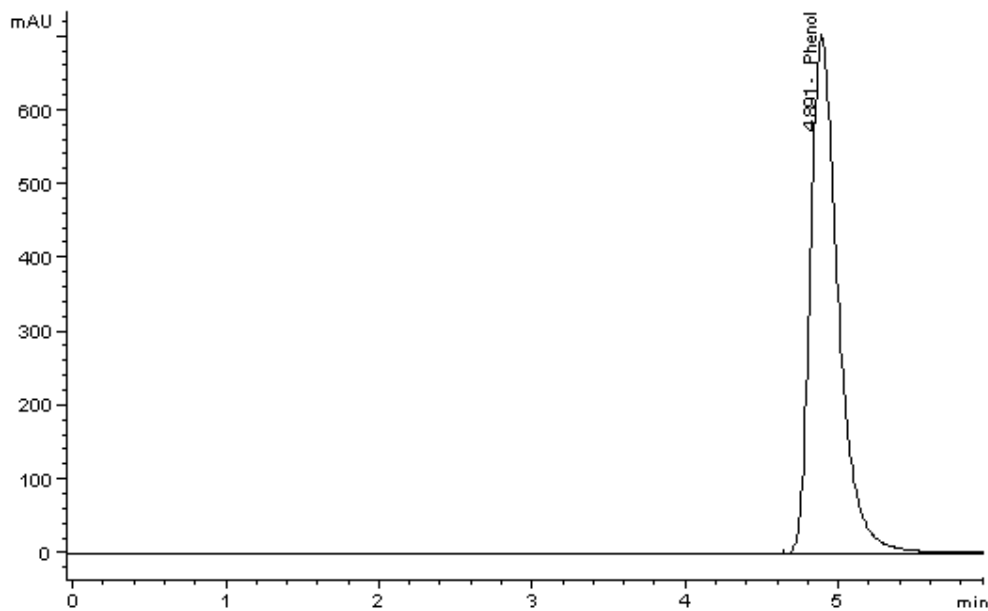
Figure 4.2. Typical HPLC chromatogram for phenol.

The conversion of phenol X_{Ph} was defined as (eq. 4.2):

$$X_{Ph}(\%) = \frac{C_{Ph_0} - C_{Ph}(t)}{C_{Ph_0}} x100 \qquad (4.2)$$

where C_{Ph_0} was the initial phenol concentration and $C_{Ph}(t)$ the phenol concentration at a given time.

The formation of some reaction products during the reaction of polymerisation was also determined by HPLC (Hypersil ODS, Agilent Technologies) with ultraviolet (270 nm) absorbance detection. The new chromatographic method was adapted from the method to determine the phenol. Standard samples were subjected to analysis by HPLC to determine retention times for products as 4,4'-Biphenol, 4-Phenoxyphenol and 2,2'-diphenol. Water and methanol were used as mobile phase. The gradient starts from 60:40 v/v of water:methanol and goes to 50:50 v/v at minute 16 and finally to 45:55 at minute 20. The gradient remains isocratic until the end of the analysis with a total time of analysis of 30 minutes using a flow rate of 1ml/min.

4.5. The activity assay of the HRP

The purpose of the enzyme activity assay was to determine the amount of the active enzyme that was present in a solution. Under saturating conditions of the phenol, the AAP (4-aminoantipiryne) and the H_2O_2, the initial rate was measured to observe the rate of colour formation in a solution. The reaction between the phenol and the H_2O_2 was catalysed by the

enzyme, for making the products of the reaction to react with the AAP and formed a red coloured solution which absorbed light at a wavelength of 510 nm.

The HRP activity test was measured using the peroxidase assay that used phenol, 4-AAP and H_2O_2. This method provided all reagents in excess except for the enzyme in order to ensure that the initial rate of the reaction was directly proportional to the amount of the HRP enzyme present.

This test determined the activity of an enzyme by monitoring the appearance of colour in the sample. The rate was measured by calculating the change in the absorbance over time (the slope of the linear change of absorbance). This slope was used to calculate the activity of the enzyme by taking into account the dilution of the sample and the extinction coefficient of the product. One activity unit was defined as the amount of enzyme that converted 1 µmol of hydrogen peroxide per minute at pH 7.4 and 25ºC. The enzyme activity was expressed in $U \cdot ml^{-1}$.

The assay mixture consisted of 95 µl of 100 mM phenol in 0.5M sodium phosphate buffer pH 7.4, 0.48 mg of 4-AAP, 1.9 µl of 100 mM H_2O_2, 50 µl of the enzyme sample and water until reaching a final volume of 1 ml. Immediately after the addition of the enzyme, the cuvette was shaken and the change of absorbance within time was monitored at a peak wavelength of 510 nm.

A DINKO UV-VIS spectrophotometer, model 8500, in combination with a personal computer equipped with uv/vis software was employed for measuring the enzyme activity and concentration.

The enzyme activity was calculated by the following steps:

1) Calculate the average slope over the linear range of the data in terms of absorbance units per unit of time (A_{510}/s).

2) Convert the rate into A_{510}/s to A_{510}/min.

3) Calculate the change in concentration using $A = \varepsilon \cdot c \cdot l$

$$\Delta c = \frac{\Delta A}{\varepsilon \cdot l}$$

(4.3)

where $\varepsilon = 6.0 \ mM^{-1} \cdot cm^{-1}$ and $l = 1.0$ cm

4) Calculate the enzyme activity in the cuvette

The above formula produce an answer that is in $mM \cdot min^{-1}$. Since the reaction occurs in 1.0 ml total volume, $mM \cdot min^{-1} \cdot ml = \mu mol \cdot min^{-1}$. Consequently, $1 \ \mu mol \cdot min^{-1} = 1$ U.

5) Calculate the activity of the sample.

Calculate the dilution factor through the dilution of the enzyme sample (determine by the fraction from the main preparation) and also by the dilution achieved by pipetting 50 µl of

sample into 1 ml of the total volume. The activity of the sample was calculated by multiplying the activity in the cuvette by the dilution factors.

This activity test was used in all the activity measurements in the different studied methods. The enzymatic activity of the native enzyme solution was also determined using this test. A HRP stock solution was prepared in order to have a 150 $U \cdot ml^{-1}$ in 0.1 M of sodium phosphate buffer pH 7.4.

The typical response of the enzyme activity determination is shown in figure 4.3. As it can be seen in the figure, the absorbance presents a linear relationship within time. In this way, the slope obtained from the points shown in the figure, permitted the determination of the activity. In this case, the enzymatic activity of the native enzyme solution was 166±3 $U \cdot ml^{-1}$.
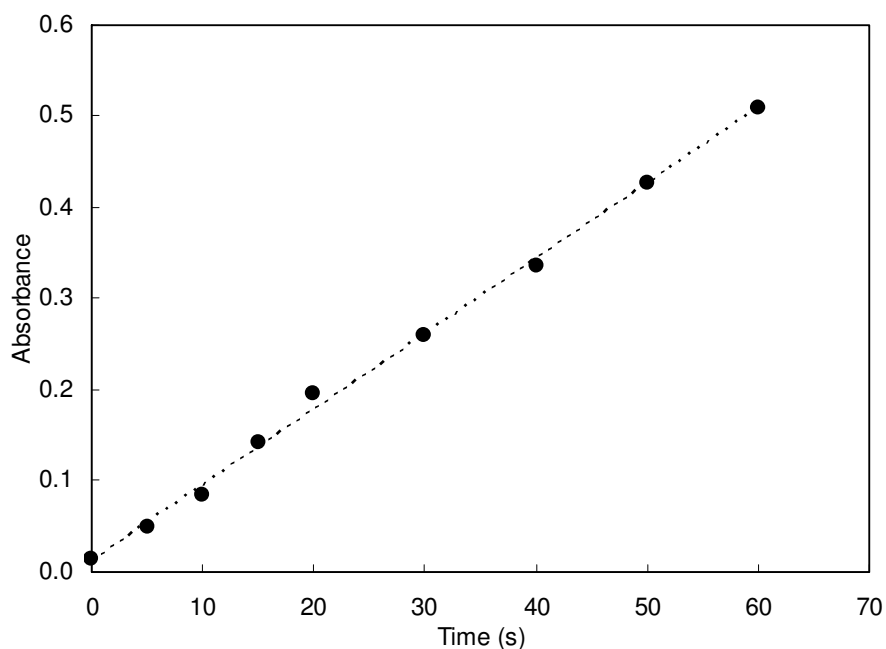
Figure 4.3. Determination of the activity of the native enzyme solution. R^2: 0.99.

Chapter 5. Results of the enzymatic elimination of phenol in the torus reactor

The enzymatic elimination of phenol was used as a model reaction to evaluate the performance of the torus reactor at different operating conditions and to compare then to a batch stirred reactor. The operating parameters studied in the enzymatic process were the hydrogen peroxide initial concentration, the phenol initial concentration and the horseradish peroxidase initial concentration.

5.1. Enzyme activity in the torus reactor

The effect of the initial HRP concentration on the removal of phenol was analysed. Different initial HRP concentrations were tested ranged between 0.08 and 1 U/ml. As it can be seen in the figure 5.1, the removal of phenol increased with an increase in the HRP concentration. This figure shows the phenol removal efficiency vs time at different initial concentrations of HRP.
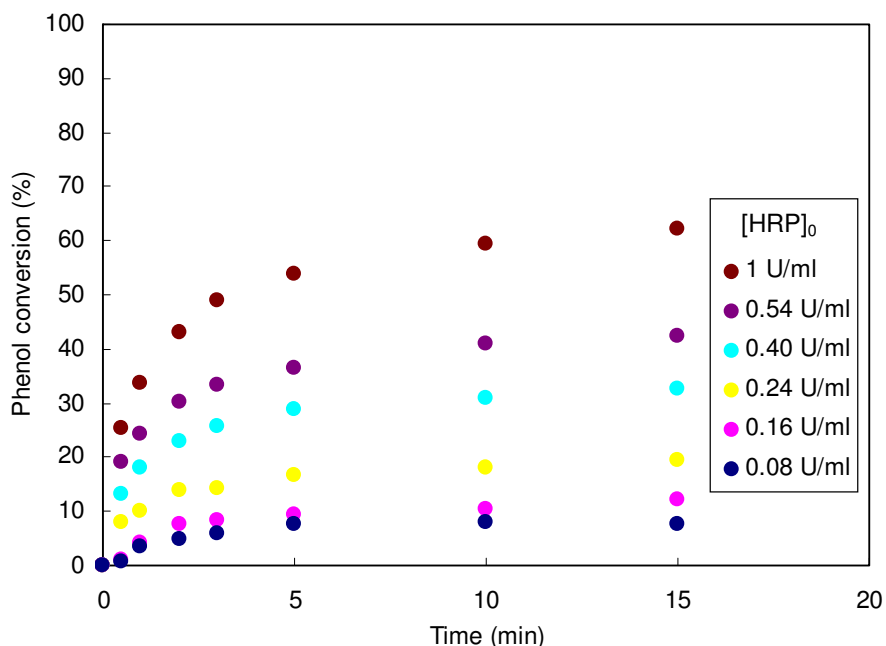
Figure 5.1.   Influence of the HRP initial concentration on the phenol conversion in the torus reactor. [Phenol]$_0$: 1.1 mM, [H$_2$O$_2$]$_0$: 0.882 mM, pH 7 and temperature of 20ºC.

In this case, for an initial concentration of phenol of 1.1 mM and an H$_2$O$_2$ initial concentration of 0.882 mM, only 8% of phenol conversion is obtained for an HRP initial concentration of $2 \cdot 10^{-5}$ mM (0.08 U/ml) whereas the phenol removal increased to approximately 62% with a concentration of $2 \cdot 10^{-4}$ mM (1 U/ml). The low conversion of phenol at low concentrations of HRP can be attributed to the inactivation of the enzyme, may be as result of the interaction of the phenoxy radicals with the enzyme's active centre and also because of the inhibition by H$_2$O$_2$. This increase in conversion of phenol with an augment of HRP concentration indicated that the

conversion of phenol to polyphenolic compounds is through the formation of free radicals as it was described in section 3.2.2.

The free HRP activity was observed from the data obtained for the removal of phenol at different HRP initial concentrations. The enzyme activity was determined calculating the slope of the apparent reaction rate versus the enzyme concentration. The initial reaction rates (V_i) were determined from the plot of the consumption of phenol as a function of time. The experimental data were fitted to a logarithmic curve and the reaction rate was determined calculating the value of derivative of the slope of the curve for a time of 0.5 min. The figure 5.2 presents the values of the apparent reaction rate for 1.1 mM of phenol and 0.882 mM of H_2O_2 initial concentrations. The calculated slope gave an activity of the free enzyme of 204±17 U/mg (µmol/min·mg enzyme). This value of the activity was very close to that one obtained from the supplier (181 U/mg).
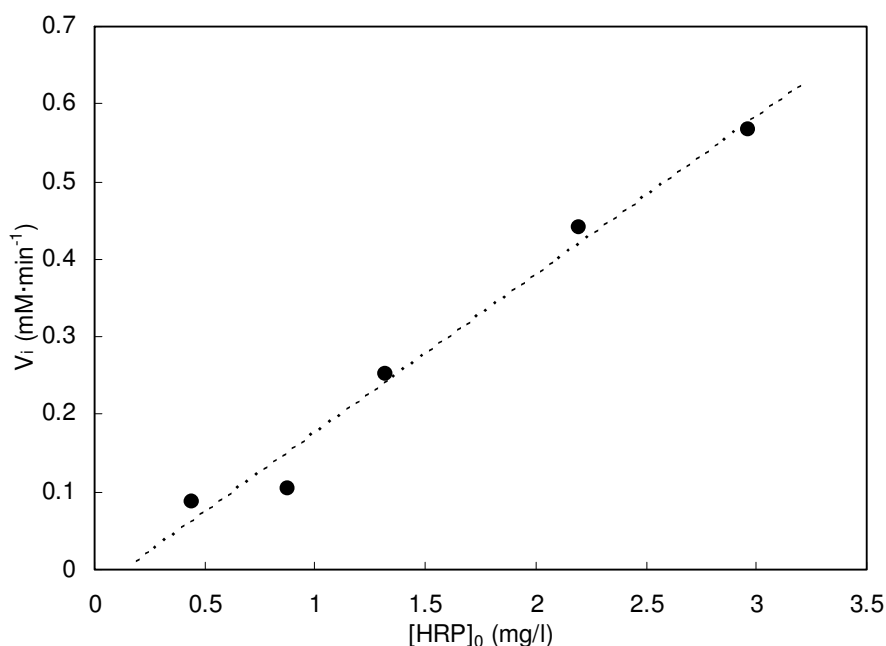
Figure 5.2.   Determination of the activity of the HRP in the torus reactor. [Phenol]$_0$: 1.1 mM, [H_2O_2]$_0$: 0.882 mM, pH 7 and temperature of 20ºC. R^2: 0.9.

5.2. Influence of the hydrogen peroxide initial concentration

The experiments to study the influence of the H_2O_2 initial concentration were carried out in batch conditions. The concentration of HRP was kept in $2·10^{-4}$ mM in all cases. The removal of the phenol was studied for different concentrations of H_2O_2 varying from 0.022 to 2.65 mM while three different phenol initial concentrations of 0.5 mM, 1.1 mM and 1.6 mM were used. A blank was made without H_2O_2 and, after several hours of reaction, the phenol concentration did not suffer any variation. In all the experiments, the solution turned dark brown immediately after the

addition of the H_2O_2. The colour of the solution depended of the concentrations of phenol and H_2O_2 used. More dark solutions were obtained with higher initial concentrations of H_2O_2 but, when an excess of H_2O_2 was added, lighter coloured solution was obtained. This fact is due to the amount of products formed increased with the amount of H_2O_2 and, therefore, the inactivation of the enzyme provokes lower levels of conversion and therefore a lower coloration of the solution. In some experiments with a high concentration of H_2O_2, it was possible to see directly into the reactor the formation of small particles of insoluble products that indicated the presence of polyphenols with more than two rings. The results of the phenol removal for the three initial phenol concentrations are illustrated in the figures 5.3, 5.4 and 5.5 respectively.
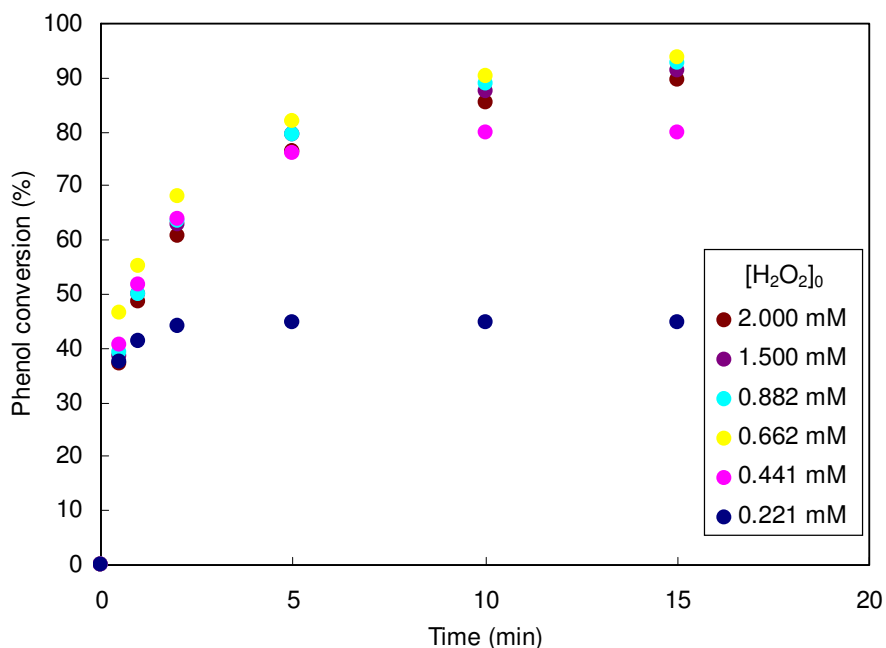
Figure 5.3.   Influence of the H_2O_2 initial concentration on the phenol conversion in the torus reactor. $[Phenol]_0$: 0.5 mM, $[HRP]_0$: $2 \cdot 10^{-4}$ mM, pH 7 and temperature of 20ºC.

As it can be seen in these figures, in all experiments, the phenol conversion reached a maximum value after few minutes for each H_2O_2 initial concentration and then, remained more or less unchanged after 10 minutes in all cases. The variances in the data are due to the experimental error fixed at 5% produced by the analytical method. An augment of the initial H_2O_2 concentration provokes an increase of the conversion of phenol until a maximum value of conversion is reached. After this point, if the H_2O_2 initial concentration is increased more, the phenol conversion began to decrease and the reaction has a slower initial reaction rate.

Around 97% of maximum phenol conversion is attained for an initial phenol concentration of 0.5 mM. In this case, when the initial H_2O_2 concentration is increased from 0 to 0.662 mM the phenol conversion increases until the optimum condition of H_2O_2 is reached (0.662 mM in this case).
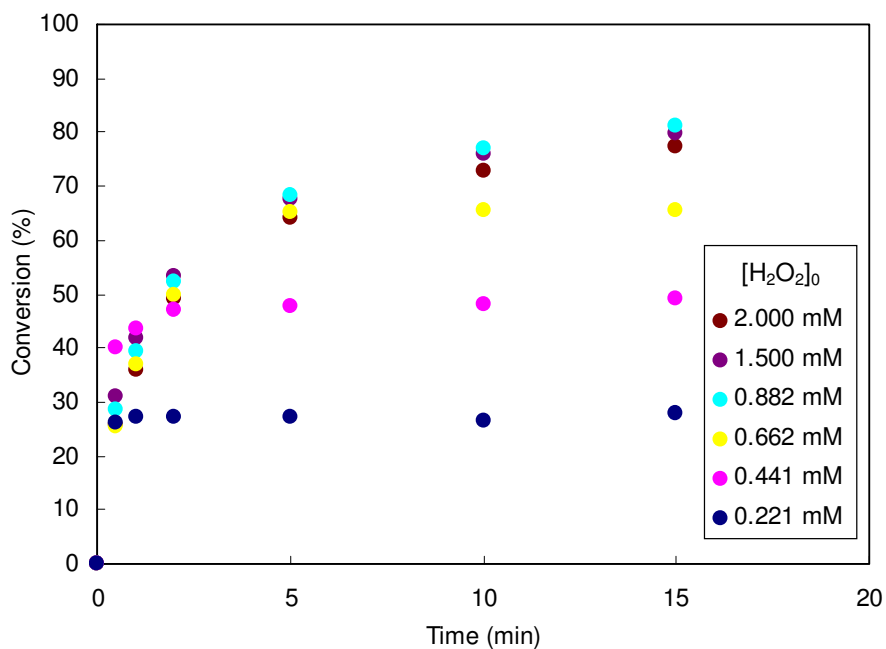
Figure 5.4.   Influence of the H_2O_2 initial concentration on the phenol conversion in the torus reactor. $[Phenol]_0$: 1.1 mM, $[HRP]_0$: $2 \cdot 10^{-4}$ mM, pH 7 and temperature of 20ºC.
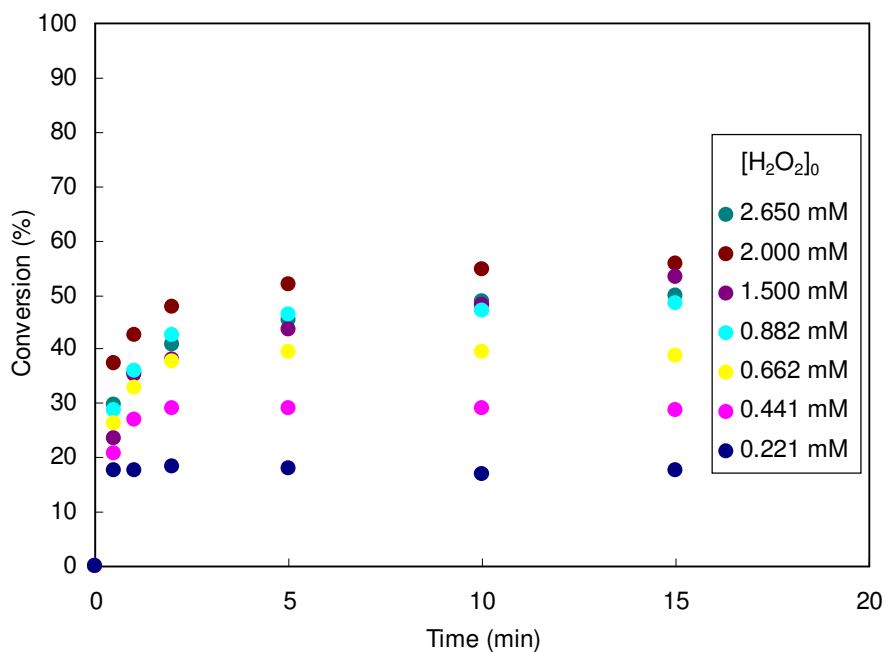
Figure 5.5.   Influence of the H_2O_2 initial concentration on the phenol conversion in the torus reactor. $[Phenol]_0$: 1.6 mM, $[HRP]_0$: $2 \cdot 10^{-4}$ mM, pH 7 and temperature of 20ºC.

Then, with a further augment of the H_2O_2 concentration, the phenol conversion began to decrease slightly. The same behaviour was observed for different initial concentrations of phenol. Around 85% of phenol conversion was obtained for 1.0 mM of phenol initial concentration for a value of H_2O_2 initial concentration of 0.882 mM and 56% of removal for 1.6

mM initial concentration of phenol for the optimum H_2O_2 initial concentration of 2 mM in this case. This behaviour can be seen in figure 5.6.
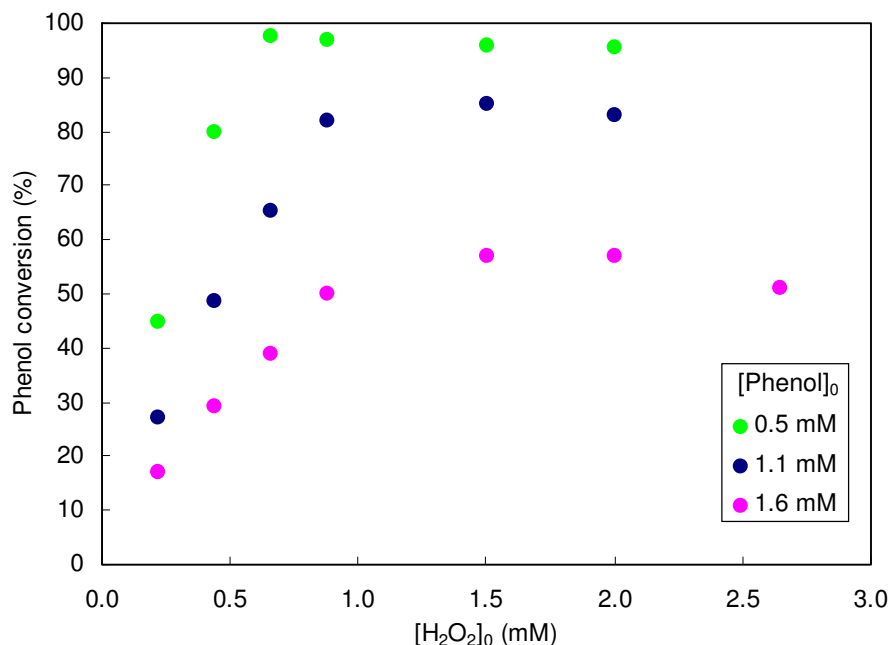
Figure 5.6.   Influence of the H_2O_2 initial concentration on the maximum phenol conversion attained in the torus reactor. $[HRP]_0$: $2 \cdot 10^{-4}$ mM, $[H_2O_2]_0$ from 0.221 to 2.65 mM, pH 7 and temperature of 20ºC.

Therefore, the optimal H_2O_2 concentration was evaluated as the concentration where the maximum conversion of phenol is reached. The optimal H_2O_2 concentration was found to be a molar relationship of 1:1 between H_2O_2 and phenol. This stoichiometry between peroxide and phenol is in agreement with the results reported by Vasudevan (1996), Nicell et al. (1992) and Buchanan et al. (1997). When the concentration of H_2O_2 is less than the optimal value, the conversion of phenol is limited by the amount of H_2O_2. However, when the concentration of H_2O_2 is increased beyond the optimal value, the removal efficiency gradually decreases, probably because the inhibition of the enzyme by H_2O_2 as predicted by Vasudevan et al. 1996.

In the mechanism of the enzymatic elimination of phenol discussed in the section 3.2.2, two free radicals were generated for every molecule of peroxide consumed. As the free radicals polymerise spontaneously, the stoichiometric ratio of peroxide to phenol should be 0.5:1. This fact assumes that the dimmers are completely soluble in water (Nicell 1992). However, some dimmers remain soluble and can react with the HRP to give more free radicals. Further, these radicals can combine themselves to form larger polymers and then precipitate. As long as the polymers remain soluble, the enzyme may catalyse the oxidation of phenol and its polymers. For this reason, the consumption of peroxide to remove the phenol therefore approaches the unity. So, the formation of large polymer molecules did not take place via a propagation step, while only the formation of free radicals, requiring the action of the HRP did it.

5.3. Influence of the phenol initial concentration

The influence of the initial phenol concentration was studied for a H_2O_2 initial concentration of 0.662 mM and initial phenol concentrations in the range of 0.5-2.7 mM. The enzyme concentration was kept at a low value in order to obtain a slower reaction rate to determine the initial reaction rate.

The experimental results of the influence of the initial phenol concentration can be observed in the figure 5.7. As it can be seen in the figure, an increase in the phenol initial concentration caused a decrease in the total phenol conversion. This fact was provoked by the ratio of the enzyme concentration to the phenol concentration. When the phenol concentration is increased, it is necessary to add a higher amount of enzyme to the reaction mixture in order to obtain the same phenol conversion. Moreover, the conversion of phenol is inversely proportional to the initial phenol concentration.
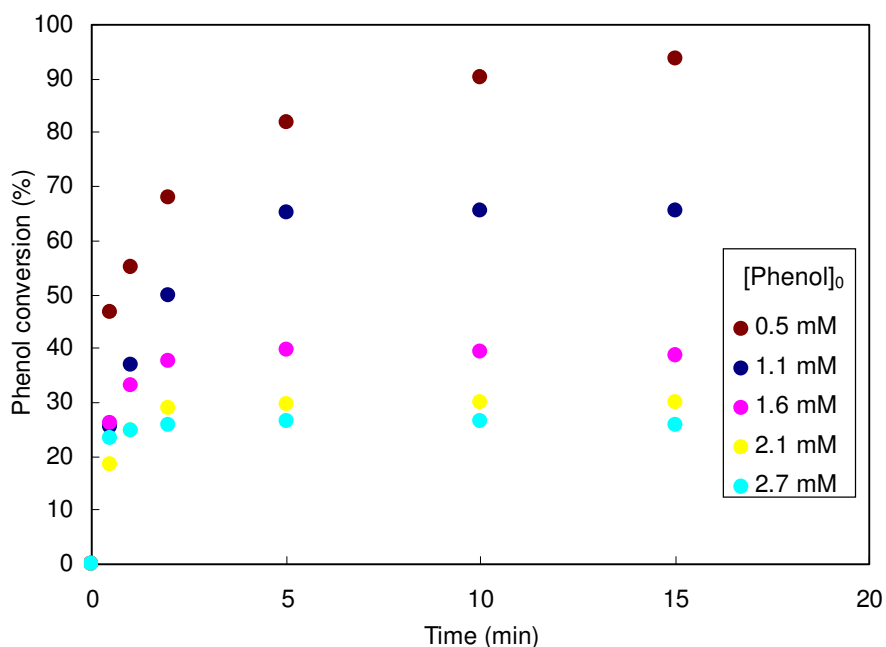
Figure 5.7.   Influence of the phenol initial concentration on the maximum phenol conversion attained in the torus reactor. $[HRP]_0$: $2 \cdot 10^{-4}$ mM, $[H_2O_2]_0$: 0.662 mM, pH 7 and temperature of 20ºC.

On the other hand, the figure 5.8 presents the amount of phenol removed as a function of the initial phenol concentration. As it can be seen in the figure, the quantity of eliminated phenol increased until a maximum is attained for an initial phenol concentration of 1.1 mM. After this value the amount of phenol removed was more or less constant. This fact seems to indicate that we are in presence of the inactivation of the enzyme, caused by the high concentration of free radicals formed during the reaction, as it was also reported by (Klibanov 1983).
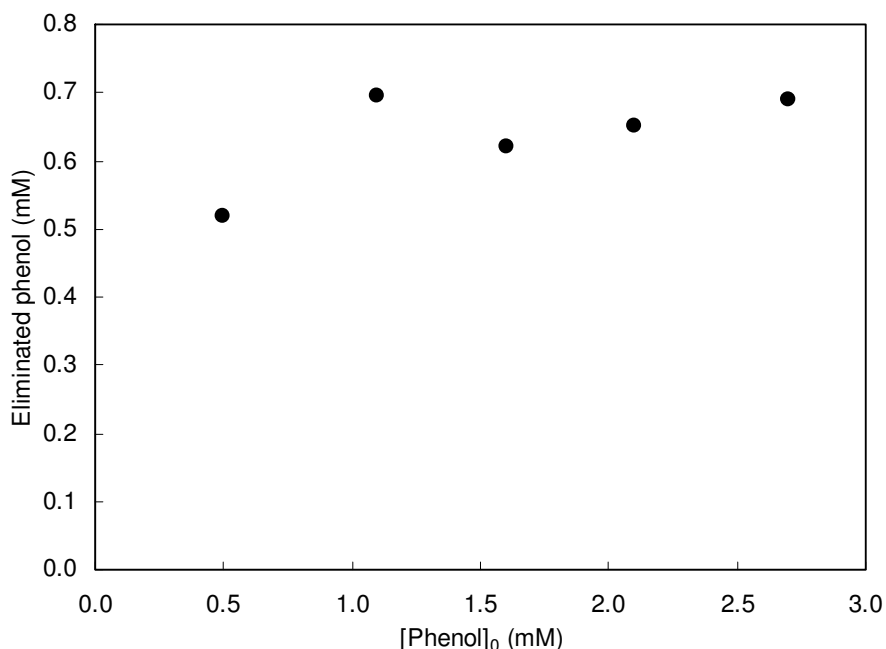
Figure 5.8.   Influence of the phenol initial concentration on the maximum yield of phenol eliminated in the torus reactor. $[HRP]_0$: $2 \cdot 10^{-4}$ mM, $[H_2O_2]_0$: 0.662 mM, pH 7 and temperature of 20ºC.

Moreover, this behaviour can be also observed for the initial rates of the reaction, V_i. The figure 5.9 presents the influence of the initial phenol concentration on the initial rates of the reaction. As it can be observed in the figure, V_i increased with the augment of the initial phenol concentration.

In addition, it was no possible to reach a total conversion of phenol even though the H_2O_2 was in excess as it was the case for $[phenol]_0$: 0.5 mM. To avoid the deactivation of the enzyme, Klibanov et al. (1980) proposed that an increase in the time of reaction could be used to increase the removal of the phenol at low enzyme concentrations but, Maloney (1986) showed that increasing the reaction time did not provoke any improvement in the conversion of phenol, where the time of reaction was maintained during 3 hours.

To confirm the deactivation of the enzyme, two experiments were made adding more H_2O_2 or more enzyme. The initial concentrations for both cases were the same: 1.1mM of phenol, 2mM of H_2O_2 and $2 \cdot 10^{-4}$ mM of HRP. In the first case, 50% more of H_2O_2 was added after 10 min of reaction, this produced a drop in the phenol conversion from 47 to 40%. This drop confirmed the inhibition of the HRP produced by the excess of H_2O_2.

On the other hand, the amount of enzyme was duplicated after 10 min of reaction in the second case. Before the addition, the phenol conversion was stable at 47%, however, after adding the extra enzyme, the conversion increased until 68%. This indicated the inhibition of the HRP by the products of the phenol oxidation, even though, after the addition, there were more available non-inhibited enzymes to keep the phenol conversion. This also indicated that there was not a lack of H_2O_2 the limiting factor for the conversion of phenol.
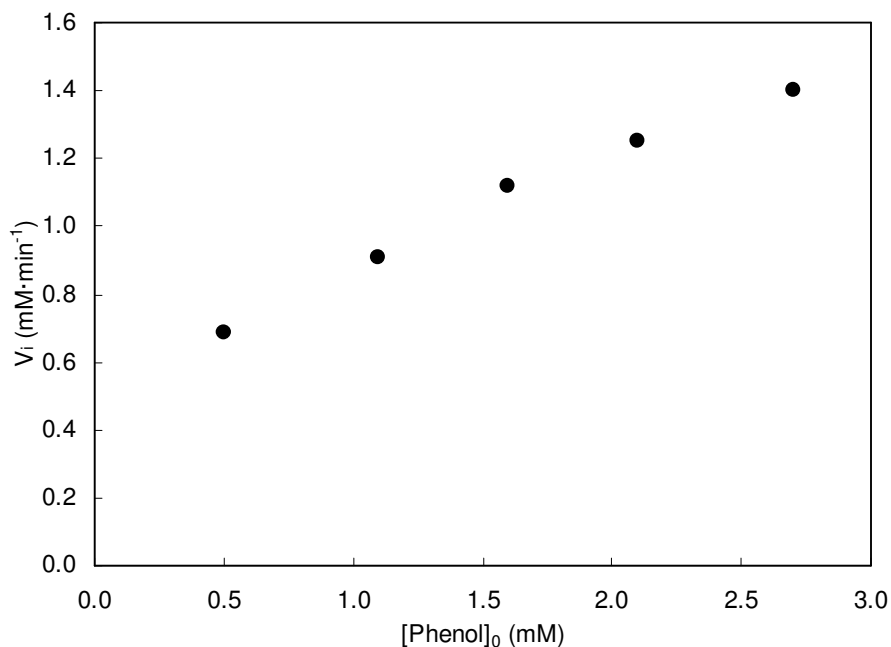
Figure 5.9.   Influence of the phenol initial concentration on the initial rates of the reaction. $[HRP]_0$: $2 \cdot 10^{-4}$ mM, $[H_2O_2]_0$: 0.662 mM, pH 7 and temperature of 20ºC.

These results are in agreement with those published by Klibanov et al. (1983). At a low H_2O_2 initial concentration, a low activity is obtained due to the high quantity of active enzyme existing in the mixture. Therefore, the lack of H_2O_2 limits the work of the enzyme. At higher H_2O_2 initial concentrations, the native enzyme concentration decreases by the formation of inactive forms. This is due to the inhibition of the reaction by the H_2O_2 concentration.

Finally, a criterion of efficiency of the enzyme activity is the turnover of the enzyme which can be defined as the number of moles of phenol converted per mole of enzyme. The number of turnover was found being around 2300 for an initial phenol concentration of 0.5 mM, 4450 for 1.1 mM and 4800 for 1.6 mM. These results are also in agreement with those obtained by Wu et al. (1993), where a turnover number of 1950 was obtained for an initial concentration of phenol of 1 mM, a phenol:H_2O_2 ratio of 1:1 and 1.2 U/ml of HRP.

5.4. Determination of the kinetic model in the torus reactor

The kinetic of the enzymatic removal of phenol was examined in the torus reactor. Different kinetic models were evaluated in order to determine the best option for the enzymatic elimination of phenol in the torus reactor. The normal kinetic model of Michaelis-Menten is presented like thus also the Michaelis-Menten model with inhibition by substrate and finally, a proposed model that considers the influence of the initial H_2O_2 concentration like the one of phenol. The models are presented as follows and the experimental data for the initial reaction rate are shown in each case. In all cases, the experimental initial reaction rates (V_i) were determined from the plot of the consumption of phenol as a function of time. The experimental data were fitted to a logarithmic curve and the reaction rate was determined calculating the value of derivative of the slope of the curve for a time of 0.5 min. This time was chosen to have enough conversion of phenol that can be measured by the analytical method and to be as near as possible to time 0 where the initial rates are higher.

5.4.1. Michaelis-Menten model

The initial reaction rate data as a function of H_2O_2 concentration are presented in figures 5.10 for and initial phenol concentration of 0.5 mM, figure 5.11 for 1.1 mM of phenol and figure 5.12 for 1.6 mM.

Figure 5.10. Influence of the H_2O_2 initial concentration on the Steady-state initial rates of phenol oxidation. Fitting obtained by the Michaelis-Menten model. [Phenol]$_0$: 0.5 mM, [HRP]: $2\cdot10^{-4}$ mM, pH 7 and temperature of 20ºC.

As it can be seen in these figures, the initial reaction rate increased with the increase of the H_2O_2 initial concentration until the optimal concentration of H_2O_2 was reached (molar ratio 1/1 for H_2O_2/Phenol ratio), and then, the initial reaction rate began to decrease.
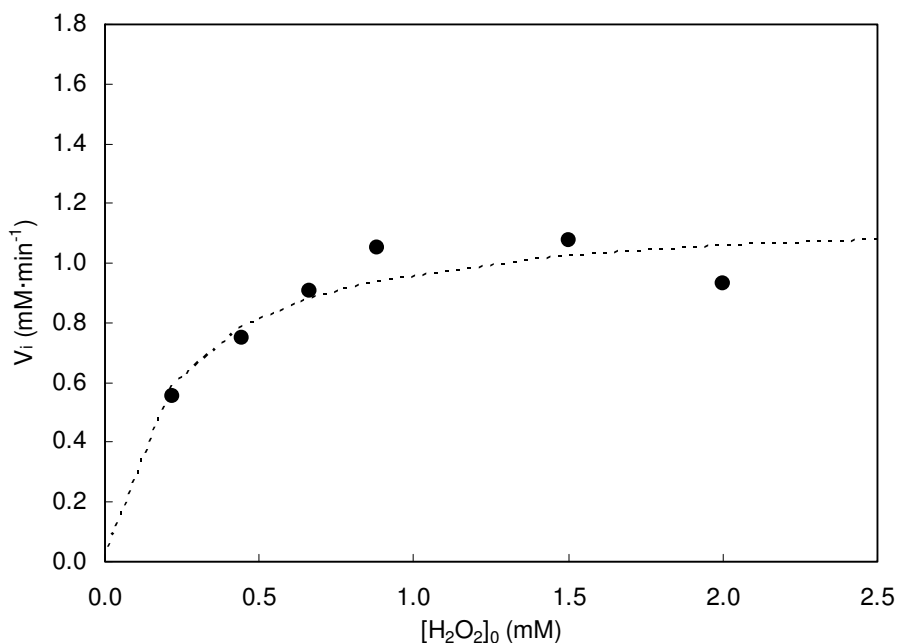
Figure 5.11.   Influence of the H_2O_2 initial concentration on the Steady-state initial rates of phenol oxidation. Fitting obtained by the Michaelis-Menten model. [Phenol]$_0$: 1.1 mM, [HRP]: $2 \cdot 10^{-4}$ mM, pH 7 and temperature of 20ºC.
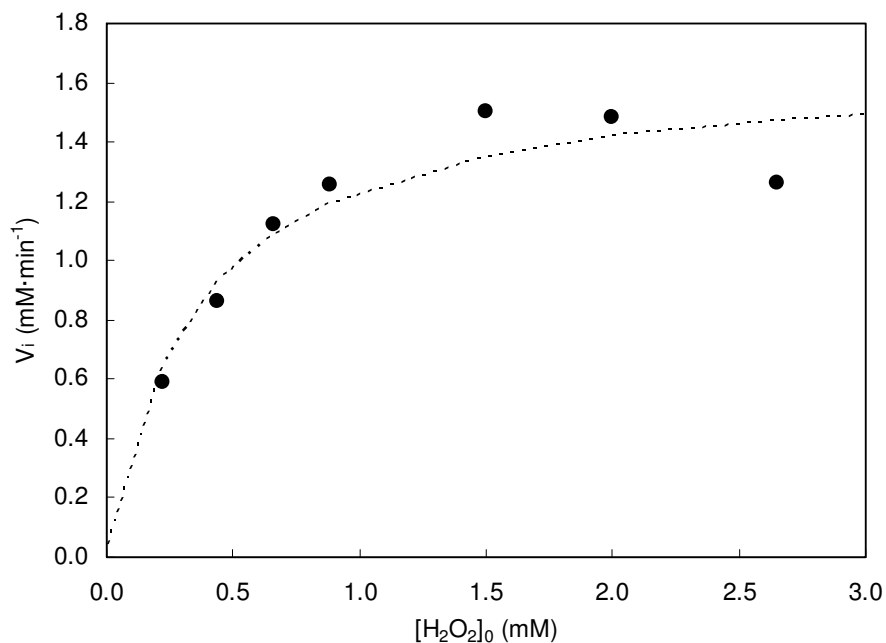
Figure 5.12.   Influence of the H_2O_2 initial concentration on the Steady-state initial rates of phenol oxidation. Fitting obtained by the Michaelis-Menten model. [Phenol]$_0$: 1.6 mM, [HRP]: $2 \cdot 10^{-4}$ mM, pH 7 and temperature of 20ºC.

A maximum value of initial reaction rate of 0.69 mM·min^{-1} was obtained for 0.5 mM of initial concentration of phenol, 1.08 mM·min^{-1} for 1.1 mM and 1.5 mM·min^{-1} for 1.6 mM of phenol.

The experimental data of initial reaction rates were fitted using an analytical equation proposed by Michaelis-Menten that is usually used in enzymatic treatments. The equation is defined by (Cornish-Bowden 2004):

$$V_i = \frac{V_{max} \cdot [H_2O_2]}{K_m + [H_2O_2]}$$
(5.1)

where the variables V_i and $[H_2O_2]$ are respectively the apparent rate of the phenol consumption and the H_2O_2 initial concentration. The apparent maximum reaction rate, V_{max}, and the apparent Michaelis constant K_m, were estimated by the least-squares approximation with the solver of MS Excel. The table 5.1 presents the values obtained for the kinetic parameters.

Table 5.1. Apparent Michaelis-Menten parameters for the reaction of HRP with Phenol and H_2O_2.

Phenol (mM)	V_{max} (mM·min^{-1})	K_m (mM)	Cumulative error
0.5	0.69	0.08	0.014
1.1	1.17	0.22	0.034
1.6	1.67	0.35	0.083

Figures 5.10, 5.11 and 5.12 also present the fitting of the experimental values of V_i. As it can be seen in the three figures, the Michaelis-Menten model did not fit well the experimental data, especially for the values of V_i after the maximum. Only the three first values are well fitted in each case and therefore, it was necessary to modify the model in order to accurate the fitting for the values of the higher initial concentrations of H_2O_2.

5.4.2. Michaelis-Menten model with inhibition by substrate

The initial reaction rates were, then fitted using another kinetic model, the Michaelis-Menten model with inhibition by substrate. The kinetic data as a function of H_2O_2 concentration are presented in figures 5.13 for and initial phenol concentration of 0.5 mM, 5.14 for 1.1 mM of phenol and 5.15 for 1.6 mM. The initial rate (V_i) vs. H_2O_2 concentration was fitted to the Michaelis-Menten equation with inhibition by substrate (Cornish-Bowden 2004):

$$V_i = \frac{V_{max} \cdot [H_2O_2]}{K_m + [H_2O_2] + K' \cdot [H_2O_2]^2}$$
(5.2)

where the variables V_i and $[H_2O_2]$ are respectively the apparent rate of the phenol consumption and the H_2O_2 initial concentration, while V_{max} is the apparent maximum reaction rate, K_m, the apparent Michaelis constant and K', the inhibition constant. As it can be seen in the figures, a good approximation of the experimental data was obtained using this model and this, for all the

range of H_2O_2. This fact confirmed that an inhibition of the enzyme by the substrate or by the products of the reaction occurred. Hydrogen peroxide interfered in the reaction by decreasing the reaction rate.
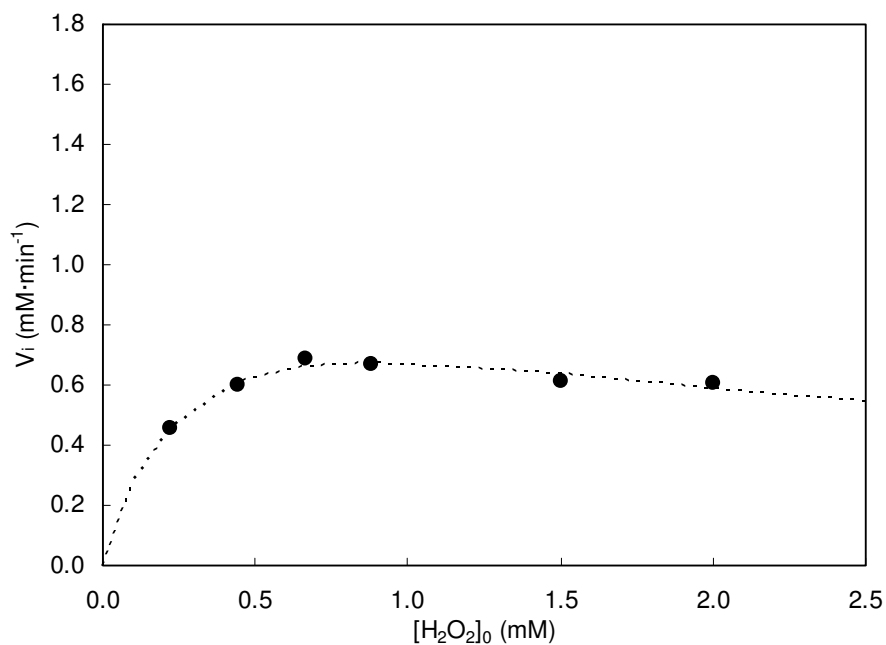
Figure 5.13. Influence of the H_2O_2 initial concentration on the Steady-state initial rates of phenol oxidation. Fitting obtained by the Michaelis-Menten model with inhibition. $[Phenol]_0$: 0.5 mM, [HRP]: $2 \cdot 10^{-4}$ mM, pH 7 and temperature of 20ºC.
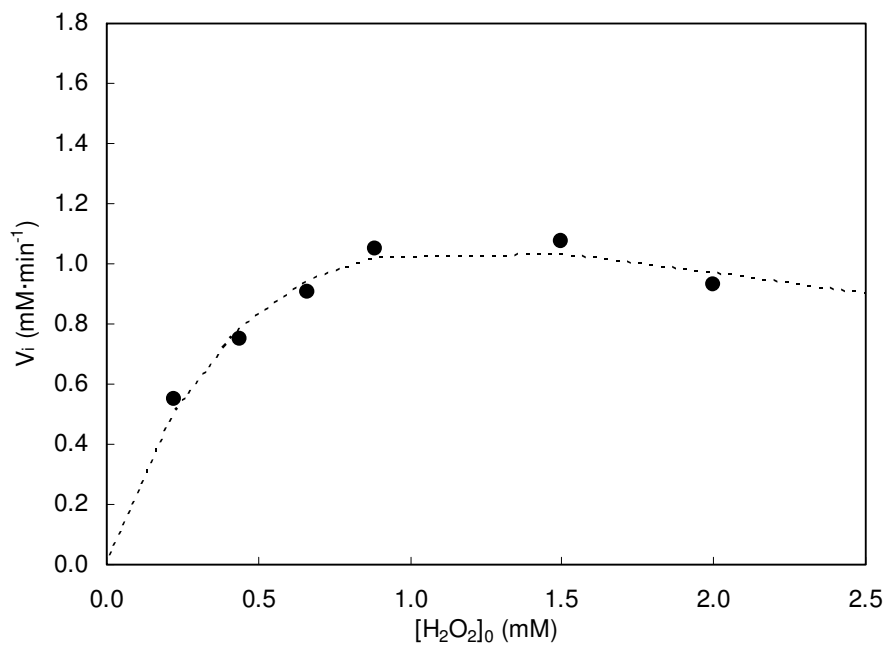
Figure 5.14. Influence of the H_2O_2 initial concentration on the Steady-state initial rates of phenol oxidation. Fitting obtained by the Michaelis-Menten model with inhibition. $[Phenol]_0$: 1.1 mM, [HRP]: $2 \cdot 10^{-4}$ mM, pH 7 and temperature of 20ºC.

The reduced reaction rate can be attributed to the formation of an oxidation state of HRP which is not catalytically active but its formation does not represent a terminal inactivation of HRP. In the presence of an excess of peroxide, the formation of this inactive form of HRP would increase resulting in suppressed catalyst performance. This fact is demonstrated by the lower initial reaction rates obtained when a higher initial concentration of H_2O_2 is added to the mixture.

On the other hand, this fact was not observed in the work of Vasudevan et al. (1996) but, in the works of Arnao et al. (1990) and Nicell et al. (1997), where it was found that the hydrogen peroxide concentration had an inhibitory effect on the catalytic activity of the enzyme. In the work of Vasudevan et al. (1996), the kinetic model of the reaction was determined using three different initial concentrations of phenol of 1.0272 mM, 2.5637 mM and 5.1750 mM, in all cases, the initial H_2O_2 concentrations used respectively were kept lower than the optimum value of 1:1 ratio with the phenol. Therefore, no inhibition by hydrogen peroxide was observed in the work and it was proposed that the reaction followed the normal Michaelis-Menten model. In Arnao et al. (1990), the inactivation process of peroxidase during the ABTS (2,2'-azino-bis(3-ethylbenzthiazoline-6-sulphonic acid)) oxidation was investigated. They have found that the HRP is inhibited by the H_2O_2 concentration. Therefore it was suggested the need to include an enzyme inactivation step in the usual schemes used for reactions catalyzed by peroxidase.
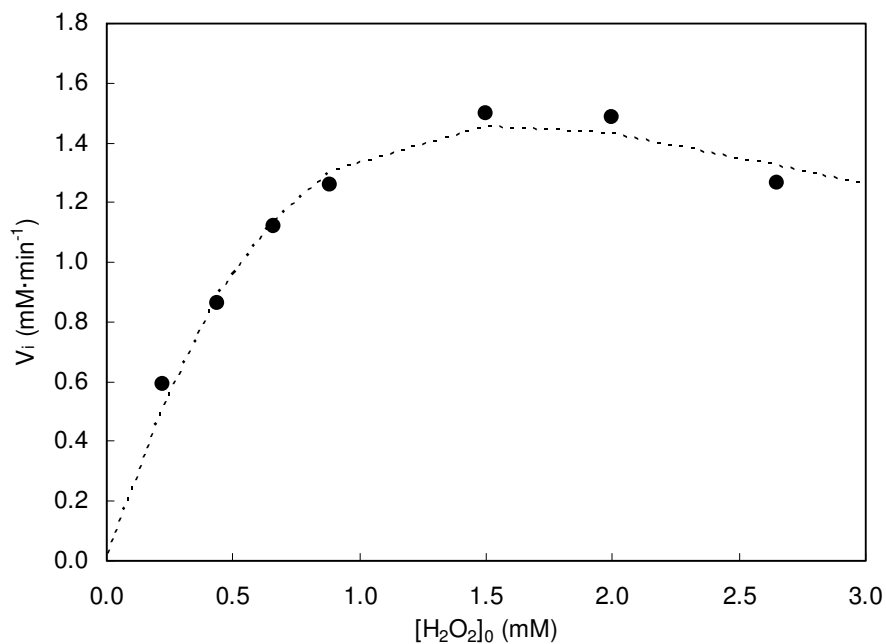
Figure 5.15.   Influence of the H_2O_2 initial concentration on the Steady-state initial rates of phenol oxidation. Fitting obtained by the Michaelis-Menten model with inhibition. [Phenol]$_0$: 1.6 mM, [HRP]: $2 \cdot 10^{-4}$ mM, pH 7 and temperature of 20ºC.

The parameters of the kinetic model V_{max}, apparent maximum reaction rate, K_m, apparent Michaelis constant, and K', inhibition constant, were estimated by the least-squares approximation with the solver of MS Excel. In this procedure for estimating constants, all the

parameters were optimised at the same time. The calculated values of the fitted parameters for different phenol concentrations are presented in table 5.2.

Table 5.2. Apparent Michaelis-Menten with inhibition parameters for the reaction of HRP with Phenol and H_2O_2.

Phenol (mM)	V_{max} (mM·min^{-1})	K_m (mM)	K' (mM^{-1})	Cumulative error
0.5	1.17	0.32	0.41	0.002
1.1	2.57	0.88	0.60	0.010
1.6	4.97	1.88	0.77	0.018

These results showed that the parameters V_{max}, K_m and K' increased when initial concentration of phenol increases. The same trend was also observed in the work of Vasudevan et al (1996).

As it can be observed, the fittings are in good agreement with the experimental data. The results of the enzymatic elimination have the same trend that those obtained by previous works (Vasudevan 1996, Nicell 1997) but the kinetic parameters can not be compared with other literature values because the kinetic model used was different. The rate constants are different for each type of peroxidase and they are function of the pH, temperature, the kind of aromatic compound that is treated and finally, with the kinetic model applied.

Although, a good fitting of the experimental data of initial reaction rate was obtained using the kinetic model of Michaelis-Menten with inhibition, it was not possible to model globally. There are different kinetic parameters for each initial phenol concentration studied.

5.4.3. Kinetic model with inhibition by H_2O_2 and influence of the phenol initial concentration

In order to have a unique kinetic model to be applied for any initial phenol concentration, a different kinetic model was proposed. This model, based on the Michaelis-Menten kinetic model with inhibition, not only contemplated the initial H_2O_2 concentration, but also the initial phenol concentration. It is important to notice that the initial phenol concentration was included in two terms. The first one multiplies the maximum reaction rate parameter, V_{max}, meaning that the phenol initial concentration contributed proportionally to the initial reaction rate. The second term related the initial phenol concentration as an inhibitor and it is expressed in the denominator of the kinetic equation, limiting the initial reaction rate for higher values of initial phenol concentration. This consideration was possible because the kinetic parameters presented a linear relationship with the initial phenol concentration.

The initial rate (V_i) vs. phenol and H_2O_2 concentrations was fitted to the kinetic model represented by the equation 5.3:

$$V_i = \frac{V_{max} \cdot [H_2O_2][Phenol]}{K_m + [H_2O_2] + K \cdot [Phenol] + K' \cdot [H_2O_2]^2} \tag{5.3}$$

where V_i is the apparent reaction rate of the phenol consumption, [Phenol] and [H_2O_2] are the phenol and the H_2O_2 initial concentrations respectively, V_{max} is the apparent maximum reaction rate while K_m, K and K' are the kinetic model constants. The kinetic data as a function of H_2O_2 initial concentration using this kinetic model are presented in figures 5.16 for and initial phenol concentration of 0.5 mM, 5.17 for 1.1 mM of phenol and 5.18 for 1.6 mM.
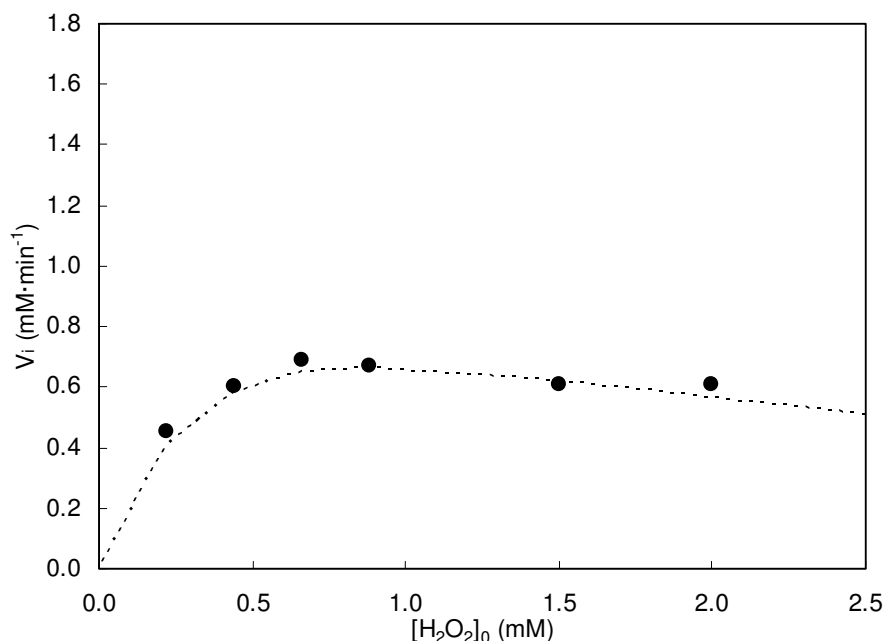
Figure 5.16.   Influence of the H_2O_2 initial concentration on the Steady-state initial rates of phenol oxidation. Fitting obtained by the modified Michaelis-Menten model with inhibition. [Phenol]$_0$: 0.5 mM, [HRP]: $2 \cdot 10^{-4}$ mM, pH 7 and temperature of 20ºC.

As it can be seen in the figures, the fittings are in good agreement with the experimental data. The parameters of the kinetic model V_{max}, apparent maximum reaction rate, K_m, apparent Michaelis constant, k and K', inhibition constants, were estimated by the least-squares approximation with the solver of MS Excel. The estimation of the parameters was made simultaneously for all the studied phenol concentrations, raising a total cumulative error of 0.04. The calculated values of the fitted parameters for different phenol concentrations are presented in table 5.3.

Table 5.3. Apparent parameters for the reaction of HRP with inhibition by Phenol and H_2O_2.

V_{max} (min^{-1})	K_m (mM)	K (*)	K' (mM^{-1})
2.72	0	0.98	0.65

* dimensionless
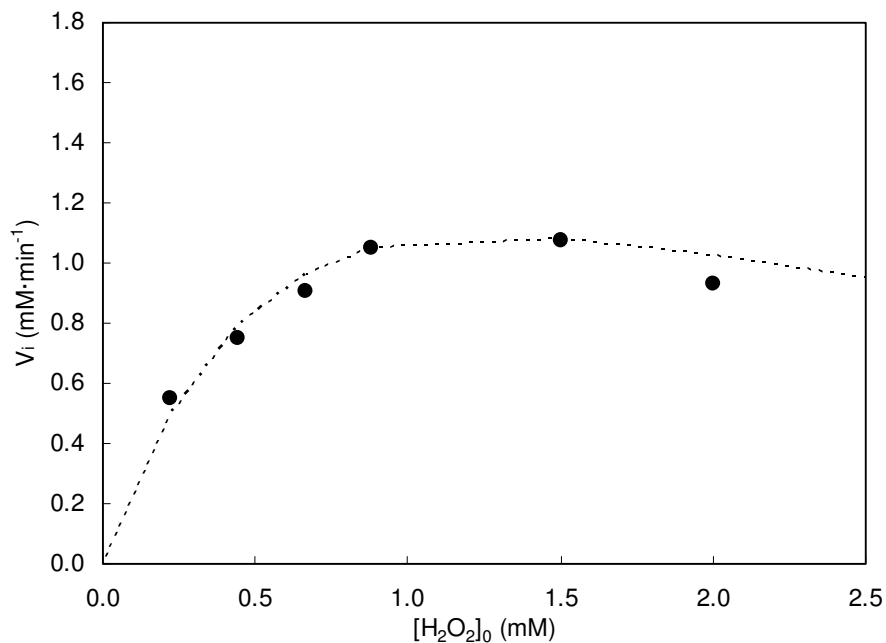
Figure 5.17. Influence of the H_2O_2 initial concentration on the Steady-state initial rates of phenol oxidation. Fitting obtained by the modified Michaelis-Menten model with inhibition. $[Phenol]_0$: 1.1 mM, [HRP]: $2\cdot10^{-4}$ mM, pH 7 and temperature of 20ºC.
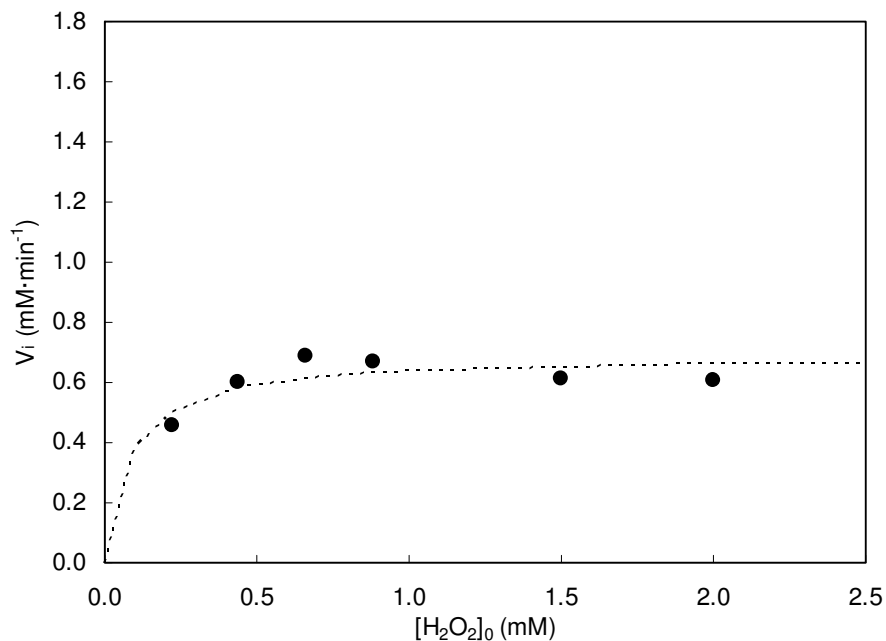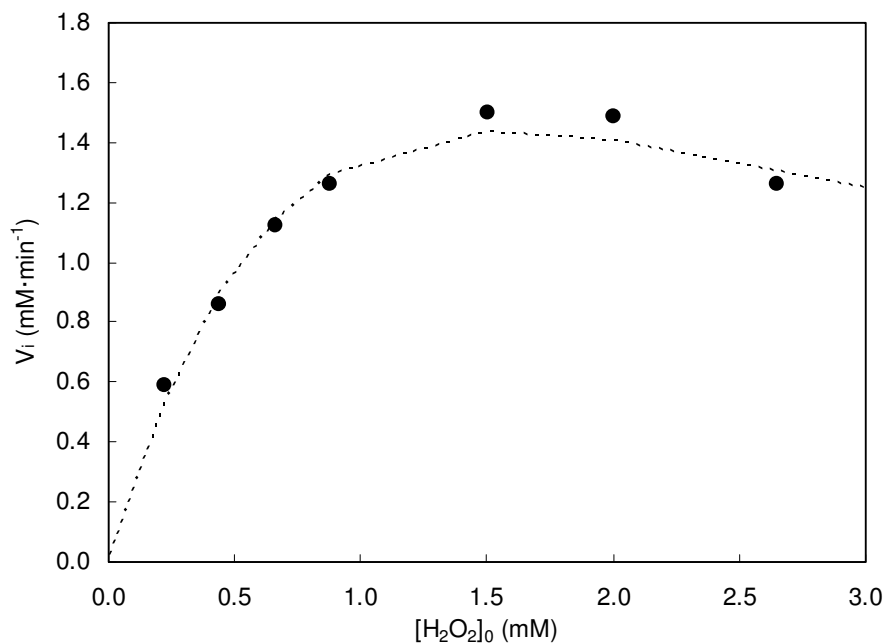

Figure 5.18. Influence of the H_2O_2 initial concentration on the Steady-state initial rates of phenol oxidation. Fitting obtained by the modified Michaelis-Menten model with inhibition. $[Phenol]_0$: 1.6 mM, [HRP]: $2\cdot10^{-4}$ mM, pH 7 and temperature of 20ºC.

Then, the definitive equation of the initial reaction rate can be written as follows:

$$V_i = \frac{2.72\cdot[H_2O_2][Phenol]}{[H_2O_2]+0.98\cdot[Phenol]+0.65\cdot[H_2O_2]^2} \qquad (5.3)$$

64

Finally, to demonstrate that the kinetic model works well, two experiments were realised to verify the predicted values of the initial reaction rates and the phenol conversion. Both experiments were not used to determine the kinetic model. The experimental conditions of both experiments were a phenol initial concentrations of 2.1 and 2.7 mM, a H_2O_2 initial concentration of 0.662 mM, a HRP initial concentration of $2 \cdot 10^{-4}$ mM, a pH of 7 and a temperature of 20ºC. The table 5.4 presents the values of this comparison.

Table 5.4. Verification of the validity of the kinetic model. $[HRP]_0$: $2 \cdot 10^{-4}$ mM, $[H_2O_2]_0$: 0.662 mM, pH 7 and temperature of 20ºC.

	[Phenol]₀: 2.1 mM		[Phenol]₀: 2.7 mM	
	Experimental	Calculated	Experimental	Calculated
Initial reaction rate	1.25 mM·min⁻¹	1.26 mM·min⁻¹	1.39 mM·min⁻¹	1.35 mM·min⁻¹
Phenol conversion	30%	31%	-	-

As it can be seen in the table, predicted or calculated and experimental values are very close giving a good validity of the kinetic model.

5.5. Mathematical modeling of the enzymatic reaction

The enzymatic reaction was modelled using numerical methods. The torus reactor was assimilated to a batch stirred tank reactor (STR). This approximation was done because the torus reactor presents a hydrodynamic behaviour similar to the stirred reactor as it will be shown in further sections. The equation of design of such kind of reactor is defined as (Fogler 2003):

$$\frac{\partial [compound]}{\partial t} = -V \tag{5.4}$$

where V represents the reaction rate. For the enzymatic reaction it was considered that both phenol and H_2O_2 concentrations have an equimolar ratio, as it was experimentally determined. This means that the reaction rate is equal for both compounds. In this way, the following equations were defined in order to obtain the phenol conversion using the kinetic model obtained in section 5.4.3:

$$\frac{\partial [H_2O_2]}{\partial t} = -V \tag{5.5}$$

$$\frac{\partial [Phenol]}{\partial t} = -V \tag{5.6}$$

$$V = \frac{V_{max} \cdot [H_2O_2][Phenol]}{K_m + [H_2O_2] + k \cdot [Phenol] + k' \cdot [H_2O_2]^2} \tag{5.7}$$

65

The differential equations were solved using Polymath. The conversion of phenol was obtained for all the studied cases. The figures 5.19, 5.20 and 5.21 present the phenol conversion obtained using the solution of the differential equations described above for an initial phenol concentration of 0.5, 1.1 and 1.6 mM and different H_2O_2 initial concentrations.
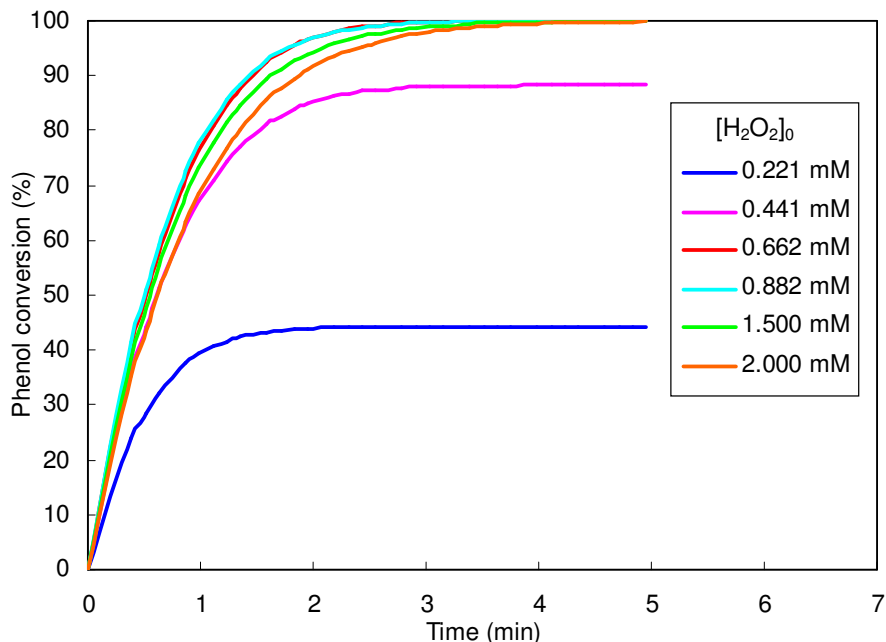
Figure 5.19.   Influence of the H_2O_2 initial concentration on the calculated phenol conversion in the torus reactor. $[Phenol]_0$: 0.5 mM and $[HRP]_0$: $2 \cdot 10^{-4}$ mM.
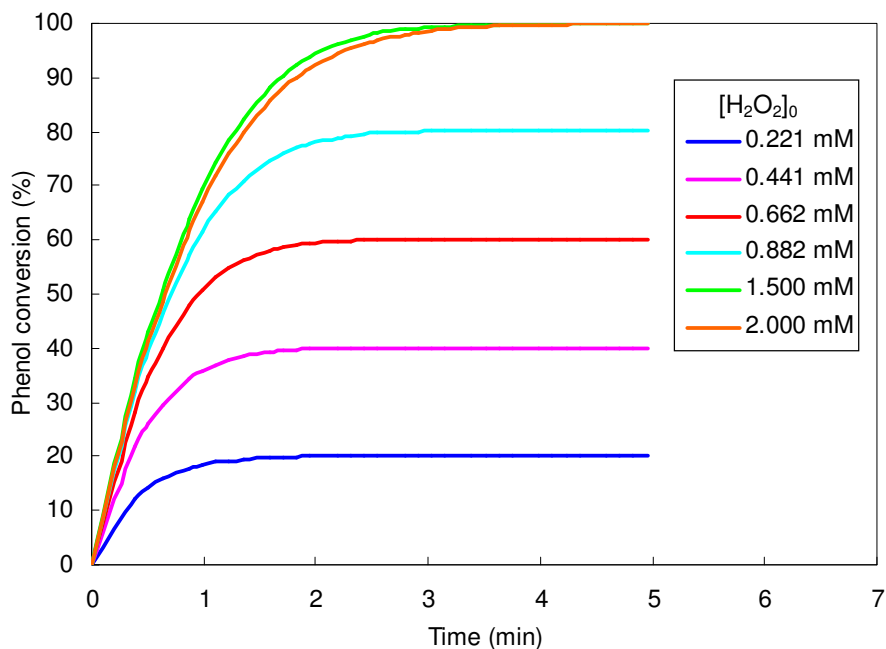
Figure 5.20.   Influence of the H_2O_2 initial concentration on the calculated phenol conversion in the torus reactor. $[Phenol]_0$: 1.1 mM and $[HRP]_0$: $2 \cdot 10^{-4}$ mM.

As it can be seen in the figures, a good approach of the phenol conversion was obtained when the H_2O_2 initial concentration was below the optimal ratio with phenol. In all cases, the curves present a similar behaviour than those observed in the experimental work, shown in section 5.2 (figures 5.3, 5.4 and 5.5 respectively). For values of H_2O_2 initial concentration above the optimal value, an overestimation of the phenol conversion was observed. However, in was not possible to find an adapted equations system that describes accurately the reaction and the phenol conversion.
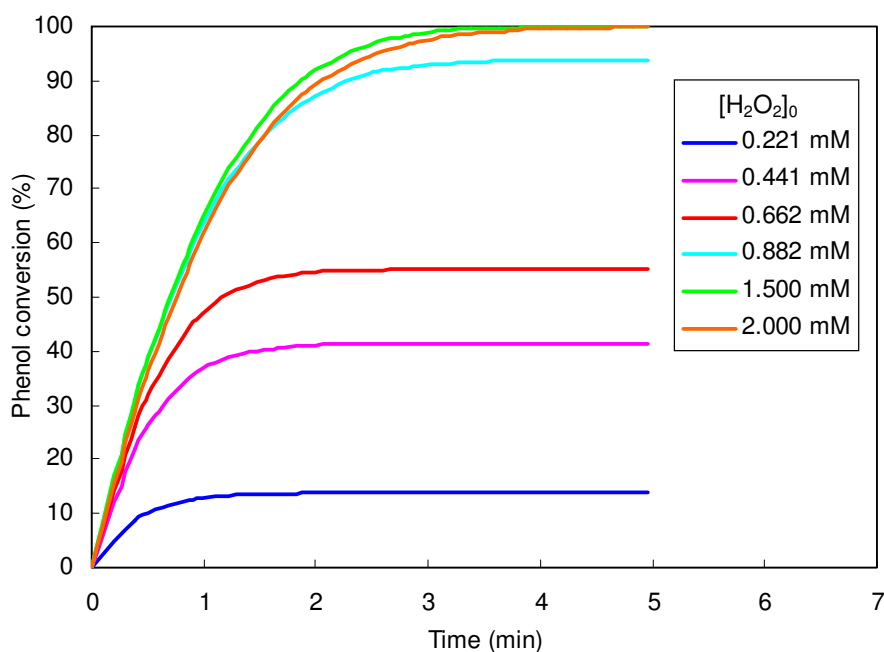
Figure 5.21. Influence of the H_2O_2 initial concentration on the calculated phenol conversion in the torus reactor. $[Phenol]_0$: 1.6 mM and $[HRP]_0$: $2 \cdot 10^{-4}$ mM.

5.6. Conclusions

The enzymatic elimination of phenol performed in the torus reactor obtained high degrees of conversion for the three initial concentrations of phenol tested.

The optimum H_2O_2 initial concentration to achieve the highest conversion of phenol must be a ratio equal to 1 between the phenol and the H_2O_2 initial molar concentration.

The excess of hydrogen peroxide in the mixture inhibits the catalytic activity of the enzyme through the conversion of peroxidase to inactive forms provoking a reduction of the phenol conversion.

The enzymatic reaction in the torus reactor follows the Michaelis-Menten equation with inhibition when the kinetic data are obtained as a function of the initial H_2O_2 concentration. But, different kinetic parameters were found for different initial phenol concentrations.

An alternative kinetic model based on Michaelis-Menten with inhibition was proposed in order to have a unique kinetic model to be applied for any initial phenol and H_2O_2 concentration. A good fitting was obtained with the proposed model for all concentrations of phenol. In this way, a model that included the effect of the H_2O_2 and the phenol initial concentrations and inhibitions was reached.

The equation of the apparent reaction rate is:

$$V_i = \frac{2.72 \cdot [H_2O_2][Phenol]}{[H_2O_2] + 0.98[Phenol] + 0.65 \cdot [H_2O_2]^2}$$

Chapter 6. Performance comparison of the torus reactor with a stirred tank reactor

The enzymatic elimination of phenol was also studied in a stirred tank reactor in order to compare the performances of the torus and the stirred tank reactors. The same initial conditions were utilised to carry out the study with the aim to see only the influence of the type of reactor.

6.1. Determination of the enzymatic activity of HRP in the stirred reactor

The enzymatic elimination of phenol was carried out in a stirred glass reactor of 100 ml. The figure 6.1 presents the phenol conversion efficiency for 1.1 mM of phenol initial concentration and 0.882 mM of H_2O_2 initial concentration using different HRP doses.

Figure 6.1.   Influence of the HRP initial concentration on the phenol conversion in the stirred tank reactor. $[Phenol]_0$: 1.1 mM, $[H_2O_2]_0$: 0.882 mM, pH 7 and temperature of 20ºC.

As it can be seen in the figure, a progressive augment of the HRP initial concentration in the reaction mixture increased the conversion of phenol in all cases. The final conversion of phenol attained was augmented from 18% for an HRP initial concentration of $3 \cdot 10^{-5}$ mM (0.15 U/ml) to 62% at $2 \cdot 10^{-4}$ mM (1U/ml). These data are very close to those obtained with the torus reactor, where the same higher conversion of phenol, 62%, was obtained with the same initial concentration of the HRP, $2 \cdot 10^{-4}$ mM.

The free HRP activity was determined in the stirred reactor as in the torus reactor using 1.1 mM of phenol, 0.882 mM of H_2O_2. The enzyme activity was again determined by the slope of the

apparent reaction rate versus enzyme concentration and the results are presented in the figure 6.2.
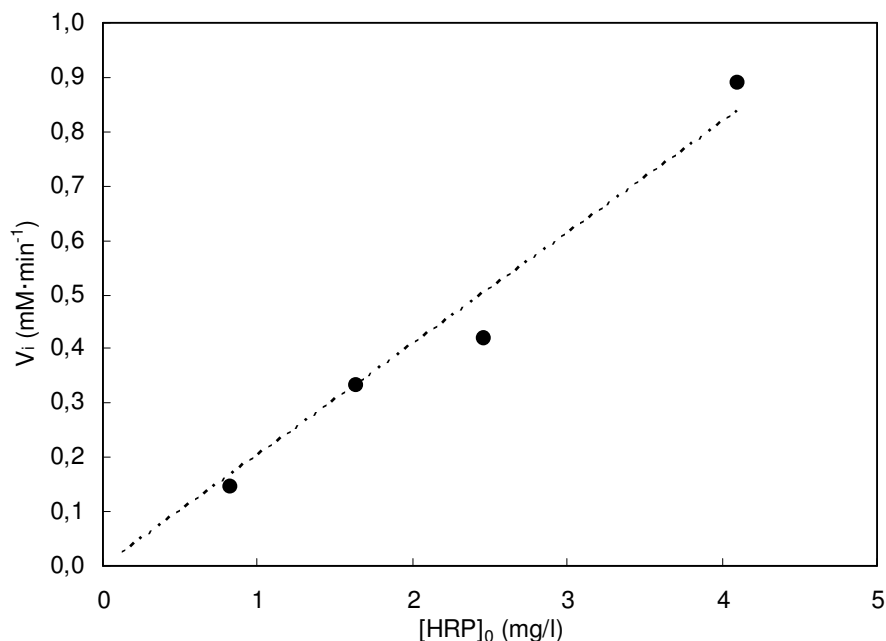
Figure 6.2.   Determination of the activity of the HRP in the stirred tank reactor. $[Phenol]_0$: 1.1 mM, $[H_2O_2]_0$: 0.882 mM, pH 7 and temperature of 20ºC. R^2: 0.98.

The activity of the free enzyme in the stirred reactor was equal to 204±22 μmol/min·mg enzyme or 204±22 U/mg. This value of the enzymatic activity is the same than the obtained with the torus reactor revealing that the activity of the enzyme is not affected by the utilisation of the torus reactor, showing the potential of this reactor geometry.

6.2. Performance comparison of the enzymatic elimination of phenol in stirred reactor

The study of the influence of the different initial concentrations was also carried out in the stirred reactor, with the same initial conditions than for the torus reactor. The phenol initial concentrations tested were in the range 0.5-1.6 mM, the H_2O_2 initial concentrations between 0.143-2.65 mM and in all cases, the HRP initial concentration was kept at $2·10^{-4}$ mM (1 U/ml).

The results of the influence of the H_2O_2 initial concentrations on the conversion of phenol in the stirred reactor are presented in figures 6.3, 6.4 and 6.5 for 0.5, 1.1 and 1.6 mM of phenol initial concentration respectively.

As it can be seen in the figure 6.3, for an initial concentration of phenol of 0.5 mM, in all experiments, the phenol conversion reached a maximum value after few minutes for each H_2O_2 initial concentration and then, remained more or less unchanged after 10 minutes in all cases.
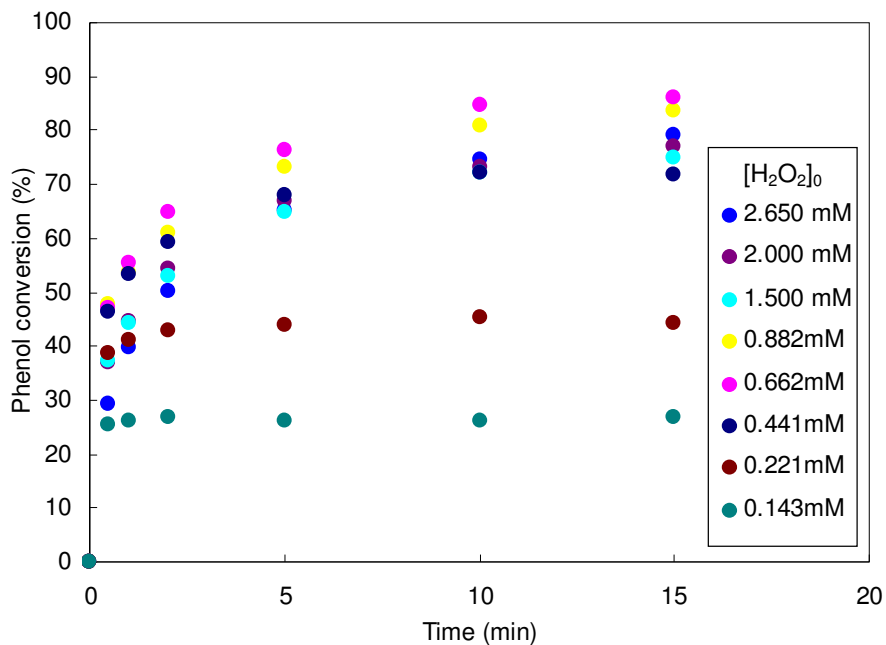
Figure 6.3.   Influence of the H_2O_2 initial concentration on the phenol conversion in the stirred tank reactor. [Phenol]$_0$: 0.5 mM, [HRP]$_0$: $2 \cdot 10^{-4}$ mM, pH 7 and temperature of 20ºC.
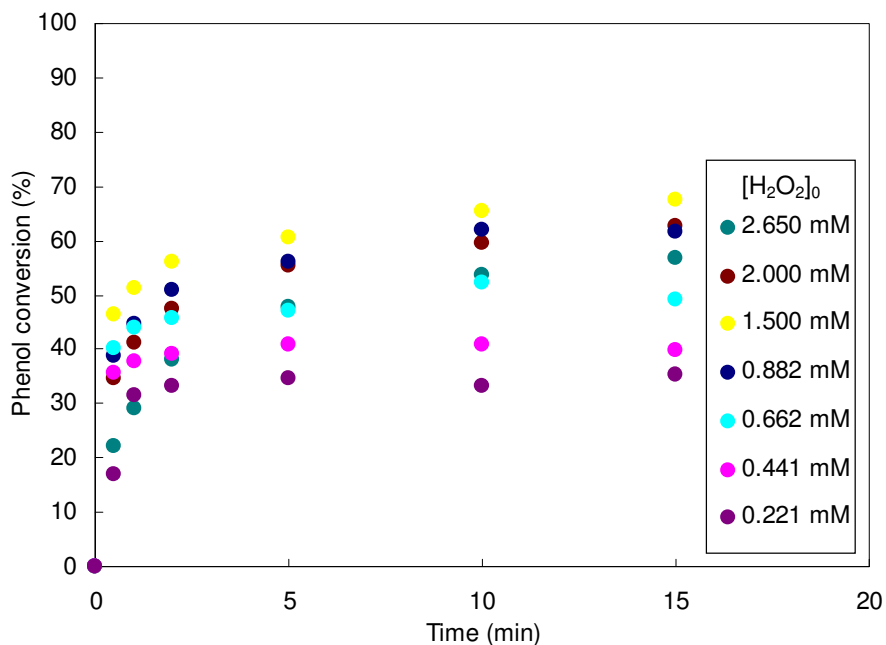
Figure 6.4.   Influence of the H_2O_2 initial concentration on the phenol conversion in the stirred tank reactor. [Phenol]$_0$: 1.1 mM, [HRP]$_0$: $2 \cdot 10^{-4}$ mM, pH 7 and temperature of 20ºC.

On the other hand, the behaviour of the conversion is equal for both reactors, the conversion of phenol augmented from the time when the H_2O_2 initial concentration increased until a maximum of the conversion is reached and then, the conversion began to diminish. Again, this fact is explained by the inactivation of the enzyme. Exactly the same behaviour can be observed for the phenol initial concentration of 1.1 and 1.6 mM.
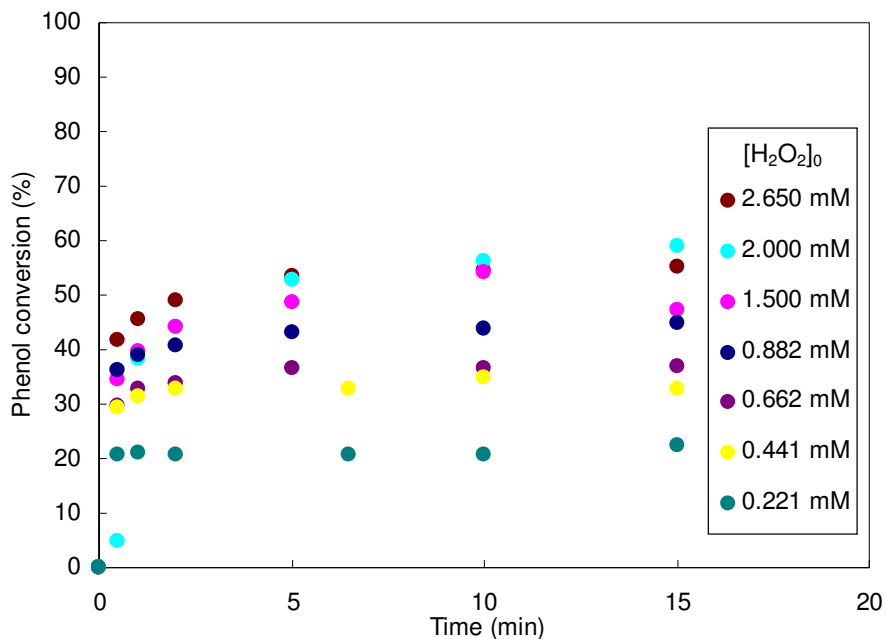
Figure 6.5.   Influence of the H_2O_2 initial concentration on the phenol conversion in the stirred tank reactor. [Phenol]$_0$: 1.6 mM, [HRP]$_0$: 2•10^{-4} mM, pH 7 and temperature of 20ºC.

To observe more clearly the behaviour of the phenol conversion for the three phenol initial concentrations, the figure 6.6 presents the maximum phenol conversion accomplished as a function of the H_2O_2 initial concentration.
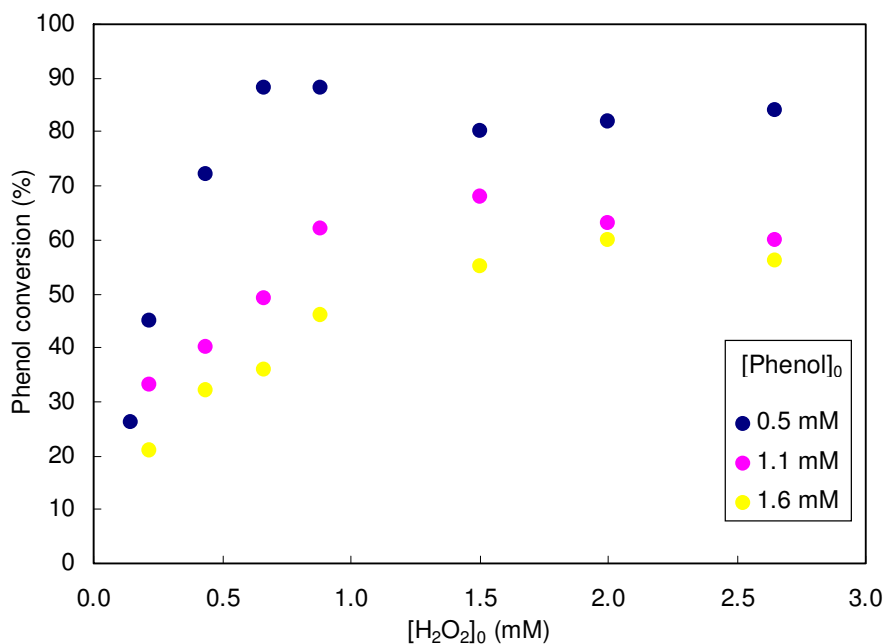
Figure 6.6.   Influence of the [H_2O_2] initial concentration on the maximum phenol conversion attained in the stirred reactor. [HRP]$_0$: 2·10^{-4} mM, [H_2O_2]$_0$ from 0.143 to 2.65 mM, pH 7 and temperature of 20ºC.

As it can be seen in the figure 6.6, the optimal initial concentration of H_2O_2 to obtain the highest phenol conversion seemed to be the ratio 1:1 between phenol and H_2O_2, exactly the same ratio obtained with the torus reactor. Again, no significative differences were observed for both reactors. Nevertheless, the conversion of phenol was always higher in the torus reactor respect to the stirred reactor for the phenol initial concentrations of 0.5 and 1.1 mM.

To confirm this fact, the figure 6.7 presents the amount of phenol eliminated during the reaction for the three different initial phenol concentrations with a stoichiometric relation of H_2O_2. As it can be seen in the figure, the quantity of eliminated phenol increased for a phenol initial concentration from 0.5 mM to 1.1 mM, however, after this value, the quantity of phenol removed stayed constant. The same behaviour was as well observed with the torus reactor, the only difference between both reactors being the extent of the elimination, always higher for the torus reactor in the tested conditions.
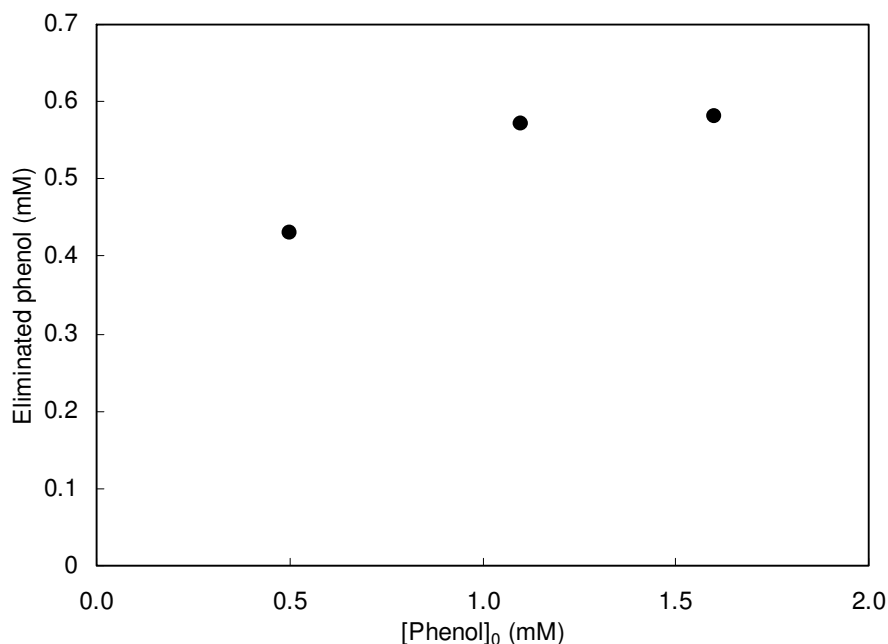
Figure 6.7.   Influence of the phenol initial concentration on the maximum yield of phenol eliminated in the stirred tank reactor. $[HRP]_0$: $2 \cdot 10^{-4}$ mM, $[H_2O_2]_0$: 0.662 mM, pH 7 and temperature of 20ºC.

Finally, to achieve the study of comparison of the performances of both reactors, the initial reaction rates were analysed in the stirred reactor. The figure 6.8 presents the influence of the phenol initial concentration on the initial rates of the reaction. As it can be seen in the figure, the reaction rates raised at the time that the initial phenol concentration increased. However, the absolute values of the initial reaction rates are lower than the obtained in the torus reactor, suggesting that the mixing in the torus reactor is better than in the stirred reactor.
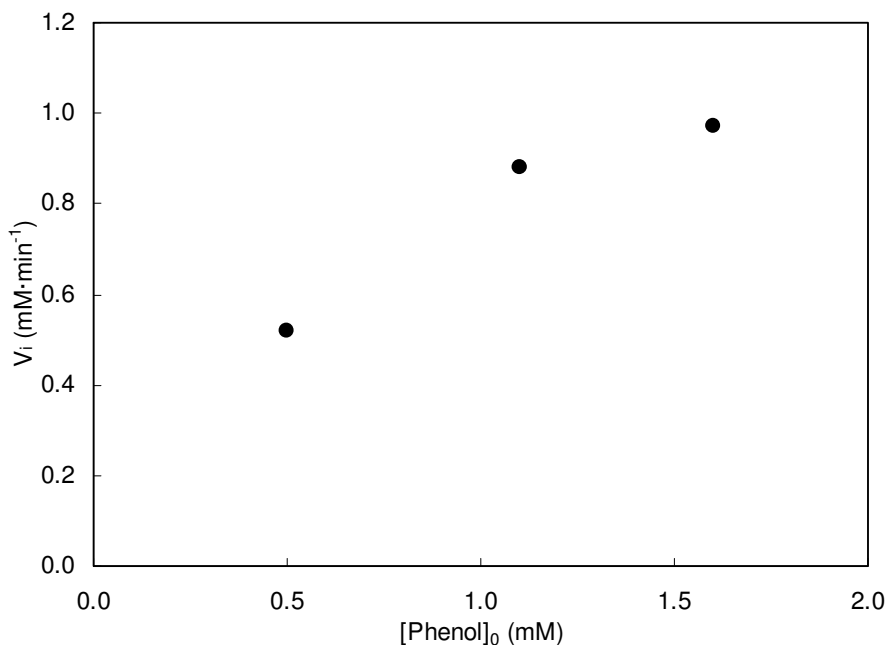
Figure 6.8.   Influence of the phenol initial concentration on the initial rates of the reaction. $[HRP]_0$: $2 \cdot 10^{-4}$ mM, $[H_2O_2]_0$: 0.662 mM, pH 7 and temperature of 20ºC.

6.3. Study at high phenol initial concentrations in the stirred reactor

With the purpose of to explore the behaviour of the enzymatic reaction with high phenol initial concentrations, several assays were performed in the 100 ml stirred batch reactor. To facilitate these assays, the initial concentrations of the H_2O_2 and of the HRP had to be increased too.

Firstly it was studied the influence of the H_2O_2 initial concentration. The main results obtained for four different phenol initial concentrations are summarised in tables 6.1, 6.2, 6.3 and 6.4.

Table 6.1. Influence of the H_2O_2 initial concentration on the phenol conversion in the stirred reactor. $[HRP]_0$: $2.48 \cdot 10^{-3}$ mM, $[Phenol]_o$: 11.0 mM, pH 7 and temperature of 20ºC.

$[H_2O_2]_0$ (mM)	X_{Phenol} (%)
5	42
10	69
14	90
19	96
29	75

Table 6.2. Influence of the H_2O_2 initial concentration on the phenol conversion in the stirred reactor. $[HRP]_0$: $2.48 \cdot 10^{-3}$ mM, $[Phenol]_o$: 13.8 mM, pH 7 and temperature of 20ºC.

$[H_2O_2]_0$ (mM)	X_{Phenol} (%)
10	42
19	69
29	72
38	97

As it can be seen in the table 6.1, 96% of phenol conversion was achieved with 19 mM of H_2O_2, however, with a H_2O_2 concentration of 29 mM, the phenol conversion decreased to 75%. This same behaviour was previously observed at low concentrations of both phenol and H_2O_2. On the other hand, for a concentration of phenol of 13.8 mM (table 6.2), the conversion of phenol increased with an augment of the H_2O_2 concentration. In contrast, if the concentration of H_2O_2 is maintained, the conversion of phenol decreased.

Table 6.3. Influence of the H_2O_2 initial concentration on the phenol conversion in the stirred reactor. $[HRP]_0$: $2.48 \cdot 10^{-3}$ mM, $[Phenol]_o$: 16.0 mM, pH 7 and temperature of 20ºC.

$[H_2O_2]_0$ (mM)	X_{Phenol} (%)
7	40
15	53
22	89
29	92

Table 6.4. Influence of the H_2O_2 initial concentration on the phenol conversion in the stirred reactor. $[HRP]_0$: $2.48 \cdot 10^{-3}$ mM, $[Phenol]_o$: 53.0 mM, pH 7 and temperature of 20ºC.

$[H_2O_2]_0$ (mM)	X_{Phenol} (%)
22	29
29	45
53	70
159	30
192	25

Exactly the same behaviour was observed for a phenol concentration of 16 mM (table 6.3), where an incremental relation of the phenol conversion respect to the H_2O_2 initial concentration. For the two largest H_2O_2 concentrations it was perceived only a small change in the conversion of phenol. Finally, the table 6.4 presents the results for an initial concentration of phenol of 53 mM. As it can be seen in the table, the tendency was similar to the one observed in table 6.1, where from a certain H_2O_2 concentration (192 mM), the conversion of phenol decreased.

Other experiments were also conducted for different initial concentrations of phenol and a fixed H_2O_2 initial concentration of 29 mM. These experiments are presented in table 6.5. Also, as it was expected, the phenol conversion decreased when the phenol initial concentration was high. Phenol conversions over 70% were reached with phenol initial concentrations lower than 16 mM, meanwhile, phenol conversion under 65% were obtained at higher initial concentrations of phenol.

Table 6.5. Influence of the Phenol initial concentration on the phenol conversion in the stirred reactor. $[HRP]_0$: $2.48 \cdot 10^{-3}$ mM, $[H_2O_2]_o$: 29.0 mM, pH 7 and temperature of 20ºC.

$[Phenol]_0$ (mM)	X_{Phenol} (%)
11.0	75
13.8	72
16.0	92
19.1	56
27.0	60
32.0	63
43.0	57
53.0	45

Tables 6.6 and 6.7 present the results of the phenol conversion conducted for an initial concentration of phenol of 11 mM and initial H_2O_2 concentrations of 10 mM and 29 mM, respectively. As expected, there was an increment in the phenol conversion due to the increment of the initial concentration of the HRP.

Table 6.6. Influence of the HRP initial concentration on the phenol conversion in the stirred reactor. $[H_2O_2]_0$: 10 mM, $[Phenol]_o$: 11.0 mM, pH 7 and temperature of 20ºC.

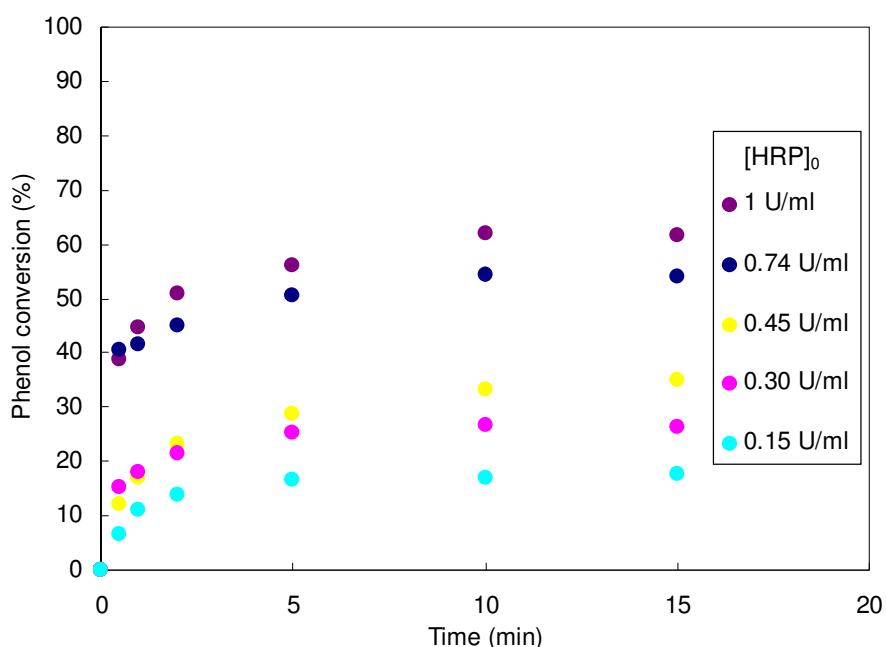| $[HRP]_0$ (mM)	X_{Phenol} (%)
$2.48 \cdot 10^{-3}$	69
$2.45 \cdot 10^{-4}$	15
$9.80 \cdot 10^{-5}$	6

Table 6.7. Influence of the HRP initial concentration on the phenol conversion in the stirred reactor. $[H_2O_2]_0$: 29 mM, $[Phenol]_o$: 11.0 mM, pH 7 and temperature of 20ºC.

$[HRP]_0$ (mM)	X_{Phenol} (%)
$4.90 \cdot 10^{-3}$	92
$2.48 \cdot 10^{-3}$	75
$2.45 \cdot 10^{-4}$	11
$9.80 \cdot 10^{-5}$	4

Nevertheless, a high initial concentration of H_2O_2 inhibited low concentrations of HRP and thus, decreased the phenol conversion. For high HRP concentrations, the concentration of H_2O_2 was not enough for inhibiting the enzyme.

A high degree of conversion was obtained for the enzymatic elimination of phenol in the stirred tank when the initial substrates concentrations were high, specially using small quantities of phenol (higher phenol/enzyme ratio).

Also, it can be observed that the enzyme-phenol ratio has an important influence on the reaction conversion percentage (between 50 and 100 %).

6.4. Kinetic model in the batch stirred reactor

The kinetic model described in section 5.4.3 was used in this analysis. This model was based in the Michaelis-Menten model with inhibition by substrate but integrate a new parameter to take

into account the effect of the phenol concentration on the initial reaction rate. The kinetic parameters of the enzymatic elimination obtained in the stirred batch reactor are shown in figures 6.9, 6.10 and 6.11 for initial phenol concentration of 0.5 mM, 1.1 mM and 1.6 mM respectively.
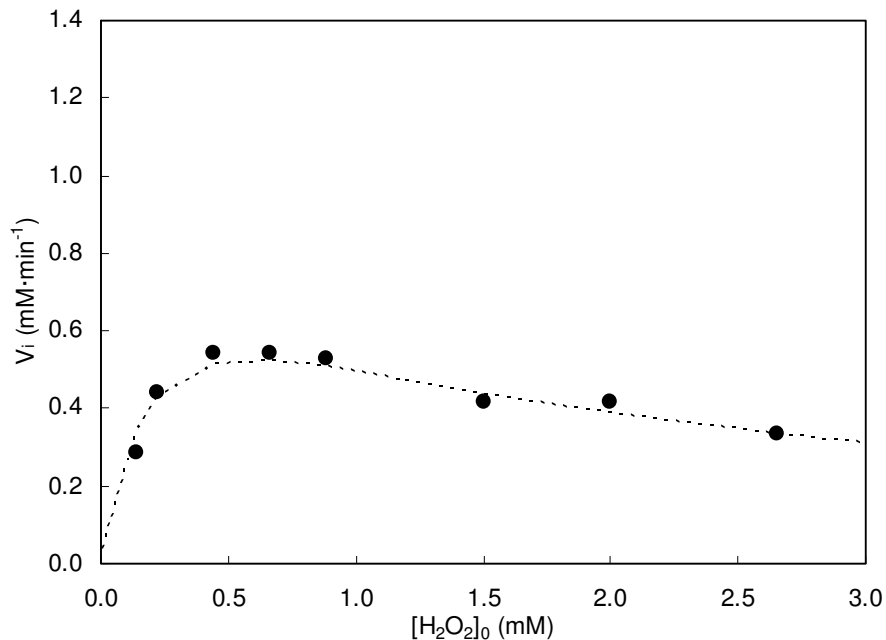
Figure 6.9.   Influence of the H_2O_2 initial concentration on the Steady-state initial rates of phenol oxidation in the stirred tank reactor. Fitting obtained by the modified Michaelis-Menten model with inhibition. [Phenol]$_0$: 0.5 mM, [HRP]: $2 \cdot 10^{-4}$ mM, pH 7 and temperature of 20ºC.
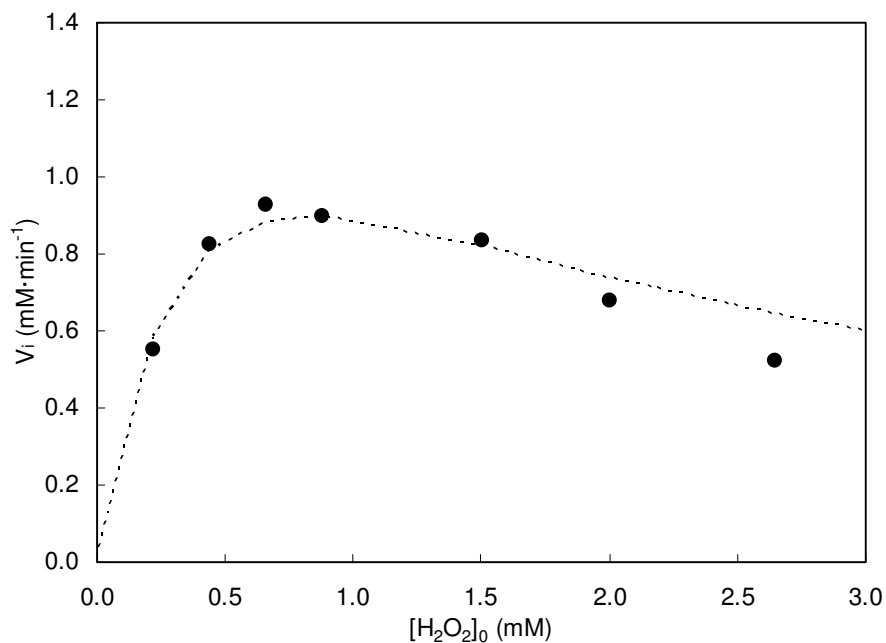
Figure 6.10.   Influence of the H_2O_2 initial concentration on the Steady-state initial rates of phenol oxidation in the stirred tank reactor. Fitting obtained by the modified Michaelis-Menten model with inhibition. [Phenol]$_0$: 1.1 mM, [HRP]: $2 \cdot 10^{-4}$ mM, pH 7 and temperature of 20ºC.
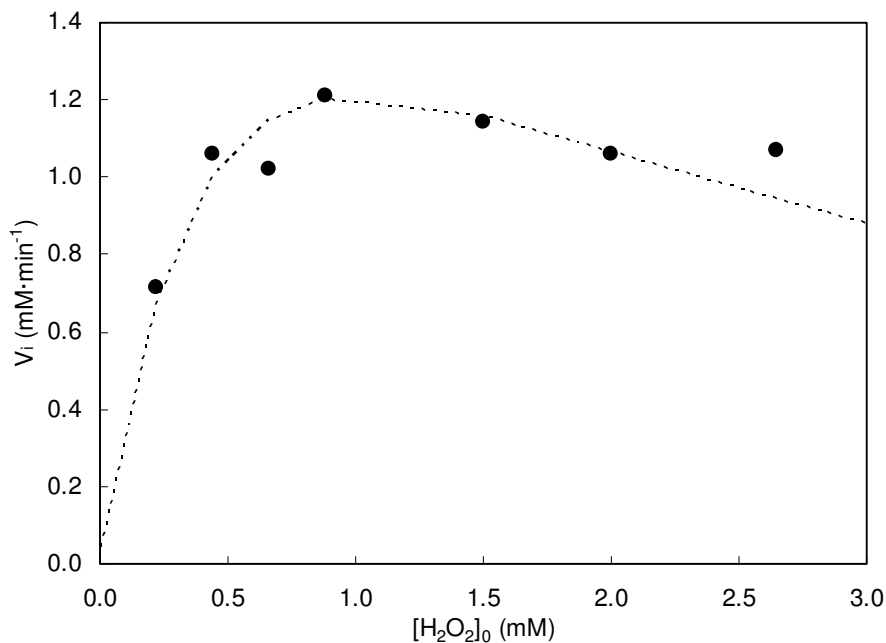
Figure 6.11. Influence of the H_2O_2 initial concentration on the Steady-state initial rates of phenol oxidation in the stirred tank reactor. Fitting obtained by the modified Michaelis-Menten model with inhibition. $[Phenol]_0$: 1.6 mM, [HRP]: $2\cdot10^{-4}$ mM, pH 7 and temperature of 20ºC.

The calculated values of the fitted parameters for different phenol concentrations are presented in table 6.8.

Table 6.8. Apparent parameters for the reaction of HRP with inhibition by Phenol and H_2O_2.

V_{max} (min^{-1})	K_m (mM)	K (*)	K' (mM^{-1})
1.76	0.01	0.41	0.65

* dimensionless

6.5. Conclusions

The optimal initial concentration of H_2O_2 to obtain the highest phenol conversion seemed to be the ratio 1:1 between phenol and H_2O_2, exactly the same ratio obtained with the torus reactor. Nevertheless, the conversion of phenol was always higher in the torus reactor respect to the stirred reactor for the phenol initial concentrations of 0.5 and 1.1 mM. The only difference between both reactors has been the extent of the elimination, always higher for the torus reactor in the tested conditions. Finally, to achieve the study of comparison of the performances of both reactors, the initial reaction rates were analysed in the stirred reactor. The reaction rates rose at the time that the initial phenol initial concentration increased. However, the absolute values of the initial reaction rates are lower than the obtained in the torus reactor, suggesting that the mixing in the torus reactor is better than in the stirred reactor.

Chapter 7. Optimisation of the process in the torus reactor: Influence of temperature, pH and ionic strength

In this chapter, the influence of the temperature, pH and ionic strength on the removal efficiency of phenol are analysed. The experimental conditions and the main results obtained are presented.

7.1. Experimental conditions

All experiments were carried out in batch conditions in the torus reactor. The reaction was initiated by adding the H_2O_2 to the reaction solution. The initial H_2O_2 concentration chosen is resulted of the previous work (analysed in section 5.1), where the optimal H_2O_2 concentration was found to be an equimolar relationship between initial H_2O_2 and phenol concentrations. The enzyme concentration was kept at a low value to slow down the reaction allowing for a better assessment of the initial reaction rate.

For the analytical procedure, in all experiments seven liquid samples (1 ml) were withdrawn at 30 s, 1, 2, 4, 6, 10 and 15 min. The reaction was stopped by the addition of 1 ml of an acetonitrile solution to the sample. Then the samples were centrifuged and analysed by HPLC.

These are common conditions to all the experiments. Specific conditions for each particular study are given in the correspondent section.

7.2. Influence of the temperature on the phenol removal

The effect of the temperature on the reaction was analysed. To study the influence of the temperature, the reaction solution containing 1.1 mM of phenol (100 mg·l^{-1}) and 2·10^{-4} mM of HRP solution was introduced into the reactor and heated until the desired temperature 10, 20, 30, 40, 50 or 60ºC. Phenol polymerizing reactions were started with the addition of the exact quantity of hydrogen peroxide into the reactor to have an initial concentration of 0.082mM. In all cases the reaction time was 15 min.

The influence of the temperature on the reaction can be observed in figure 7.1. In this case, for 1.1 mM of phenol and 0.882 mM of H_2O_2, the reaction was carried out at 10, 20, 30, 40, 50 and 60ºC.

In all experiments, the solution turned dark brown immediately after the addition of H_2O_2 signifying the polymer formation. The phenol removal efficiency reached always its maximum value after two minutes.
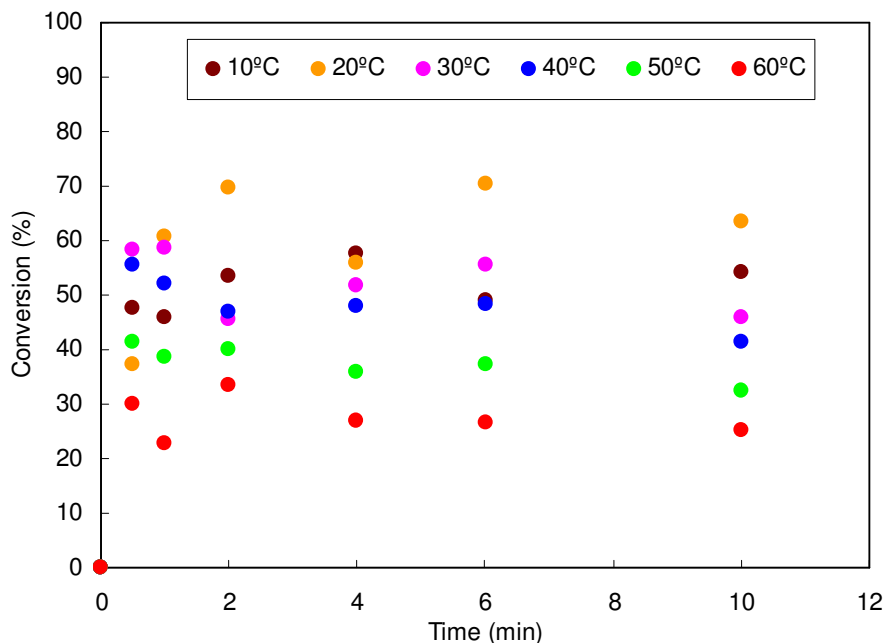
Figure 7.1.   Influence of the initial temperature on the phenol conversion in the torus reactor. $[Phenol]_0$: 1.1 mM, $[HRP]_0$: $2 \cdot 10^{-4}$ mM, $[H_2O_2]_0$: 0.882 mM and pH 6.6.

Table 7.1 presents the results of phenol removal efficacies at the studied temperatures. These values were calculated when the phenol concentration became stable (less than 3% in the variation of the phenol concentration).

Table 7.1. Phenol removal efficiency as a function of the reaction temperature.

Temperature	Phenol removal efficiency	Relative removal efficiency
10ºC	54 %	83 %
20ºC	65 %	100 %
30ºC	50 %	77 %
40ºC	46 %	71 %
50ºC	36 %	56 %
60ºC	28 %	43 %

As it can be seen in the table, the maximum phenol removal efficiency was reached at 20ºC (65 %). At a lower temperature (10ºC) the conversion was an acceptable 54 %. The diminution of the temperature did not affect greatly the activity of the HRP as published by Nicell et al (1992). They have shown that HRP can exhibit activity above 5ºC. On the other hand, an augment of the temperature provoked a constant diminution of the phenol conversion. At 60ºC, the conversion achieved was only 28 % with a relative phenol removal efficiency of 43 %. These results are in agreement with other studies (Nicell 1992) where it was stipulated that the enzyme was rapidly inactivated at temperatures above 45ºC. In the work of Nicell et al. (1992),

they have shown that the number of turnovers of HRP decreased from 9300 in the range of 5ºC to 4100 at 65ºC. Therefore, more than twice the HRP was required to precipitate the same amount of 4-chlorophenol at 65ºC as at 35ºC. This effect was also observed by Bodalo et al. (2006) between 25 and 40ºC but with less difference. They have shown only a little effect on the maximum elimination between this range of temperature. This fact can be considered advantageous because it will not be necessary to control exhaustively the temperature as normally occurs in enzymatic systems where temperature is a critical variable.

Only few researches have studied the influence of the temperature on the conversion of phenol (Nicell 1992, Masuda 2001, Song 2003) and they have suggested that the removal efficiency decreases with an increase in the reaction temperature as it was obtained in this work.

Figure 7.2 presents the values of the initial reaction rates at the different temperatures. As it can be seen in the figure, the maximum rate was obtained at 20ºC, confirming the best values of phenol conversion. Increasing the temperature, the rate decreased slowly until 40ºC. At higher temperatures the values diminished fastly exhibiting a high enzyme inactivation. These results are in agreement with those obtained by Nicell et al. (1992). At these high temperatures, significant phenol removal is possible but with an increase of the initial concentration of the enzyme that implies also an increase of the cost of the process.
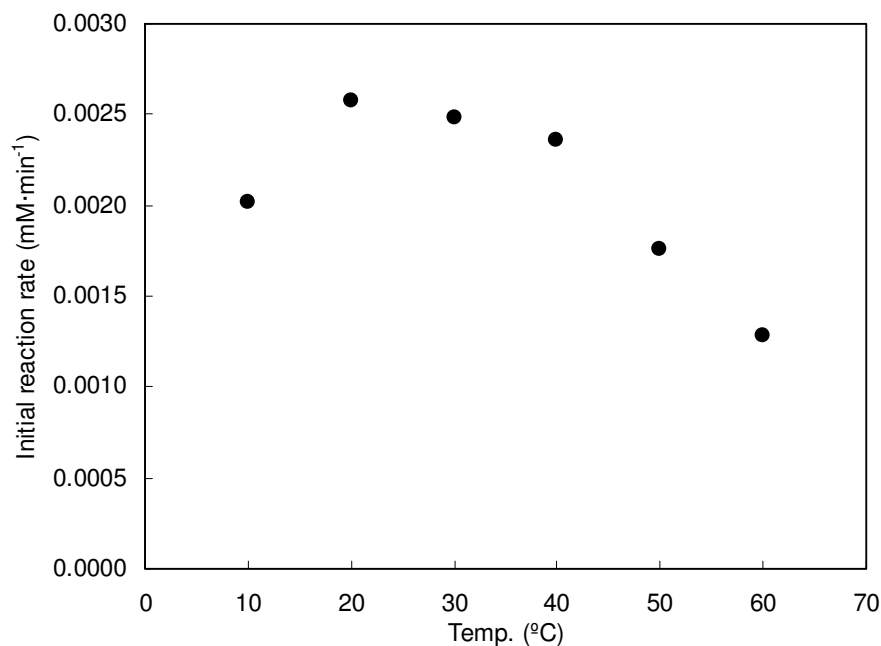
Figure 7.2.   Influence of the initial temperature on the Steady-state initial rates of phenol oxidation in the torus reactor. $[Phenol]_0$: 1.1 mM, [HRP]: $2 \cdot 10^{-4}$ mM, $[H_2O_2]_0$: 0.882 mM and pH 6.6.

7.3. Influence of the pH

Phenol removal efficiency as a function of pH was studied in the range of 2.7-10.9. The buffers were prepared as follows: buffer A (pH=2.7), 1.201 g of acetic acid and 0.360 g of sodium chloride were dissolved in 200 ml of deionised water; buffer B (pH=7.4), 0.120 g of hydrogenophosphate of disodium dihydrated and 0.745 g of sodium chloride were dissolved in 100 ml of deionised water and then the pH was adjusted to 7.4 with sodium hydroxide (0.05N) and chlorhydric acid (0.1N); buffer C (pH=7.7), 0.120 g of hydrogenophosphate of disodium dihydrated and 0.759 g of sodium chloride were dissolved in 100 ml of deionised water and then the pH was adjusted to 7.4 with chlorhydric acid (0.1N); buffer D (pH=8.4), 0.120 g of hydrogenophosphate of disodium dihydrated and 0.745 g of sodium chloride were dissolved in 100 ml of deionised water and then the pH was adjusted to 7.4 with sodium hydroxide (0.05N) and chlorhydric acid (0.1N); buffer E (pH=9.5), 0.67 g of sodium phosphate dibasic were dissolved in 250 ml of deionised water and then the pH is adjusted to 9.5 using sodium hydroxide (0.1N); buffer F (pH=10.9) was prepared in the same way that buffer E but adjusting the pH to 10.8 with sodium hydroxide (0.1N). The initial phenol concentration was 1.1 mM (100 mg·l^{-1}) and the initial H_2O_2 concentration of 1.5 mM. The concentration of HRP was kept to $2 \cdot 10^{-4}$ mM. In all experiments, the HRP dissolution was added to the phenol dissolution buffered or not. When the operating temperature is reached, T=20ºC, the hydrogen peroxide is added and the reaction is started.

To examine the impact of the initial pH on phenol removal, the reactions were performed with a solution of an initial concentration of phenol of 1.1 mM (100 mg·l^{-1}) and an initial concentration of HRP of $2 \cdot 10^{-4}$ mM (1 U·ml^{-1}). The temperature was always 20ºC while the initial pH examined was in the range from 2.7 to 10.9. The reaction was started by the addition of the exact quantity of H_2O_2 to attain a concentration of 1.496 mM in solution. The colour of the reaction solution turned instantly after the addition of the peroxide, but its intensity depended of the initial pH checked. In some experiments it was possible to see directly the formation of small particles indicating the presence of insoluble polymers, moreover, the size of the polymers was unequivocally depending of the initial pH. The results of the phenol removal as a function of the pH value can be seen in figure 7.3.
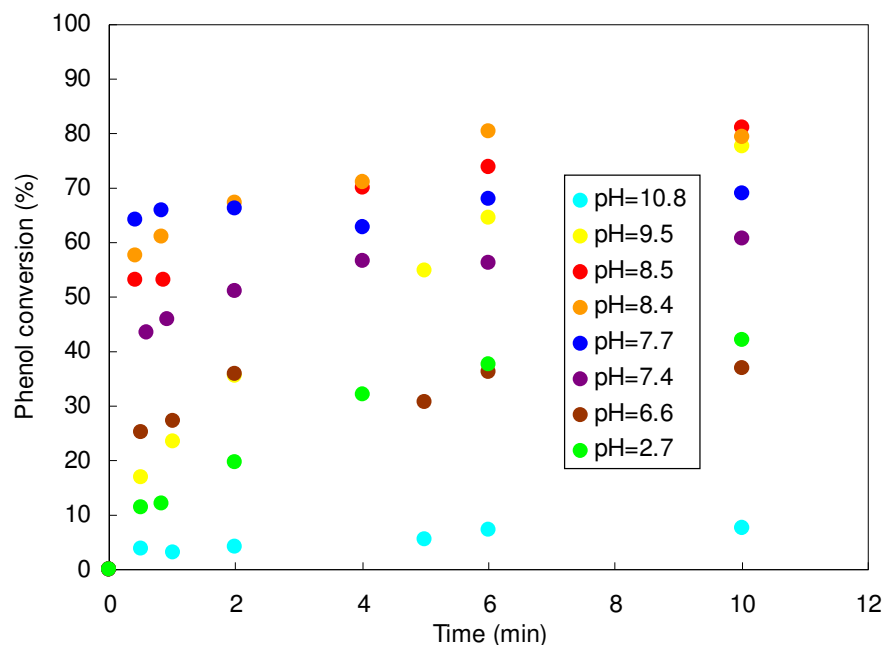
Figure 7.3.   Influence of the pH on the phenol conversion in the torus reactor. [Phenol]$_0$: 1.1 mM, [HRP]$_0$: 2•10^{-4} mM, [H$_2$O$_2$]$_0$: 0.882 mM and temperature of 20ºC.

Table 7.2 presents the results of phenol removal efficacies at the different initial pH after 6 minutes of reaction. These values were also calculated when the phenol concentration became steady (less than 3% in the variation of the phenol concentration). As it can be seen in the table, the phenol removal efficiency increased as the initial pH value is augmented until the optimum value of pH is reached (8.4) where 80% of phenol conversion was attained. After this value, the phenol conversion decreased firstly slowly (64% at a pH of 9.5) and drastically, less than 7% at a pH of 10.9. All the curves showed a similar behaviour except for the experiment without buffer, experiment at an initial pH of 6.6 provoked by the phenol initial concentration.

Table 7.2. Influence of the initial pH on the phenol removal efficiency.

Initial pH	Phenol removal efficiency	Relative removal efficiency
2.7	38 %	47 %
6.6	50 %	63 %
7.4	56 %	70 %
7.7	68 %	85 %
8.4	80 %	100 %
9.5	64 %	80 %
10.9	7 %	9 %

A good removal of phenol was obtained over the pH range of 7.4-9.5, with conversion values higher than 60% in all cases, the best result of phenol conversion being 80% for a pH of 8.4 after 6 minutes of reaction time. This trend was in agreement with the data obtained by Wu et

al. (1993). These authors have studied the influence of pH in a range form 4 to 10 for the same initial phenol and H_2O_2 concentration but with and without an additive (PEG). It was found that, in absence of an additive, a good removal of phenol was observed over the pH range from 6 to 9 with an optimum value at pH 8.5. In presence of PEG, the optimum value of pH for the removal of phenol was shifted from 8.5 to 8.

These results were also consistent with those reported by Nicell et al. (1992). They have tested three different phenolic compounds and, for all cases, HRP demonstrated some catalytic ability between pH' 4 and 10 but only accomplished good removal over the pH range of 6 to 9.

The Figure 7.4 presents the values of the initial reaction rates as a function of the initial pH values. As it can be observed in the figure, the initial reaction rate increased with the pH until to reach a maximum value for a pH of 7.7 and remained more or less constant although the pH of 8.4 where the maximum phenol conversion was obtained. After this value, the initial reaction rate decreased very fastly. As reported by Masuda et al. (2002), the electrostatic interactions might contribute to the adsorption of the enzyme on the precipitate provoking it inactivation and/or on the solubility of the products might depend on the initial value of the pH, and removal efficiency is improved drastically when the pH is changed.
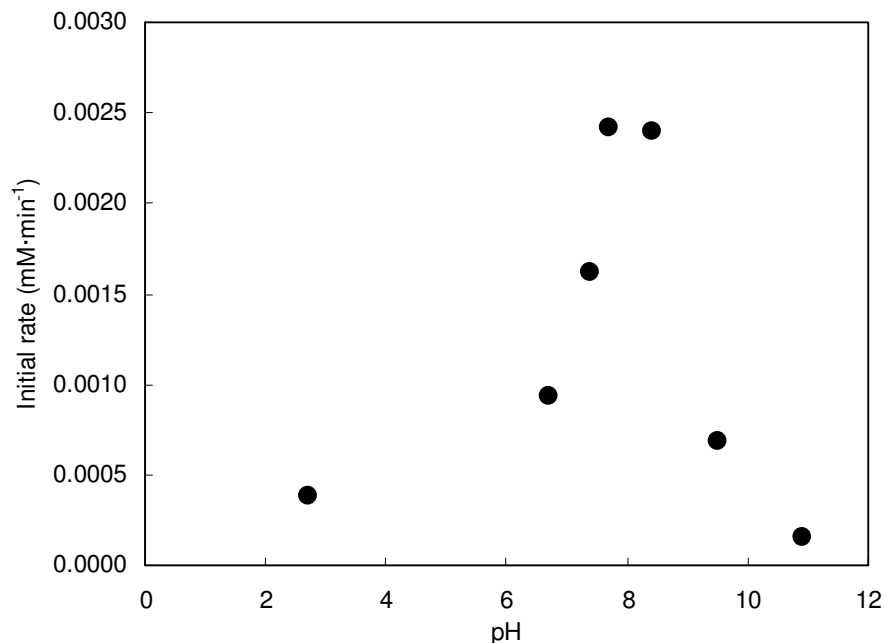
Figure 7.4.   Influence of the initial pH on the Steady-state initial rates of phenol oxidation in the torus reactor. [Phenol]$_0$: 1.1 mM, [HRP]: $2 \cdot 10^{-4}$ mM, [H$_2$O$_2$]$_0$: 1.5 mM and temperature of 20ºC.

On the other hand, table 7.3 presents the retention time distributions of the products obtained in the samples after 6 minutes. As it can be seen in table 7.3, three soluble products S_1, S_2 and S_3 were detected at a shorter retention time than the phenol for initial pH values of 2.7, 7.4 and 8.4. In the same way, three soluble products C_1, C_2 and C_3 were detected at a higher retention time than the phenol and only at an initial pH of 2.7. This arrangement of groups was selected in

function of the retention time. S represents products with lower retention time than phenol and C compounds with higher ones.

For the other experiments the possible products were not detected with the analytical procedure (only a few traces of the different studied compounds were observed). Some authors have demonstrated that the HRP phenol polymerisation can lead to the formation of dimers, trimers, and quinones as o-phenoxyphenol, p-phenoxyphenol, o,o'-biphenol, 2,4'-biphenol, p-p'-biphenol and others (Aitken 1994, Huixian 1994). In the present work, the reaction soluble products were analysed by HPLC and identified by their retention time as in the cited works. Obviously, this method did not permit identification nor a quantification of such products but it was possible to follow their presence by the existence of their different peaks in the chromatograms. Finally, other insoluble products are also formed throughout the polymerisation of the phenol and precipitated during the reaction. These products can be also dimers, trimers and polymers with higher molecular weights (Huixian 1994).

Table 7.3. Example of the reaction products formed during the enzymatic reaction of phenol.

				Retention time (min)				
pH	H_2O_2	S_1	S_2	S_3	Phenol[a]	C_1	C_2	C_3
all	2.01				5.27			
2.7	2.05	2.42	2.86	3.11	5.27	7.15	7.96	8.51
7.4	2.12			3.12	5.26			
8.4	2.02	2.38		3.16	5.15			

[a] Phenol retention time

The distribution of these reaction products seemed to be dependent on the pH of the reaction solution. In the case of a pH of 2.7, the lower tested, the higher quantity of soluble reaction products with shorter retention time than the phenol were produced while, products with higher retention time than phenol were also detected in this case. Nevertheless, the final phenol conversion at a pH of 2.7 is one of the lowest and the quantity of the reaction products the highest. When the value of pH is increased, just a few soluble products are detected in the samples. As it can be deduced, the precipitate formation depends of the pH of the reaction.

The results may indicate that the adsorption of HRP on the insoluble reaction products was enhanced at low pH values. It is known that phenol self-coupling reactions resulted primarily in polymeric phenolic products like benzenes linked by ether or C-C bonds bearing multiple phenolic groups (Wu 1999, Huixian 1994). The pH-dependent behaviour observed experimentally suggested that a fraction of the phenolic sites present on the products may be dissociable around the neutral pH. This fact was consistent with a previous electrophoresis analysis conducted by Huang and Weber (2004). They have reported that the phenol coupling products are negatively charged and the protonation of the proton-disassociated sites was able to reduce the ionic character of the products and increased the tendency to precipitate.

7.4. Influence of the ionic strength

To examine the power of the ionic strength on the phenol elimination, three additional reactions were performed with an initial concentration of phenol of 1.1 mM (100 mg·l^{-1}) and an initial concentration of HRP of 2·10^{-4} mM (1 U·ml^{-1}). Sodium chloride was added to the solutions to attain the concentrations of 30, 180 and 480 mM of NaCl, giving ionic strengths of 0.05, 0.20 and 0.50 respectively while the experiment without salt addition had an ionic strength of 0.02. The temperature and the initial pH were always 20ºC and 6.6 respectively. The buffer was prepared weighting 0.6 g of hydrogenphosphate of sodium and adding 500 ml of deionised water. The reaction was initiated by the addition of the correct quantity of H_2O_2 to reach a concentration of 1.5 mM in solution. When the operating temperature is reached, T=20ºC, the hydrogen peroxide is added and the reaction started. The colour of the reaction solution turned instantly after the addition of the peroxide. The figure 7.5 presents the phenol removal efficiency with time for the different ionic strength studied.
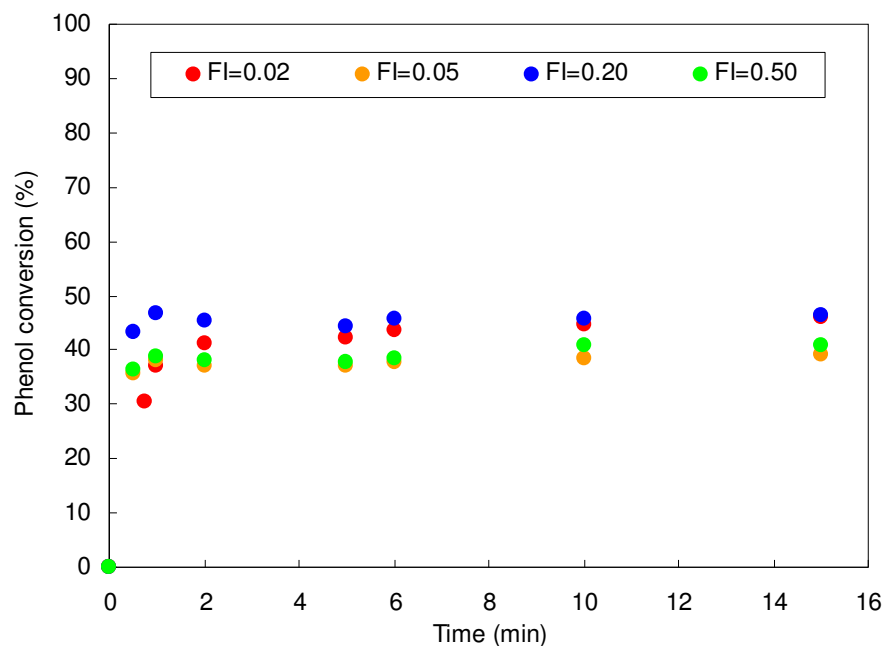
Figure 7.5.   Influence of the initial ionic strength on the phenol conversion in the torus reactor. [Phenol]$_0$: 1.1 mM, [HRP]$_0$: 2•10^{-4} mM, [H_2O_2]$_0$: 0.882 mM, pH 6.6 and temperature of 20ºC.

It was possible to observe experimentally, that the amount of precipitated products increased significantly when the salt concentration was augmented, indicating that some soluble products of reaction became insoluble. This fact was also observed by Huang et al. (2004), showing that if the ionic strength is augmented, various dissolved reaction products turned out to be further precipitable.

Table 7.4 presents the data of the influence of the ionic strength on the phenol conversion. As it can be seen in the table, the phenol removal was practically not influenced by the salt concentration. A final conversion of 40-45% was obtained in all cases.

Table 7.4. Influence of the ionic strength on the phenol removal efficiency.

Initial ionic strength	Phenol removal efficiency	Relative removal efficiency
0.02	46 %	100 %
0.05	39 %	85 %
0.20	46 %	100 %
0.50	41 %	89 %

The Figure 7.6 presents the values of the initial reaction rates as a function of the ionic strength. As it can be observed in the figure, the reaction rate was influenced by the sodium chloride concentration. When the salt concentration increased, the initial reaction rate augmented from $0.8 \cdot 10^{-3}$ $M \cdot min^{-1}$ without salt addition until a maximum value of $2.0 \cdot 10^{-3}$ $M \cdot min^{-1}$ for an ionic strength of 0.20. After this value the initial rate decreased with a further augmentation of salt that signified none additional benefit for the process.
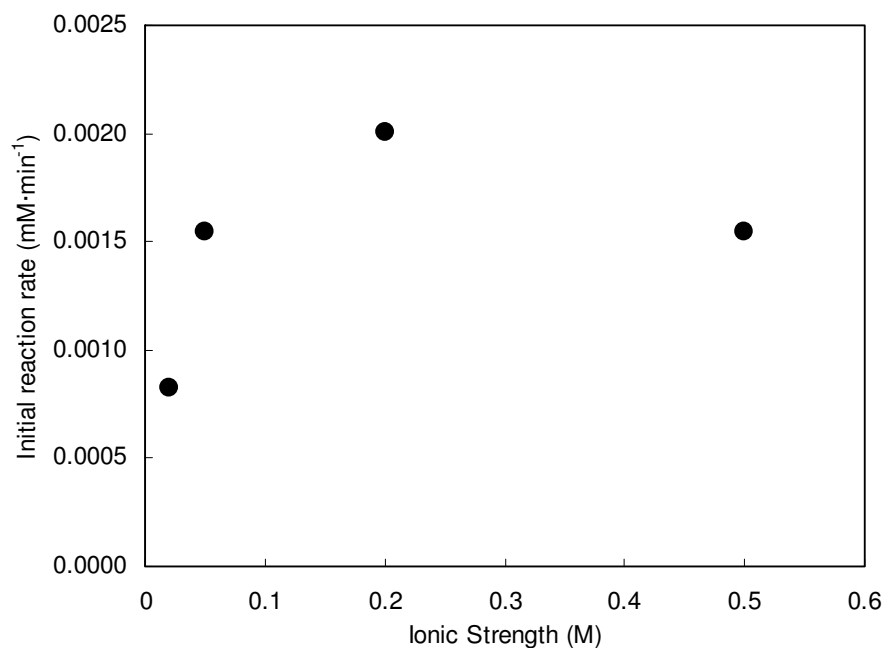
Figure 7.6. Influence of the initial ionic strength on the Steady-state initial rates of phenol oxidation in the torus reactor. $[Phenol]_0$: 1.1 mM, [HRP]: $2 \cdot 10^{-4}$ mM, $[H_2O_2]_0$: 1.5 mM, pH 6.6 and temperature of 20ºC.

7.5. Conclusions

The best operating conditions for the enzymatic elimination reaction, temperature, initial pH and ionic strength were determined. The optimum temperature to carry out the experiments was 20ºC with a phenol conversion of 65%. A lower o higher temperature of 20ºC allowed a relative removal efficiency of 83 and 77% respectively. The most favourable pH was of 8.4 with a phenol conversion of 80%. Highest initial reaction rate was obtained for this pH value. The use

of added salt contributed to increase the initial reaction rate but had no any significant influence on the final phenol conversion. In this case, a higher level of products precipitation was noted.

Chapter 8. Elimination of phenol with immobilised enzyme

This chapter describes a new method for the covalent immobilisation of the HRP on Eupergit C. In order to design a productive horseradish peroxidase system for the enzymatic elimination of the phenol, three different approaches for the covalent immobilisation of the enzyme were explored: a direct HRP binding to the polymers via their oxirane groups, a HRP binding to the polymers via spacer made from adipic dihydrazide and the HRP binding to amino-reactive polymer surfaces through the enzyme carbohydrate moiety previously modified by periodate oxidation.

8.1. Immobilisation of the HRP by oxirane groups

One of the most used methods to immobilise enzymes on Eupergit supports involves the direct binding of the enzyme onto the polymers via the oxirane groups. The oxirane functional group is a subset of organic cyclic ether compounds. Cyclic refers to the fact that the oxirane atoms (two atoms of carbons and an oxygen in a three-membered ring) and "ether" that indicates that there is a carbon-oxygen-carbon bonding arrangement.

In this case, 50 mg of unmodified Eupergit C was incubated with different amounts of the native HRP solution in 0.1 M of sodium phosphate buffer (pH 7.4) at 4 ºC. The effect of the amount of enzyme mixed with the Eupergit support was studied and the activity of the immobilised enzyme was used as parameter to compare. The amount of enzyme was ranged between 0.44-5.28 mg. In each experiment, several samples were taken consecutively in order to determine the variations of the enzyme activity in the supernatant solution. The immobilisation will be stopped when the activity of the enzyme in the supernatant solution will be constant. An example of the results obtained with this method of immobilisation is shown in figure 8.1.

As it can be seen in the figure, the activity of the enzyme diminish from 166 U·ml^{-1}, value of the activity of the free enzyme, to more or less 140 U·ml^{-1}. Almost all the linked enzymatic activity was coupled before the first three hours of experimentation and it will not be necessary to maintain the procedure of immobilisation.

After the time of incubation, in this case 24 h, the beads were washed with demineralised water and with a sodium phosphate buffer. Then, the immobilised enzyme was collected and stored in sodium a phosphate buffer at a pH of 7.4. The activity of the HRP immobilised onto Eupergit was determined for each immobilisation.

Figure 8.1.   Influence of the extent of the immobilisation on the enzymatic activity of the loading enzyme
solution by the method of the oxirane groups.

The figure 8.2 presents the influence of the quantity of enzyme in solution with the support on

the activity of the immobilised enzyme and on the yield of the activities of the coupled enzyme

over the initial activity.

Figure 8.2.   Influence of the quantity of enzyme loading on support on: (●) the activity of the immobilised
enzyme and, (O) the coupling yield of activity.

As it can be seen in the figure, the activity of the immobilised enzyme was not proportional to

the amount of the attached enzyme. Below 35 mg·g^{-1} of HRP loading on support, the activity of

the immobilised enzyme increased with the amounts of enzyme per gram of support. The

maximum activity of the immobilised enzyme (73 U·g^{-1}) was obtained when 17.6 mg of enzyme was loading per gram of support. However, after this value, the activity of the immobilised enzyme decreased. Also, the coupling yield of activity was decreasing with an increase in the amount of enzyme loading on the support. This fact indicated that, even though higher amounts of enzyme were available, they were not linked to the support.

8.2. Immobilisation of the HRP by adipic dihydrazide treatment

A second alternative method was studied for the HRP immobilisation by adipic dihydrazide pre-treatment of the support. In this case, the immobilisation procedure consisted of two main steps: the pre-treatment of the polymer beads with adipic dihydrazide (ADH) and after, the coupling of the enzyme to the polymers surface.

The ADH was chosen to conjugate the enzyme because the hydrazide groups of the ADH offer several advantages over simple amino compounds (O'Shannessy 1987 and King 1986). The main benefit is the product of the reaction of a hydrazide and an aldehyde in neutral and acidic pH: a hydrazone linkage. This functional link is stable and does not require reduction with cyanoborohydride thereby circumventing one of the reactions associated with labelling with amino compounds.

The activation of the acrylic particles of the Eupergit was carried out with 0.1 M of Adipic dihydrazide solution in phosphate buffer for 4 h at room temperature at pH 7.4 and slow shaking. In all experiments, 3 ml of the adipic dihydrazide solution was added to 50 mg of the solid beads. After that, the polymers were washed several times with water and phosphate buffer.

Activated polymers were then incubated with different amounts of native horseradish peroxidase solution in 0.1 M of sodium phosphate buffer at pH 7.4 and 4 ºC for 24 h under slow shaking. Several samples of supernatant enzyme solution were taken over time in order to determine the variations of the enzymatic activity in the solution. An example of the obtained results using this method of immobilisation is shown in figure 8.3.

As it can be seen in the figure, almost all the linked enzymatic activity was coupled in the first sixteen hours of experimentation. Unlike the previous immobilisation method (3 hours of coupling time), the immobilisation method using ADH took 16 hours for the same purpose. This difference can be explained as the extra time used by the enzyme to get attached to a more specific binder that will also suppose an improvement in the immobilised activity. After the binding, the support was washed with water and sodium phosphate buffer, pH 7.4 and stored in this buffer at 4 ºC until use.

Chapter 8. Elimination of phenol with immobilised enzyme
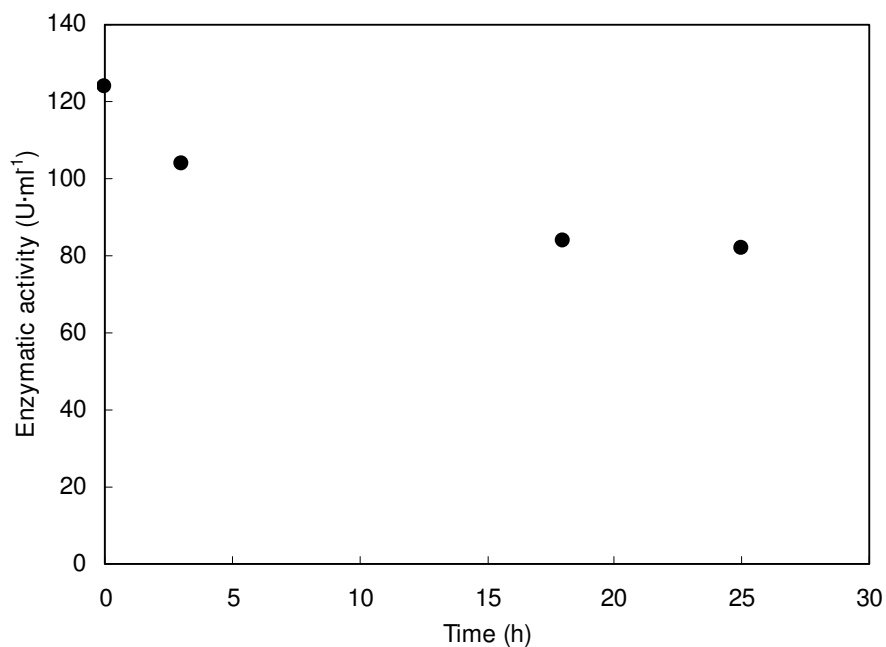
Figure 8.3.   Influence of the extent of the immobilisation on the enzymatic activity of the loading enzyme solution by the method with adipic dihydrazide.

The effect of different amounts of enzyme loading to the Eupergit support on the immobilised enzyme activity was studied in the range of 0.44-3.52 mg of HRP. The activity of the obtained immobilised enzyme-Eupergit was determined in each experiment. Using this immobilisation technique by the treatment with adipic dihydrazide, the main results obtained are shown in figure 8.4.
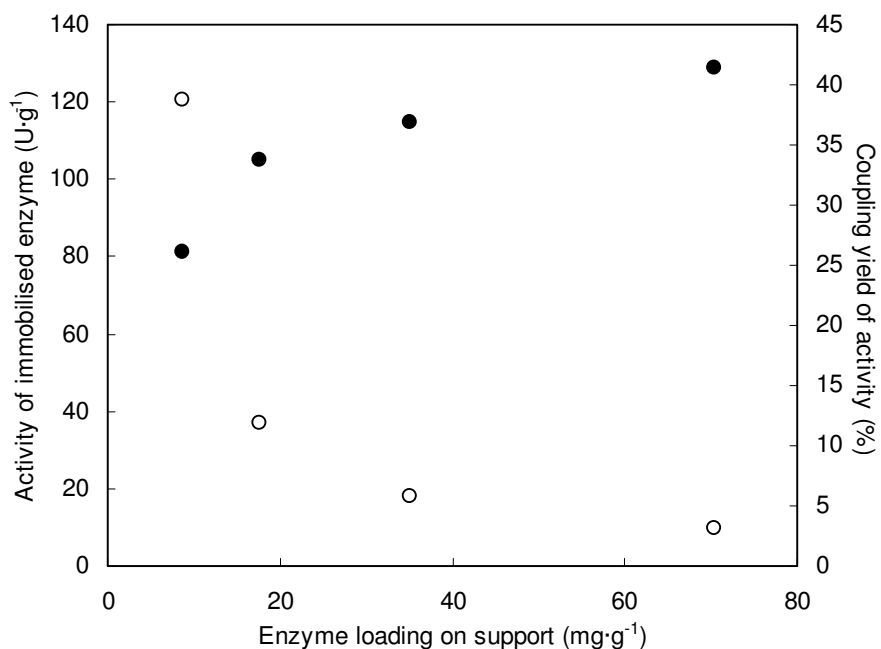
Figure 8.4.   Influence of the quantity of enzyme loading on support on: (●) the activity of the immobilised enzyme and, (O) the coupling yield of activity. Immobilisation method with ADH.

As it can be seen in the figure, the enzymatic activity of the immobilised enzyme increased with an increase in the enzyme loading on the support. Also in this immobilisation method, a fast diminution was obtained for the coupling yield of the activity.

The maximum enzymatic activity of the immobilised enzyme was found to be 128 $U \cdot g^{-1}$ using the immobilisation method of HRP by treatment with ADH.

8.3. The immobilisation of the HRP by the periodate method

8.3.1. Classical method

Finally, the periodate method was also evaluated for the covalent immobilisation of HRP. The immobilisation procedure consisted on three main steps: oxidation of the horseradish peroxidase by sodium periodate, the polymer pre-treatment with adipic dihydrazide and the coupling of the oxidised enzyme to the amino-Eupergit support. A schematic illustration of this method is shown in figure 8.5.
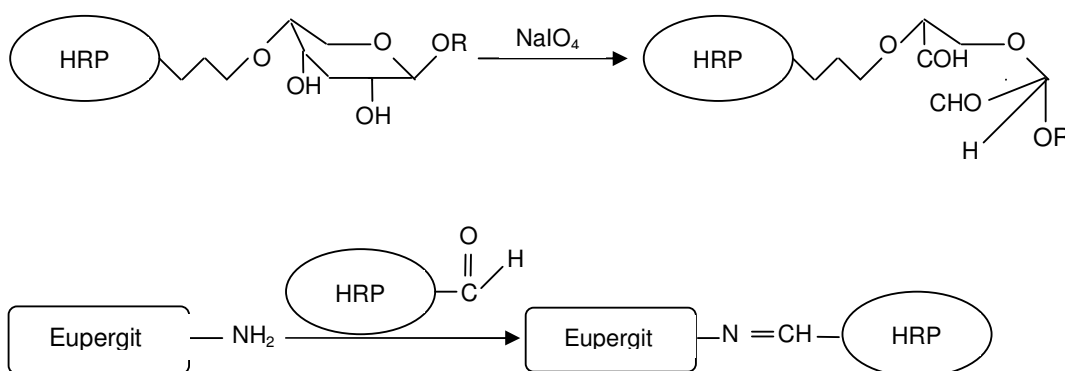
Figure 8.5. Schematic illustration of the covalent method for the HRP immobilisation on Eupergit support.

The periodate reaction was chosen because of the absence of reactions in the lateral chains, its high yield of formation of aldehyde groups and the fact that it can be carried out in aqueous solution at or near neutral pH.

A possible side-effect of the sodium periodate treatment is the oxidation of some amino acids which may alter the conformation of the protein molecules. The oxidation of amino acids with periodate appears to be a problem only under conditions of extensive oxidation (room temperature for several hours and a very high concentration of periodate).

The necessary conditions for the optimal periodate oxidation of the HRP were investigated by Kurstak et al. (1988). In their investigations, 4 to 8 mM was found to be the optimum concentration range.

The oxidation of the HRP was initiated by mixing 10 ml of the stock sodium metaperiodate and 10 ml of the stock enzyme. The reaction mixture was incubated for 2 h at room temperature in complete darkness. Excess periodate was destroyed with the addition of 0.1 ml of ethylene glycol and incubation for 20 minutes at room temperature in complete darkness.

The resulting oxidised HRP was isolated by the use of a dialysis membrane to remove other molecules in solution after the enzyme modification. The solution, containing the enzyme and other molecules, was placed into a semipermeable dialysis bag, such a cellulose membrane with pores, and sealed. The dialysis tube used was 18/32'' with a molecular weight cut-off (MWCO) of 12000-14000 Da.

The sealed bag was introduced in a container and the dialysis was carried out against 0.1 M phosphate buffer, pH 7.4 for 4 h. Molecules small enough to pass through the tube (water, salt and small molecules) tended to move into or out of the dialysis bag, in the direction of decreasing concentration. Larger molecules such as the enzyme that have dimensions greater than the pore diameter were retained inside the dialysis bag.

The concentrations of the oxidised enzyme before and after the dialysis process were checked by spectrophotometric analysis, and the activity test was conducted.

The Eupergit C (50mg) support was conjugated with 0.1 M of Adipic Dihydrazide in 0.1 M phosphate buffer (pH 7.4). The support and the ADH were incubated for 4 h at room temperature. Then the support was washed several times with water and sodium phosphate buffer.

Finally, the oxidised enzyme was conjugated with the support in 0.1 M sodium phosphate buffer at pH 7.4, for 24 h at 4ºC and slow shaking. The concentration and activity tests were conducted.

At the periodate concentration used, with a 2 h reaction period, the specific activity of the oxidised enzyme was almost the same as the original (specific activity of oxidised and original enzymes were 124 and 166 U·mg^{-1}, respectively).

The effect of the enzyme loading on immobilised enzyme activity was studied by varying the amount of the HRP offered (0.22-2.64 mg of HRP) to a fixed amount of supports (50 mg). Samples of the enzyme solution were taken before and after the immobilisation for the activity assay. An example of the results obtained using this method of immobilisation is shown in figure 8.6.

As it can be seen in the figure, the entire free enzyme was coupled after 24 hours. This time is comparable with the 16 hours that were necessary for the immobilisation of the HRP on the ADH pre-treated support. The use of specific binders increased the needed time for the immobilisation of the enzyme on the support, but also supposed an improvement in the immobilised activity.
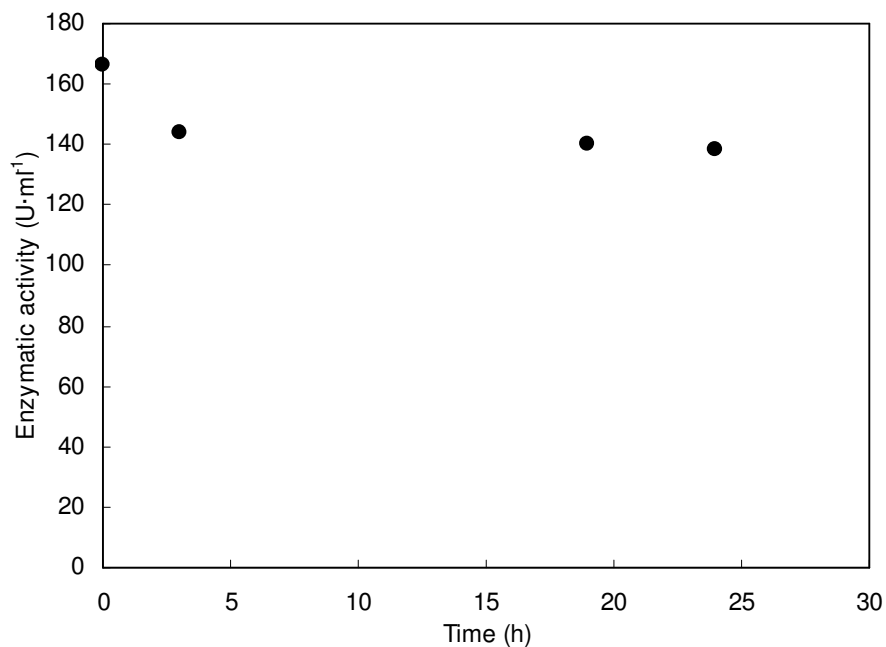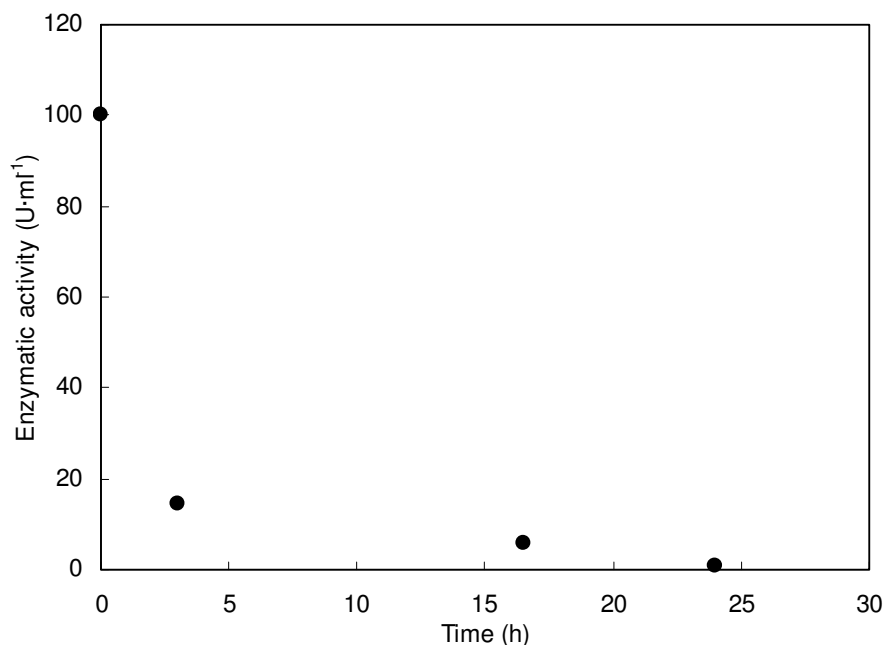
Figure 8.6.   Influence of the extent of the immobilisation on the enzymatic activity of the loading enzyme solution by the periodate method.

In order to obtain an industrial feasible biocatalyst and trying to obtain an immobilised enzyme with higher enzymatic activity, the immobilisation method by periodate was optimised. The influence of the amount of HRP in the attachment solution was analysed. The study was carried out in the range of 0.22-2.64 mg of the total protein loading on the amino-Eupergit. In each experiment, 50 mg of modified polymer particles were immersed in a certain volume of enzyme solution. The aim was to determine an efficient relationship between the enzyme and the support. The figure 8.7 shows the enzyme loading along with the enzyme coupling yield on the support tested.

It is seen in the figure that the enzyme loading increased as the HRP amount was increased. The enzyme coupling yield was in the range of 38 to 99 %. However, it can be noticed from the figure that the activity yield was not proportionally to the amount of enzyme bound. After a certain value of enzyme loading on support, the activity yield did not show an increase possibly due to the close packing of the enzyme on the support surface, which could limit the access of substrates needed in the hydrolysis reaction.

It was known that the catalytic efficiency of immobilisation processes decreased when enzyme loading exceeded a certain value and an optimum activity should be selected (Al-Duri 2000). Using the periodate method as enzyme immobilisation technique, the maximum value of enzymatic activity was found to be 126 $U \cdot g^{-1}$. This value of enzymatic activity was very close to the one obtained using the immobilisation method by adipic dihydrazide (128 $U \cdot g^{-1}$). The loading of 17.6 $mg \cdot g^{-1}$ (or 0.88 mg of enzyme loading in 50 mg of Eupergit support) seemed to be most appropriate for use, resulting in a rather high activity yield.
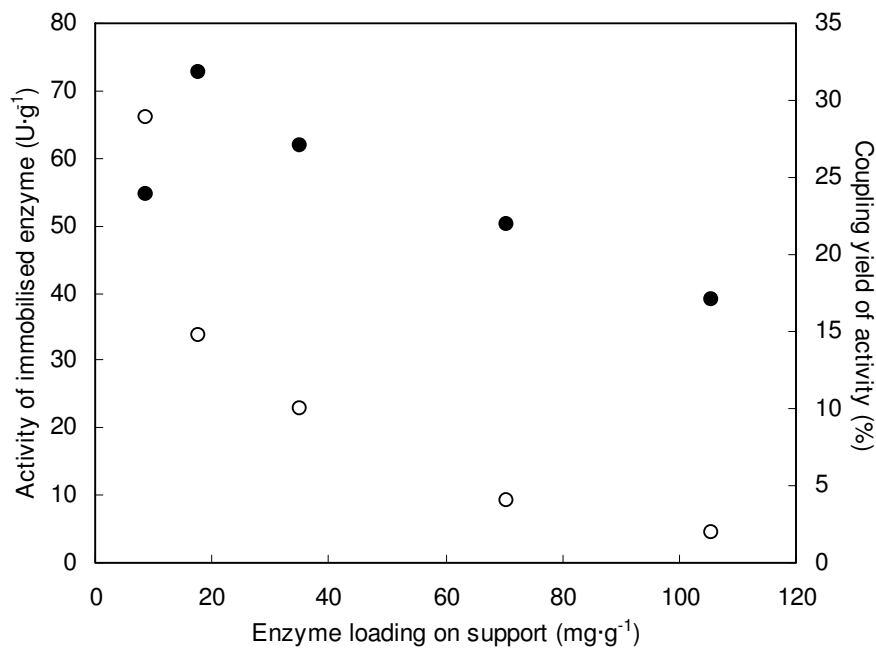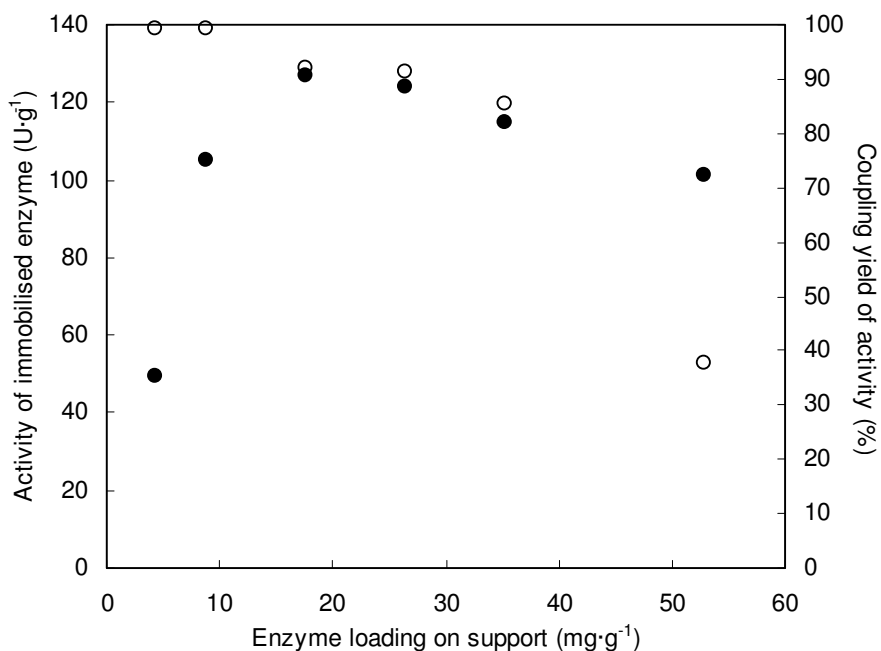
Figure 8.7.   Influence of the quantity of enzyme loading on support on: (●) the activity of the immobilised enzyme and, (O) the coupling yield of activity. Immobilisation method by periodate treatment.

8.3.2. Optimisation of the ADH concentration in the periodate treatment

The effect of the ADH amount on activity retention was studied. Different ADH amounts ranging from 0.1-0.9 mmol were used for immobilising HRP to Eupergit by the periodate method. The effect of the ADH concentration is illustrated in table 8.1. As it can be observed in the table, an increase in the ADH concentration provoked an augment in the amount of enzyme covalently attached to the matrix. At low concentrations of ADH seemed to be a smaller number of bonds formed between enzyme and the support. Hence, a lower enzymatic activity of the immobilised enzyme was obtained. As the concentration of ADH increased, more enzyme molecules were covalently bound to the support through the bonds between the amino groups of Eupergit and the groups of the enzyme. Moreover, when the concentration was increased further, a decrease in the enzymatic activity of the immobilised enzyme was observed may be due to the non-specific activation of the groups. Therefore, the optimum value of ADH to obtain a high enzymatic activity in the immobilised enzyme was found to be 0.3 mmol.

Table 8.1. Effect of the ADH concentration on the enzymatic activity for the immobilisation method by periodate.

ADH (mmol)	Enzyme loading ($mg_{enzyme}/g_{support}$)	Enzyme activity ($U \cdot ml^{-1}$)	Coupling yield (%)
0.1	26.4	31.95	96.09
0.2	26.4	31.99	94.80
0.3	26.4	113.48	91.30
0.5	26.4	48.84	84.30
0.9	26.4	59.29	77.40

The effect of the incubation period on the activity was studied. The obtained data are shown in table 8.2. As it can be observed in the table, an optimum incubation period of 24 h was required for the maximum immobilisation of HRP on Eupergit.

Table 8.2. Effect of the incubation time on activity.

Incubation period (h)	Enzyme loading ($mg_{enzyme}/g_{support}$)	Enzyme activity ($U \cdot ml^{-1}$)	Coupling yield (%)
4	35.2	21.86	27.0
14	35.2	16.39	66.7
21	35.2	36.06	76.2
24	35.2	49.00	85.4
28	35.2	44.00	80.0

8.4. Determination of the activity of the immobilised HRP

The activity of the immobilised HRP has been determined in both stirred and torus reactors. To do this, the removal of phenol was studied for different initial concentrations of HRP, from 0.001 U/ml to 0.006 U/ml, for a phenol initial concentration of 0.5 mM and finally, for a H_2O_2 initial concentration of 0.662 mM. The figure 8.8 presents the results of the conversion of phenol as a function of time obtained with the immobilised enzyme.

As it can be seen in the figure, the reaction realised in the 100 ml stirred reactor showed that it is possible to reach very high degrees of removal of phenol, around 92%, with the horseradish peroxidase immobilised on Eupergit. With the experimental conditions, 0.006 U/ml of the immobilised enzyme, the reaction took approximately 4 h to reach the final conversion of phenol of 92%. This value of phenol conversion was almost the same value that those obtained using free enzyme with a concentration of 1.0 U/ml. This fact seemed to indicate that the immobilisation process improved the enzymatic stability as it was predicable. Moreover, the immobilisation process appears to protect the enzyme from its inhibition by the products of reaction or by the substrates.
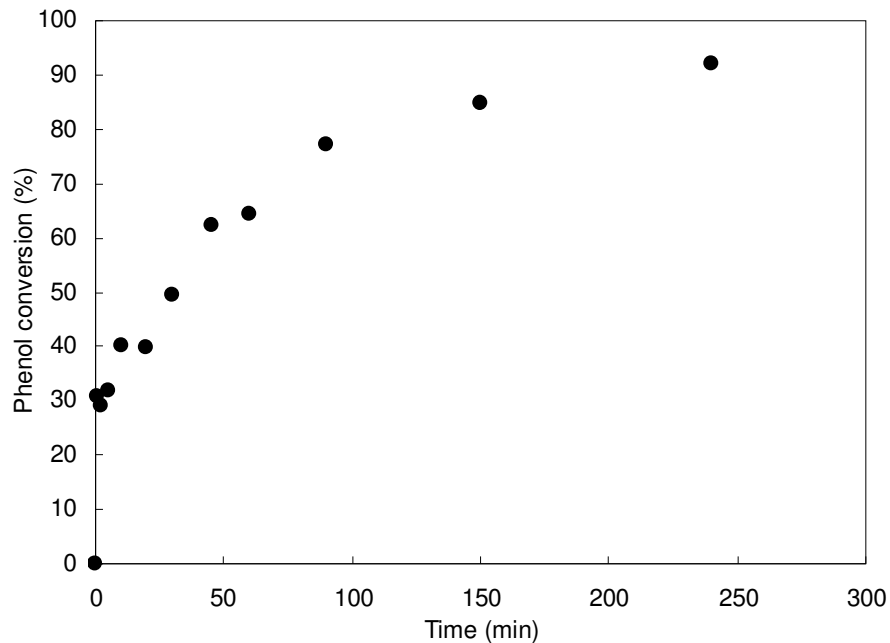
Figure 8.8.   Influence of the time of reaction on the phenol conversion in the stirred tank reactor with immobilised HRP. $[Phenol]_0$: 0.5 mM, $[HRP]_0$: 0.006 U/ml, $[H_2O_2]_0$: 0.662 mM, pH 7 and temperature of 20ºC.

The figure 8.9 presents the influence of the immobilised HRP initial concentration on the phenol conversion for a phenol initial concentration of 0.5 mM and finally, for a H_2O_2 initial concentration of 0.662 mM.
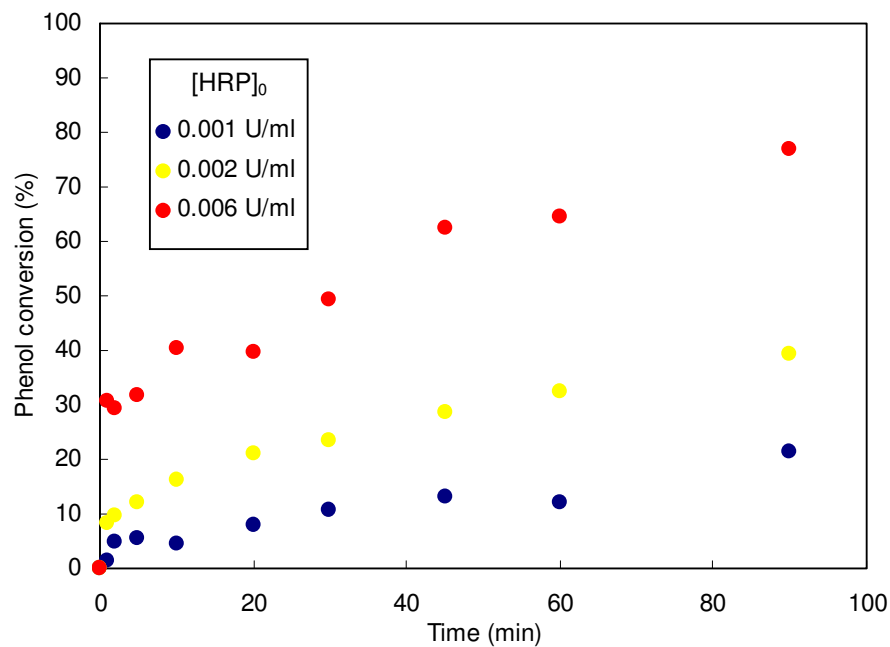
Figure 8.9.   Influence of the immobilised HRP initial concentration on the phenol conversion in the stirred tank reactor. $[Phenol]_0$: 0.5 mM, $[H_2O_2]_0$: 0.662 mM, pH 7 and temperature of 20ºC.

As it can be seen in the figure and, as it was expected by the results obtained with the free enzyme, the conversion of phenol increased with an augment of the immobilised HRP initial concentration. The enzymatic activity of the immobilised HRP was determined from these results calculating the initial reaction rates as previously explained. The activity of the immobilised enzyme is shown in figure 8.10. From the value of the slope it was found an enzyme activity of 28.3±0.1 U/mg. The immobilisation of the enzyme produced a great reduction of the activity of the enzyme from 204±22 to the 28.3±0.1 U/mg, signifying loos of 86% of the activity. The cause of this usual trend could be the formation of multilayers or a bad orientation of the active site of the enzyme.
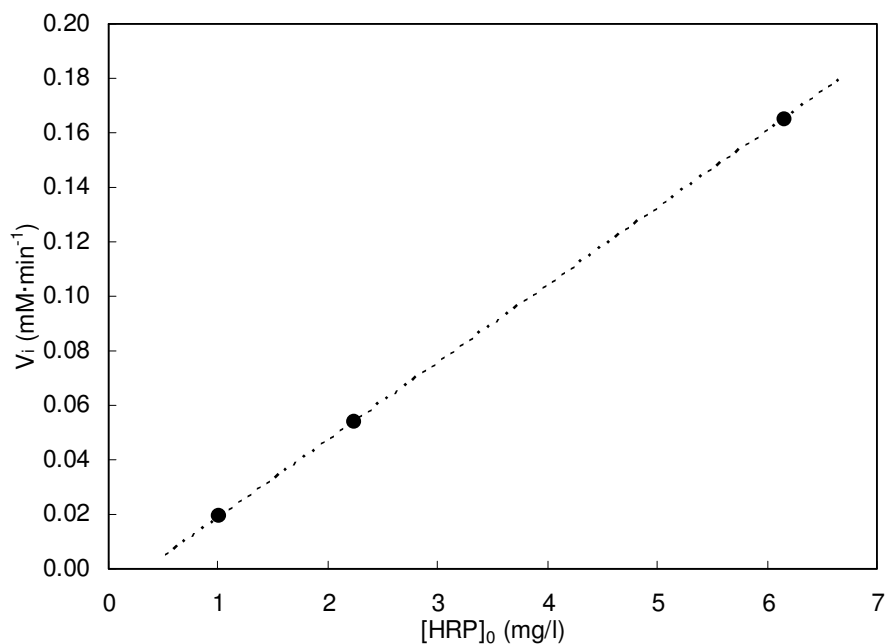
Figure 8.10. Determination of the activity of the immobilised HRP in the stirred tank reactor. $[Phenol]_0$: 0.5 mM, $[H_2O_2]_0$: 0.662 mM, pH 7 and temperature of 20ºC. R^2: 0.999.

The same study was carried out using the torus reactor. The figure 8.11 presents the phenol conversion as a function of time for the case 0.5 mM of initial phenol concentration and 0.662 mM of H_2O_2 initial concentration. Different enzyme concentrations were tested in the range 0.001-0.004 U/ml.

As it can be seen in the figure, the same trend and almost the same phenol conversion was obtained using the torus reactor. In the same way, the enzyme activity using the torus reactor was also calculated.
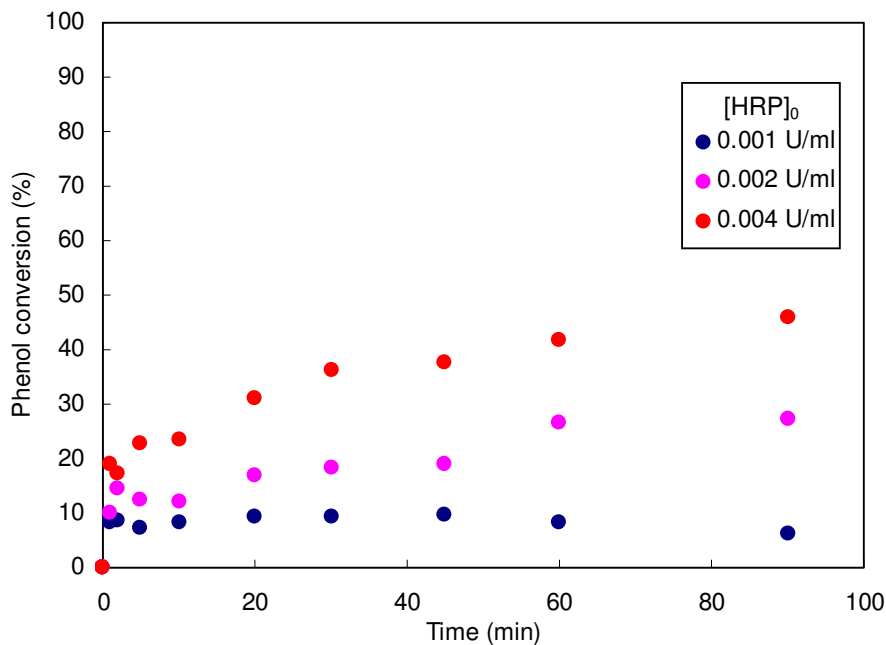
Figure 8.11.   Influence of the immobilised HRP initial concentration on the phenol conversion in the torus reactor. [Phenol]$_0$: 0.5 mM, [H$_2$O$_2$]$_0$: 0.662 mM, pH 7 and Temperature of 20ºC.

The figure 8.12 shows the initial reaction rate as a function of the initial HRP concentration in order to determine the enzyme activity in the torus reactor.
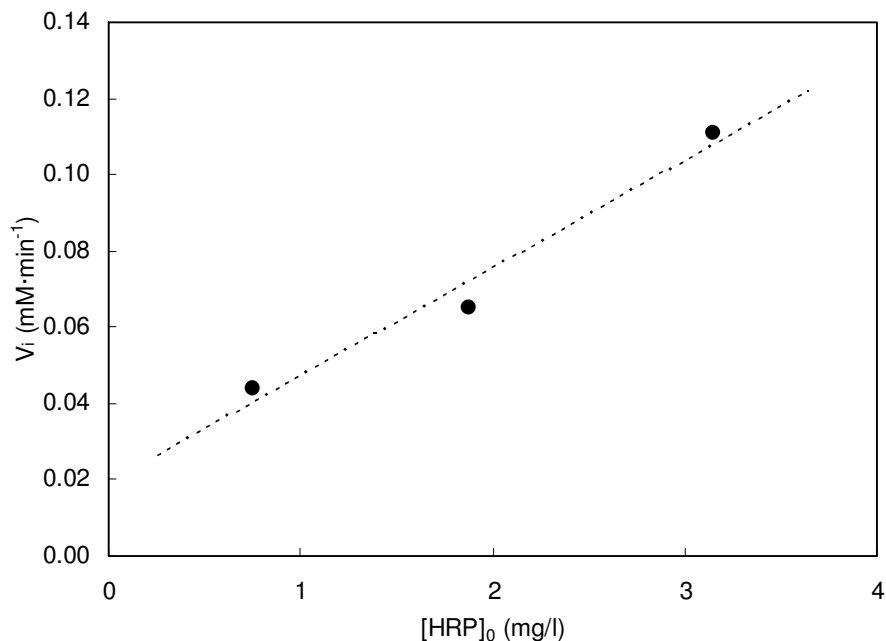
Figure 8.12.   Determination of the activity of the immobilised HRP in the torus reactor. [Phenol]$_0$: 0.5 mM, [H$_2$O$_2$]$_0$: 0.662 mM, pH 7 and Temperature of 20ºC. R^2: 0.969.

In this case, the enzyme activity was 28.1±5.0 U/mg. The same activity was obtained in both reactors. Therefore, the activity of the enzyme is not affected by the type of reactor used as it was deduced with free enzyme in section 6.1. Again the diminution of enzyme activity is exactly

the same as it was predictable. As both reactors have the same behaviour, the end of this study will be achieved with the stirred reactor.

8.5. Influence of the hydrogen peroxide initial concentration

To study the influence of the H_2O_2 initial concentration, different experiments were carried out in the stirred reactor in batch conditions. In all cases the concentration of immobilised HRP was kept in 0.002 U/ml or $3 \cdot 10^{-7}$ mM. The conversion of phenol was studied for different initial concentrations of H_2O_2 varying from 0.221 to 2.650 mM while, three different initial concentrations of phenol of 0.5 mM, 1.1 mM and 1.6 mM were used. The results of the phenol conversion are illustrated in the figures 8.13, 8.14 and 8.15.
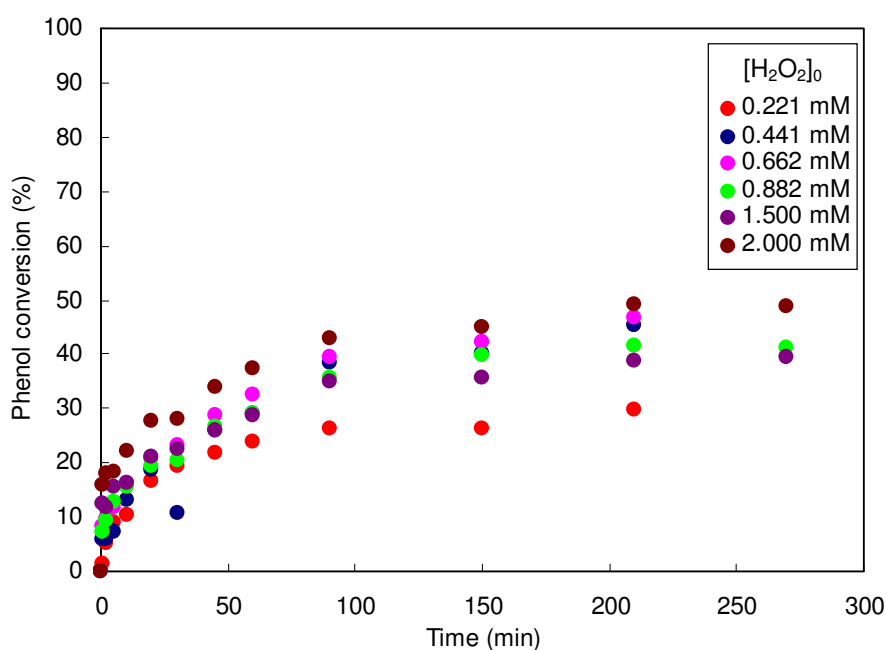
Figure 8.13. Influence of the H_2O_2 initial concentration on the phenol conversion in the stirred tank reactor using immobilised enzyme. [Phenol]$_0$: 0.5 mM, [HRP]$_0$: $3 \cdot 10^{-7}$ mM, pH 7 and temperature of 20ºC.

As it can be seen in the figures, the behaviour of the curves is similar than the obtained with the free enzyme. The phenol conversion attained is around 50, 40 and 26% for an initial phenol concentration of 0.5, 1.1 and 1.6 mM respectively. These values of conversion are almost a half part of the phenol conversion obtained using free enzyme in all cases. On the other hand, it is remarkable that the quantity of immobilised enzyme necessary to convert the phenol is inferior in three orders of magnitude than with the free enzyme.
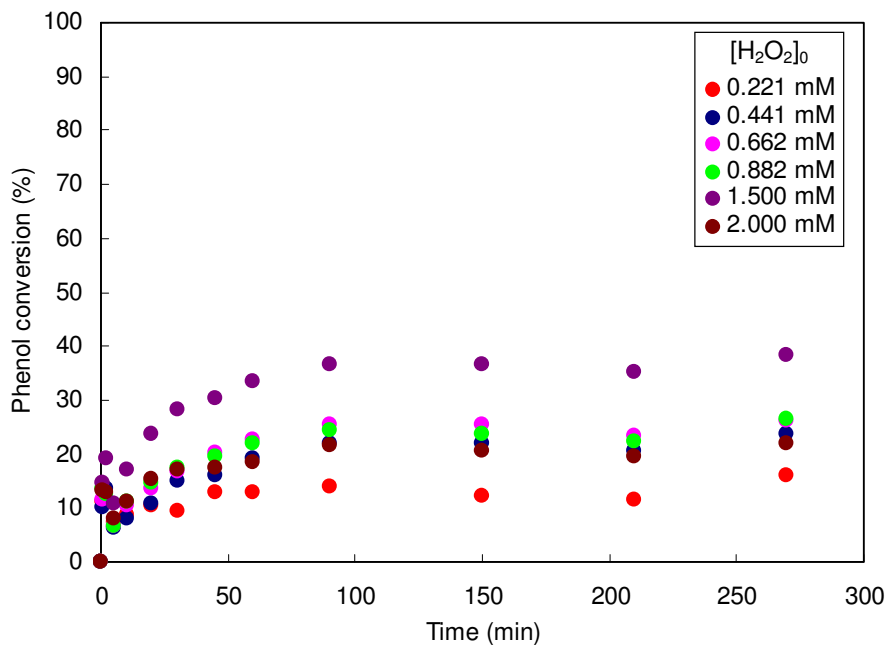
Figure 8.14. Influence of the H_2O_2 initial concentration on the phenol conversion in the stirred tank reactor using immobilised enzyme. [Phenol]$_0$: 1.1 mM, [HRP]$_0$: $3 \cdot 10^{-7}$ mM, pH 7 and temperature of 20ºC.
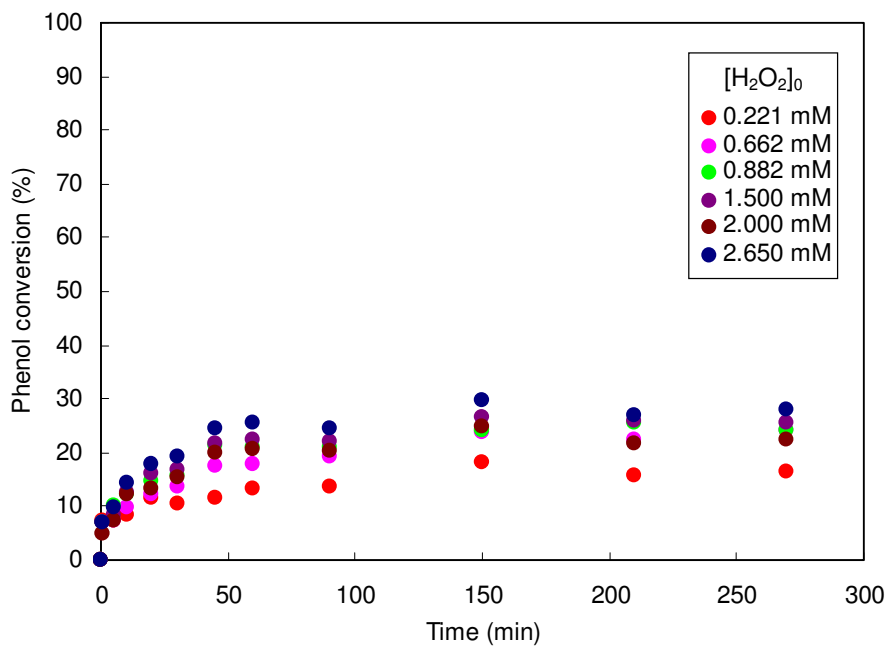
Figure 8.15. Influence of the H_2O_2 initial concentration on the phenol conversion in the stirred tank reactor using immobilised enzyme. [Phenol]$_0$: 1.6 mM, [HRP]$_0$: $3 \cdot 10^{-7}$ mM, pH 7 and temperature of 20ºC.

8.6. Kinetics of the immobilised HRP

The determination of the kinetics of the immobilised enzyme in the stirred reactor was realised exactly in the same conditions than for the free enzyme detailed in the section 5.4. The kinetic model described in section 5.4.3 for free enzyme was now utilised in this determination:

$$V_i = \frac{V_{max} \cdot [H_2O_2][Phenol]}{K_m + [H_2O_2] + K \cdot [Phenol] + K' \cdot [H_2O_2]^2} \tag{5.3}$$

where V_i is the apparent reaction rate of the phenol consumption, [Phenol] and [H_2O_2] are the phenol and the H_2O_2 initial concentrations respectively, V_{max} is the apparent maximum reaction rate while K_m, K and K' are the kinetic model constants.

The initial reaction rates of the enzymatic elimination obtained in the stirred reactor are shown in figures 8.16 and 8.17 for an initial phenol concentration of 0.5 mM and 1.1 mM respectively.
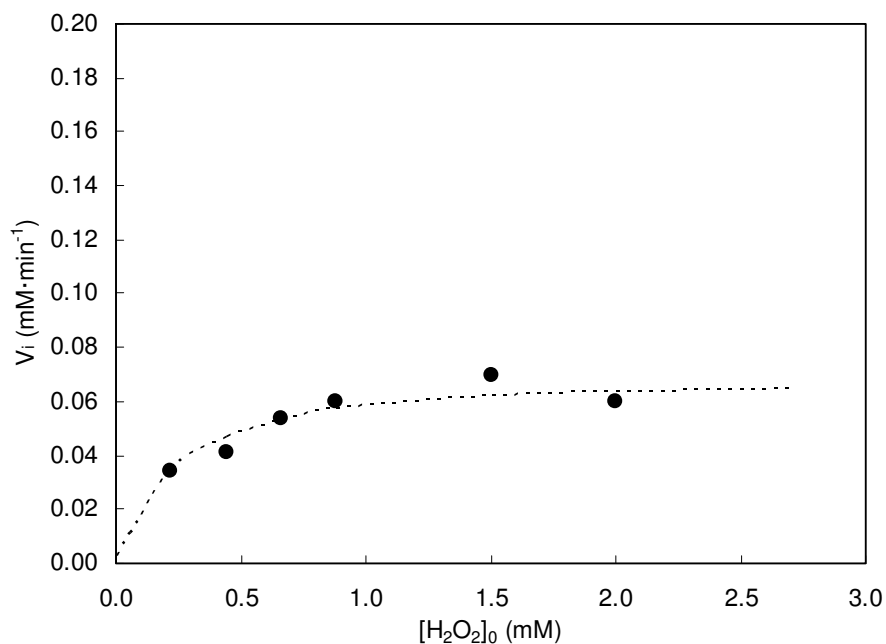
Figure 8.16.   Influence of the H_2O_2 initial concentration on the Steady-state initial rates of phenol oxidation in the stirred tank reactor for immobilised enzyme. Fitting obtained by the modified Michaelis-Menten model with inhibition. [Phenol]$_0$: 0.5 mM, [immobilised HRP]: $3 \cdot 10^{-7}$ mM, pH 7 and Temperature of 20ºC.

As it can be seen in the figures, the reaction using immobilised enzyme follows the same kinetic model than the free enzyme.
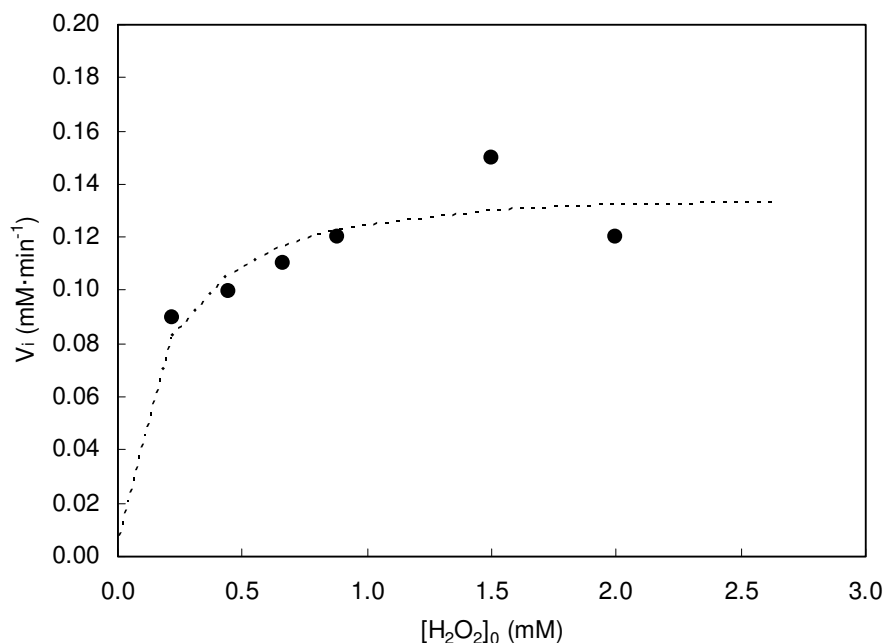
Figure 8.17. Influence of the H_2O_2 initial concentration on the Steady-state initial rates of phenol oxidation in the stirred tank reactor for immobilised enzyme. Fitting obtained by the modified Michaelis-Menten model with inhibition. $[Phenol]_0$: 1.1 mM, [immobilised HRP]: $3 \cdot 10^{-7}$ mM, pH 7 and Temperature of 20ºC.

The calculated values of the fitted parameters are presented in table 8.3.

Table 8.3. Apparent parameters for the reaction of HRP with inhibition by Phenol and H_2O_2 for immobilised enzyme.

V_{max} (min^{-1})	K_m (mM)	K (*)	K' (mM^{-1})
0.14	0.35	0.16	0.02

* dimensionless

8.7. Conclusions

Three different approaches for the covalent immobilisation of HRP were explored. In a first case, the direct HRP binding to polymers was studied via their oxirane groups. In this case, almost all the linked enzymatic activity was coupled before the 3 first hours of experimentation. Also, using this immobilisation technique, a maximum value of enzymatic activity of 73 U·g^{-1} was obtained for the immobilised enzyme on Eupergit support.

As a second approach, the HRP was bound to the polymer via the spacer made from adipic dihydrazide. Using this method of immobilisation, the maximum enzymatic activity of the immobilised enzyme was found to be 128 U·g^{-1}. Only a 3% of coupling of the enzyme activity was obtained for an enzyme loading on the support of 70.4 mg·g^{-1}.

Finally, the HRP binding was studied into amino-reactive polymer surfaces through the enzyme carbohydrate moiety previously modified by periodate oxidation. In this case, a maximum value of the immobilised enzyme activity of 126 $U \cdot g^{-1}$ was found using an enzyme loading on the support of 17.6 $mg \cdot g^{-1}$.

Therefore, almost the same activity of the immobilised HRP on Eupergit was obtained using the immobilisation techniques of pre-treatment of the support by adipic dihydrazide or by the periodate method. The last method allowed the use of a reduced amount of enzyme in order to obtain the same enzymatic activity.

In this way, the periodate-mediated covalent immobilisation of HRP on Eupergit was found to be an effective method for the preparation of stable biocatalysts.

The reaction of enzymatic elimination of phenol using immobilised enzyme showed that it was possible to reach high degrees of removal (around 12%) with the horseradish peroxidase immobilised on Eupergit. For example, using 0.011 $U \cdot ml^{-1}$ of immobilised enzyme, the reaction took approximately 2 h to reach the final conversion of phenol. The value of removal of phenol obtained was almost the same that those obtained using 0.15 $U \cdot ml^{-1}$ of the free enzyme. This fact seemed to indicate that the immobilisation process improved the enzymatic stability. Moreover, the immobilisation process could protect the enzyme from its inhibition by products or substrates.

PART III. Computational Fluid Dynamic study of the torus reactor and the enzymatic reaction

Chapter 9. Literature review

This chapter summarises some of the most important works that have been carried out on the CFD studies about the torus reactor. Moreover, this chapter describes the more relevant studies of flow modeling and the hydrodynamics determination of different reactors in batch and continuous operating. Finally, the fundamental bases of CFD are presented.

9.1. Previous CFD studies about the torus reactor

The torus reactor used in this study was a 100 ml reactor built in Poly(methyl-methacrylate) (PMMA). The reactor has an annular square section with a gap width of D = 25 mm. The agitation into the reactor was done by a three blades marine impeller with a blade pitch angle of 45º and an external diameter of 15 mm (for a detailed description of the reactor see section 4.1).

Despite experimental studies have confirmed efficiency of the torus geometry, the optimal conception of torus reactors and their utilisation in industrial scale production require still theoretical research. Few information about hydrodynamic characteristics involved in torus shape reactors is known. Khalid et al. (1996, 2001) emphasized the main features of the flow, and especially the high degree of mixing and the decay of the swirling motion when moving far from the impeller zone.

Other studies were mainly restricted to global measurements, like the circulation time as a function of the impeller rotation speed (Sato 1979), or a general overview of the flow structure using tracer methods (Legrand 2002). This is mainly explained by the difficulties encountered to conduct an experimental investigation of the complex flow obtained in torus geometries. The combined effects of the bend curvature and the impeller rotation generate a complex flow inside the reactor. But the hydrodynamics resulting of its complexity also explains the reactor efficiency, and for this reason such kind of investigations is of primary interest.

Sato et al. (1979) have studied the hydrodynamics in continuous loop reactors of rectangular form for the polymerization of olefins. The loop reactor used was constructed of four pieces of 10 cm with straight acrylic tubes connected with four bends in a rectangular loop. They have found that the average circulation velocity is proportional to impeller speed and the sine of the impeller blade angle. Moreover average circulation velocity depended upon Reynolds number and the dimensions of the impeller. Also, the influence of baffles and impeller geometry was analysed. In the case of unbaffled conditions, fluid flows in a helical motion and the intensity of this motion increased with impeller speed and pitched angle. In the case of baffled conditions,

tangential velocity component was suppressed. They showed that the flow distribution was influenced by the presence of baffles and by the type of impeller used.

On the other hand, Murakami et al. (1982) studied the influence of energy dissipation in a loop reactor of rectangular form. They were interested in the influence of the diameter and the angle of inclination of the blades impeller, the length of the reactor, the number of elbows constituting this loop reactor, the baffles and in the operating (continuous and batch) mode. Measurements of power consumption in a loop reactor of 10 cm i.d. with pitched paddle impellers were carried out in the range of mixing Reynolds number $Re = 10^2$ to $2 \cdot 10^5$. They have found no influence of baffle condition and no difference between batch and continuous operations.

Finally, Ronze et al. (1991) studied the residence time distribution in an open reactor composed of a cylindrical tube with an axial distributor. They were interested in the heat transfer in these reactors, and showed that the heat transfer was independent of the flow regime, which was characterized by micromixing state inside the reactor.

9.2. Flow characteristics

The flow modeling of a circular sectioned toroidal reactor in batch and continuous operating modes was studied by Benkhelifa et al. (2000) using a reactor with a volume of 5.25 litres. They determined the tracer evolution in a batch system and the residence time distribution in continuous mode. The flow in the reactor has been modelled with a plug flow with axial dispersion and total or partial recirculation in order to determine the axial dispersion coefficient in the reactor and to optimise the other experimental parameters such as the mean circulation time and the recycling factor. The determination of the Péclet number showed that the axial dispersion coefficient in the torus reactor is nearly constant whatever the operating mode and the flow regime. The axial dispersion is close to that obtained in vortex flows which are characterized by well-defined flow structures (Kataoka 1977) and allowed good mass and heat transfers. However, despite its interest in reactor running modeling, especially when reactions are occurring, such kind of investigation gives only a general representation of the flow in the geometry.

Moreover, Belleville and Legrand (1992) have showed that the torus reactors are characterised by an efficient radial mixing and the absence of dead volume which allow an easy scale-up due to the absence of dead volume. They studied the influence of the viscosity of the solution and the geometry of the mobile of agitation on the mean velocity of circulation in a torus reactor.

The effect of various parameters, such as the depth of the impeller, the circumferential position of the probe, the diameter of the impeller, the inclination angle of the blades, the geometry of the impeller and the volumes of the torus reactor, was studied by Nasrallah et al. (2008). The flow circulation inside the torus reactor was investigated in terms of circulation Reynolds number and the circulation number in function of the mixing Reynolds number. In this work three torus

reactors of circular section have been studied with volume of 2, 4.2, and 13 L. This study has shown that an efficient mixing is obtained in the toroidal geometry. The helicoidal flow generated by the impeller is accentuated in the four bends. Consequently, this type of reactor has not dead volume, leading to an easier extrapolation of these performances with respect to the classical stirred tanks. They have found that the only parameters influencing the flow and the mixing are the rotating speed of the impeller, the diameter and the type of the impeller. Finally, they showed that a better circulation is ensured by a marine screw impeller with respect to a pitched blade.

The torus reactor can be operated in continuous regime, this means with inlet and outlet flow rates. When operated in continuous mode, mixing performance can be modified (Benkhelifa 2000), due to the effect of the inlet and outlet flow, that can alter the flow structure inside the reactor. This is obviously a function of the feeding flow rate, and thus of the residence time in the reactor.

The main studies carried out in loop reactors are summarised in table 9.1 (Nasrallah 2008).

Table 9.1. Main studies in loop reactors.

Reactor	Re_m*	Type of studies	Types of impeller	Reference
Batch rectangular loop reactor	$2.3 \cdot 10^3$-$2 \cdot 10^5$	Determination of the circulation velocity	Marine screw	Sato et al. (1979)
Batch circular loop reactor	$2 \cdot 10^3$-$4 \cdot 10^4$	Determination of the mixing characteristics	Pitched blade with pale right-hand side-tilted	Tanaka et al. (1989)
Batch circular loop reactor	$2 \cdot 10^3$-$3 \cdot 10^4$	Flow modeling	Marine screw	Belleville et al. (1992)
Batch circular and rectangular torus reactor	$2 \cdot 10^3$-$3 \cdot 10^4$	Mixing characterization in a batch and continuous torus reactor	Marine screw	Nouri et al. (1997)
Batch and continuous torus reactor	$Re_m < 3 \cdot 10^3$ laminar regime and $Re_m > 6 \cdot 10^3$ turbulent regime	Experimental study and modeling of the flow in a batch and continuous torus reactor	Marine screw	Benkhelifa et al. (2000)

*Re_m: Mixing Reynolds number

9.3. Computational fluid dynamic

Computational fluid dynamics (CFD) is one of the branches of fluid mechanics that uses numerical methods and algorithms to solve and analyse problems that involve fluid flows. Computers are used to perform the millions of calculations required to simulate the interaction

of fluids and gases with the complex surfaces used in engineering. Even with simplified equations and high-speed supercomputers, only approximate solutions can be achieved in many cases.

The fundamental bases of any CFD problem are the Navier-Stokes equations, which define any single-phase fluid flow. These equations can be simplified to the Euler equations by removing terms that describes viscosity. A further simplification can also be achieved by removing terms describing vorticity until reaching the full potential equations. Finally, these equations can be linearized to yield the linearized potential equations.

The development of the initial methods was focused on the solution of Linearized Potential equations. After 1930, two-dimensional methods were developed using conformal transformations of the flow about a cylinder to the flow about an airfoil. However, the development of three-dimensional methods was paced by the available computational power.

The application of the CFD has been an established engineering tool in automotive and aerospace industry for many years. Recently, the CFD found increasing applications in chemical, biomedical and food industry (Ghani 1999, Hu 2000, Verboven 1997). On the other hand, the CFD has been used to simulate aqueous flow-fields in UV reactors (Lyn 1999). In this study, inactivation kinetics and radiation intensity have been combined with CFD generated flow-field to predict the reactor performance. Moreover, the CFD has also been applied to simulate surface reactions in catalytic reactors. In this sense, Seo et al. (2003) performed CFD simulation of the surface reactions in a catalytic heat exchanger using Fluent and obtained reasonable agreement between the simulation and the experimental results. Finally, other studies were carried out modeling processes with CFD e.g. simulation of polyphenol oxidation during tea fermentation (Lian 2002) or simulation of UV photocatalytic reactors (Pareek 2003) in order to predict reactor performances.

In this context, Computational Fluid Dynamics appears as an interesting tool to conduct a further analysis of flow structures. The modeling of the entire flow in torus reactor is however not easy, because of the combined effects of the bend curvature and the impeller rotation. Interaction between the helical motions with Dean vortices can be strong, as shown in Pruvost et al. (2004a), where a numerical study of the flow in a U-bend using the commercial code Fluent was conducted. In this study, it was studied the numerical flow prediction for two different bends and the results established the effectiveness of the numerical approach to determine the flow conditions for both 90º and 180º bends. For a better understand of the swirl effect in a bend flow, different values of the swirl number were applied at the bend entry. The competition between Dean vortices and swirl was emphasized, linked to the perturbation by the swirl motion of the radial pressure gradient due to the bend curvature. For small values of the swirl number, the flow at the bend outlet was found to result from a complex interaction between Dean vortices and swirl motion. For higher values, the influence of the swirl motion increased corresponding to the Dean vortices disappearance.

In Pruvost et al. (2004b), the numerical investigation was extended to the case of the torus reactor geometry using a reactor with straight parts fitted with a marine impeller. This study was devoted to a numerical analysis of the particular flow conditions involved in a torus geometry, and especially the competition between the swirling motion, due to the impeller rotation, with Dean vortices generated by the bends. The numerical tool was used to analyse the particular behaviour of the flow in torus reactor, and specially its evolution along the distance from the marine impeller. Two major characteristics were observed, the first related to the particular motion involved by the impeller in the first downstream bend. The second characteristic was the competition between centrifugal forces and Dean vortices provoked by the bends. In the classical bend pipe flows, the maximum axial velocity was located in the outer part of the bend curvature due to the centrifugal force. On the contrary, the position of the maximum axial velocity in the torus reactor was reversed in the inner part of the reactor.

Results achieved with the commercial code Fluent being satisfactory, same authors (Pruvost et al. 2006) have also applied CFD to the particular case of a square-sectioned photobioreactor of torus geometry. For the photoreactor optimization, two different types of impeller were studied. The investigations concluded to the interest of a classical three blades marine impeller because it had a more efficient flow circulation and mixing. Relevant characteristics for this application were investigated, like mixing time, radial mixing and shear stress. But it must be noticed that only batch configuration was considered.

The aim of the present study is to characterize the flow behaviour of a square sectioned torus reactor in continuous and batch conditions, by combining both experimental and numerical approaches. For the continuous mode, simulations were validated with experimental residence time distribution determination (chapter 10). Next, the CFD was employed to explain reactor behaviour by numerically investigating the flow structure. The study was finally focused on the perturbation occurring in continuous mode for high feeding flow rates (chapter 11).

Further, the influence of the inlet positions of the flow rates was analysed. Different configurations were considered and the influence was study following the mean residence time in the reactor.

In the last part of this section, a scale-up of the reactor volume in presented. A torus reactor with a volume of 300 ml was studied using CFD. The geometry and the mesh were created and some simulations were carried out to determine the mean velocities inside the reactor in order to compare the performance with a 100 ml reactor.

Finally, the present study was the first attempt to model the enzymatic elimination of phenol. The goal of chapter 12 was to study the enzymatic elimination of phenol in a torus reactor. CFD was used to analyze the coupling between flow and enzymatic reaction. A validation of the enzymatic reaction implementation in CFD code is presented, by comparing numerical predictions to experimental results of enzymatic conversion rates.

Chapter 10. Experimental investigation in continuous conditions

This chapter presents the concept of residence time distribution and mean residence time as well as the way to obtain the RTD in a reactor. The conductimetric method is described and presented as a tool to obtain the experimental mean residence time.

10.1. Residence time distribution and mean residence time

The concept of residence time distribution (RTD) has been introduced by Danckwerts (1953) with the purpose of to study and to describe real reactors. This distribution function, likewise accessible by experience, gives more global information about the fluid circulation inside the reactor than the classical hydrodynamic equations of fluid mechanical. The utilization of RTD permits the knowledge and the extrapolation of hydrodynamic characteristics of the reactor and can be applied to complex reactor geometries and for different fluid natures.

In a real reactor, the molecules, which enter at given instant, do not leave the reactor at the same time. So, exists a residence time distribution t_s around the average residence time $\overline{t_s}$. This distribution noted E(t) depends on the flow hydrodynamic and the reactor geometry. It has an influence on the reactor chemical performances (conversion, selectivity, yield…) and is a fundamental concept to reactor design.

The RTD for process equipment is typically measured using stimulus-response tracer experiments to detect design flaws such as bypass, channelling, and dead zones, in addition to characterizing a reactor's mean residence time and standard deviation. This measurement has been done, historically, when a complete velocity distribution map for the fluid in the vessel is not available. Because CFD is capable of predicting the complete velocity distribution in a vessel, it provides an alternative, indeed, simpler means of determining the RTD.

The development of Computer Fluid Dynamics will improve the comprehension and optimisation of such processes. However, this approach remains difficult in case of complex industrial processes. Therefore, the extension of the RTD concept is an alternative way to obtain hydrodynamic data and help for improvement of the processes.

A parameter frequently used is the space-time or average residence time τ, which is defined as being equal to V/v. It will be shown that for a particular reactor, ideal or nonideal, this nominal time, τ, is equal to the mean residence time, t_m, for incompressible fluid. As is the case with other variables described by distribution functions, the mean value of the variable is equal to the first moment of the RTD function, E(t). The definition of the mean residence time is depicted in the figure 10.1.

$$t_m = \int_0^\infty t \cdot E(t)\,dt$$
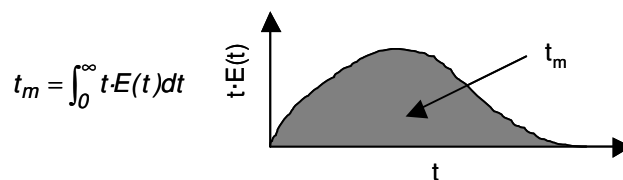
Figure 10.1. Main residence time.

10.2. Conductimetric method

The tracer method is based on the labelling of the entering molecules in the reactor and to follow their displacement into the reactor bulk. For this, the tracer used can be radioactive, a coloured or chemical substance, with the same properties than the fluid, but with a characteristic physic property like the electric, thermal or conductivity.

The conductimetric method is one of the traced methods allowing the experimental determination of RTD. It has been chosen for its easy utilization and to need commercially accessible products. Moreover, is one of the methods more used in numerous works (Gibson 1963, Brodberger 1983).

This technique consists in to register the temporal evolution of the electric conductivity of a concentrated solution of a tracer. The tracer is injected at some time $t = 0$ and then measuring the tracer concentration, C, in the effluent stream as a function of time. In addition to being a nonreactive species that is easily detectable, the tracer should have physical properties similar to those of the reacting mixture, and be completely soluble in the mixture. It also should not absorb on the walls or other surfaces in the reactor. The latter requirements are needed so that the tracer's behaviour will honestly reflect that of the material flowing through the reactor. The two most used methods of injection are pulse input and step input.

The pulse input was used in the study, where an amount of tracer N_0 is suddenly injected in one shot into the feed stream entering the reactor in the shorter time as possible. The outlet concentration is then measured as a function of time. The effluent concentration-time curve is referred to as the *C* curve in RTD analysis.

From the exit tracer concentration, we can determine the *Residence Time Distribution function* defined as *(E(t))* or sometimes called the *exit-age distribution function*:

$$E(t) = \frac{C_T(t)}{\int\limits_0^\infty C_T(t)\,dt} \tag{10.1}$$

This function describes in a quantitative manner how much time different fluid elements have spent in the reactor.

The principal difficulties with the pulse technique lie in the problem to obtain a reasonable pulse at the reactor entrance. The injection must take place over a period, which is very short compared with the residence time in various sections of the reactor or in the entire reactor. On the other hand the injection must produce a negligible amount of dispersion between the point of injection and the entrance of the reactor.

10.3. RTD measurements

The determination of the residence time distribution is carried out by measuring evolution of a tracer concentration using a conductimetric method. A two-points detection method is used, allowing the measurement of the concentration evolutions at both inlet and outlet of the reactor.

The hydraulic circuit is constituted by a vessel containing feed water, a moto-pump Stepdos 08RC (Knf Flotdos) and the inlet and outlet lines. The inlet tube is located at a distance of z/L_z between 0.75 and 0 (in reference with the impeller) and the outlet tube is located at $z/L_z = 0.5$ as it can be seen in figure 10.2.
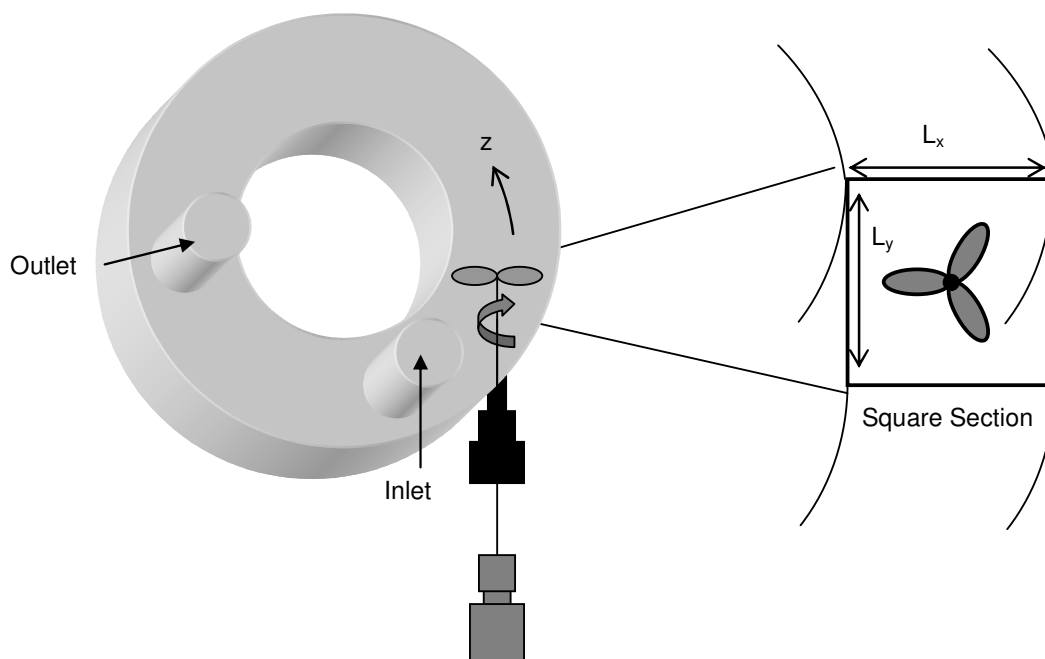
Figure 10.2. Continuous torus reactor (showing inlet and outlet lines).

The two conductimetric probes are identical and constituted both by two hemicylindrical nickel sheets (figure 10.3). Each probe is connected to a variable frequency conductimeter (Tacussel CD810). An operating frequency of 16.000 Hz was adopted in order to avoid the polarization of the electrodes and also to ensure a linear relationship between the conductivity and the tracer concentration. Both concentration signals, obtained at the inlet and at the outlet of the reactor

respectively, are sampled using an AOIP model SA32 data acquisition device, connected to a Personal Computer (PC).
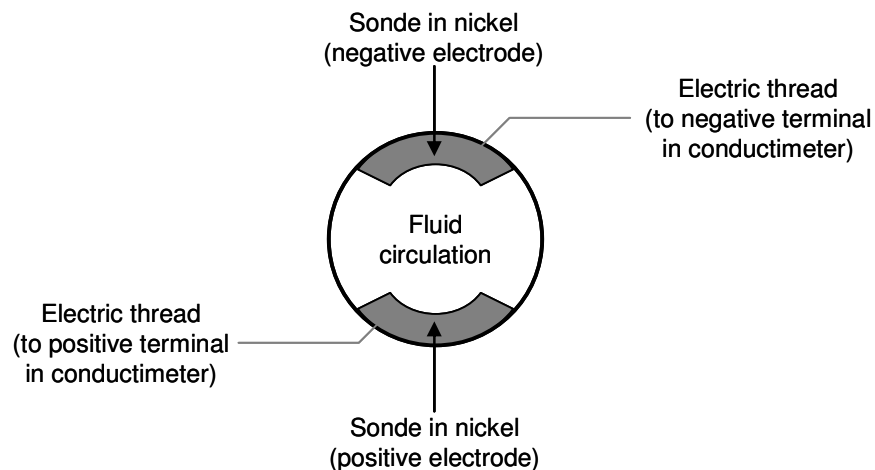
Figure 10.3.Conductimetric sonde scheme.

The tracer was prepared with a solution of sodium chloride (4N) in demineralised water. A small quantity (1 ml) of the tracer was injected with a syringe in the inlet tube to simulate a pulse and do not disturb the flow inside the reactor. The obtained outlet curve and its comparison to the inlet one allowed the estimation of the mean residence time. Different operating conditions have been tested, with impeller rotation velocities N of 500, 1000, 1500 and 1800 rpm and also different flow rates, Q, ranged between 180 and 1200 ml/h.

10.4. Results

Figure 10.4 shows an example of the curves obtained at the inlet and at the outlet of the reactor. These curves were obtained for N = 1500 rpm and Q = 1200 ml/h (Re = 7200) and are representative of all tested experimental conditions. The experimental mean residence times were obtained using the conductimetric method. On one hand, it can be seen that the conductivity signal of the inlet presented a very narrow distribution that verified the pulse-type injection of the tracer into the reactor. On the other hand, the outlet conductivity signal had a wider shape which describes the exit distribution of the tracer in the reactor. This second signal presented also a lower peak, and a delay related with the time spent by the tracer to move from the inlet to the outlet port.
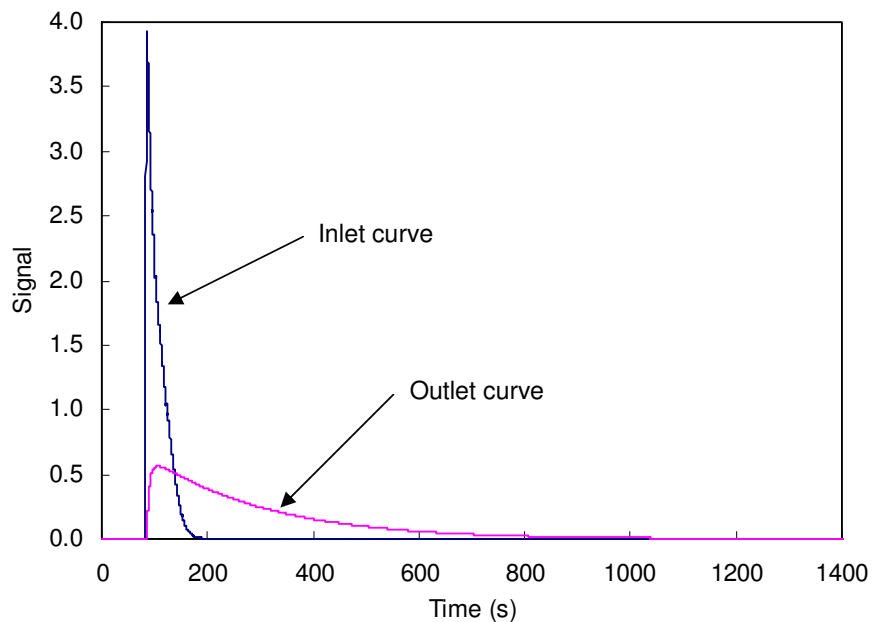
Figure 10.4.   Typical response of the conductimetric method: inlet and outlet signals (N = 1500 rpm, Q = 1200 ml/h).

When the flow rate was increased, the residence time quickly decreased as it can be seen in figure 10.5. For incompressible flows, the mean residence time must satisfy $\tau = V/Q$, and is thus independent of the impeller rotation speed. These theoretical values are also shown in figure 10.5.
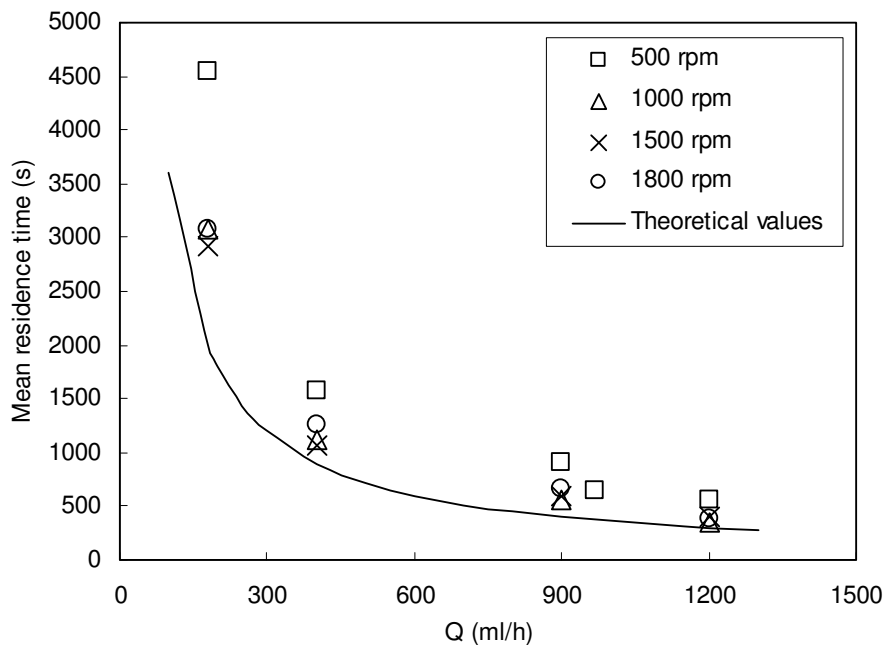
Figure 10.5. Experimental values of the mean residence time.

The comparison between theoretical models and the values obtained experimentally gave and estimation of the accuracy of the experimental method. Some differences were observed for the same flow rates but different impeller rotation speeds. Thus, there was a lack of precision in the calculations, especially for small flow rates and small rotation speeds. The residence time of the tracer was very dispersed in these cases.

10.5. Conclusions

The characterisation of the hydrodynamics in the torus reactor was carried out with the use of tracers and the conductrimetric method. The tracer was successfully detected in the inlet and outlet ports. This detection allowed the verification of the pulse-like injection of the tracer into the reactor, and also revealed its signal disappearance after about 100 seconds. The detection of the tracer in the outlet port showed a delay related to its residence time and a wide distribution characterised by an initial low peak and a subsequent decrease of the signal until almost disappearing after 600 seconds.

The measurement of the mean residence time with a variation of flow rate and the impeller rotation speed showed a good approximation to the theoretical model. However, the experimental values presented higher values of mean residence time compared to the theoretical model for low flow rates. This is specially true for the lowest impeller rotation speed (i.e. 500 rpm) at low flow rates (i.e. 180 and 400 ml·h^{-1}), where the mean residence time presented an important difference with the theoretical model. This difference could be due to the setup of the experiment, even though, it is remarkable the good fitting of the theoretical model with the experimental data at high flow rates.

Chapter 11. Numerical simulation

This chapter summarises the methodology used for the hydrodynamic characterization of the torus reactor in both batch and continuous conditions with numerical simulation. The different steps necessaries to solve the problem are presented. In the last part of the chapter, the numerical results are analysed for different configurations, batch and continuous mode, different reactor geometries and, also, a scale-up of the reactor volume are presented.

11.1. Methodology

The hydrodynamic characterization of the torus reactor in both batch and continuous conditions was carried out with numerical simulation using the commercial code Fluent® (Fluent Inc.).

To solve the problem, different steps are necessaries. The first step consisted in to create the reactor geometry and the grid. The torus reactor geometry was three-dimensionally meshed using Gambit Software (Fluent Inc.). This software permitted to carry out the geometry, the mesh and to specify the boundary conditions. To mesh the region near the impeller a refinement function (named size function in Fluent) is applied in this area to control the cells density in boundary layers. This function fixes the size of the first near-wall elementary volume and the discretization step. The size of the first cell can be chosen with respect to two different near-wall considerations, being a standard approach with application of a wall-function based on the universal logarithmic profile (standard wall-function), and the second a full resolution of momentum equations in the boundary layer using a Low-Re Model. Pruvost et al. (2004b) have investigated the effect of the near-wall consideration for the torus reactor simulation and the standard approach was found to give satisfactory results. Despite the fact that an improvement can be expected with an approach involving a full resolution of in the boundary layer like with a Low-Re model, the great increase in the grid refinement in the near-wall region, and thus in time computing, was not found justified, only a slight difference being observed between both approaches (Pruvost et al. 2004b).

The second step of the modeling was to choice the solver formulation. Fluent propose three different formulations to solve: segregated, coupled explicit and coupled implicit. The Segregated (separated resolution) and Coupled (coupled or simultaneous resolution) scheme are different because their different approach to the resolution of the equations of movement quantity, continuity and energy. The Segregated scheme solve the equations in a sequential manner, meanwhile the Coupled scheme does it simultaneously. The resolution of additional equations (turbulent…) is sequential for the two approaches. The Segregated scheme is traditionally employed in the case of incompressible flow or easily compressible. The Coupled method has been developed for high velocity and compressible regimes.

The third step was to select the basic equations as they can be momentum and pressure, and their interpolation scheme for the continuity equation: first order, second order, QUICK or

power-law. The second order scheme is the most advised interpolation scheme to use, except if some problems with the convergence are found. A second order interpolation scheme is applied for all discretized transport equations (pressure, momentum and turbulent characteristics). The transport equations were numerically solved using a segregated method, which implies to solve the pressure-velocity coupling with an iterative correction procedure "SIMPLEC". The computations were performed until the convergence of all residual criteria with no variation of the values.

For all simulations, the defaults constants of Fluent were retained for the turbulent models and the steady-state calculation was done. A large number of models exist to model the turbulence. Two mean categories can be considered: one, based in the medium Reynolds equations (RANS) named one point model and the second one, the large scale simulations method (LES for Large Eddy Simulation). The one point model (RANS) is normally used because it gives more accurate results for this type of configuration. They are based in the statistical equations to partial derivated obtained for the mean Navier-Stokes equation. The more industrial used models are mixture length, k-ε and RSM (Reynolds Stress Model). The k-ω model (Wilcox, 1998) was found to give the most accurate prediction by using the commercial code Fluent in the case of torus reactor simulation (Pruvost, 2004b). This model was therefore used for the turbulence modeling into the torus reactor.

In the next steps, it was necessary to specify the materials (fluids or mixtures and physical properties) and to define the boundary conditions. Fluent proposes different types of boundary conditions: inlet and outlet (pressure inlet, velocity inlet, mass flow inlet, inlet vent, intake fan, pressure outlet, pressure far-field, outflow, outlet vent, exhaust vent), wall (wall, symmetry, periodic, axis), mesh internal (fluid, solid, porous) and faces internal conditions (fan, radiator, porous jump, wall, interior).

In the torus reactor, the flow resulted by the impeller rotation, which is the only driving mechanism in the reactor working in batch. In continuous, the driving force is the impeller rotation and the inlet-outlet flow rate. The moving parts in the geometry are modeled using a Multiple Reference Frames (MRF) resolution. With the MRF approach, the solution is achieved by solving the equations of motion in two different reference frames, one being the absolute inertial frame and the other attached to the impeller being in rotation with a rotation velocity equal to that the impeller.

Then, it is necessary to adjust the resolution parameters. An under-relaxation parameter is available for each equation solved. If this value (between 0 and 1) is high, the needed time to get convergence is shorter, but the risk of having divergence is bigger. For defect, Fluent gives the appropriate values for each case but is possible to modify the values during the resolution.

The last steps of the modeling were to initialize the flow and to calculate the solution. For facilitate the convergence, it is recommended to initialize the solution in the entire domain. In this step, it is necessary to choice the iteration numbers, the reporting interval and when the convergence criterion is verified.

In this work, the torus shape was three-dimensionally meshed using the Gambit Software® (Fluent Inc.). Due to the impeller, a regular mesh is difficult to apply in the entire geometry. So, the reactor was divided in two different zones. The first one, the marine impeller vicinity, has been meshed using tetrahedral volumes and prisms. A regular mesh with elementary hexahedral volumes has been used in the remaining part of the torus. The grid discretisation in this regular part is uniform, whereas cells density is gradually increased when coming closer to the impeller. To mesh the region near the impeller, a refinement function (named "size function" in Fluent) is applied to control the cells density in boundary layers. This function determines the size of the first near-wall elementary volume and the discretisation step. The grids for the reactor and the impeller are presented in figure 11.1 and 11.2 respectively.
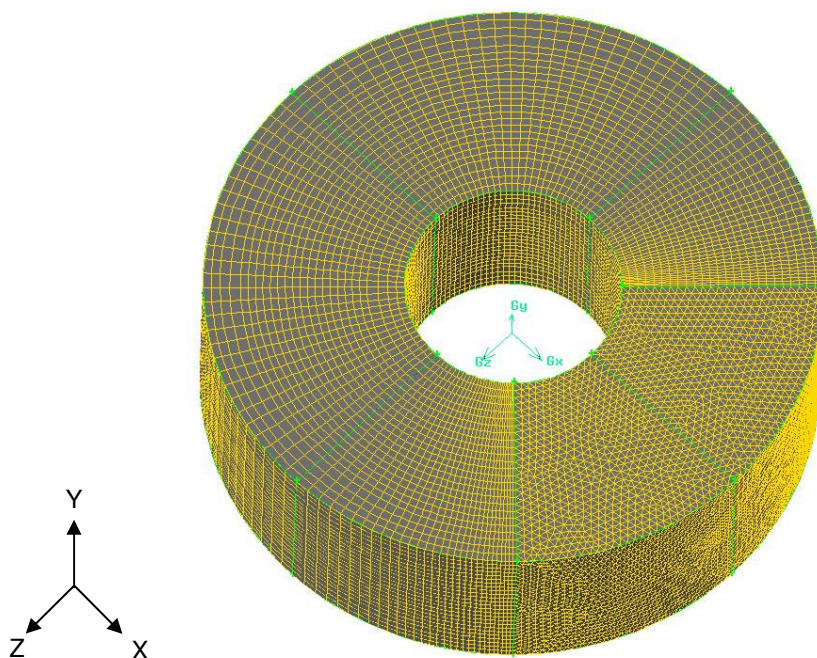
Figure 11.1. Batch torus reactor grid.
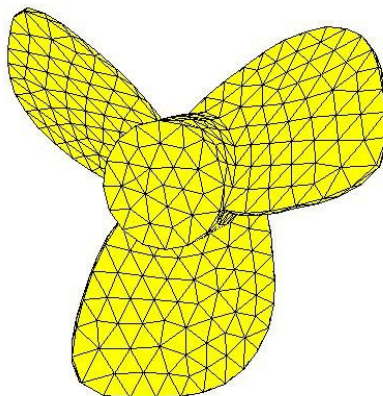
Figure 11.2. Marine impeller grid.

The motion of the impeller was modelled using the Multiple Reference Frames (MRF) resolution. This model is based on the division of the total volume of the reactor into two concentric blocks, in which the inner one contains the impeller. The results obtained by this method were more accurate than the ones obtained by a method that did not include implicitly the impeller, as long as, empiric data in the close region of the impeller were unknown, Brucato et al. (1998). The same model was used for the torus geometry in Pruvost et al. (2004b). The flow-field was obtained using the k-ω turbulence model (Wilcox 1998). This model was found to give good results for torus geometry (Pruvost 2004a, Pruvost 2004b, Pruvost 2006). Boundary layers were meshed using a standard wall-function approach, as in Pruvost et al. (2006), with an appropriate meshing in the wall region.

All computations were performed on an Intel® Pentium® core-Duo processor (3.00 GHz, 3.01 GHz, 2 GB RAM).

11.2. Simulation of the reactor in batch conditions

In order to study the torus reactor in batch conditions, the geometry and the mesh of the reactor were created. To ensure grid independency of the results, three meshes (301473 cells, 338973 cells and 348531 cells) have been tested. The results of convergence showed that the data of flow velocities were totally independent of the number of cells of the grid.

To model the batch configuration, the torus reactor was considered closed (no inlet or outlet conditions were applied) and the flow was only driven by the impeller rotation. The only boundary condition to be specified in this case was the rotation speed of the impeller.

The mixing performance in the torus reactor was numerically evaluated by determining the mixing time. Value was obtained by the simulation of a pulse tracer injection. In the case of turbulent flows, the diffusion process had to be taken into account by means of the turbulent mass diffusivity D_{jt}, expressed by the turbulent Schmidt number. The value in turbulent flow for the Schmidt number was set to $Sc_t = 1$ as described by Pruvost et al. (2004). Next, the tracer dispersion was determined by solving the unsteady formulation of the mass transport equation. Because the tracer injection was considered to not influence the flow, the steady solution of the flow-field inside the reactor could be used. In this case, only mass transport equation was solved with an unsteady resolution.

The simulated injection point was located at a distance $Z_{imp} = z/L_z = 0.25$ from the impeller as it can be seen in figure 11.3.

In the unsteady resolution of the tracer transport, the mixing time was determined by the evolution of the averaged tracer concentration on a given cross-section with respect to time. This cross-section, used for the injection point, was always located at the same distance from the impeller.
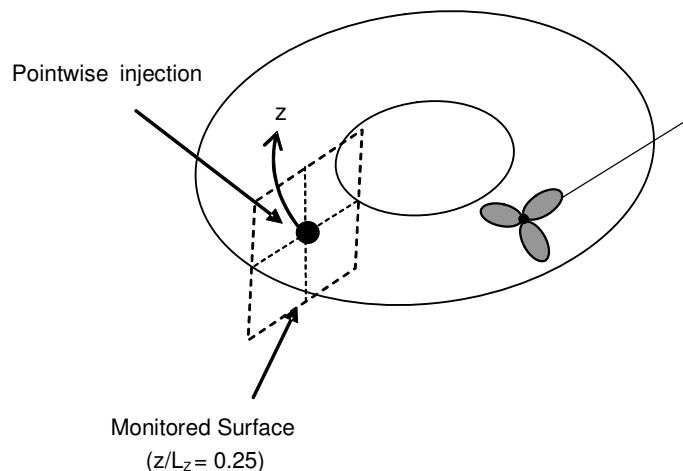
Figure 11.3.   Passive tracer injection: visualization of the monitored surface and the injection point in batch reactor.

For the unsteady resolution of the mass transport equation, it is necessary to specify a time step Δt, which has been chosen enough small to ensure accurate results. For this, different tests have been done to determine the time step effect. The figure 11.4 presents the influence of the values of the time step on the average simulated concentration for N = 800 rpm. The values of the time step used were between 0.100, 0.050, 0.010, 0.005 and 0.001 s. The numerical results show that a time step around 0.005 s can be used, because the curves obtained for 0.001 and 0.005 s are very similar, and for this, in all calculations, a time step of 0.005 s will be used to save calculation time.
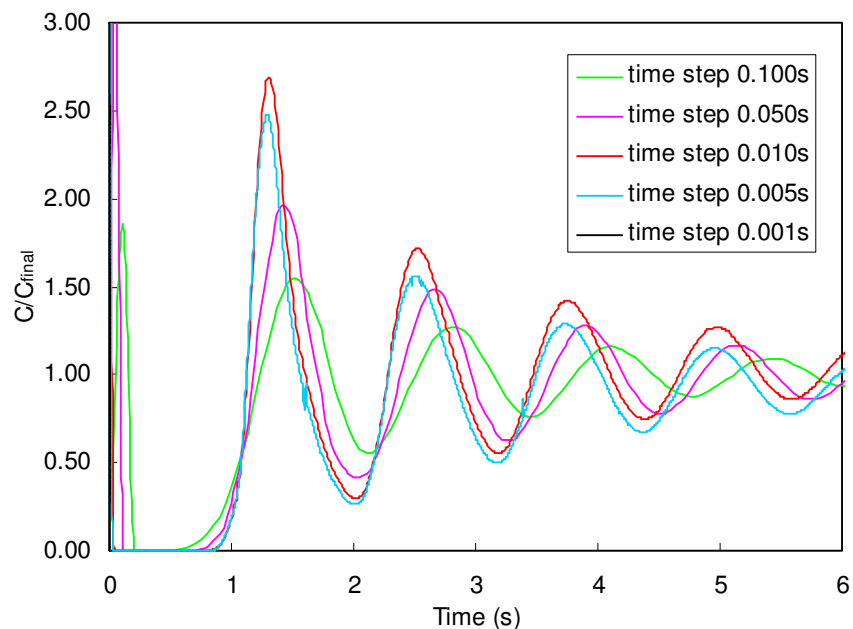
Figure 11.4.   Time evolution of the normalized concentration averaged on a given flow cross-section (z/L_z = 0.25): influence of the time step on the unsteady resolution (N = 800 rpm).

11.3. Simulation of the reactor in continuous conditions

The torus reactor was also studied in continuous conditions. For the continuous regime, the reactor mesh was modified by introducing pipes for the inlet and outlet flows. The irregular zone which is located near the impeller was meshed in the same way that for the batch conditions. The inlet and outlet zones were meshed using hexagonal/wedge volumes because they were also considered as irregular zones. These irregularities were presented due to the junctions between the inlet and outlet tubes and the surface of the reactor. The resulting grid was composed of 349981 cells and it can be seen in the figure 11.5.
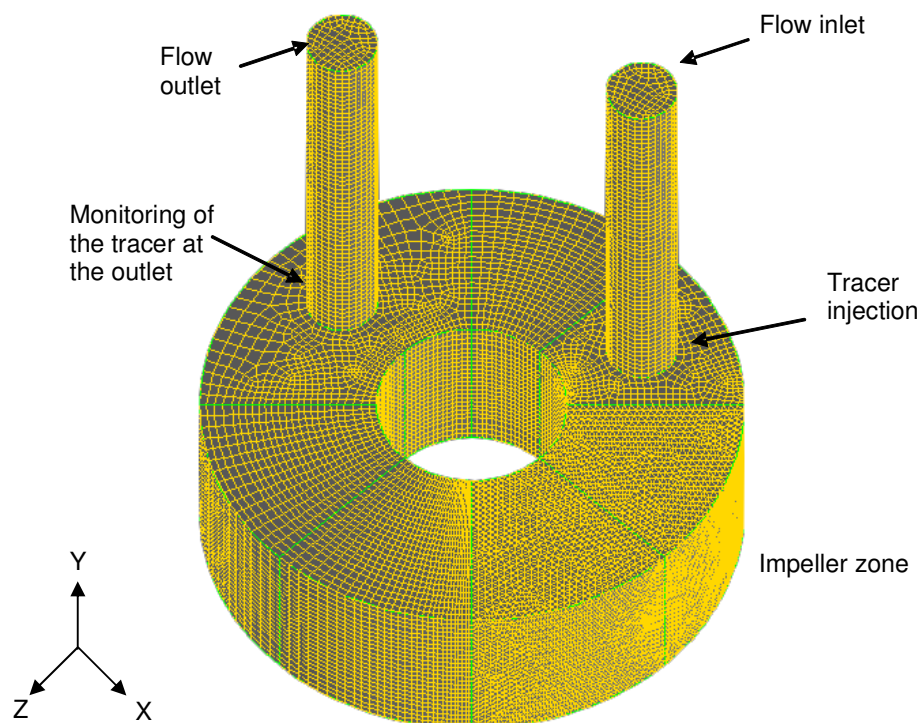
Figure 11.5.   Continuous torus reactor grid (349981 cells) and localisation of the surface for the simulation of the tracer injection.

In continuous conditions, the hydrodynamics are the result of the impeller rotation and the flow rate applied in the inlet of the reactor. A MRF resolution was then conducted, with investigated flow-rates applied in flow-inlet as boundary condition.

As it was the case in batch conditions, the tracer dispersion was solved using the mass-transport equation. To simulate the two-point RTD experimental measurement, the passive tracer was introduced as a pulse by changing its concentration in the feed. Figure 11.5 shows the modified grid of the reactor, the locations of the injection of the passive tracer and the point where it is monitored. As illustrated, the averaged tracer concentration was monitored as a function of time at the outlet of the reactor. The results obtained provide the exit age distribution of the tracer between the inlet and the outlet of the reactor, and therefore, represent the RTD of the reactor.

11.4. Validation in continuous regime

For the continuous regime, the validation was achieved by comparing simulated RTD to experimental ones. An example of results is given in figure 11.6, showing agreement between numerical simulations and experimental measurements. As it can be seen in the figure, the impeller rotation speed had only a strong influence when the inlet flow rate is small (i.e. 180 and 400 ml·h^{-1}), confirming previous assumption of a possible flow disturbance inside the reactor for given operating conditions. As for the experimental characterization, a lack of accuracy is observed for small values of the impeller rotation speeds and flow rates, explained by the poor mixing in those conditions, resulting in a very dispersed distribution of the exit age of the injected tracer that makes difficult the calculation of the mean residence time. Obviously, the mean residence time is not sufficient to validate the numerical simulation, this value being fixed by the feeding flow rate and reactor volume only (τ = V / Q). In figure 11.6, experimental, numerical and theoretical values of the mean residence time are also shown, where theoretical values were calculated with the previously mentioned equation for τ.
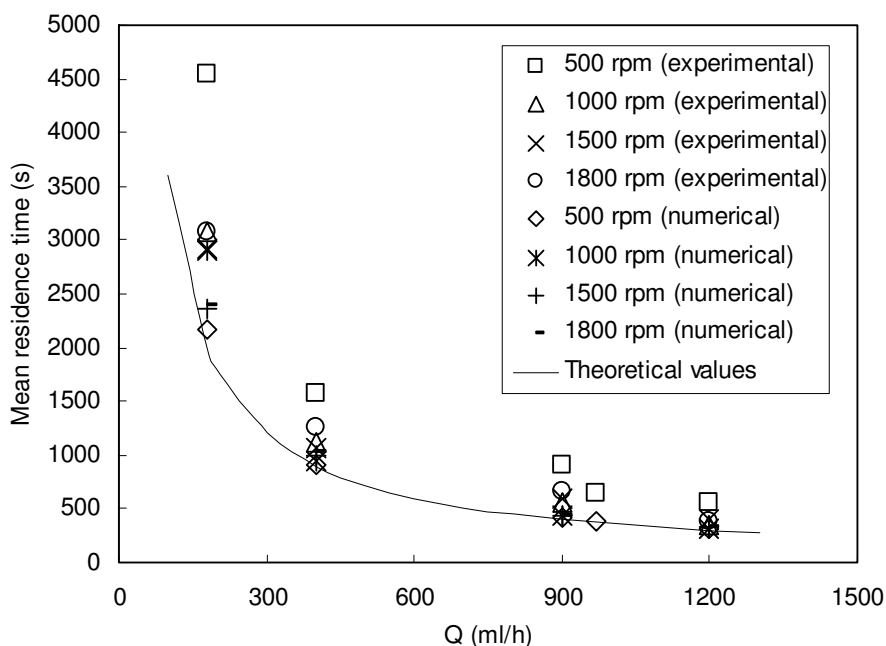
Figure 11.6. Experimental and simulated values of the mean residence time.

On the other hand, the figure 11.7 presents the outlet curves achieved numerically and experimentally for the residence time distribution. As it can be seen in the figure, the same shape was obtained. The curves are not identical but a relative agreement between them is observed, however, for low flow rates (i.e. 180 and 400 ml/h) the mean residence time was higher for the experimental and numerical data than the theoretical calculation. This difference in the values of mean residence time diminished meanwhile the flow rate increased, being almost negligible at 1200 ml/h. It is indeed difficult to obtain an accurate determination of RTD, especially due to its dispersed nature.
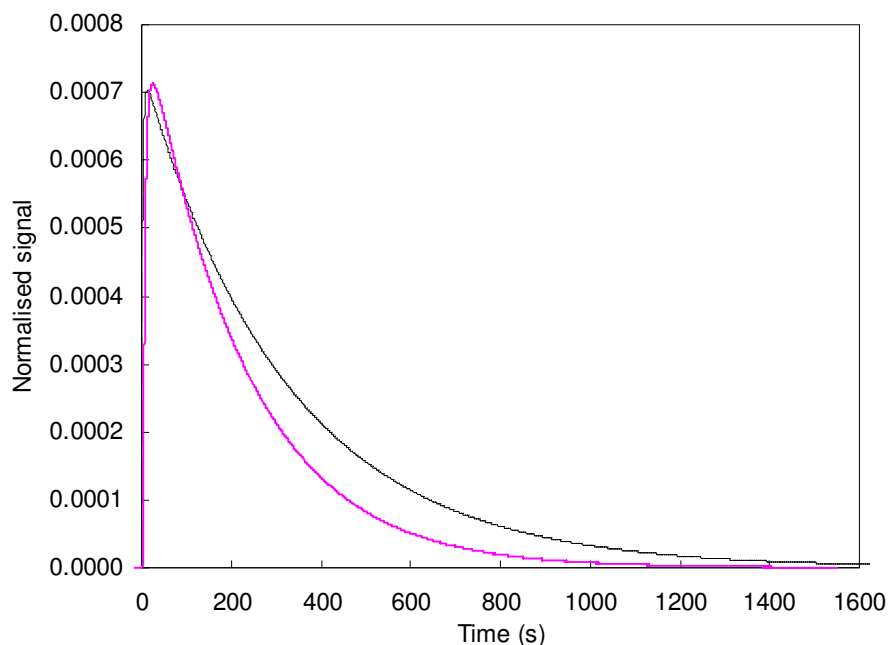
Figure 11.7. Experimental and numerical prediction of the residence time distribution.

For a deep investigation of the flow structure, experimental validation by only RTD is not sufficient, because of the global nature of this characteristic (different flow structures can give same RTD). But, considering previous characterization on almost same reactor geometries (Pruvost 2006), and the aim of this study that is to have only a global overview of the mixing efficiency in continuous and batch modes, such validation can be considered as sufficient.

11.5. Results of the numerical investigation in batch mode

11.5.1. Influence of the impeller rotation speed on the bulk velocity

The circulation velocity U_0 and the mixing time T_m are the two values of primary relevance for the study of the influence of the impeller rotation speed on the hydrodynamic of the torus reactor. To do this, the numerical procedure described above has been retained, consisting in the use of the k-ω model and the multiple reference frames for the simulation of the impeller. The values of U_0 are deduced from the axial component of velocity (z-direction) by a simple spatial averaging in a cross-section of the reactor. The figure 11.8 presents the values of U_0 in batch mode for impeller rotation velocities varying from 200 rpm to 2000 rpm.

As it can be seen in the figure, the circulation velocity obtained with Fluent increased with the impeller rotation speed with a linear proportion. The solid line represents the empirical equation obtained by Belleville et al. (1992).
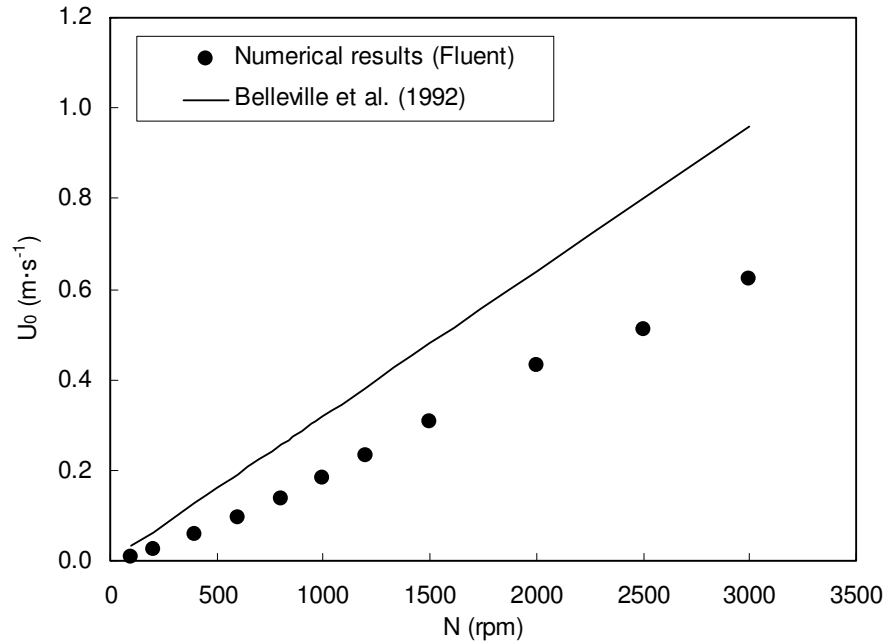
Figure 11.8.   Mean bulk velocity as a function of the impeller rotation speed: comparison with the empirical correlation of Belleville et al. (1992).

They used a torus reactor consisting of four flanged smooth bends without straight lengths of pipes with a total volume of 2 L. In this work, they have proposed a model whereby the mean circulation velocity is calculated as a function of U', which is the velocity related to the volumetric rate of discharged flow from the impeller. From their results, they established the following correlation:

$$U_0 = 0.06 F_g N \tag{11.1}$$

where U_0 is the mean bulk velocity, N the rotation speed of the impeller and F_g a geometric factor defined by:

$$F_g = \frac{d_1^2 - d_2^2}{D^2} tg\phi \tag{11.2}$$

The parameters d_1 and d_2 are the inner and outer diameters of the impeller, ϕ is the pitch angle of the blades and D the pipe inner radius. Those results were further confirmed by Khalid et al. (1996) using also a torus reactor with circular section.

For our case, the reactor had a square section and the diameter used in the equation was the hydraulic one. F_g is constant and equal to 0.32. It must be noticed that the relation between the circulation velocity and the impeller rotation speed is strictly linear, that is in agreement with the correlation presented by Belleville et al. (1992). However, the mean bulk velocity obtained for a fixed impeller rotation speed is even lower in the case of a square-sectioned reactor. As it was described by Pruvost et al. (2004), the use of a square-sectioned geometry reduces the induced flow rate in the torus geometry, because the swirling flow is better maintained in circular-sectioned pipes.

127

On the other hand, it is interesting to introduce the Reynolds number in order to characterise the flow. In a mixing tank, where there is no bulk velocity, the Reynolds number is given as the mixing Reynolds number:

$$Re_m = \rho \cdot N \cdot D^2 / \mu \qquad (11.3)$$

In the torus reactor, the Reynolds number can be calculated by the equation:

$$Re = \rho \cdot U_0 \cdot D / \mu \qquad (11.4)$$

with the values of U_0 obtained in previous results. In the case of batch torus reactor, the relation between Re and Re_m is given by (Legrand 1997):

$Re_m > 4500\text{-}5500$ $\qquad\qquad\qquad Re = 0.1109 \cdot Re_m^{1.16}$ $\qquad\qquad (11.5)$

$Re_m < 4500$ $\qquad\qquad\qquad\qquad Re = 0.0027 \cdot Re_m^{1.59}$ $\qquad\qquad (11.6)$

These equations were obtained for a square-sectioned torus reactor of 0.1 L. Figure 11.9 shows the correlations of Reynolds number as a function of the mixing Reynolds number for a torus reactor and also the results obtained by numerical prediction. The results are in agreement with the predicted correlations, especially for Reynolds numbers higher than 1000, however, for lower values of the mixing Reynolds number numerical results were slightly higher than the predicted ones.
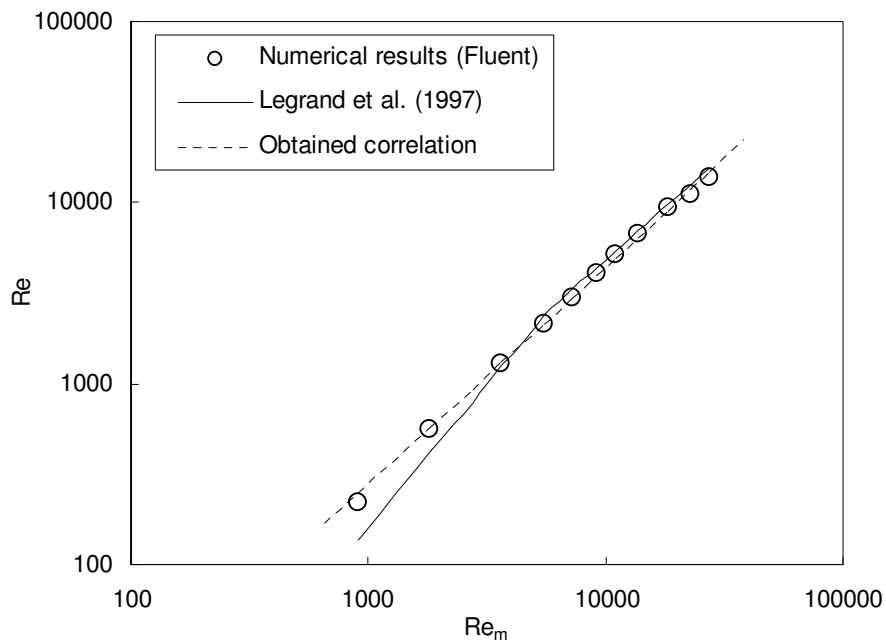
Figure 11.9. Variation of the Reynolds number as function of the mixing Reynolds number.

In the same way, it was possible to obtain a correlation between the mixing Reynolds number and the Reynolds number. The relationship is given in equation 11.7.

$$Re = 0.0695 \cdot Re_m^{1.2} \qquad (11.7)$$

128

This relationship was obtained for values of N ranged between 200 and 3000 rpm and for Reynolds numbers between 550 and 13700. It is noticed that there is no breakdown in this relationship, that it linear in the studied range.

Finally, it was determined the behaviour of the axial component U of the mean velocity for a monitor area located at different distances from the impeller and for different impeller rotation velocities. The figure 11.10 presents the behaviour of U for z/L_z ranges between 0 and 0.75 and for velocities between 200 and 3000 rpm.
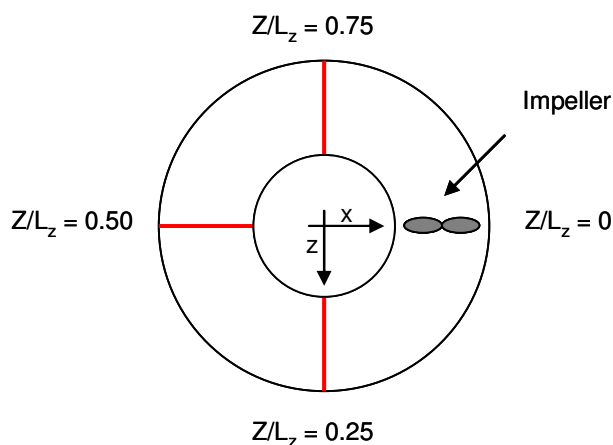
Figure 11.10a. Position of the monitoring areas in the torus reactor.
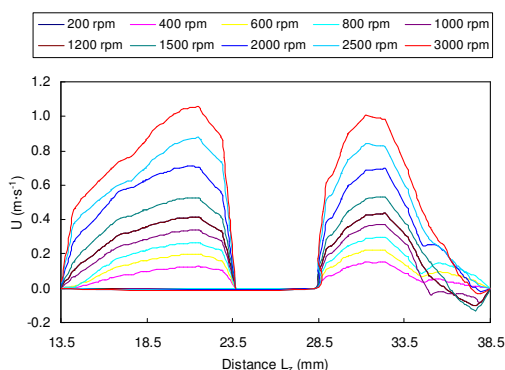
Figure 11.10b. Axial velocity for $Z/L_z=0.00$.
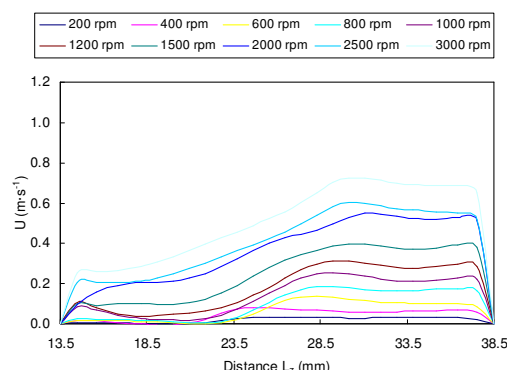
Figure 11.10c. Axial velocity for $Z/L_z=0.25$.
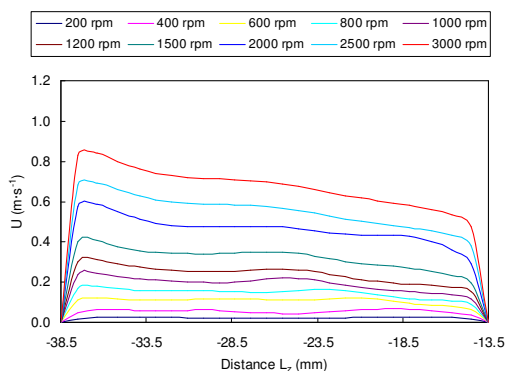
Figure 11.10d. Axial velocity for $Z/L_z=0.50$.
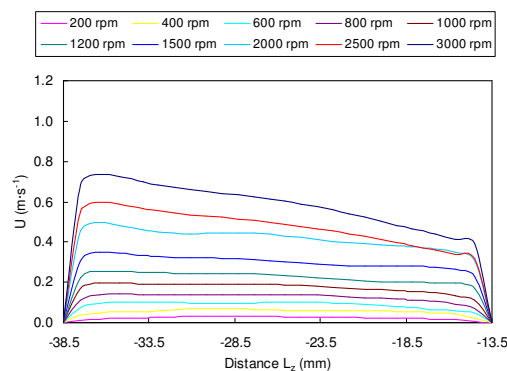
Figure 11.10e. Axial velocity for $Z/L_z=0.75$.

As it can be seen in the figure, the bulk velocity and the axial velocity profile increased with the impeller rotation speed. At z/L_z=0.00, the axial velocity profiles described a null middle zone that corresponded to the impeller wall, and maximum axial velocities after this area in both directions. The axial velocities decreased towards both reactor walls, the internal (x=13.5 mm) and the external (x=38.5 mm). A maximum axial velocity of around 1.1 was achieved with an impeller rotation speed of 3000 rpm. The maximum axial velocities in the other areas (z/L_z=0.25, 0.50 and 0.75) were lower due to the non presence of the impeller. In the case of z/L_z=0.25, the presence of high turbulence could probably explain the lower values of maximum axial velocities compared with the last two areas (z/L_z=0.5 and 0.75). For zones situated far from the impeller (z/L_z=0.50 and 0.75), the centrifugal force, induced by the bend configuration, shifts the maximum velocity towards the outer part of the bend curvature.

11.5.2. Influence of the impeller rotation velocity on the flow-field inside the reactor

The presence of the impeller generates different flow profiles inside the reactor, depending how far or not is the impeller. In figure 11.11, the velocity contours were analysed for two different impeller rotation velocities. As it can be seen in the figures, different velocity contours are generated depending of the impeller velocity for the same location of the test. As higher the impeller rotation is, the turbulence inside the reactor is increased as is shown for 200 and 3000 rpm. Also, for the same impeller velocity, it is obtained different profile of velocities depending if the test is located close or far from the impeller. The impeller generates a swirl flow with a high circumferential velocity, which decreases along the flow path to tend a pure axial flow (Pruvost et al. 2004b).

11.5.3. Determination of the mixing time in batch

By definition, the mixing time is the time necessary to achieve the total homogenisation in the concentration inside the reactor. In this study, the mixing time, T_m, was determined by monitoring the evolution of the tracer concentration into the reactor. The figure 11.12 gives an example of the time-variation of the concentration for an impeller rotation speed of 1500 rpm. The relative height of the peaks and their number depend on the axial dispersion into the reactor. With a high axial dispersion, the reactor is mixed during one circulation, thus, peak values will decrease faster and consequently less time is needed for obtaining a homogenous mixture. After a given time, corresponding to the mixing time, the tracer is totally homogenised and the concentration inside the reactor reaches a constant value. Moreover, T_m is defined as the time to achieve the final concentration obtained at the final dilution, C_{final}, with a variance value of 5%.
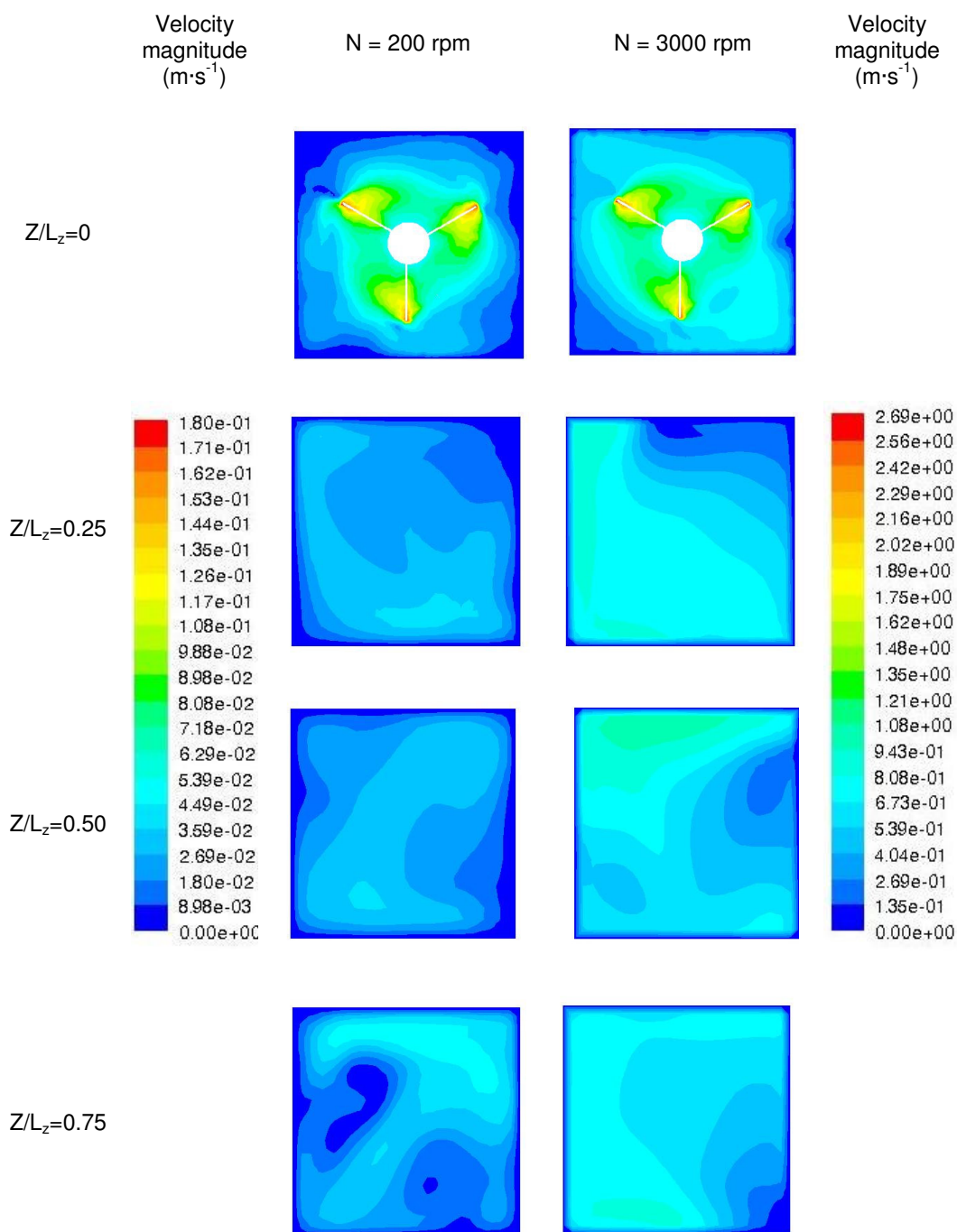
Figure 11.11. Velocity contours inside the reactor for two different impeller rotation speed and different positions.

On the other hand, the mean circulation time corresponds to the time between two consecutive peaks on the response curve.
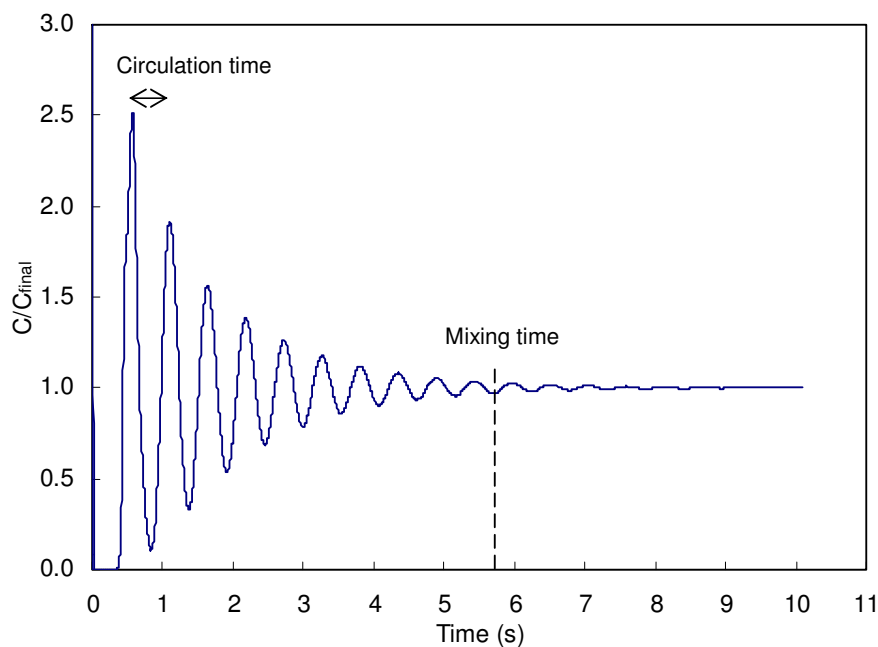
Figure 11.12. Example of mixing time determination: time evolution of the normalized concentration averaged on the monitored surface (z/L_z = 0.25, N = 1500 rpm).

Figure 11.13 depicts the variation of the mixing time as a function of the impeller rotation speed. As it can be seen in the figure, the mixing time decreases rapidly with the increase of the impeller rotation speed.
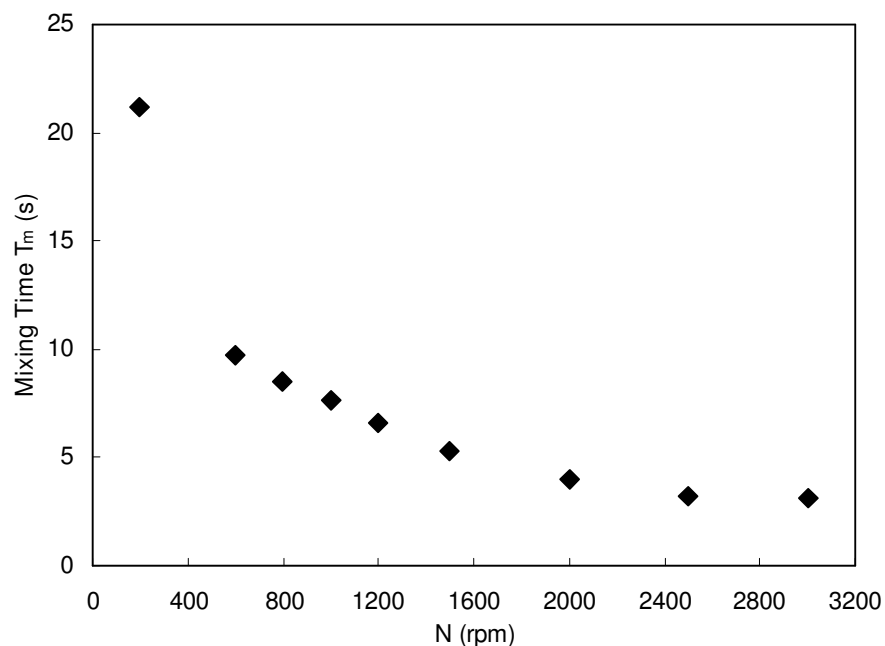
Figure 11.13. Mixing time numerical prediction: evolution of the mixing time with the impeller rotation velocity.

As expected, the same trend was obtained by Pruvost et al. (2006) working with a photobioreactor of 1.3 L volume.

The maximum value of the mixing time was calculated to 21s for a speed of the impeller rotation of 200 rpm. Even for small impeller rotation speeds, mixing time can be considered sufficiently short to achieve rapid concentration homogeneity in the reactor. After an impeller velocity value of 1200 rpm, a mixing time smaller than 5 s is necessary to achieve a total homogenisation inside the reactor. In terms of circulations, the mixture needed 3.4 turns to obtain a homogenous concentration inside the reactor using an impeller rotation speed of 200 rpm. Likewise, it took 8.7 turns for an impeller rotation speed of 1000 rpm and 12.3 turns for an impeller rotation speed of 3000 rpm to obtain a total homogenous concentration of the mixture inside the reactor.

Another important parameter to be analysed is the dimensionless mixing time T_m^*, defined by (Harnby 1997):

$$T_m^* = N.T_m \tag{11.8}$$

where N is the impeller rotation velocity. This parameter is important because it allows a comparison with classical geometries, like mixing tanks, where this parameter is found to be independent of the Reynolds number when turbulent regime is achieved (Harnby 1997). Figure 11.14 presents the values of T_m^* for impeller rotation speeds varying from 200 rpm to 2000 rpm. As it can be seen in the figure, T_m^* is found to be constant for values of N higher than 1200 rpm, corresponding to a Reynolds number of 5800 and to a fully turbulent regime (Benkhelifa et al. 2000). A better mixing is obtained in turbulent flow due to a better dispersion, but the energy consumption is also greater. Generally, a compromise has to be found.
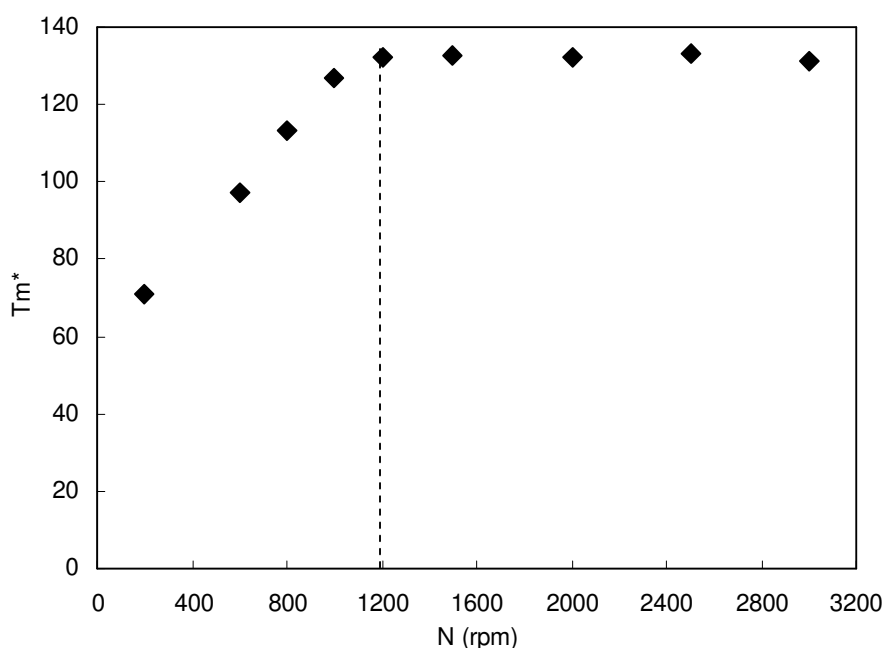
Figure 11.14. Numerical prediction: dimensionless mixing time.

On the other hand, the visualisation of the mixing along a single revolution for the tracer can be seen in figure 11.15. As it can be seen in the figure, the tracer cloud is time-dispersed.

11.6. Results of the CFD study in continuous mode

11.6.1. Mean velocities and circulation times

The mean velocity is defined as the average velocity of all the particles inside the reactor. The mean velocities in continuous were obtained into the reactor using a CFD analysis. Due to the presence of inlet and outlet flow, the continuous regime can lead to different hydrodynamics with respect to the batch one. The relation between N and U_0 could be modified due to the effect of the entering flow rate through the inlet. This entering flow rate can modify the U_0 by increasing it or by decreasing it due to a possible effect in the circulation. Table 11.1 presents the results obtained for the mean circulation velocities U_0 into the reactor for different impeller rotation speeds ranged from 0 to 2000 rpm and, for different flow rates, varying from 180 to 1200 ml/h. As it can be seen in the table, the mean velocities inside the reactor increased with an augment in the impeller rotation velocity. Also, the inlet flow rate has a small influence on the mean velocity except for small agitation speeds. With the higher inlet flow rates the mean velocities are lightly smaller, may be due to the perturbation of the flow inside the reactor. Finally, for all flow rates, the results are mainly dependent on the impeller rotation speed, the same behaviour was observed in batch conditions.

Table 11.1. Mean circulation velocities ($m \cdot s^{-1}$) into the reactor for different impeller rotation speeds.

Speed	U_0 ($m \cdot s^{-1}$)				
		Continuous			
N (rpm)	Batch	Q=180 ml·h^{-1}	Q=400 ml·h^{-1}	Q=900 ml·h^{-1}	Q=1200 ml·h^{-1}
0		0.0002	0.0005	0.0008	0.0012
200	0.0224	0.0256	0.0257	0.0256	0.0258
400	0.0538				
500	0.0744	0.0784	0.0784	0.0782	0.0781
600	0.0915				
800	0.1302				0.1285
1000	0.1766	0.1848	0.1856	0.1850	0.1838
1200	0.2247			0.2322	0.2225
1500	0.2971	0.3024	0.3026	0.3019	0.2919
1800	0.3518	0.3754	0.3754	0.3751	0.3617

t=0.025s

t=0.225s

y
z
x

t=0.325s

t=0.475s

t=0.625s

t=0.775s

t=0.975s

t=1.225s
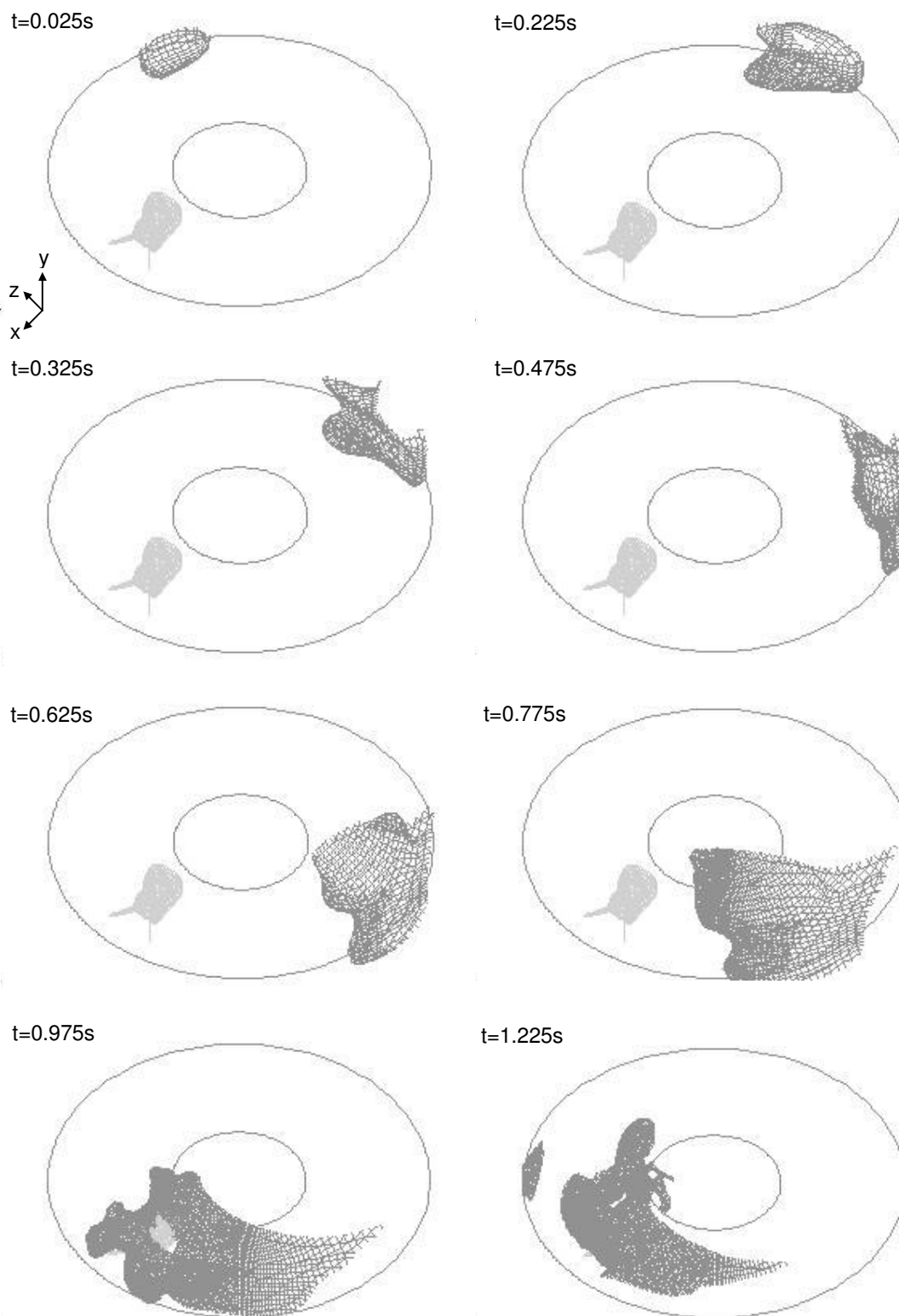
Figure 11.15. Example of mixing in a single revolution for N = 800 rpm and different times.

On the other hand, figure 11.16 presents the mean circulation times in batch and continuous conditions for a flow rate of 1200 ml/h and different impeller rotation speeds. As it can be seen in the figure, the differences between batch and continuous conditions are very low, both curves having the same behaviour and similar to that presented by Benkhelifa et al. (2000). Only a slight difference can be observed for low rotation speeds.
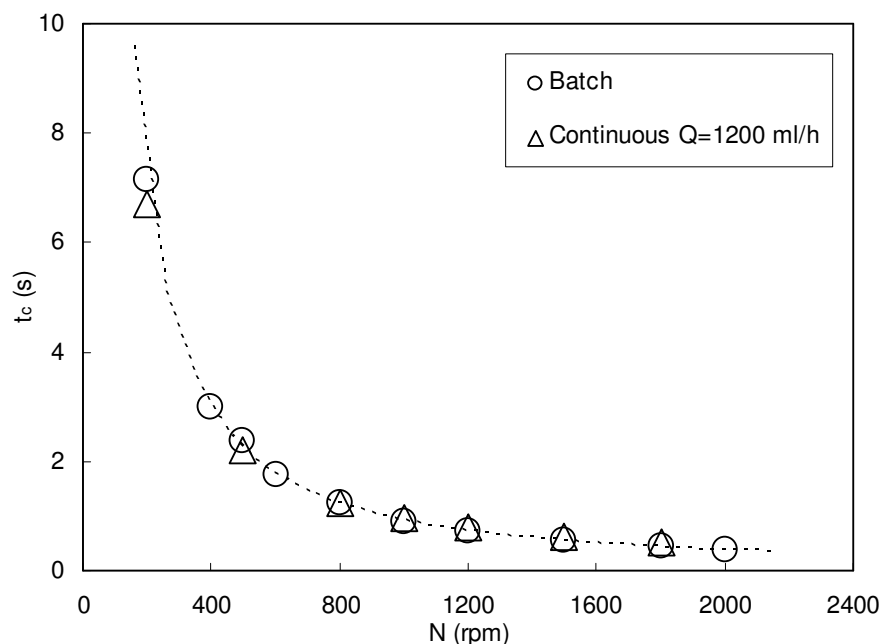
Figure 11.16. Mean circulation times obtained for batch and continuous conditions for different impeller rotation speeds and for a flow rate of 1200 ml/h.

Moreover, the circulation time can be defined as the time necessary for a fluid element to traverse a torus reactor loop. The circulation time was studied for continuous and also for batch reactors. For the continuous reactors, the mean circulation time was denominated t_{cc}, for the batch reactors, it was called t_{cb}. This study was carried out in order to determine the effect of the inlet flow rate into the circulation inside the reactors.

For a given speed, the figure 11.17 presents the evolution of the ratio between t_{cc} and t_{cb}, as a function of τ/t_{cc}, where τ is defined as:

$$\tau = \frac{V}{Q} \tag{11.9}$$

The ratio between the residence time, τ, and the mean circulation time in continuous mode characterised the importance of the inlet flow rate on the circulation. The t_{cc}/t_{cb} ratio was nearly equal to 1.1 for high values of τ/t_{cc}, and less than 1 when the rotation speed was low (less than 800-1000 rpm). This fact indicates that the hydrodynamics inside the reactor were perturbed in particular conditions, for small values of N, or for high values of Q, depending of the ratio characterised by τ/t_{cc}.
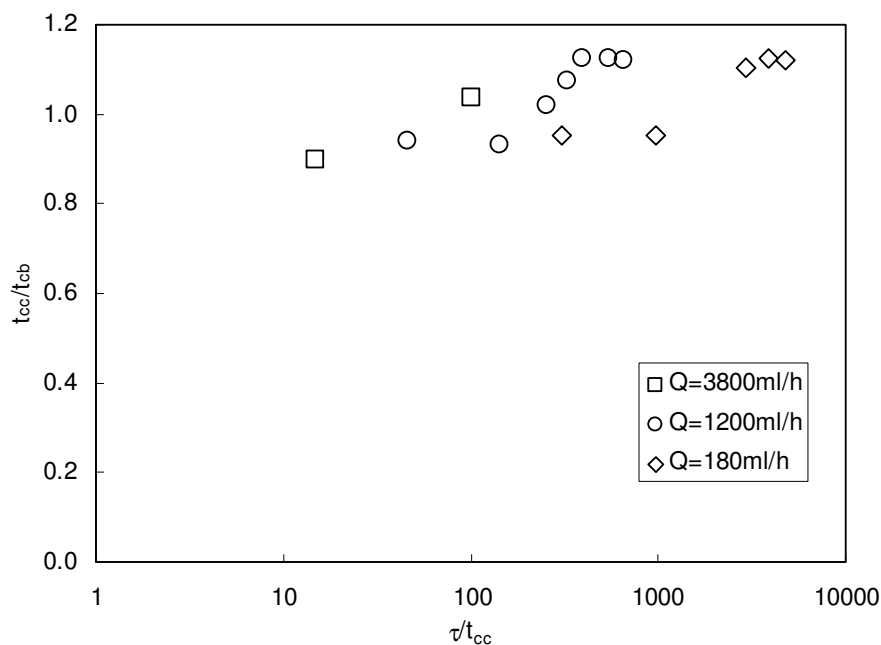
Figure 11.17. Comparison of the mean circulation time in continuous and batch conditions as a function of the τ/tcc ratio for different flow rates.

Finally, the impeller rotation velocity plays a major role in the hydrodynamics. Figure 11.18 presents the comparison of the mean circulation time in continuous and batch conditions as a function of the impeller rotation speed for different flow rates. As it can be seen in the figure, below a given value of the rotation speed, all feeding flow rates in continuous conditions have an influence on the circulation inside the reactor, which is accelerated. At high impeller rotation speed, more than 1000 rpm, the inlet flow rate had no influence on the circulation, giving the same t_{cc}/t_{cb} ratio.

Benkhelifa et al. (2000) reported a diminution in the mean circulation time, especially important when the value of τ/t_{cc} is smaller than 20 ($t_{cc}/t_{cb} < 0.8$). In this work, the inlet injection was in the same direction of the flow circulation, favouring the circulation inside the reactor. Unlike this, in the case under study, the inlet injection was perpendicular to the circulation flow. This important change might explain the reduction in the effect of the inlet flow rate, and thus, this could not be observed in this study.
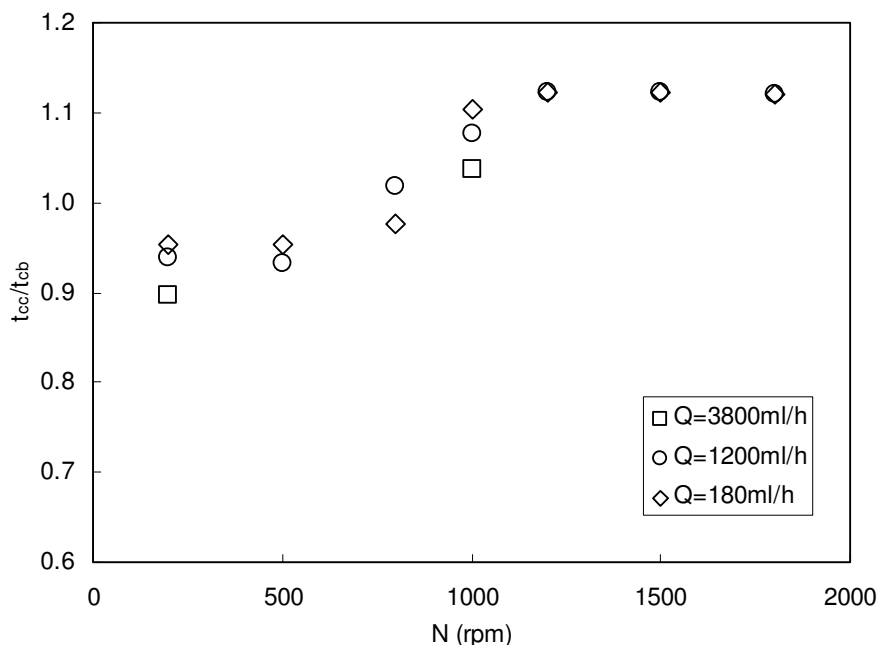
Figure 11.18. Comparison of the mean circulation time in continuous and batch conditions as a function of the impeller rotation speed for different flow rates.

11.6.2. Influence of the inlet flow rate on the flow inside the reactor

The influence of the inlet flow rate on the flow structure in the entrance of the reactor was investigated. By the conception of the experimental reactor, the flow inlet is set perpendicular to the reactor and has thus a small influence. Depending of the impeller rotation speed, the circulation time inside the reactor can even be increased or decreased. For small values of N, feeding flow rate accelerated the circulation inside the reactor, on the contrary, deceleration of the flow circulation was observed for values of N > 1000 rpm.

Figure 11.19 presents the differences in the flow structures due to the influence of the inlet flow rate. In this figure, it is possible to see the velocity contours inside the reactor and the flow rate leads to a negligible perturbation at small flow rate of 180ml/h and a higher for high feeding flow rates of 7200 ml/h. The same trend was observed when the velocity vectors are depicted.

However, such operating conditions correspond to the two extreme cases, lowest and highest flow rates available experimentally, the influence on the flow structure in normal operating conditions remains limited. The reactor hydrodynamics in continuous regime will be mainly the result of the influence of the impeller rotation.
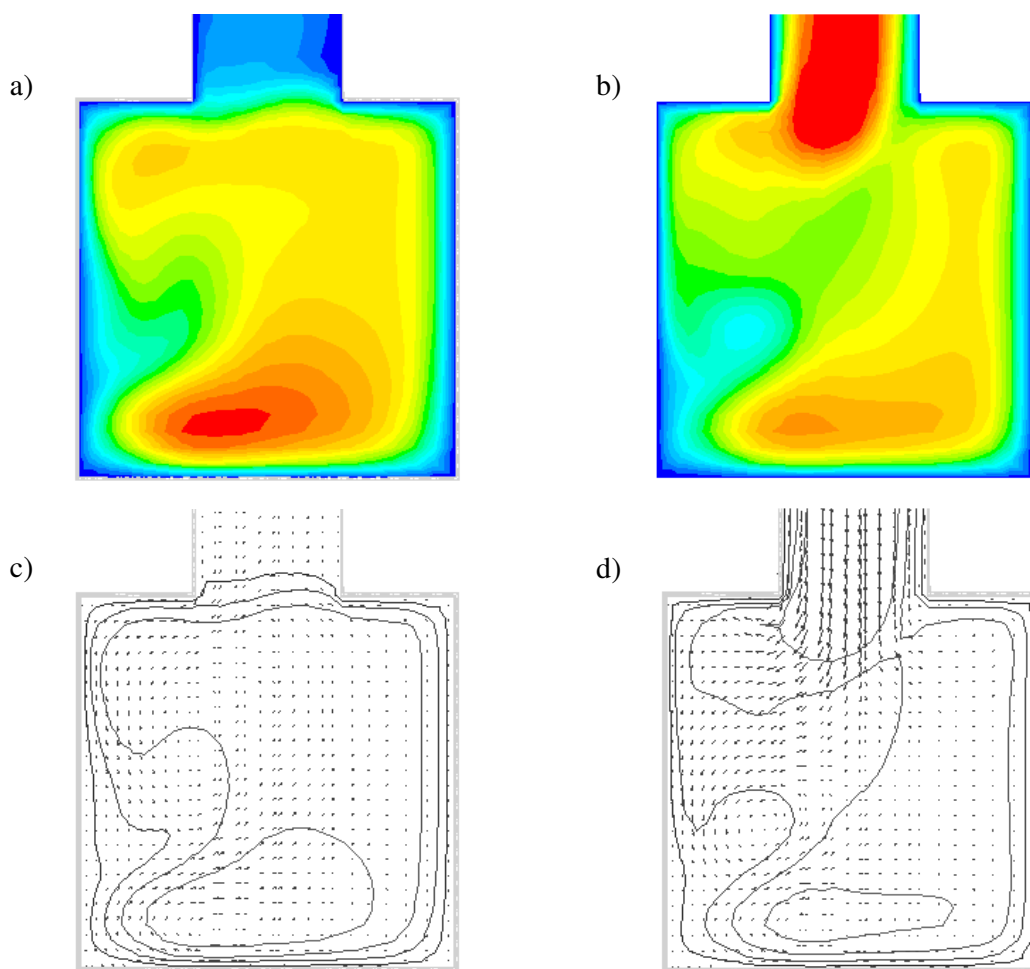
Figure 11.19. Modification of the flow structure due to the feeding injection. Velocity contours inside the reactor for a) 200 rpm, 180 ml/h and b) 200 rpm, 7200 ml/h. Velocity vectors showing the flow disturbance c) 200 rpm, 180 ml/h and d) 200 rpm, 7200 ml/h.

11.7. Influence of the inlet flow rate position on the mixing time in continuous

The hydrodynamic study of the torus reactor in continuous mode has been evaluated and presented in section 11.6. In order to improve the reactor performance, it was investigated the influence of the inlet flow rate on the hydrodynamic characteristics in the reactor.

Different geometries were used to determine the influence of the position of the inlet flow rate varying its location onto the reactor. The outlet was kept in the same position, at ϕ=180º from the impeller, for all the cases. Inlets were placed at: ϕ=-68º for the original grid, ϕ=-112º for grid 1, ϕ=-90º for grid 2 and ϕ=90º for grid 3. For all cases, the geometry of the reactor and the outlet was constant and then, the inlet was placed in the desired position. Due to the change in the inlet position, a different geometry and grid were obtained for each case. The different configurations studied and the angular differences between the inlet and the outlet are shown in figure 11.20.
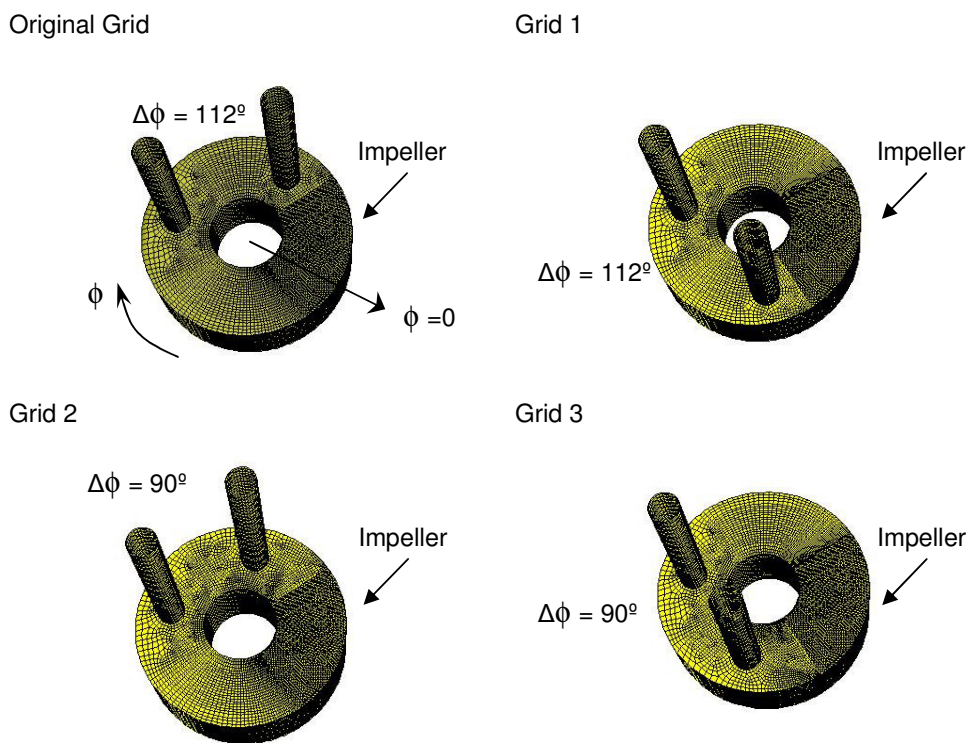
Figure 11.20. Different configurations for the inlet flow rate.

The figures 11.21 show the mixing time obtained for each configuration and for two different inlet flow rates, 180 and 1200 ml/h.
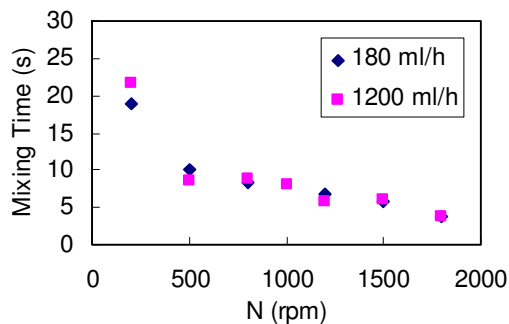
Figure 11.21a. Mixing time obtained for grid 1.
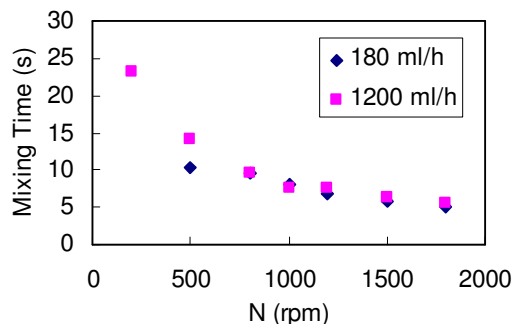
Figure 11.21b. Mixing time obtained for grid 2.

As it can be observed in the figures, only a small difference in the mixing times is observed for small values of impeller rotation speeds (200 rpm). For higher velocities of rotation, negligible differences have been found for the different configurations. Therefore, the inlet flow rate position has not influence on the hydrodynamic of the torus reactor and the flow inside the reactor when the entrance of the flow in located in a perpendicular form to the flow circulation inside the reactor.
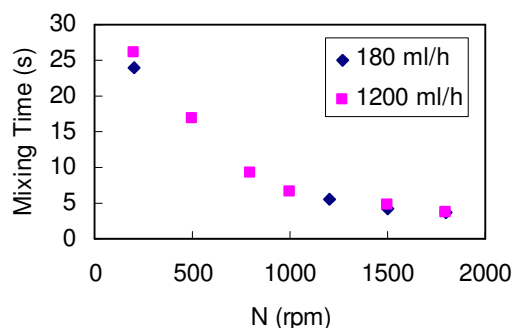
Figure 11.21c. Mixing time obtained for grid 3.

Also, the flow rate has not influence on the flow inside the reactor in the studied ranges. These results can be compared with those obtained by Benkhelifa et al. (2000), where they have seen perturbation of the flow when the inlet flow rate is located in a parallel form respect to the reactor, where the inlet flow rate benefits the circulation inside the reactor.

11.8. Comparison with a circular-sectioned torus reactor in batch conditions

A new geometry and grid were created for the torus reactor but using a circular-sectioned reactor. Figure 11.22 shows the mesh of the torus reactor with a circular section.
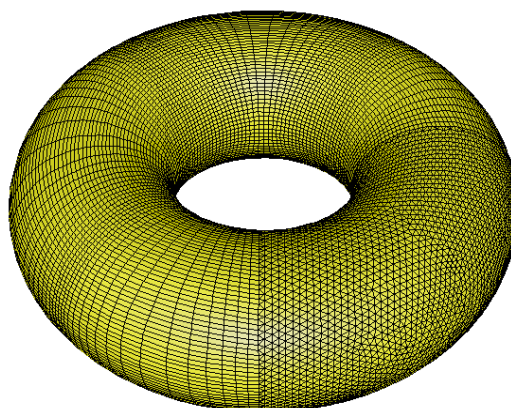
Figure 11.22. Grid for the circular-sectioned torus reactor.

For this, the same methodology was kept as in section 11.1. In this case, the regular part of the reactor was created using the default toroidal geometry available in Gambit, however, in order to include the impeller, the irregular part had to be modified and rebuilt to be compatible with the rest of the geometry. Once the geometry was finished, the mesh was created resulting in a regular mesh in ¾ of the reactor and an irregular mesh for the quarter that contained the impeller. The used impeller corresponded to the geometry described in section 11.1. The resulting mesh with 328691 cells has been tested.

The mean bulk velocities inside the circular-sectioned torus reactor were determined using CFD. As can be seen in figure 11.23, the mean velocities in the circular-sectioned reactor showed the same trend than the square-sectioned torus reactor.
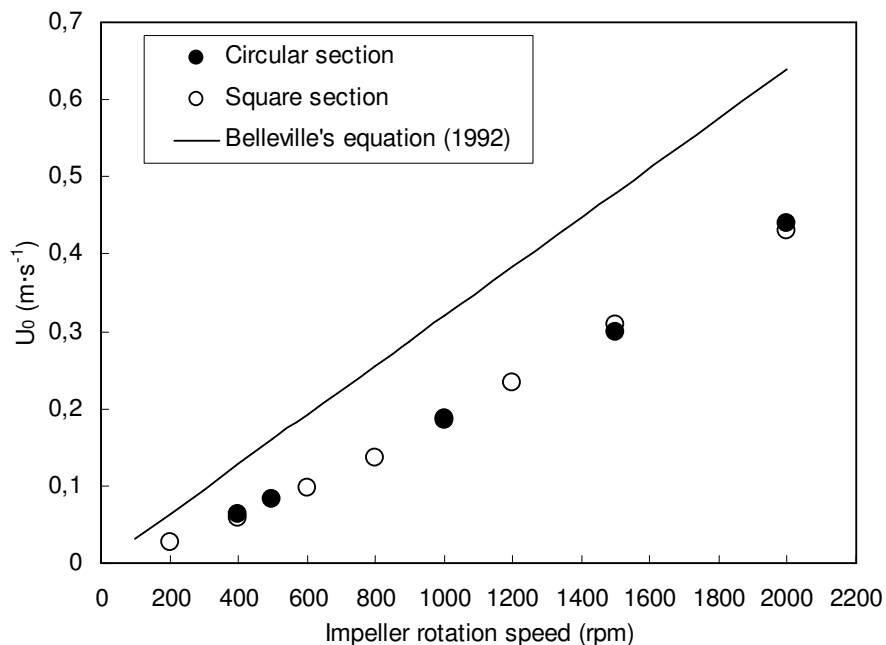
Figure 11.23. Mean bulk velocities in the circular-sectioned torus reactor.

As it can be observed in the figure, negligible differences were observed comparing square and circular-sectioned torus reactor. This fact can be due to the small volume of the reactor and the high turbulence generate inside it.

Different flow profiles are generated inside the reactor depending where the test is located respect to the impeller. Figures 11.24 show the flow profiles for two different impeller rotation velocities, 200 and 2000 rpm. As it can be seen in the figures, different velocity contours are generated depending of the impeller velocity for the same location of the test. As high the impeller rotation is, the turbulence inside the reactor is increased. Also, for the same impeller velocity, it is obtained different velocity profile depending if the test is located close or far from the impeller. A decaying swirl flow is generated by the impeller. The swirl intensity decreases with the circumferential distance from the impeller.
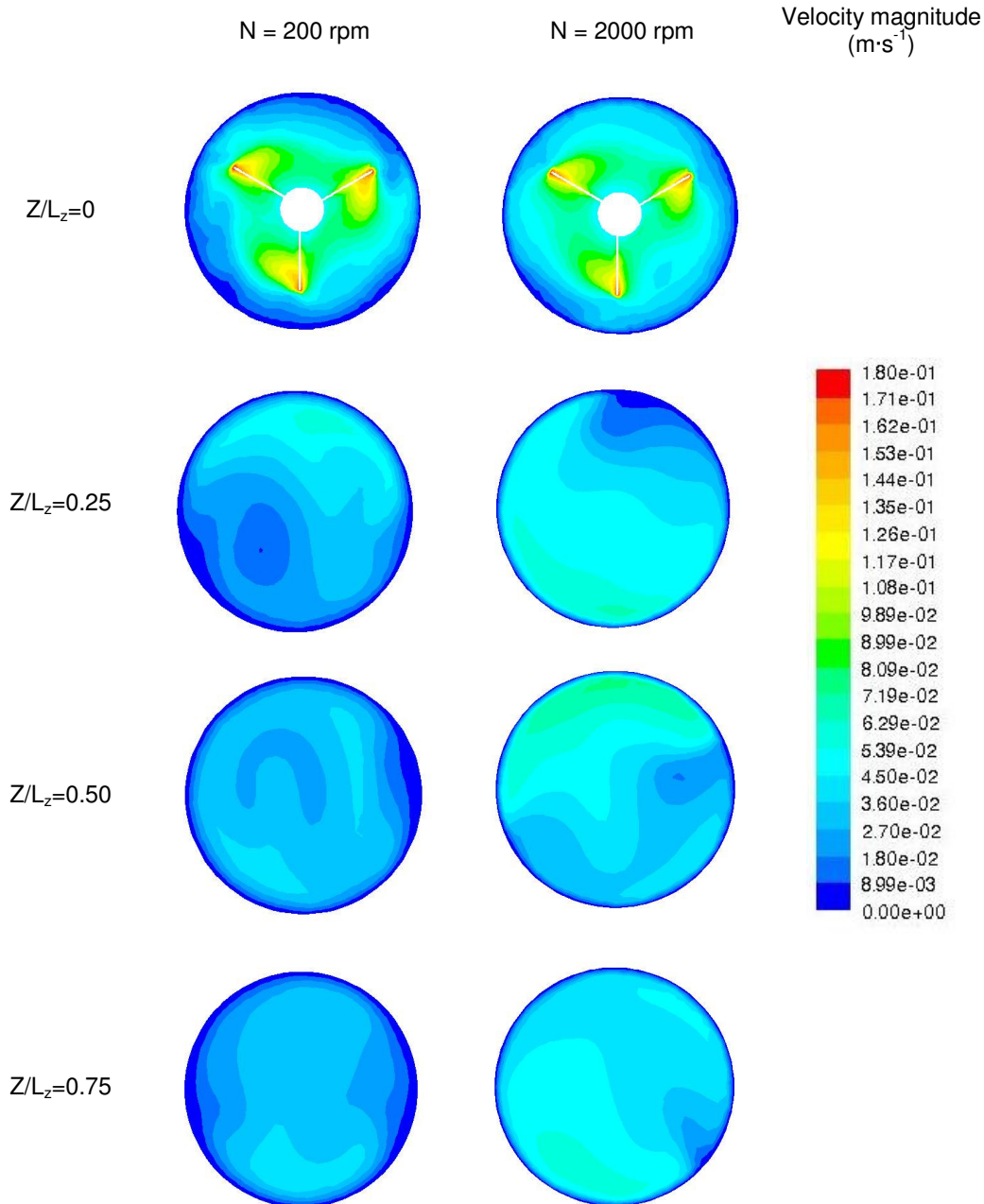
Figure 11.24. Flow profile in the circular-sectioned torus reactor at different positions.

11.9. Scale-up of the torus reactor volume

Finally, a scale-up to 300 ml of the square-sectioned torus reactor was realised with a new mesh of 1126746 cells. The geometry and mesh for this new torus reactor were made in the same way the geometry and mesh of the reactor from section 11.1 were created. Due to the impeller, a regular mesh was difficult to apply to the entire geometry. The reactor was divided in

two different zones: the marine impeller vicinity, which was meshed using tetrahedral volumes and prisms; and the remaining part of the reactor that was meshed with regular elementary hexahedral volumes. The impeller used in this study was the same presented in section 11.1. Figure 11.25 presents the geometry and the mesh for the reactor of 300 ml.
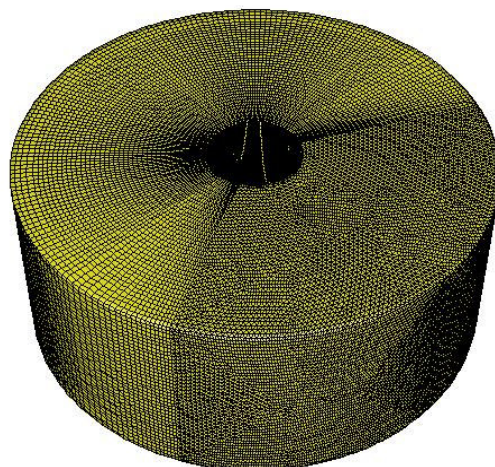
Figure 11.25. Mesh of the 300 ml square-sectioned torus reactor.

To compare the performance of the 300 ml reactor, the mean bulk velocities were calculated. The mean velocities inside the reactor are shown in figure 11.26.
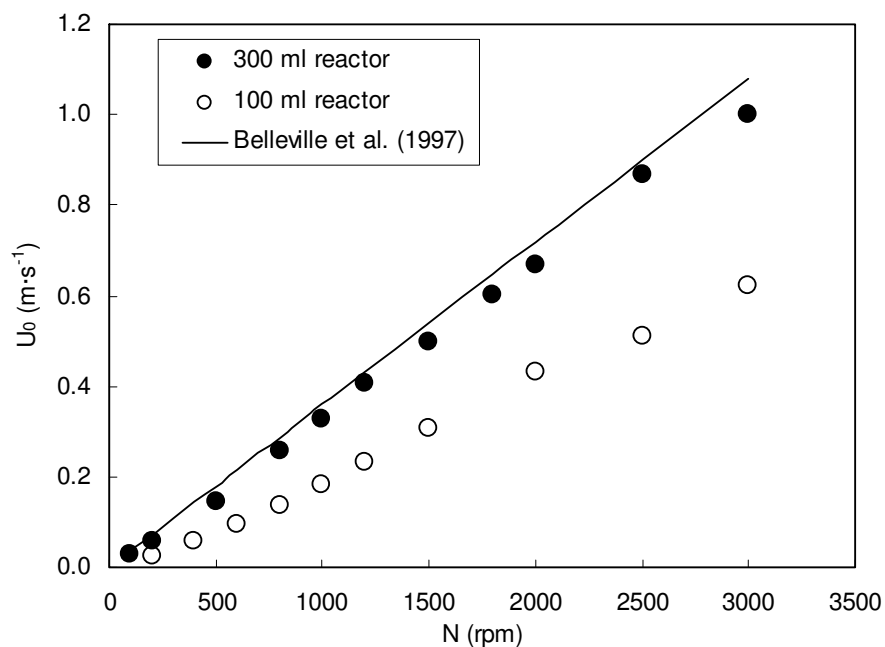
Figure 11.26. Mean bulk velocities in the 300 ml square-sectioned torus reactor.

As it can be seen in the figure, the mean velocities obtained for the 300 ml square-sectioned reactor presented a linear relation between U_0 and the impeller rotation speed. These mean

velocities were higher compared with the ones obtained for the 100 ml square-sectioned reactor.

A higher volume of the reactor, with a bigger impeller, could be the reason for this behaviour. The impeller for this case had an external diameter of 25 mm and an internal diameter of 7 mm, keeping the same pitch angle. In comparison with the empirical equation obtained by Belleville et al. (1992) for a torus reactor with circular section, the mean velocities obtained in this case were slightly smaller. It is possible that the flow in the model used by Belleville et al. (1992) that consisted of four flanged smooth bends without straight lengths of pipes with a total volume of 2 L, behaves in a similar way than in this 300 ml square-sectioned torus reactor. This might be possible supposing that large diameter reactors behaves in a similar way.

On the other hand, the Reynolds and the Reynolds mixing numbers for the 300 ml reactor were also calculated and are presented in figure 11.27. A linear relation between the Reynolds and the Reynolds mixing numbers was obtained. This relation is comparable to the one obtained for the 100 ml torus reactor (eq. 11.7), thus, the same approximation was used.

$$Re = 0.0695 \cdot Re_m^{1.2} \tag{11.7}$$

In the same way a linear relation was obtained for the 100 ml torus reactor, the 300 ml reactor presented a linear relation without the breakdown point presented by Legrand et al. (1997).
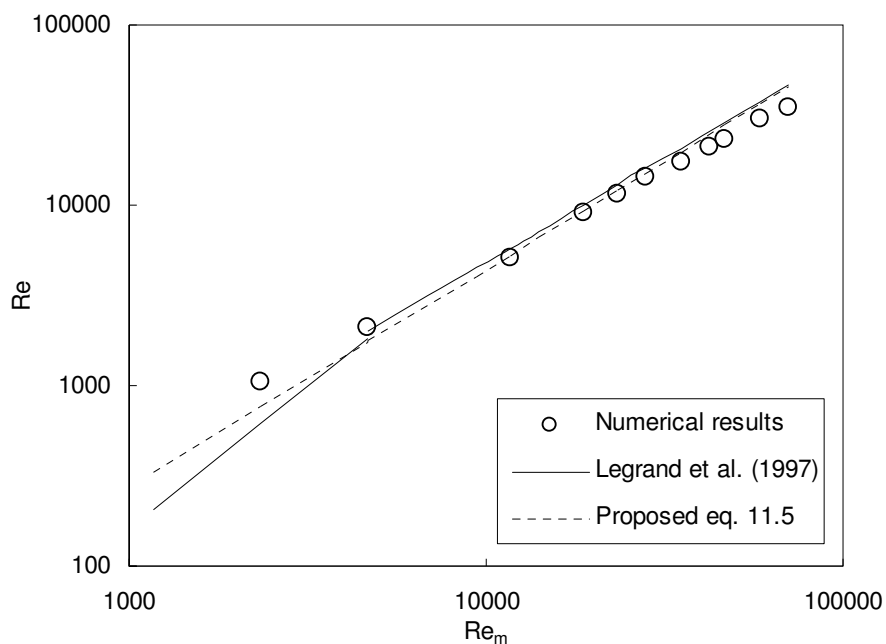
Figure 11.27. Reynolds vs. Reynolds mixing number in the 300 ml square-sectioned torus reactor.

145

11.10. Conclusions

The characterization of the flow-field in a torus reactor of 100 ml similar to the experimental reactor was carried out for two different configurations, batch and continuous reactor. In batch conditions, a linear evolution of the mean circulation velocities with respect to the impeller rotation speed was obtained, as it was already determined by Belleville et al. for a circular-sectioned torus reactor.

The mixing time values obtained in all hydrodynamic conditions were short, less than 21s in all studied cases, to achieve rapid concentration homogeneity into the reactor. The dimensionless mixing time was determined and was found to be independent of the Reynolds number when the impeller rotation speed is greater than 1200 rpm (Re > 5800). Thus, fully turbulent regime should be obtained into the torus reactor from these values of Reynolds number, achieved from N = 1200 rpm.

In continuous mode, the torus reactor can exhibit a more complex behaviour, due to the perturbation of the inside flow by the feeding injection (acceleration or deceleration of the flow circulation in the reactor). This was shown for particular conditions of impeller rotation speeds and feeding flow rates. For common operating conditions, the hydrodynamics is however mainly a function of the impeller rotation speed. Further study will quantify influence of such perturbation in the case of enzymatic conversion using the torus reactor in continuous regime.

When different inlet flow rates are compared in order to determine the best configuration to be used, only a small difference in the mixing times was observed for small values of impeller rotation speeds (200 rpm). For higher velocities of rotation, negligible differences have been found for the different configurations. So, it could be deduced that when the flow inlet in located in a perpendicular form to the flow circulation inside the reactor, it has not influence on the hydrodynamic of the reactor.

A circular-sectioned torus reactor was tested by CFD to compare the performance with a square-sectioned one. Negligible differences were found due to the small volume of the reactor and the high turbulence generate inside it.

Finally, a 300 ml square-sectioned reactor was studied by CFD. This reactor seems to be more effective than the 100 ml one because it presents higher bulk velocities and similar to those predicted by the empirical equation proposed for a torus reaction with circular section.

Chapter 12. Modelling the enzymatic reaction with CFD

This chapter presents a numerical approach of the enzymatic elimination of phenol using CFD. Different alternatives are analysed and the most relevant results are summarised.

12.1. Numerical approach

To validate the numerical simulation of the torus reactor, the enzymatic reaction of phenol with HRP was also modelled using CFD. To allow the validation, the kinetics of the enzymatic reaction was coupled with the flow study. To do this coupling, the reaction option has to be activated in the software and various species as reactants, products and enzyme, have to be defined. Their transport is therefore represented with the flow-field.

Then, the reaction mechanism has to be defined to simulate the enzymatic reaction. For this, two different strategies were studied. In the first one, while the enzyme concentration was kept small, only two reactions were taken into consideration, and in this case, the reaction mechanism defined in Fluent was:

$$E+H_2O_2 => C_1+H_2O \tag{12.1}$$

$$C_1+PhOH => E+PhO\bullet+H_2O \tag{12.2}$$

where C_1 represents an active intermediate form of the enzyme E.

The second strategy was studied because inhibition of the reaction was found for some initial concentrations of the reagents. In this case, the reaction mechanism was basically the same, with the equations 12.1 and 12.2 but, adding a third reaction necessary to take in account the step of the inhibition of the enzyme. Then, the reaction mechanism was:

$$E+H_2O_2 => C_1+H_2O \tag{12.1}$$

$$C_1+PhOH => E+PhO\bullet+H_2O \tag{12.2}$$

$$E+H_2O_2 => E_i+H_2O \tag{12.3}$$

where E_i represents the inactive form of the enzyme.

The next step was the definition of the reaction rate in Fluent by the utilisation of a user-defined function (UDF). To do this, it was necessary to write a small program in C language and coupling it to Fluent using the UDF utility. The reaction rate was defined in the UDF utility using the kinetic parameters obtained experimentally. After that, a patch (assignation of an initial value to variables into different cells) was done for each initial concentration of the reagents into the reactor. Finally, to simulate the enzymatic reaction, it was used the kinetic model with inhibition by H_2O_2 and taking into account the influence of the phenol initial concentration, presented in the section 5.4.3.

The simulations were carried out in unsteady-state mode, by solving the transport equations for each reactive and for the local enzymatic reaction rates. The phenol conversion was determined in each case by monitoring the species concentrations versus time.

12.2. Numerical simulation of the reaction using the global kinetic model

12.2.1. Simulation of the reaction using the mechanism without inhibition

In a first phase of the study, it was used the mechanism of the reaction described only by equations 12.1 and 12.2. In this case, the inhibition of the enzyme was not taken in account. The figures 12.1, 12.2 and 12.3 present the influence of the H_2O_2 initial concentration on the phenol conversion for an initial phenol concentration of 0.5, 1.1 and 1.6 mM respectively.

Figure 12.1.   Influence of the H_2O_2 initial concentration on the simulated phenol conversion in the torus reactor without inhibition. [Phenol]$_0$: 0.5 mM and [HRP]$_0$: $2 \cdot 10^{-4}$ mM.

As it can be seen in the three figures, the phenol conversion reached a maximum value after few minutes for each H_2O_2 initial concentration and then, remained more or less invariable. The conversion of phenol increased when the H_2O_2 initial concentration was raised until a maximum value of conversion was reached. After this point, if the H_2O_2 initial concentration was increased, the final phenol conversion was decreased and the reaction had a slower initial reaction rate.

Figure 12.2.   Influence of the H_2O_2 initial concentration on the simulated phenol conversion in the torus reactor without inhibition. $[Phenol]_0$: 1.1 mM and $[HRP]_0$: $2 \cdot 10^{-4}$ mM.

Figure 12.3.   Influence of the H_2O_2 initial concentration on the simulated phenol conversion in the torus reactor without inhibition. $[Phenol]_0$: 1.6 mM and $[HRP]_0$: $2 \cdot 10^{-4}$ mM.

On the other hand, the phenol conversion curves present a similar behaviour than those observed in the experimental work, shown in section 5.2 (figures 5.3, 5.4 and 5.5 respectively). The simulated phenol conversions are in agreement with the experimental ones but only, for an H_2O_2 initial concentration that remained below the optimal value. When this value is reached, the phenol conversions are overestimated.

149

12.2.2. Simulation of the reaction using the mechanism with inhibition

In a second step, the reaction described by equation 12.3 was included in the mechanism of the reaction. In this case, the inhibition of the enzyme was taken in account. The figures 12.4, 12.5 and 12.6 present the influence of the H_2O_2 initial concentration on the phenol conversion for an initial phenol concentration of 0.5, 1.1 and 1.6 mM respectively.
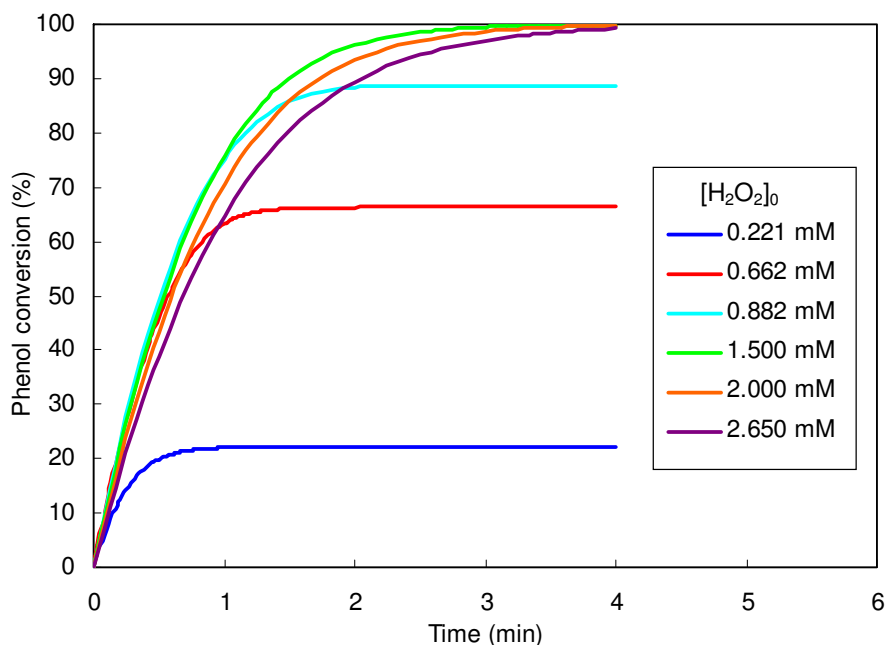
Figure 12.4. Influence of the H_2O_2 initial concentration on the simulated phenol conversion in the torus reactor with inhibition. $[Phenol]_0$: 0.5 mM and $[HRP]_0$: $2 \cdot 10^{-4}$ mM.

As it can be seen in the figures, a good agreement with the experimental data was obtained for values of H_2O_2 initial concentrations higher than the optimal value (figures 5.3, 5.4 and 5.5 respectively). For smaller values of H_2O_2, an underestimation was observed for the phenol conversion in all cases.

Therefore, it would be necessary to combine two mechanisms in order to well simulate the enzymatic reaction for all values of H_2O_2 initial concentrations. In this sense, a mechanism without inhibition of the enzyme has to be applied below the optimal value of H_2O_2 initial concentration and a mechanism taking into account the inhibition of the enzyme has to be applied above.

Chapter 12. Modelling the enzymatic reaction with CFD
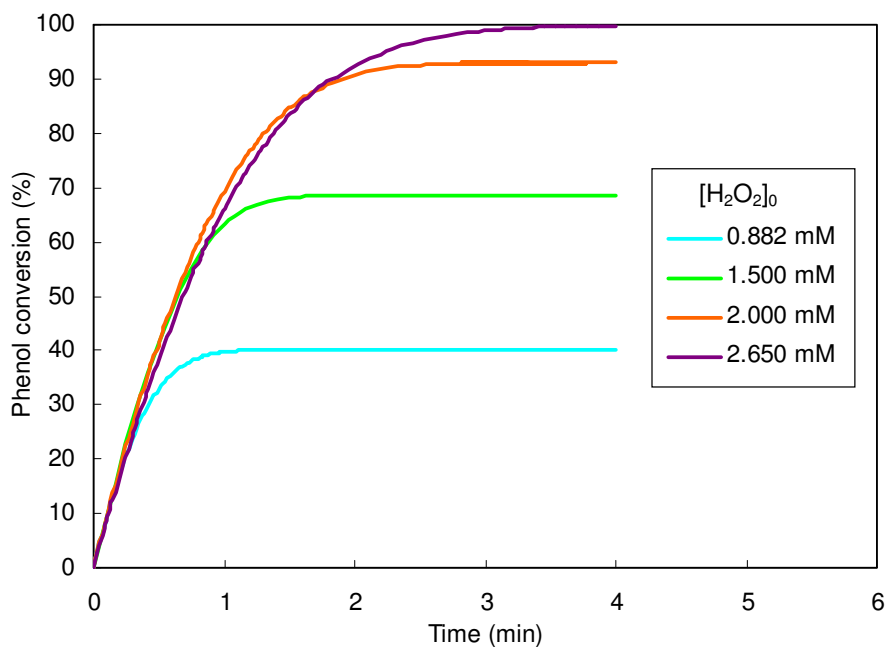
Figure 12.5. Influence of the H_2O_2 initial concentration on the simulated phenol conversion in the torus reactor with inhibition. $[Phenol]_0$: 1.1 mM and $[HRP]_0$: $2 \cdot 10^{-4}$ mM.
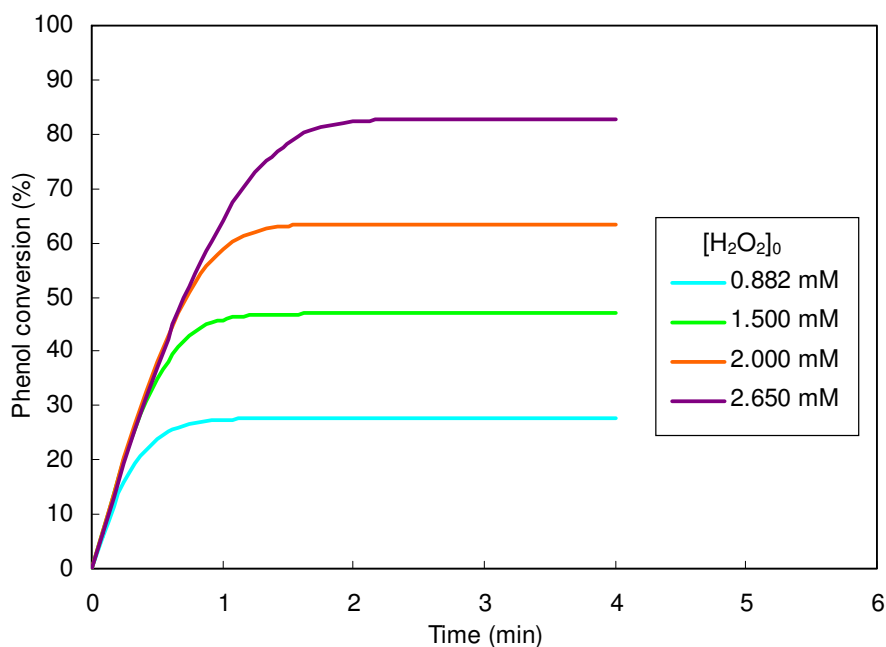
Figure 12.6. Influence of the H_2O_2 initial concentration on the simulated phenol conversion in the torus reactor with inhibition. $[Phenol]_0$: 1.6 mM and $[HRP]_0$: $2 \cdot 10^{-4}$ mM.

The figures 12.7, 12.8 and 12.9 present the influence of the H_2O_2 initial concentration on the phenol conversion for an initial phenol concentration of 0.5, 1.1 and 1.6 mM respectively, with both mechanisms used.
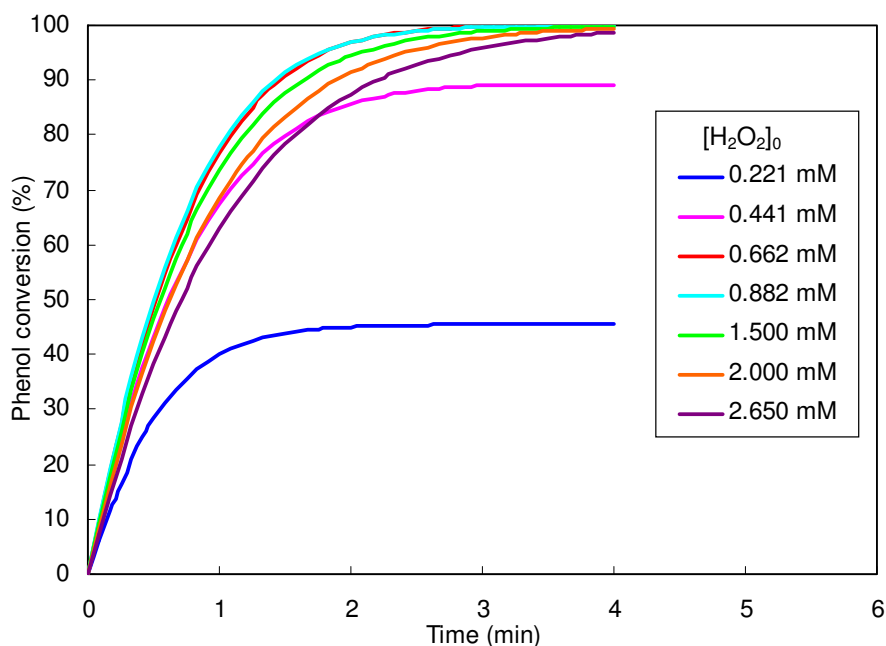
Chapter 12. Modelling the enzymatic reaction with CFD
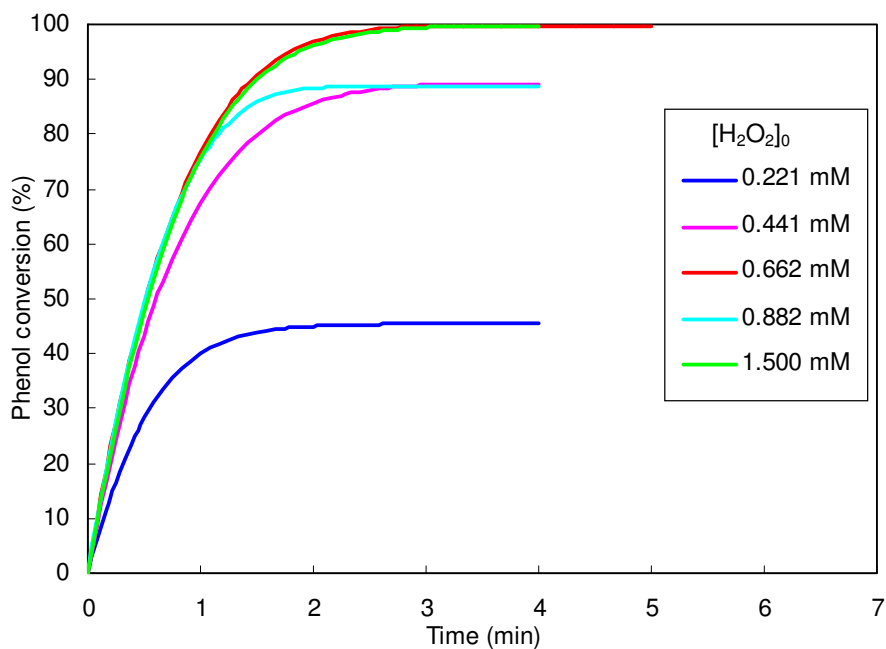
Figure 12.7.   Influence of the H_2O_2 initial concentration on the simulated phenol conversion in the torus reactor calculated with both mechanisms. $[Phenol]_0$: 0.5 mM and $[HRP]_0$: $2 \cdot 10^{-4}$ mM.
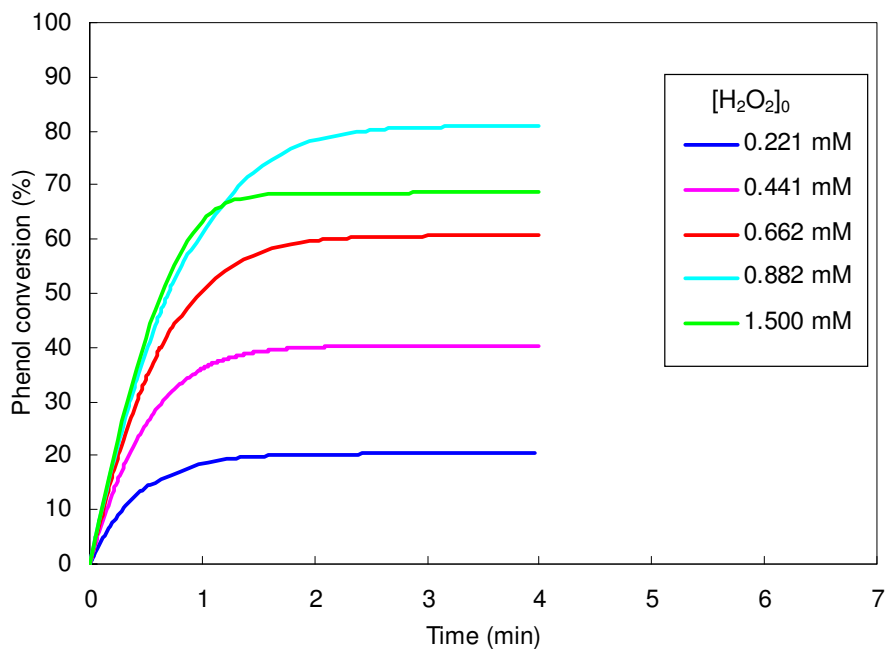
Figure 12.8.   Influence of the H_2O_2 initial concentration on the simulated phenol conversion in the torus reactor calculated with both mechanisms. $[Phenol]_0$: 1.1 mM and $[HRP]_0$: $2 \cdot 10^{-4}$ mM.

Using simultaneously, the two different mechanisms, a better agreement was obtained in all cases with the experimental data of the phenol conversion (see figures 5.3, 5.4 and 5.5 respectively).
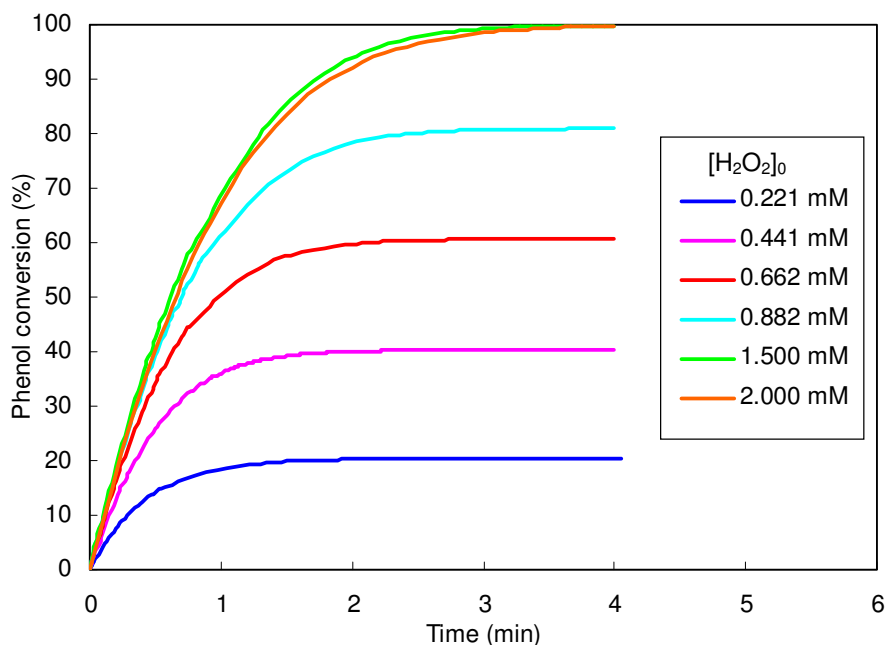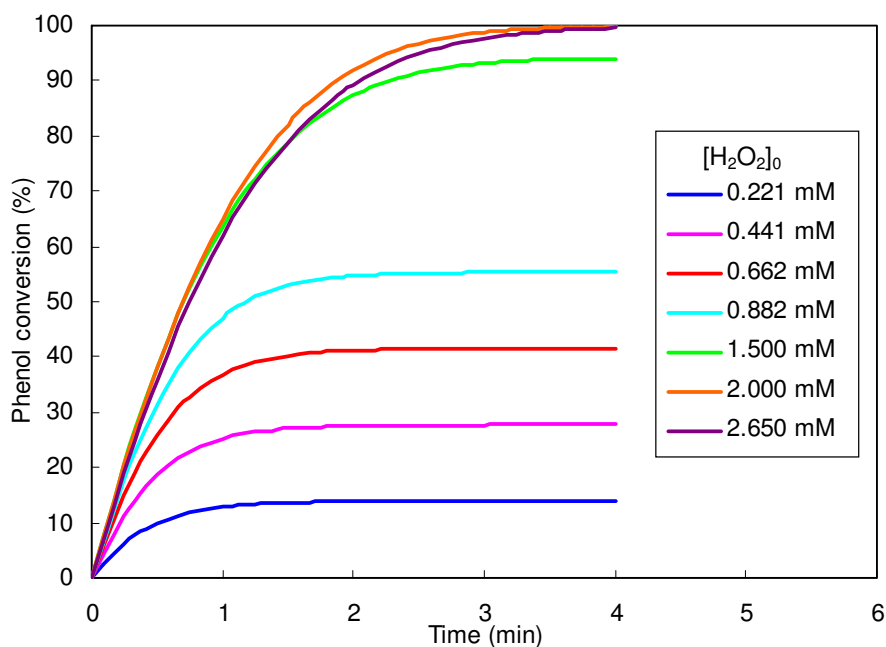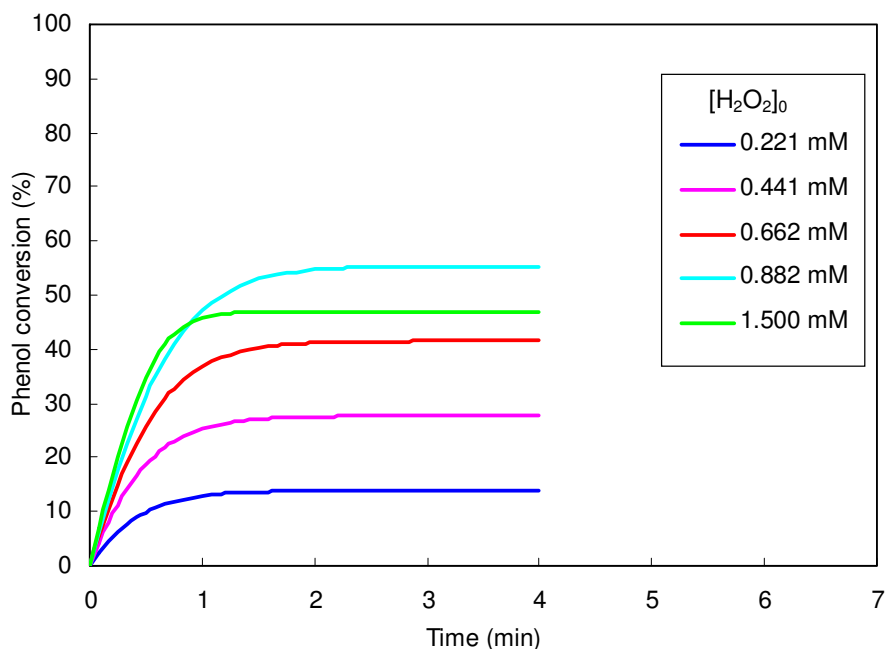
Figure 12.9.   Influence of the H_2O_2 initial concentration on the simulated phenol conversion in the torus reactor calculated with both mechanisms. [Phenol]$_0$: 1.6 mM and [HRP]$_0$: $2 \cdot 10^{-4}$ mM.

12.3. Numerical simulation of the kinetics of the reaction

The simulated initial reaction rates were calculated from the simulated curves of phenol conversion using the model with the mechanism with inhibition of the enzyme. The figures 12.10, 12.11 and 12.12 present the influence of the H_2O_2 initial concentration on the simulated initial reaction rates for an initial phenol concentration of 0.5, 1.1 and 1.6 mM respectively.

As it can be seen in the three figures, the simulated initial reaction rates are significantly in agreement with the experimental values for the three initial concentrations of phenol. The relative difference between simulated and experimental values is comprised in the range of 2 to 20%, while the higher variation is always obtained for the lower H_2O_2 initial concentration, where the difference is elevated. Moreover, in the three figures again, the simulated values fit better the kinetic model than the experimental values.

All these results validate the effectiveness of the coupling of the kinetic model obtained experimentally with the model of the torus reactor obtained by CFD. This fact proves that the CFD is a very useful tool to predict results of conversion and reaction rates without the necessity to make both extensive and expensive experimental research.
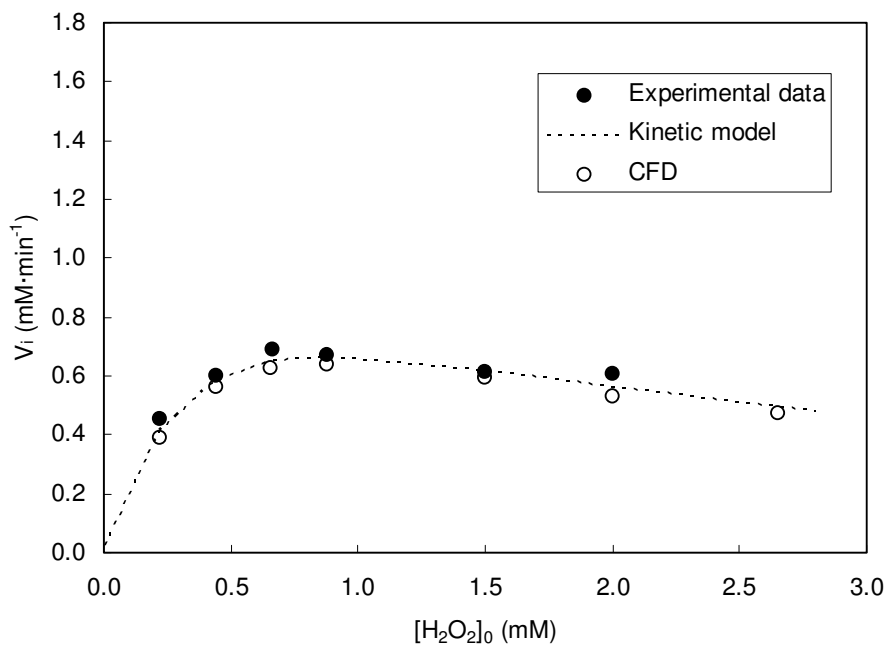
Figure 12.10. Influence of the H_2O_2 initial concentration on the Steady-state initial rates of phenol oxidation. Fitting and CFD obtained by the Michaelis-Menten model with inhibition. Experimental conditions: $[Phenol]_0$: 0.5 mM, [HRP]: $2 \cdot 10^{-4}$ mM, pH 7 and temperature of 20ºC.
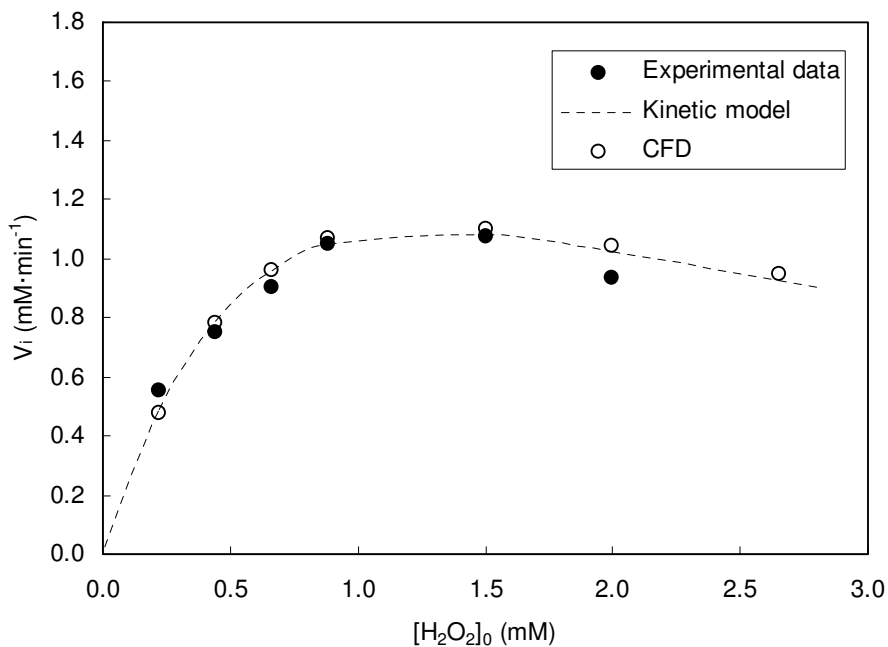
Figure 12.11. Influence of the H_2O_2 initial concentration on the Steady-state initial rates of phenol oxidation. Fitting and CFD obtained by the Michaelis-Menten model with inhibition. Experimental conditions: $[Phenol]_0$: 1.1 mM, [HRP]: $2 \cdot 10^{-4}$ mM, pH 7 and temperature of 20ºC.
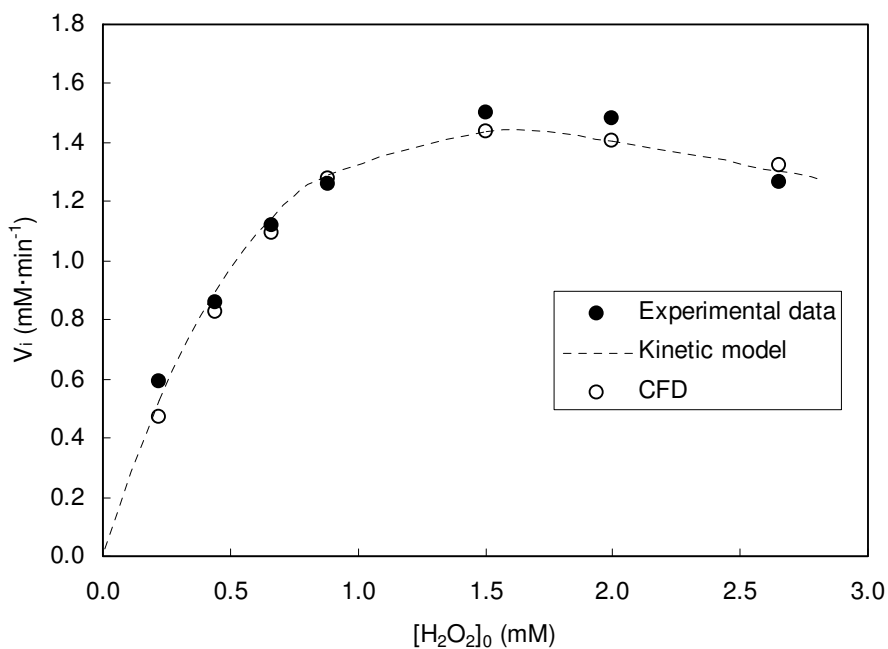
Figure 12.12. Influence of the H_2O_2 initial concentration on the Steady-state initial rates of phenol oxidation. Fitting and CFD obtained by the Michaelis-Menten model with inhibition. Experimental conditions: $[Phenol]_0$: 1.6 mM, [HRP]: $2 \cdot 10^{-4}$ mM, pH 7 and temperature of 20ºC.

12.3. Conclusions

Optimization of enzymatic elimination of the phenol process in a torus reactor requires an understanding of the complex enzymatic reactions of phenol under various process conditions. The CFD model developed in the study made it feasible to analyze such complex behaviour. By coupling a kinetic model of the enzymatic reaction to flow simulation, optimization of torus reactor hydrodynamics can be envisaged so as to eliminate phenol. In this study, a good agreement was obtained between experimental data of enzymatic elimination of phenol and its numerical simulation using CFD.

PART IV. Conclusions and future work

Chapter 13. Conclusions

The enzymatic elimination of phenol has been studied in a torus reactor. The most relevant conclusions are:

• Experimental results show that the enzymatic process is a good option to treat phenolic compounds.

• The maximum phenol conversion is 97% when the optimal concentrations of substrates are used.

• It is observable an inhibition of the enzyme when high concentrations of hydrogen peroxide are employed.

• The performance of the torus reactor is compared with a stirred reactor. The enzyme activity is identical in both reactors.

• A lower removal of phenol is obtained using the stirred tank reactor.

• Higher initial reaction rates are obtained using the torus reactor. This fact can be related to a more efficient mixing of the reactants in the torus reactor.

• The kinetic model and the parameters are determined for both reactors. A kinetic model that takes into account the initial phenol concentration, the initial hydrogen peroxide concentration and the inhibition of the enzyme is obtained.

• A good method for the covalent immobilisation of the enzyme is achieved. This method is a new alternative for the HRP immobilisation.

• The activity of the immobilised enzyme is lower than the activity of the free enzyme; however, a higher degree of phenol conversion is obtained using a lower concentration of enzyme.

The hydrodynamic characterization of the torus reactor in batch and continuous conditions has been carried out by numerical simulation using CFD. The mainly significant conclusions are:

• In batch conditions, the influence of the impeller rotation speed provokes a linear increase of the mean circulation velocity.

• The mixing time values are in all cases brief, less than 21s, achieving a rapid homogeneity of the concentration into the reactor.

• The dimensionless mixing time is independent of the Reynolds number when the impeller rotation speed is greater than 1200 rpm (Re > 5800), thus, fully turbulent regime is.

• In continuous mode the hydrodynamic is mainly a function of the impeller rotation speed.

- The location of the flow inlet in the reactor has no influence on the hydrodynamics.

- For low impeller rotation speeds, only a small difference is observed in the mixing times. For higher speeds, there are negligible differences in the mixing times.

Finally, the enzymatic elimination of phenol is modelled using CFD by the coupling between the experimental kinetic model and the flow-field characterisation of the torus reactor. The principal conclusions are:

- The CFD numerical simulations have a very good agreement with the experimental data.

- Again, the reaction rates reached by numerical simulation are extremely close to the experimental.

- The good agreement between experimental and simulation allows the possibility to predict the experimental results.

- These results allow the possibility to optimise and scale-up the process using the CFD.

How to continue the work

The continuation of the work has to have some guidelines.

- After the promising results of the removal of phenol in the torus reactor with immobilised enzyme, the next step of study will be to drive an open configuration with the torus reactor containing immobilized enzymes working in continuous flow.

- The integration of membranes in the process to separate the products of reaction.

- The modelisation of the continuous torus reactor and of the whole process by CFD.

How to continue the work

How to continue the work

Bibliography

Abdel-Fattah A.F., Osman-Mona Y., Abdel-Naby M.A., 1997. Production and immobilisation of cellobiase from Aspergillus niger A20. Chem Eng J 68: 189-196.

Adler I., Fiechter A., 1986. Valuation of bioreactors for low viscous media and high oxygen transfer demand. Bioproc. Eng. 1: 51-59.

Agency for Toxic Substances and Disease Registry (ATSDR), 1998. Toxicological profile for phenol, Update, Atlanta, USA.

Agency for Toxic Substances and Disease Registry (ATSDR), 2006. Toxicological Profile for Phenol (Draft for Public Comment). Atlanta, GA: U.S. Department of Health and Human Services, Public Health Services.

Aggelis G., Iconomou D., Christou M., Bokas D., Kotzailias S., Christou G., Tsagou V., Papanikolaou S., 2003. Phenolic removal in a model olive oil mill wastewater using Pleurotus ostreatus in bioreactor cultures and biological evaluation of the process. Wat. Res. 37: 3897-3904.

Aitken M., 1993. Waste treatment applications of enzymes: opportunities and obstacles. Chem. Engng. J. 52: B49-B58.

Aitken M., 1994. Characterization of reaction products from the enzyme catalyzed oxidation of phenolic pollutants. Wat. Res. 28: 1879-89.

Al-Duri B., Yong Y.P., 2000. Lipase immobilisation:an equilibrium study of lipase immobilised on hydrophobic and hydrophilic/hydrophobic supports, Biochem. Eng. J. 4(3): 207-215.

Arica M.Y., Bayramoglu G., Bicak N., 2004. Characterization of immobilised tyrosinase onto spacer-arm attached glycidyl methacrylate based reactive microbead, Process Biochem. 39: 2007–2017.

Arnao M.B. et al., 1990. Inactivation of peroxidise by hydrogen peroxide and its protection by a reductant agent. Bioch. et Bioph. Acta 1038: 85-89.

Artiga P., Oyanedel V., Garrido J.M., Méndez R., 2005. An innovative biofilm-suspended biomass hybrid membrane bioreactor for wastewater treatment. Desalination 179: 171-179.

Bayramoglu G., Arica M.Y., 2008. Enzymatic removal of phenol and p-chlorophenol in enzyme reactor: Horseradish peroxidase immobilised on magnetic beads. J. of Hazard. Mater., doi: 10.1016/j.jhazmat.2007.12.008.

Bayramoglu G., Yilmaz M., Arica M.Y., 2004. Immobilisation of a thermostable α-amylase onto reactive membranes: kinetics characterization and application to continuous starch hydrolysis. Food Chem. 84: 591–599.

Belleville P., Legrand J., 1992. Influence de la viscosité de la solution et de la géométrie de l'agitateur sur les caractéristiques de l'agitation dans un réacteur torique. Récents progrès en Génie des Procédés, Lavoisier Technique et Documentation Paris 6: III-20-III-25.

Belleville P., Nouri L., Legrand J., 1992. Mixing characteristics in the torus reactor. Chem. Eng. Technol. 15: 282-289.

Benkhelifa H., Bengoa C., Larre C., Guibal E., Popineau Y., Legrand J., 2005. Casein hydrolysis by immobilised enzymes in a torus reactor. Proc. Biochem. 40: 461-467.

Benkhelifa H., Legrand J., Legentilhomme P., Montillet A., 2000. Study of the hydrodynamic behaviour of the batch and continuous torus reactors in laminar and turbulent flow regimes by means of tracer methods. Chem. Eng. Sci. 55: 1871-1882.

Bertanza G., Collivignarelli C., Pedrazzani R., 2001. The role of chemical oxidation in combined chemical-physical and biological process: experiences of industrial wastewater treatment. Water Sci. Technol. 44(5): 109-116.

Bódalo A., Gómez J.L., Gómez E., Bastida J., Máximo M.F., 2006. Comparison of commercial peroxidases for removing phenol from water solutions. Chemosphere 63: 626–632.

Bollag J.M., Sjobtad R.D., Minard R.D., 1977. Polymerization of phenolic intermediates of pesticides by a fungal enzyme. Experientia 33: 1564-1566.

Borja R., Martfla A., Maestro R., Luque M., Durfinet M., 1993. Enhancement of the anaerobic digestion of wine distillery wastewater by the removal of phenolic inhibitors. Biores. Technol. 45: 99-104.

Bouchra H., 1988. PhD Thesis. Preparation and characterization of defined conjugated of glucose oxidase and peroxidase. University of Windsor.

Brodberger L.F., 1983. A conductimetric method for the study of mixing phenomena in liquids. Electrochim. Acta 28: 619-626.

Brucato A., Ciofalo M., Grisafi F., Micale G., 1998. Numerical prediction of flow-fields in baffled stirred vessels: a comparison of alternative modeling approaches. Chemical Engineering Science 53(21): 3653-3684.

Buchanan I.D., Nicell J.A., 1997. Model development for horseradish peroxidase catalyzed removal of aqueous phenol. Biotechnology and Bioengineering 54(3): 251-261.

Bungay H.R., 1989. Basic biochemical Engineering. BiLine Associate.

Carvalho G.M., Alves T.L., Freire D.M., 2000. Appl Biochem Biotechnol 84: 791.

Chellapandian M., Krishnan M. R. V., 1998. Chitosan-poly (glycidyl methacrylate) copolymer for immobilisation of urease. Process Biochem 33: 595-600.

Chibata I., 1978. Immobilised Enzyme. Kodansha Ltd, Halsted Press.

Cochranea C.F., Petacha H.H., Hendersona W., 1996. Application of tris(hydroxymethyl)phosphine as a coupling agent for alcohol dehydrogenase immobilisation. Enzyme Microb Technol 18(5): 373-378.

Cornish-Bowden A., 2004. Fundamentals of Enzyme Kinetics (3rd edition). Published by Portland Press: ISBN 1 85578 1581.

Danckwerts P.V., 1953. Continuous flow systems: distribution of residence times. Chemical Engineering Science 2: 1-13.

Danner D.J., Brignac P.J. Jr, Arcenaux D., Patel V., 1973. The oxidation of phenol and its reaction product by horseradish peroxidase and hydrogen peroxide. Arch. Biochem. Biophys. 156: 759-763.

Dec J., Bollag J.M., 1990. Detoxification of substituted phenol by oxidoreductive enzymes through polymerization reactions. Arch. Environ. Contamination Toxicol. 19: 543-50.

Decision No 2455/2001/EC of the European Parliament and of The Council of 20 November 2001 establishing the list of priority substances in the field of water policy and amending Directive 2000/60/EC, Official Journal of the European Communities, 15.12.2001, L 331, pp. 1-5.

Delincee H., Radola B.J., 1975. Fractionation of horseradish peroxidase by preparative isoelectric focusing, gel chromatography and ion-exchange chromatography. Eur. J. Biochemistry 52: 321–330.

Deshpande S.S., 1996. Enzyme Immunoassays, From Concept to Product Development. Chapman and Hall, 169–171.

Directive 2000/53/EC of 18 September 2000. Official Journal of the European Communities, 21.10.2000, L 269, pp. 34-43

Directive 2000/60/EC of 23 October 2000. Official Journal of the European Communities, 22.12.2000, L 327, pp 1-72.

Directive 2002/95/EC of 13.02.2003. Official Journal of the European Communities, 13.02.2003, L 37, pp. 19-23.

Directive 2002/96/EC of 13.02.2003. Official Journal of the European Communities, 13.02.2003, L 37, pp. 24-39

Directive 75/442/EEC of 15 July 1975. Official Journal of the European Communities 25.07.1975, L 194, pp. 39-41.

Dojilido R., Best G.A., 1993. Chemistry of waters and water pollution. Ellis Horwood, New York.

Duarte-Vazquez M., 2002. Removal of aqueous phenolic compounds from a model system by oxidative polymerization with turnip (Brassica napus L var purple top white globe) peroxidase. J. of chem. Techn. and biotechn. 78: 42-47.

Dumitriu S., Magny P., Montagne D., Vidal P.F., Chornet E., 1994. Polyionic Hydrogel Obtained by Complexation Between Xanthan and Chitosan: Their Properties as Supports for Enzyme Immobilisation, Journal of Bioactive and Compatible Polymers 9(2): 184–210.

Dunford H, Stillman J., 1976. On the function and mechanism of action of peroxidases. Coordination Chem. Rev. 19: 187-251.

Dunford H. et al., 1991. Horseradish Peroxidase: structure and kinetic properties. Peroxidases in Chemistry and Biology. Everse, J., Everse, K., and Grisham, M., Boca Raton, Fla, CRC Press. II: 1-24.

Eftaxias A., 2001. Catalytic wet air oxidation of phenol in a trickle bed reactor: Kinetics and reactor modelling, Ph.D. dissertation, Universitat Rovira i Virgili, Tarragona, Spain. Access: http://www.tesisenxarxa.net/TESIS_URV/AVAILABLE/TDX-1103103-094925//EftaxiasThesis.pdf

EPER, The European pollutant Emission Register, 2004. http://www.eper.ec.europa.eu/eper/

European Pollutant Emission Register. March 2008, In: www.eper.eea.eu.int

Fogler S., 2003. Elementos de ingeniería de la reacción química (3rd edition). Publisher by Prentice Hall Mexico.

Fortuny A., Bengoa C., Font J., Castells F., Fabregat A., 1999. Water pollution abatement by catalytic wet air oxidation in trickle bed reactor, Catalysis Today 53: 107.

Fortuny A., Font J., Fabregat A., 1998. Wet Air Oxidation of Phenol Using Active Carbon as Catalyst, Applied Catalysis B: Environmental 19: 165.

Fortuny A., Miró C., Font J., Fabregat A., 1999. Three-phase Reactors for Environmental Remediation: Catalytic Wet Oxidation of Phenol using Active Carbon, Catal. Today 48: 323.

Ghani A.G.A. et al., 1999. An investigation of deactivation of bacteria in a canned liquid food during sterilisation using computational fluid dynamics (CFD). J. Food Eng. 42: 207-214.

Gibson C., Schwarz H., 1963. Detection of conductivity fluctuations in a turbulent flow field. J. Fluid Mech. 16: 357-364.

González Siso M.I., Lang E., Carreno-Gómez B., Becerra M., Otero F., Blanco Méndez J., 1997. Enzyme encapsulation on chitosan microbeads. Process Biochem 32(3): 211-216.

Greenwood N.N., Earnshaw A., 1997. A great description of properties & chemistry of H_2O_2. Chemistry of the Elements, 2nd ed., Butterworth-Heinemann, Oxford, UK.

Griffin B., 1991. Chloroperoxidase: a review. Peroxidases in chemistry and biology. J. Everse, Everse, K. and Grisham, M. Boca Raton, Fla, CRC. II: 85-137.

Hage R., Lienke A., 2005. Applications of Transition-Metal Catalysts to Textile and Wood-Pulp Bleaching. Angewandte Chemie International Edition 45(2). doi: 10.1002/anie.200500525.

Hammel K.E., Tardone P.J., 1988. The oxidative dechlorination of polychlorinated phenols is catalyzed by extracellular fungal lignin peroxidases. Biochemistry 27: 6563-6568.

Hancock F.E., 1999. Catalytic strategies for industrial water re-use. Catalysis Today 53: 3.

Harnby N., Edwards M., Nienow A., 1997. Mixing in the process industries. Butterworth Heinemann, London.

Hernaiz M.J.,. Crout D.H.G., 2000. Immobilisation/stabilization on Eupergit C of the □-galactosidase from B. circulans and an a-galactosidase from Aspargillus oryzae, Enzyme Microb. Technol. 27: 26–32.

Horan N.J., 1990. Biological Wastewater Treatment Systems. Theory and Operation. Chichester, England, Jhon Wiley & Sons Ltd.

Hosogai K., Tanaka M., 1992. Study of suspension polymerisation of styrene with a circular loop reactor. Polymer Eng. Sci. 32: 431-437.

Hu Z.H. et al., 2000. CFD simulation of heat and moisture transfer for predicting cooling rate and weight loss of cooked ham during air-blast chilling process. J. Food Eng. 46: 189-197.

Huang Q., Tang J., Weber Jr., 2005. Precipitation of enzyme-catalyzed phenol oxidative coupling products: Background ion and pH effects. Wat. Res. 39: 3021-7.

Huang Q., Weber Jr., 2004. Interactions of soil-derived dissolved organic matter with phenol in peroxidise-catalyzed oxidative coupling reactions. Environ. Sci. Technol. 38: 338-44.

Huixian Z., Taylor K., 1994. Products of oxidative coupling of phenol by horseradish peroxidase. Chemosphere 28(10): 1807-1817.

Huzjak D., Krizanic J., 1993. The stability of b-galactosidase (Aspergillus oryzae) immobilised on Eupergit C. Annual Meeting of Croatian Biochemists, Zagreb, p. 84. Abstract.

Hyndmann D., Burell R., Lever G., Flynn G. T., 1992. Biotechnol Bioeng 40: 1326.

Ikehata K., 2002. Screening of Coprinus species for the production of extracellular peroxidase and evaluation of the enzyme for the treatment of aqueous phenol. Environ. Techn. 23: 1355-1367.

Ikehata K., Buchanan I.D., Pickard M.A., Smith D.W., 2005. Purification, characterization and evaluation of extracellular peroxidase from two Coprinus species for aqueous phenol treatment. Bioresource Techn. 96: 1758–1770.

Industrial waste treatment with hydrogen peroxide (1980). FMC Corporation, Philadelphia, PA.

Irvine R.L., Wilderer P.A., 1988. Aerobic processes. Standard Handbook of Hazardous Waste Treatment and Disposal. H.M. Freeman (ed), McGraw-Hill, New York.

Itoyama K., Tokura S., Hayashi T., 1994. Biotechnol Prog 10: 225.

Ivanov A.E., Schneider M.P., 1997. Methods for the immobilisation of lipases and their use for ester synthesis, J. Mol. Catal. B: Enzymatic 3: 303–309.

Jones C.W., Clark J.H., 1999. Applications of Hydrogen Peroxide and Derivatives. Royal Society of Chemistry.

Karam J., Nicell J., 1997. Potential applications of enzymes in waste treatment. J. Chem. Technol. Biotechnol. 69: 141-153.

Karube I., 1987. In: Kennedy, J.F. (ed.), Enzyme Technology in Biotechnology, Vol. 7a: 685. VCH Verlagsgesellschaft, Weinheim, Germany.

Kataoka K., Doi H., Komai T., 1977. Heat/mass transfer in Taylor vortex flow with constant axial flow rates. Int. J. Heat Mass Transfer 20: 57-63.

Katchalski-Katzir K., Kraemer D.M.,2000. Eupergit® C, a carrier for immobilisation of enzymes of industrial potential. J. Mol. Catal. B: Enzymatic 10: 157–176.

Khalid A., Legrand J., 2001. Energy dissipation distribution and mixing in a torus reactor. Chem. Eng. Com. 185: 141-164.

Khalid A., Legrand J., Rosant J.M., 1996. Turbulent flow induced by an impeller in a closed toroidal loop. J. Fluids Eng. 118(4): 677-684.

King T.P., Zhao S.W., Lam T., 1986. Preparation of Protein Conjugates via Intermolecular Hydrazone Linkage. Biochemistry 25: 5774-5779.

Kirk T. et al., 1987. Lignin-degrading enzymes. Phil Trans. R. Soc. Lond. A 321: 461-474.

Klibanov A.M. et al., 1983. Peroxidase catalyzed removal of phenols from coal-conversion wastewaters. Science 221: 259-261.

Klibanov A.M., Alberti B.N., Morris E.D., Felshin L.M., 1980. Enzymatic removal of toxic phenols and anilines from wastewaters. J. Appl. Biochem. 2: 414–421.

Knezevic Z., Milosavic N., Bezbradica D., Jakovljevic Z., Prodanovic R., 2006. Immobilisation of lipase from Candida rugosa on Eupergit® C supports by covalent attachment. Biochemical Engineering J. 30: 269–278.

Krajewska B., Leszko M., Zaborska W., 1990. Urease Immobilised on Chitosan Membrane : Preparation and Properties, J. Chem. Tech. Biotechnol. 48: 337–350.

Kramer D.M., Lehmann K., Pennewiss M., Plainer H., 1975. Photo-beads and oxirane beads as solid supports for catalysis and biospecific adsorption. In: Peeters H (editor). Protides of Biological Fluids 23rd Colloquium. Oxford: Pergamon Press p. 505–511.

Kramer D.M., Lehmann K., Pennewiss M., Plainer H., 1978. Oxirane-acrylic beads, preparation 2878-C. Enzyme Engineering 4. In: Broun GB, Manecke G, Wingard LB, editors. New York: Plenum Publishing, p. 153–154.

Laederach H., Widmer F., 1984. Le bioréacteur torique. Inf. Chim. 249: 157-160.

Lanz K., Scheuer S., 2001. EEB Handbook on EU Water Policy under the Water Framework Directive, Brussels.

Legrand J., Belleville P., 2002. Flow characteristics and transport phenomena in toroidal loop reactors. Chem. Eng. Technol. 25(6): 667-670.

Legrand J., Guéguen J., Bérot S., Popineau Y., Nouri L., 1997. Acetylation of pea isolate in a torus microreactor. Biotech. Bioeng. 53: 409-414.

Lian G. et al., 2002. CFD simulation of heat transfer and polyphenol oxidation during tea fermentation. Comp. and Elec. in agric. 34: 145-158.

Liu J., Song H., Weng L., Ji L., 2002. Increased thermostability and phenol removal efficiency by chemical modified horseradish peroxidase. J. of Molecular Catalysis B: Enzymatic 18: 225-232.

Lyn D.A. et al., 1999. Numerical modeling of flow and disinfection in UV disinfection channels. J. of Envir. Eng. 125: 17-23.

Magnin D., Dumitriu S., Chornet E., 2003. Immobilisation of Enzymes into a Polyionic Hydrogel: ChitoXan. Journal of Bioactive and Compatible Polymers 18: 355-373.

Malcata F.X., Reyes H.R., Garcia H.S., Hill C.G. Jr., Amundson C.H., 1990. Immobilised Lipase Reactors for Modification of Fats and Oils. A Review, J. Am. Oil Chem. Soc., 67: 890–910.

Maloney W., 1986. Transformation of trace organic compounds in drinking water by enzymatic oxidative coupling. Environ. Sci. Technol. 20: 249-253.

Masuda M., 2001. Effect of reaction conditions on phenol removal by polymerization and precipitation using Coprinus cinereus peroxidase. Enzyme and Microbial Techn. 28: 295-300.

Matatov-Meytal Y.I., Sheintuch M., 1998. Catalytic Abatement of Water Pollutants. Ind. Eng. Chem. Res. 37(2): 309-326.

Miao Y., Tan S.N., 2001. Amperometric hydrogen peroxide biosensor with silica sol–gel/chitosan film as immobilisation matrix. Anal Chim Acta 437(1): 87-93.

Miland E., Smyth M., Ó Fágáin C., 1996. Phenol removal by modified peroxidases. J. Chem. Technol. Biotechnol. 67: 227-236.

Minard R.D., Liu S.Y., Bollag J.M., 1981. Oligomers and quinones from 2,4-dichlorophenol. J. Agric. Fd Chem. 29: 250-253.

Mishra S., Mahajani V.V., Joshi J.B., 1995. Wet Air Oxidation, Industrial and Engineering Chemistry Research 34: 2.

Murakami Y., Hirose T., Ono S., Eitoku H., Nishijima T., 1982. Power consumption and pumping characteristics in a loop reactor. Ind. Chem. Eng. Proc. Des. Dev. 21: 273–276.

Nasrallah N., Legrand J., Bensmaili A., Nouri L., 2008. Effect of impeller type on the mixing in torus reactors. Chemical Engineering and Processing doi: 10.1016/j.cep.2007.11.008.

Nicell J.A., 1994. Kinetics of horseradish Peroxidase catalysed polymerization and precipitation of aqueous 4-chlorophenol. J. Chem. Tech. Biotechnol. 60: 203-215.

Nicell J.A., 1995. Phenol polymerization and precipitation by horseradish peroxidase enzyme and an additive. Biores. Technol. 54: 5-16.

Nicell J.A., Al-Kassim L., Bewtra J.K., Taylor K.E., 1993. Wastewater treatment by enzyme catalysed polymerization and precipitation. Biodeterioration Abstracts, 7(1) 1: 1-8.

Nicell J.A., Bewtra J.K., Taylor K.E., Biswas N., St. Pierre C., 1992. Enzyme catalysed polymerisation and precipitation of aromatic compounds from wastewater. Wat. Sci. Technol. 25(3): 157-64.

Nicell J.A., Wright H., 1997. A model of peroxidase activity with inhibition by hydrogen peroxide. Enzyme Microb. Technol. 21: 302-310.

Noda T., Furuta S., Suda I., 2001. Sweet potato β-amylase immobilised on chitosan beads and its application in the semi-continuous production of maltose. Carbohydr Polym 44(3), 189: 195.

Nouri L., Legrand J., Popineau Y., Belleville P., 1997. Enzymatic hydrolysis of wheat proteins. Part II: comparison of performance of batch-stirred and torus reactors. Chem. Eng. J. 65: 195-199.

O'Shannessy D.J., Quarles R.H., 1987. Labelling of the oligosaccharide moieties of immunoglobulins. J. Immunol. Meth 99: 153-161.

Okuma H., Takahashi H., Yazawa S., Sekimukai S., 1992. Development of a System with Double Enzyme Reactors for the Determination of Fish Freshness. Analytica Chimica Acta, 260: 93–98.

Ozmen M., Ayas Z., Güngördü A., Ekmekci G., Yerli S., 2008. Ecotoxicological assessment of water pollution in Sariyar Dam Lake, Turkey. Ecotoxicology and Environmental Safety 70: 163–173.

Pacific Northwest Pollution Prevention Resource Center, January 2006. Topical Reports Northwest Guide to Persistent, Bioaccumulative Toxins (PBT), in: http://www.pprc.org/pubs/pbt.cfm

Pareek V.K. et al., 2003. Computational fluid dynamic (CFD) simulation of a pilot-scale annular bubble column photocatalytic reactor. Chem. Eng. Sci. 58(3-6): 859-865.

Pruvost J., Legrand J., Legentilhomme P., 2004a. Numerical investigation of bend and torus flows, part I: effect of swirl motion on flow structure in U-bend. Chem. Eng. Sci. 59: 3345-3357.

Pruvost J., Legrand J., Legentilhomme P., Rosant J.M., 2004b. Numerical investigation of bend and torus flows. Part II: Flow simulation in torus reactor. Chemical Engineering Science 59(16): 3359-3370.

Pruvost J., Pottier L., Legrand J., 2006. Numerical investigation of hydrodynamic and mixing conditions in a torus photobioreactor. Chem. Eng. Sci. 61: 4476-4489.

Ravindranath N.H., Sathaye J.A., 2002. Climate Change and Developing Countries. Springer. ISBN 1402001045.

Robb D., 1984. Tyrosinase. Copper proteins et copper enzymes. L. R. Boca Raton, Fla, CRC Press. II, 207.

Rocchietti S., San Vicente Urrutia A., Pregnolato M., Tagliani A., Guissan J.M., Fernandez-Lafuente R., Terreni M., 2002. Influence of the enzyme derivative preparation and substrate structure on the enantioselectivity of penicillin G acylase, Enzyme Microb. Technol. 31: 88–93.

Roman R., Dunford H.B., 1972. pH dependence of the oxidation of iodide by compound I of horseradish peroxidase. Biochemistry 11: 2076.

Ronze D., Pierrard P., Zoulalian A., 1991. Influence de la DTS du fluide sur la détermination de la conductance globale de transfert thermique entre un fluide en écoulement et la paroi d'un système ouvert. Entropie 166: 21–27.

Rubalcaba A., Suárez-Ojeda M.E., Carrera J., Font J., Stüber F., Bengoa C., Fortuny A., Fabregat A., 2007. Biodegradability enhancement of phenolic compounds by Hydrogen Peroxide Promoted Catalytic Wet Air Oxidation. Catalysis Today 124: 191–197.

Ryu K., McEldoon J., Pokora A., Lyms W., Dordick J., 1993. Numerical and Monte Carlo Simulations of Phenolic Polymerizations Catalyzed by Peroxidase. Biotechnol. Bioeng. 42: 807-14.

Santoleri J.J., 1988. Liquid-injection incinerators. Standard Handbook of Hazardous Waste Treatment and Disposal, H.M. Freeman (ed), McGraw-Hill, New York.

Sato Y., 1979. Flow pattern, circulation velocity and pressure loss in loop reactor. J. Chem. Eng. Japan 12: 448-453.

Sawahata T., Neal R.A., 1982. Horseradish Peroxidase mediated oxidation of phenol. Biochem. biophys. Res. Commun. 109: 988-994.

Schwartz R.D., Hutchinson D.B., 1981. Microbial and enzymatic production of 4,4'-dihydroxybiphenyl via phenol coupling. Enzyme Microb. Technol. 3: 361-363.

Scully C., Collins G., O'Flaherty V., 2006. Anaerobic biological treatment of phenol at 9.5–15ºC in an expanded granular sludge bed (EGSB)-based bioreactor. Wat. Res. 40: 3737-44.

Seo Y.S. et al., 2003. The catalytic heat exchanger using catalytic fin tubes. Chem. Eng. Sci. 58 (1): 43-53.

Shannon L.M., Key E., Lew J.Y., 1966. Peroxidase isoenzymes from horseradish roots. Isolation and Physical Properties. J. Biol. Chem. 241: 2166–2172.

Shin H.J., Park J.M., Yang J.W., 1998. Continuous production of galacto-oligosaccharides from lactose by Bullera singularis β-galactosidase immobilised in chitosan beads. Process Biochem 33(8), 787: 192.

Simsek S., Yemenicioglu A., 2007. Partial purification and kinetic characterization of mushroom stem polyphenoloxidase and determination of its storage stability in different lyophilized forms. Process Biochem. 42: 943–950.

Song H.Y., Liu J.Z., Xiong Y.H., Weng L.P., Ji L.N., 2003. Treatment of aqueous chlorophenol by phtalic anhydride-modified horseradish peroxidase. J. Mol. Catal. B:Enzyme 22: 37-44.

Spagna G., Barbagallo R.N., Casarini D., Pifferi P.G., 2001. A novel chitosan derivative to immobilise α-L-rhamnopyranosidase from Aspergillus niger for application in beverage technologies. Enzyme Microb Technol 28(4-5): 427-438.

Spanish Pollutant Emission Register, 2008, In: http://www.eper-es.es

Spanish Water Act 1/2001: Real Decreto Legislativo 1/2001, BOE 176 del 24 de Julio de 2001, pp. 26791-26817.

Stanisavljević M., Nedić L., 2004. Removal of phenol from industrial wastewaters by horseradish (*Cochlearia Armoracia L*) peroxidase. Working and Living Environmental Protection 2(4): 345 – 349.

Stirling D.A., 2000. Persistent Organic Pollutants. An Overview of Historical Manufacturing and Use. Chemistry Preprint Archive, 1-4.
http://www.sciencedirect.com/preprintarchive/journal/15740331.

Strukul G. (Ed), 1992. Catalytic oxidation with hydrogen peroxide as oxidant. Kluver Academic Publishers, Dordrecht, The Netherlands, Chapters 1-2, 4, 6.

Suarez-Ojeda M.E., Guisasola A., Baeza J.A., Fabregat A., Stüber F., Fortuny A., Font J., Carrera J., 2007. Integrated catalytic wet air oxidation and aerobic biological treatment in a municipal WWTP of a high-strength o-cresol wastewater. Chemosphere 66: 2096–2105.

Suarez-Ojeda M.E., Stüber F., Fortuny A., Fabregat A., Carrera J., Font J., 2005. Catalytic wet air oxidation of substituted phenols using activated carbon as catalyst. Applied Catalysis B: Environmental 58: 105–114.

Suarez-Ojeda M.E., Stüber F., Fortuny A., Fabregat A., Carrera J., Font J., 2005. Catalytic wet air oxidation of substituted phenols using activated carbon as catalyst. Applied Catalysis B: Environmental 58: 105–114.

Tanaka M., Sendai T., Hossogai K., 1989. Flowing characteristics in a circular loop reactor, Chem. Eng. Res. Dev. 67: 423–427.

Tatsumi K., Ichikawa H., Wada S., 1994. Dephenolization from aqueous solution by treatment with peroxidase and a coagulant. Wat. Sci. Technol. 30: 79–86.

Tien M., 1987. Properties of ligninase from Phanerochaete chrysosporium and their possible applications. CRC Crit. Rev. Microbiol. 15: 141-168.

Tong Z., Qingxiang Z., Hui H., Qin L., Yi Z., 1997. Removal of toxic phenol and 4-chlorophenol from waste water by horseradish peroxidase. Chemosphere 34(4): 893-903.

UNEP International Environment, 2002. Environmentally Sound Technology for Wastewater and Stormwater Management: An International Source Book. IWA Publishing. ISBN 1843390086.

Vasudevan P., 1996. Kinetics of phenol oxidation by peroxidase. Applied Biochemistry and Biotechnology 60: 203-215.

Vasudevan P., Li L.O., 1996. Peroxidase catalyzed polimerization of phenol. App. Biochem. and Biotech. 60: 73-82.

Verboven P. et al., 1997. The local surface heat transfer coefficient in thermal food process calculations: a CFD approach. J. Food Eng. 33: 15-35.

Verschueren K., 1977. Handbook of environmental data on organic chemicals. New York.

Voet D. and J., 1995. Biochemistry, 2nd edition, John Wiley & Sons Inc.

Voice T.C., 1988. Activated carbon adsorption. Standard Handbook of Hazardous Waste Treatment and Disposal, H.M. Freeman (ed), McGraw-Hill, New York.

Wehtje E., Adlercreutz P., Mattiasson B., 1992. Improved activity retention of enzymes deposited on solid supports. Biotechnol Bioeng 41: 171.

Welinder K.G., 1979. Amino acid sequence studies of horseradish peroxidase Eur. J. Biochem. 96: 483–502.

Wilcox D.C., 1998. Turbulence modeling for CFD. DCW Industries, Inc., La Canada, California.

Wirz B., Barner R., Huebscher J., 1993. Facile chemoenzymic preparation of enantiomerically pure 2-methylglycerol derivatives as versatile trifunctional C4-synthons. J. Am. Chem. Soc. 58: 3980–3984.

Wu J., Bewtra T. K., and Taylor K., 1993. Optimization of the reaction conditions for enzymatic removal of phenol from wastewater in the presence of polyethylene glycol. Water Res. 27(12): 1701-1706.

Wu J., Taylor K., Biswas N., Bewtra N., 1999. Kinetic model for removal of phenol by horseradish peroxidase with PEG. J. Environ. Eng. 125: 451-8.

Yildiz H.B., Sahmetlioglu E., Boyukbayram A.E., Toppare L., Yagci Y., 2007. Immobilisation of tyrosinase and alcohol oxidase in conducting copolymers of thiophene functionalized poly(vinyl alcohol) with pyrrole. Int. J. Biol. Macromol. 41: 332–337.

Yu J., Taylor K.E., Zou H., Biswas N., Bewtra J.K., 1994. Phenol conversion and dimeric intermediates in horseradish peroxidase-catalyzed phenol removal from water. Environ. Sci. Technol. 28: 2154-60.

Zollner H., 1993. Handbook of Enzyme Inhibitors, 2nd Ed., Part A: 367–368.

Biographical note

Name: Laura Mariela Pramparo

Education:

- 1996-2001: Chemical Engineer, Universidad Nacional de Río Cuarto, Córdoba, Argentina.

- 2003-2005: Research Sufficiency (Diploma d'Estudis Avançats, DEA), Universitat Rovira i Virgili, Tarragona, Spain.

Publications in Journals:

- Pramparo, L.; Pruvost, J.; Stüber, F.; Font, J.; Fortuny, A.; Fabregat, A.; Legentilhomme, P.; Legrand, J.; Bengoa, C. Mixing and Hydrodynamics investigation using CFD in a square-sectioned torus reactor in batch and continuous regimes. Chem. Eng. J. 137(2008):386-395.

- Pramparo L.; Stüber, F.; Font, J.; Fabregat, A.; Fortuny, A.; Bengoa, C. Kinetic model and parameters of the enzymatic elimination of phenol in a torus reactor. In preparation.

- Pramparo L.; Stüber, F.; Font, J.; Fortuny, A.; Fabregat, A.; Bengoa, C. Optimization of the operating conditions in the enzymatic elimination of phenol in a torus reactor. In preparation.

- Pramparo, L.; Pruvost, J.; Stüber, F.; Font, J.; Fortuny, A.; Fabregat, A.; Legentilhomme, P.; Legrand, J.; Bengoa, C. Numerical approach for the enzymatic elimination of phenol in a torus reactor. In preparation.

Chapters in books:

- Pramparo, L.; Sanchez, I.; Stüber, F.; Font, J.; Fortuny, A.; Fabregat, A.; Bengoa, Ch. Enzymatic Elimination of Phenol in Stirred and Torus Reactor. Chemical Industry and Environment V. Ed. Ferdinand Berger & Söhne GmbH, Horn, Austria. Vol. I:362-370, 2006. ISBN: 3 900 554 57 9.

- Sanchez, I.; Pramparo, L.; Stüber, F.; Font, J.; Fortuny, A.; Fabregat, A.; Bengoa, Ch. Phenol Oxidation by Chelated iron: Initial pH Influence. Chemical Industry and Environment V. Ed. Ferdinand Berger & Söhne GmbH, Horn, Austria. Vol. I:371-378, 2006. ISBN: 3 900 554 57 9.

- Pramparo, L.; Castro, U.I.; Stüber, F.; Font, J.; Fortuny, A.; Fabregat, A.; Bengoa, Ch. Enzymatic Elimination of Phenol in a Torus Reactor: Reaction Kinetic Study. International

Biographical note

Water Conference 2006, Ed. Centro de Estudos de Água 27-34, 2006, Portugal. ISBN: 972 8688 40 7.

- Pramparo, L.; Sanchez, I.; Legentilhomme, P.; Pruvost, J.; Legrand, J.; Stüber, F. ; Font, J.; Fabregat, A.; Fortuny, A.; Bengoa, C. Numerical simulation of a torus reactor. CHISA 2006, Ed. Process Engineering Publisher, Vol. 5, 2006, Czech Republic. ISBN: 80 86059 45 6.

- Pramparo L.; Stüber F.; Font, J.; Fortuny A.; Fabregat, A.; Bengoa Ch. Enzymatic elimination of phenol: pH influence. Récents Progrès en Génie des Procédés, Ed. SFGP, Vol. 94, 2007, France. ISBN: ISBN 2-910239-6.

- Pramparo L.; Stüber F.; Font, J.; Fortuny A.; Fabregat, A.; Bengoa C. Determination of the kinetic model and parameters of the enzymatic elimination of phenol in a torus reactor. Récents Progrès en Génie des Procédés, Ed. SFGP, Vol. 96, 2007, France. ISBN: 2-910239-70-5.

Contributions in congresses and scientific meetings:

- Pramparo, L.; Stüber, F.; Font, J.; Fortuny, A.; Fabregat, A.; Legentilhomme, P.; Pruvost, J.; Legrand, J.; Bengoa, C. Immobilized enzymatic elimination of phenol in a torus reactor. Preliminary flow study. Poster, Forum FLUENT 2005, Madrid (Spain), 2005.

- Pramparo, L.; Stüber, F.; Font, J.; Fortuny, A.; Fabregat, A.; Legentilhomme, P.; Pruvost, J.; Legrand, J.; Bengoa, C. Elimination of phenol by immobilized enzyme in a torus reactor. Preliminary flow study. Poster, 10th Mediterranean Congress of Chemical Engineering, Barcelona (Spain), 2005.

- Pramparo, L.; Stüber, F.; Font, J.; Fortuny, A.; Fabregat, A.; Legentilhomme, P.; Pruvost, J.; Legrand, J.; Bengoa, C. Elimination of phenol by immobilized enzyme in a torus reactor. Preliminary flow study. Poster, IV Jornadas Doctorales URV, Tarragona (Spain), 2005.

- Torrens, E.; Bernat, X.; Suárez, M.E.; Rubalcaba, A.; Baricot, M.; Prámparo, L.; Sánchez, I.; Castro, U.I.; Mezohegyi, G.; Daghsteib, S.A.; Bengoa, C.; Stüber, F.; Fortuny, A.; Font, J.; Fabregat, A. Grupo de Ingeniería de la Reacción Química e Intensificación de Procesos. Poster, Mesa Española de Tratamiento de Aguas (META), Valencia (Spain), 2006.

- Pramparo, L.; Sanchez, I.; Stüber, F.; Font, J.; Fortuny, A.; Fabregat, A.; Bengoa, Ch. Enzymatic Elimination of Phenol in Stirred and Torus Reactor. Poster, 5th European Meeting on Chemical Industry and Environment (EMCHIE), Vienna (Austria), 2006.

- Sánchez, I.; Pramparo, L.; Font, J.; Fortuny, A.; Stüber, F.; Fabregat, A.; Bengoa, Ch. Phenol oxidation promoted by chelated iron: initial PH influence. Poster, 5th European Meeting on Chemical Industry and Environment, Vienna (Austria), 2006.

Biographical note

- Pramparo, L.; Font, J.; Bengoa, Ch. Enzymatic Elimination of Phenol in Stirred and Torus Reactors. Poster, V Jornadas Doctorales DEQ, Tarragona (Spain), 2006.

- Pramparo, L.; Sanchez, I.; Stüber, F.; Font, J.; Fortuny, A.; Fabregat, A.; Legentilhomme, P.; Pruvost, J.; Legrand, J.; Bengoa, Ch. Numerical Simulation of a Torus Reactor. Poster, CHISA, Prague (Czech Republic), 2006.

- Pramparo, L.; Castro, U.I.; Stüber, F.; Font, J.; Fortuny, A.; Fabregat, A.; Bengoa, C. Enzymatic elimination of phenol: pH influence. Poster, 1st International Congress on Green Process Engineering, Toulouse (France), 2007.

- Pramparo, L.; Stüber, F.; Font, J.; Fortuny, A.; Fabregat, A.; Bengoa, C. Determination of the kinetic model and parameters of the enzymatic elimination of phenol in a torus reactor. Poster, 11e Congrès de la Société Française de Génie de Procédés (SFGP), Saint Etienne (France), 2007.

- Pramparo, L.; Bengoa, C. Performance study of a torus reactor using enzymatic elimination of phenol. Poster, 6th PhD Day of the programme in Chemical, Environmental and Process Engineering, Tarragona (Spain), 2007.

- Pramparo, L.; Pruvost, J.; Stüber, F.; Font, J.; Fortuny, A.; Fabregat, A.; Legentilhomme, P.; Legrand, J.; Bengoa, C. Numerical approach for the enzymatic elimination of phenol in a torus reactor. Poster, 18th European Symposium on Computer Aided Process Engineering (ESCAPE-18), Lyon (France), 2008.

Research stays:

- University of Windsor, Windsor (ON), CANADA, 2007. Duration: 45 days. Topic: Enzyme immobilization. Supervisor: Dr. K. Taylor.

- Université de Nantes, Saint Nazaire, FRANCE, 2006. Duration: 3 months. Topic: Modelization and numerical simulation of the kinetic reaction in the torus reactor. Supervisor: Dr. J. Pruvost.

- Université de Nantes, Nantes, FRANCE, 2005. Duration: 5 months. Topic: Modelization and simulation of a torus reactor with Fluent (CFD). Supervisor: Dr. J. Pruvost.